

**LEVEL**



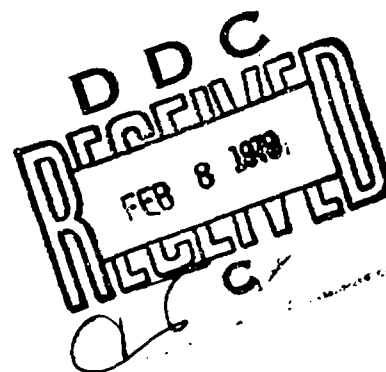
12

AD A 064318

USARTL-TR-78-26

**DESIGN, TEST, AND ACCEPTANCE CRITERIA FOR  
HELICOPTER TRANSPARENT ENCLOSURES**

Bruce F. Kay  
Sikorsky Aircraft Division  
United Technologies Corp.  
Stratford, Conn. 06602



DDC FILE COPY

November 1978

Final Report for Period 27 June 1974 - 26 July 1976

Approved for public release;  
distribution unlimited.

Prepared for  
APPLIED TECHNOLOGY LABORATORY  
U. S. ARMY RESEARCH AND TECHNOLOGY LABORATORIES (AVRADCOM)  
Fort Eustis, Va. 23604

79 02 07 003

## APPLIED TECHNOLOGY LABORATORY POSITION STATEMENT

The high replacement cost of helicopter transparencies in terms of maintenance, aircraft availability, mission performance, and dollars is a serious problem. Recognizing this, the Applied Technology Laboratory funded PPG Industries and Good-year Aerospace Corporation to assess the problem and recommend remedial action. They reported that abrasion is a serious problem, and many windshields with degraded visibility are "lived with" in the field - partly because interchangeable parts are virtually nonexistent. Helicopter windshields are being replaced every 200 to 300 flight hours. This generally low reliability was largely attributed to the fact that the Army had neither a specification nor any design guidelines addressing helicopter cockpit enclosures as a subsystem. Instead, each Army helicopter has its own Army/contractor negotiated model specification, giving rise to a generally low reliability. The needs were for a specification with "teeth" in its qualification and acceptance criteria, together with a design handbook giving designers and procurement agencies alike insight into what is required for a better performing, more reliable product.

The objectives of this contract were to develop a draft specification and a comprehensive design handbook. The results are published in two reports: TR 78-26, Design, Test and Acceptance Criteria for Helicopter Transparent Enclosures; and TR 78-26A and B, Helicopter Transparent Enclosures, Volume I being the Design Handbook and Volume II being the General Specification.

In this program, emphasis was devoted to structural integrity, including the interactive effects of airframe stiffness, edge attachments, structural loads, thermal variations, vibration, and windshield manufacturing tolerances based on induced loads resulting from windshield/airframe contour mismatch. A NASTRAN finite element analysis of a windshield and its airframe support structure was used to analyze the structural interaction between fuselage deformation, airframe/cockpit enclosure loads, and windshield strains and deformations. Subsequent tests demonstrated the need for more refined NASTRAN modeling.

A General Specification has been developed with minimum performance levels stated for those characteristics/features considered common to all transparent enclosures, together with a set of qualification and acceptance test criteria to ensure conformance. The key aspect of the qualification and acceptance tests is the development of an integrated-endurance test. This test realistically combines operational loads and environmental extremes cyclically in a severely accelerated life cycle exposing failure modes, permitting an assessment of expected service life. This test puts "teeth" into the specification, and its implementation should afford a cost-effective means for substantiating windshield reliability. A realistic windshield wiper abrasion test has been embodied in the General Specification. At this time, there is insufficient data for relating results from this test to service life.

The General Specification and Design Handbook are responsive to the Army's need. Their implementation is encouraged.

This program was conducted under the technical cognizance of Joseph H. McGarvey, Military Operations Technology Division.

### DISCLAIMERS

The findings in this report are not to be construed as an official Department of the Army position unless so designated by other authorized documents.

When Government drawings, specifications, or other data are used for any purpose other than in connection with a definitely related Government procurement operation, the United States Government thereby incurs no responsibility nor any obligation whatsoever; and the fact that the Government may have formulated, furnished, or in any way supplied the said drawings, specifications, or other data is not to be regarded by implication or otherwise as in any manner licensing the holder or any other person or corporation, or conveying any rights or permission, to manufacture, use, or sell any patented invention that may in any way be related thereto.

Trade names cited in this report do not constitute an official endorsement or approval of the use of such commercial hardware or software.

### DISPOSITION INSTRUCTIONS

Destroy this report when no longer needed. Do not return it to the originator.

REPORT DOCUMENTATION PAGE		READ INSTRUCTIONS BEFORE COMPLETING FORM	
1. REPORT NUMBER USARTL-TR-78-26	2. GOVT ACCESSION NO.	3. RECIPIENT'S CATALOG NUMBER	
4. TITLE (and Subtitle) DESIGN, TEST, AND ACCEPTANCE CRITERIA FOR HELICOPTER TRANSPARENT ENCLOSURES		5. TYPE OF REPORT & PERIOD COVERED Final Report, 21 Jan 74 - 26 Jul 76	
7. AUTHOR(s) Bruce F. Kay		6. PERFORMING ORG. REPORT NUMBER SER-50967	
9. PERFORMING ORGANIZATION NAME AND ADDRESS Sikorsky Aircraft Division United Technologies Corp. Stratford, Conn. 06602		8. CONTRACT OR GRANT NUMBER(s) DAAJ02-74-C-0065	
11. CONTROLLING OFFICE NAME AND ADDRESS Applied Technology Laboratory, US Army Research and Technology Laboratories (AVRADCOM) Fort Eustis, Va. 23604		10. PROGRAM ELEMENT, PROJECT, TASK AREA & WORK UNIT NUMBERS 62203A/1F262203AH86 03 009 BX	
14. MONITORING AGENCY NAME & ADDRESS (if different from Controlling Office)		12. REPORT DATE November 1978	
		13. NUMBER OF PAGES 326	
		15. SECURITY CLASS. (of this report) Unclassified	
		15a. DECLASSIFICATION/DOWNGRADING SCHEDULE	
16. DISTRIBUTION STATEMENT (of this Report) Approved for public release; distribution unlimited.			
17. DISTRIBUTION STATEMENT (of the abstract entered in Block 20, if different from Report)			
18. SUPPLEMENTARY NOTES			
19. KEY WORDS (Continue on reverse side if necessary and identify by block number) Transparent Enclosures    Fail Safety    Endurance Testing Abrasion    Ballistic Impact    Usage Spectrum Interlayers    Optical Factors    Adhesion Finite-Element Analysis    Spall    Edge Attachments			
20. ABSTRACT (Continue on reverse side if necessary and identify by block number) This report describes a series of analytical and experimental studies that were performed to develop and substantiate the design, acceptance, and test criteria for Army helicopter transparent enclosures. Primary emphasis was placed on structural substantiation methods and the airframe interface. Wind-shield endurance tests were performed in a manner intended to duplicate actual service conditions. Suitable instrumentation was used to determine critical loading combinations. (over)			

325 800 79 02 07 003 JCL

20. ABSTRACT - Continued

A NASTRAN finite-element analysis was performed to demonstrate the applicability of this type of structural analysis for helicopter cockpits. The analysis showed the benefits of using NASTRAN to evaluate transparency stresses in curved panels, and stresses resulting from fuselage wracking.

As abrasion has been the primary cause for helicopter transparency replacements, a series of tests were conducted to enable simulation of the various forms of abrasion in the laboratory. The tests were conducted on glass, acrylic, and polycarbonate; the acrylic and polycarbonate materials were with and without abrasion-resistant hard coats.

Ballistic tests were performed on a variety of transparent materials to quantify spall characteristics. The test data were compared to empirical relationships used to equate spall energy with probability of skin penetration.

ACCESSION for	
NTIS	White Section <input checked="" type="checkbox"/>
FDC	Buff Section <input type="checkbox"/>
UNANNOUNCED	<input type="checkbox"/>
JUSTIFICATION	
BY	
DISTRIBUTION/AVAILABILITY CODES	
Dist.	AvAIL and/or SPECIAL
<b>R</b>	

## PREFACE

The work reported herein was authorized by Contract DAAJ02-74-C-0065 awarded by the Eustis Directorate, U. S. Army Air Mobility Research and Development Laboratory (USAAMRDL)\*, Fort Eustis, Virginia. The work was performed by the Sikorsky Aircraft Division, United Technologies Corporation, Stratford, Connecticut.

This work was performed under the supervision of Mr. B. F. Kay, Airframe Design & Development Section, who served in the capacity of Program Manager and Principal Investigator. The Technical Monitor for this program was Mr. J. H. McGarvey, Military Operations Technology Division, USAAMRDL.

Grateful acknowledgement is extended to the following corporations, Government agencies and individuals at Sikorsky Aircraft that contributed information used in this report:

### INDUSTRIAL

PPG Industries, Huntsville, Alabama  
Sierracin/Sylmar, Sylmar, California  
Swedlow, Inc., Garden Grove, California  
Triplex Safety Glass Co. Ltd., Birmingham, England  
Goodyear Aerospace Corp., Phoenix, Arizona  
Remington Arms Corp., Bridgeport, Conn.  
Gentex Corp., Carbondale, Pennsylvania

### GOVERNMENT AGENCIES

Army Materials & Mechanics Research Center, Watertown, Mass.  
Army Aeromedical Research Laboratory, Fort Rucker, Alabama  
Army Test Board, Fort Rucker, Alabama  
Army Flight School, Fort Rucker, Alabama  
Ballistic Research Laboratory, Aberdeen, Maryland

### SIKORSKY PERSONNEL

A. Stave, Human Factors Section  
Dr. P. Dinyovszky, Structures and Materials  
C. L. DeGeorge, Structures Analysis  
J. T. Abbe, Loads and Criteria  
R. T. Welge, Airframe Design & Development  
W. G. Degnan, Materials  
A. Thompson, Ground Test  
J. Perschbacker, Ground Test  
H. Kearney, Ground Test

---

\*Redesignated Applied Technology Laboratory, U. S. Army Research and Technology Laboratories (AVRADCOM), effective 1 September 1977.

TABLE OF CONTENTS

	<u>Page</u>
PREFACE . . . . .	3
LIST OF ILLUSTRATIONS . . . . .	8
LIST OF TABLES . . . . .	20
INTRODUCTION . . . . .	24
ABRASION TESTS . . . . .	26
Abrasion Test Methods . . . . .	29
Abrasion Test Results . . . . .	29
Correlation of Test Results . . . . .	42
Abrasion Test Conclusions . . . . .	43
STRUCTURAL ADHESION TESTS . . . . .	44
Bond Tensile Test . . . . .	47
Bond Shear Test . . . . .	51
Bond Cleavage Test . . . . .	56
Flexural Tests . . . . .	60
Structural Adhesion Test Conclusions . . . . .	84
NASTRAN FINITE ELEMENT ANALYSIS . . . . .	85
Investigative Study . . . . .	85
NASTRAN Finite Element Theory . . . . .	87
NASTRAN Finite Element Capabilities for Nonlinear Problems . . . . .	88
Structural Description . . . . .	90
NASTRAN Models Description . . . . .	93
NASTRAN Output Format . . . . .	100
Loading Conditions . . . . .	103
Results . . . . .	104
NASTRAN Conclusions . . . . .	127
THERMAL EXPANSION, INSTALLATION PRELOAD AND ASSEMBLY TESTS . . . . .	128
Tensile Stiffness Test . . . . .	130
Thermal Tests . . . . .	134
Installation Preload Test . . . . .	137
Assembly Tests . . . . .	143
Thermal Expansion, Installation Preload and Assembly Test Conclusions . . . . .	157

TABLE OF CONTENTS (Continued)

	<u>Page</u>
ASSESSMENT OF RESIDUAL VISIBILITY THROUGH FRACTURED GLASS PANELS . . . . .	158
Objective Measures . . . . .	165
Subjective Measures . . . . .	166
Results . . . . .	166
Residual Visibility Conclusions . . . . .	168
FIELD SURVEY OF ARMY HELICOPTER TRANSPARENCIES . . . . .	169
Pilot Haze Ratings . . . . .	169
Tinted Window Light Transmission . . . . .	172
Pilot Questionnaire . . . . .	173
Photographic Data . . . . .	182
Discussion and Observations . . . . .	199
Field Study Conclusions . . . . .	201
BALLISTIC DAMAGE TOLERANCE TESTS . . . . .	202
Screening Test . . . . .	206
Ballistic Impact Test Procedure . . . . .	208
Fail Safe Test . . . . .	208
Results . . . . .	211
Spall Criteria . . . . .	230
Ballistic Test Conclusions . . . . .	233
LOW-ENERGY IMPACT TESTS . . . . .	234
Test Procedure . . . . .	237
Results . . . . .	239
Impact Test Conclusions . . . . .	253
USAGE SPECTRUM . . . . .	254
Temperature Environment From Natural Climatic Conditions . . . . .	254
Structural Loading Conditions . . . . .	258
Vibration . . . . .	260
Structural Loading Spectrum . . . . .	262

TABLE OF CONTENTS (Continued)

	<u>Page</u>
INSTRUMENTED WINDSHIELD TESTS . . . . .	263
Test Specimens . . . . .	263
Specimen Installation . . . . .	267
Test Parameters . . . . .	267
Procedure . . . . .	269
Test Facility . . . . .	272
Instrumentation . . . . .	278
Results . . . . .	283
Analysis of Results . . . . .	287
Instrumented Test Conclusions . . . . .	295
WINDSHIELD ENDURANCE TESTS . . . . .	297
Test Description . . . . .	297
Results . . . . .	298
Endurance Test Conclusions . . . . .	303
MAJOR CONCLUSIONS . . . . .	308
RECOMMENDATIONS . . . . .	310
APPENDIXES	
A    ABRASION TEST METHODS . . . . .	313
Dry Rubbing Abrasion Test . . . . .	313
Falling Sand Test . . . . .	315
Windshield Wiper Test . . . . .	316
Wet Rubbing Abrasion Test . . . . .	318
Blowing Sand and Dust Test . . . . .	220
B    ANALYSIS OF INSTRUMENTATION DIFFICULTIES WITH STRAIN MEASUREMENTS AT NONAMBIENT TEMPERA- TURES . . . . .	321

LIST OF ILLUSTRATIONS

<u>Figure</u>		<u>Page</u>
1	Windshield Wiper Abrasion Damage . . . . .	26
2	Dry Rubbing Abrasion Test Results . . . . .	32
3	Specimen From Dry Rubbing Abrasion Test . . . . .	33
4	Falling Sand Test Results . . . . .	35
5	Windshield Wiper Test Results . . . . .	37
6	Windshield Wiper Test Abraded Sample . . . . .	38
7	Wet Rubbing Abrasion Test Results . . . . .	40
8	Specimen From Wet Rubbing Abrasion Test . . . . .	41
9	Baldwin Model 3LH PIE-132 Universal Testing Machine	46
10	Bond Tensile "T" Blocks . . . . .	47
11	Test Coupon-Tensile Bond . . . . .	48
12	Bond Tensile Test Setup . . . . .	49
13	Bond Shear Test Fixture . . . . .	51
14	Bond Shear Test Specimen . . . . .	52
15	Bond Shear Fixture . . . . .	53
16	Shear Stress Distribution in Interlayer . . . . .	54
17	Cleavage Test Fixture With Restrainer to Prevent Loading Pin Deflecting Away From Coupon .	56
18	Cleavage Test Fixture . . . . .	57
19	Bond Cleavage Test Specimen. . . . .	57
20	Cleavage Test Setup Shown in the Environmental Chamber on the Baldwin . . . . .	58
21	Flexural Test Setup . . . . .	61
22	Flexural Test Fixture. . . . .	61
23	Strain Measuring Equipment . . . . .	62

LIST OF ILLUSTRATIONS (Continued)

<u>Figure</u>		<u>Page</u>
24	Strain Gauge Thermal Compensation . . . . .	62
25	Flexure Test Specimen . . . . .	63
26	Flexure Test Setup Shown in the Environmental Chamber on the Baldwin . . . . .	65
27	Beam Loading Geometry . . . . .	67
28	Load Deflection Test Data, Polyester/PVB/Acrylic Laminate with Coating . . . . .	70
29	Load Deflection Test Data, Glass/PVB/Acrylic Laminate with Coating . . . . .	71
30	Load Deflection Test Data, Glass/PVB/Acrylic Laminate, No Conductive Coating . . . . .	72
31	Load Deflection Test Data, Glass/ETP/Polycarbonate Laminate with Coating . . . . .	73
32	Variation in Stiffness With Temperature, Polyester-PVB-Stretched Acrylic . . . . .	75
33	Variation in Stiffness With Temperature, Glass-ETP-Polycarbonate . . . . .	76
34	Variation in Stiffness With Temperature, Glass-PVB-Stretched Acrylic . . . . .	77
35	Strain Distribution in Uncoupled and Partially Coupled Composite Beam . . . . .	82
36	Sikorsky YUH-60A UTTAS . . . . .	90
37	Sikorsky YUH-60A Structural Arrangement . . . . .	92
38	Cockpit NASTRAN Model . . . . .	93
39	Cabin NASTRAN Model . . . . .	94
40	Cockpit NASTRAN Model Without Windshields . . . . .	96
41	Refined Model of Center Windshield . . . . .	96
42	NASTRAN Numbering Sequence for Windshields . . . . .	97
43	Cathode Ray Tube Display . . . . .	99

LIST OF ILLUSTRATIONS (Continued)

<u>Figure</u>		<u>Page</u>
44	Missing Element Detection by CRT . . . . .	99
45	Reference Coordinate System . . . . .	100
46	Force Output for BAR and Plate Elements . . . . .	101
47	Stress Output for Plate Elements . . . . .	102
48	Resolution of Normal Stresses into Bending and In-Plane Stresses . . . . .	102
49	Distinction Between Normal and Principal Stresses.	103
50	Stress Pattern in Flat Windshield . . . . .	106
51	Support Constraints for Plate Analysis . . . . .	107
52	Deflections, 1 psi Pressure Load, Glass/Glass Windshield . . . . .	109
53	Stress Distributions, 0.3 psi Pressure Condition, Glass/Glass Windshield . . . . .	112
54	Windshield Deflections Under 0.3 psi Pressure, Outboard Glass/Glass Panel . . . . .	113
55	In-Plane Forces Normal to B.L. 10 Post, 0.3 psi Pressure Loading Condition . . . . .	113
56	Differential Stiffness Effects on Center Windshield Deflection . . . . .	114
57	Major Principal Stress, 1 psi Pressure on Center Windshield . . . . .	115
58	Displacements, 1 psi Pressure on Center Windshield . . . . .	117
59	Symmetrical Pullout Maneuver . . . . .	118
60	Schematic Representation of Windshield Structure Reaction to Inertia Loading . . . . .	120
61	Moment Definition for Posts and Sills . . . . .	120
62	Displacements, Vertical Bending, Differential Stiffness Solution . . . . .	122
63	Deformed Shape of Windshield Cavity . . . . .	123

LIST OF ILLUSTRATIONS (Continued)

<u>Figure</u>		<u>Page</u>
64	Deflection Mode for Windshield Post . . . . .	123
65	Major Principal Stresses, Vertical Bending Condition . . . . .	124
66	In-Plane Forces Normal to B.L. 10 Post, Vertical Bending Condition . . . . .	125
67	Laminated Test Specimen Edge Configurations . . .	131
68	Stiffness Test Setup . . . . .	132
69	Spring Rate Test Data . . . . .	132
70	Load vs Stress Test Data . . . . .	133
71	Laminated Windshield Thermal Test at Low Temperature . . . . .	135
72	Thermal Test, Temperature vs Stress, Glass/ Acrylic Specimen . . . . .	136
73	Thermal Test, Temperature vs Stress, Glass Panel With Rigid Edging . . . . .	138
74	Thermal Test, Temperature vs Stress, Glass Panel With Flexible Edging . . . . .	139
75	Schematic Representation of Cambering Fixture . .	140
76	Contour Mismatch Test Setup . . . . .	140
77	Torquing Sequence . . . . .	141
78	Windshield Installation Preload Test, Induced Stress vs Camber . . . . .	142
79	Assembly Test Setup . . . . .	144
80	Assembly Tensile Test, 1/8" Neoprene Gasket, 0.190" Dia Holes, 30 in.-lb Torque, Glass/Acrylic Specimen . . . . .	146
81	Assembly Tensile Test, 1/8" Neoprene Gasket, 0.190" Dia Holes, 30 in.-lb Torque, All-Glass Laminated Specimens. . . . .	147

LIST OF ILLUSTRATIONS (Continued)

<u>Figure</u>		<u>Page</u>
82	Uneven Torquing of Bolts . . . . .	148
83	Assembly Thermal Tests, 1/8" Neoprene Gasket, 0.190" Dia Holes, 30 in.-lb Torque, Glass/Acrylic Specimen . . . . .	149
84	Assembly Thermal Tests, 1/8" Neoprene Gasket, 0.190" Dia Holes, 30 in.-lb Torque, All-Glass Laminated Specimen . . . . .	150
85	Assembly Tensile Tests, 1/8" Neoprene Gasket, 0.310" Dia Holes, 30 in.-lb Torque, Glass/Acrylic Specimen . . . . .	151
86	Assembly Tensile Tests, 1/8" Neoprene Gasket, 0.310" Dia Holes, 30 in.-lb Torque, All-Glass Laminates . . . . .	152
87	Assembly Tensile Tests, EC-1675 Wet Sealant, 0.310" Dia Holes, 30 in.-lb Torque, Glass/Acrylic Specimen . . . . .	153
88	Assembly Tensile Test, EC-1675 Wet Sealant, 0.310" Dia Holes, 30 in.-lb Torque, All-Glass Laminates . . . . .	154
89	Assembly Tensile Test, EC-1675 Wet Sealant, 0.310" Dia Holes, 10 in.-lb Torque, Glass/Acrylic Specimen . . . . .	155
90	Assembly Tensile Test, EC-1675 Wet Sealant, 0.310" Dia Holes, 10 in.-lb Torque, All-Glass Laminates . . . . .	156
91	Thermally Tempered Glass (16,000 psi) Fracture Pattern . . . . .	159
92	Thermally Tempered Glass (20,000 psi) Fracture Pattern . . . . .	159
93	Chemically Tempered Glass (40,000 psi) Fracture Pattern - 250 Particles/ft <sup>2</sup> . . . . .	160
94	Chemically Tempered Glass (50,000 psi) Fracture Pattern - 30,000 Particles/ft <sup>2</sup> . . . . .	160
95	Fracture Pattern From Pressure Test . . . . .	161

LIST OF ILLUSTRATIONS (Continued)

<u>Figure</u>		<u>Page</u>
96	Particle Density, 250 Per Square Foot . . . . .	162
97	Particle Density, 1600 Per Square Foot . . . . .	162
98	Horizontal Cracks, Particle Density, 4300 Per Square Foot . . . . .	163
99	Vertical Cracks, Particle Density, 5200 Per Square Foot . . . . .	163
100	Particle Density, 18,000 Per Square Foot . . . . .	164
101	Particle Density, 30,000 Per Square Foot . . . . .	164
102	Typical Target Card . . . . .	165
103	Effect of Crack Density on Visual Response Time.	167
104	Lateral Crack Pattern vs Angle of Incidence (Effects on Residual Visibility) . . . . .	167
105	Viewer for Rating Haze Levels . . . . .	169
106	Plot of Unsatisfactory Pilot Ratings vs Haze . .	171
107	Army Pilot Haze Ratings . . . . .	172
108	Test Grid Used to Measure Distortion . . . . .	182
109	CH-53 Windshield Delamination . . . . .	183
110	External View of CH53 Delamination . . . . .	184
111	AH-1 Cobra, Overall View . . . . .	185
112	AH-1. Left Side Window . . . . .	185
113	AH-1 Front Windshield, Bulls' Eye Distortion . .	186
114	AH-1 Windshield Scratches . . . . .	186
115	UH-1 Windshield Wiper Scratches From Vibration .	187
116	UH-1, Front Door Window, Wave Distortion . . . .	188
117	UH-1, Crew Door Window Abrasion . . . . .	188

LIST OF ILLUSTRATIONS (Continued)

<u>Figure</u>		<u>Page</u>
118	UH-1, Overall View . . . . .	189
119	OH-58, Overall View . . . . .	190
120	OH-58, Bottom Front Window, Edge Distortion . .	190
121	OH-58, Stone Strike, Grid Distortion . . . . .	191
122	OH-58, Stone Strike, External View . . . . .	191
123	CH-47, Windshield Delamination . . . . .	192
124	CH-47, Center Windshield Distortions . . . . .	193
125	CH-47, Center Windshield Scratches . . . . .	193
126	CH-47, Windshield Deletion Line . . . . .	194
127	CH-47, Overall View . . . . .	194
128	TH-55, Overall View . . . . .	195
129	TH-55, Front Windshield Distortions . . . . .	196
130	TH-55, Repaired Cracks . . . . .	196
131	TH-55, Grid Distortion From Repaired Cracks . .	197
132	OH-6, Bottom Window Distortion . . . . .	198
133	OH-6, Overall View . . . . .	198
134	OH-6, Side Window Obstructions, Plastic Stiffeners . . . . .	199
135	Patch Method of Repair . . . . .	200
136	Pressure Box and Pump . . . . .	204
137	Methods of Attaching Test Specimens . . . . .	204
138	Mann Barrel and Mount . . . . .	205
139	Velocity Measurement Equipment . . . . .	205
140	Multiple Ballistic Impacts . . . . .	207

LIST OF ILLUSTRATIONS (Continued)

<u>Figure</u>		<u>Page</u>
141	Screening Test Fixture . . . . .	207
142	Damaged Ballistic Test Specimen . . . . .	209
143	Ballistic Impact on Damaged Specimen . . . . .	209
144	Soft Rubber Patch Maintains Vacuum for Fail Safe Test . . . . .	211
145	Ballistic Penetration of Polycarbonate . . . . .	213
146	Ballistic Penetration of Stretched Acrylic . . . . .	214
147	Ballistic Penetration of 0.080 inch Cast Acrylic . . . . .	214
148	Ballistic Penetration of 0.187 inch Cast Acrylic . . . . .	215
149	Ballistic Penetration of All-Glass Laminate . . . . .	215
150	All-Glass Laminate After Ballistic Impact . . . . .	216
151	Penetration of Glass-Acrylic Laminate . . . . .	216
152	Glass-Acrylic Laminate After Ballistic Impact . . . . .	217
153	Fail-Safe Test of Glass-Acrylic Laminate at 1 psi . . . . .	217
154	Typical Witness Sheet Penetration for Polycarbonate . . . . .	220
155	Typical Witness Sheet Penetration Pattern for Stretched Acrylic . . . . .	220
156	Typical Witness Sheet Penetration Pattern for Cast Acrylic . . . . .	221
157	Typical Witness Sheet Penetration Pattern for Glass/Acrylic Laminate . . . . .	221
158	Typical Witness Sheet for All-Glass Laminate . . . . .	222
159	Typical Witness Sheet Penetration Pattern for All-Glass Laminate . . . . .	222
160	Typical Witness Sheet Penetration Pattern for Clamped All-Glass Laminate . . . . .	223

LIST OF ILLUSTRATIONS (Continued)

<u>Figure</u>		<u>Page</u>
161	Typical Spall Fragments From All-Glass Laminate.	225
162	Typical Spall Fragments From Glass/Acrylic Laminate . . . . .	229
163	Typical Spall Fragments From Acrylic Specimen .	229
164	Wounding Model, Skin Laceration By Glass Fragments	230
165	Spall Data Compared to Wounding Model . . . . .	232
166	Dart Impact Test Setup . . . . .	235
167	Clamped Attaching Arrangement . . . . .	235
168	Bolted Attaching Arrangement . . . . .	236
169	Impact Dart . . . . .	236
170	0.080-Inch Stretched Acrylic Specimen, Low-Temperature Impact Test . . . . .	246
171	0.080-Inch Stretched Acrylic Specimen, High-Temperature Impact Test . . . . .	246
172	Glass/Glass Laminate, Ambient-Temperature Impact Test . . . . .	247
173	Glass/Acrylic Laminate, Ambient-Temperature Impact Test . . . . .	247
174	Glass/Acrylic Laminate, Low-Temperature Impact Test . . . . .	248
175	Glass/Acrylic Laminate Broken in Environmental Chamber at Low Temperature . . . . .	248
176	Close-Up of Glass/Acrylic Laminate Impact Area .	249
177	Close-Up of Glass/Glass Laminate Impact Area . .	249
178	Glass/Glass Laminate, High-Temperature Impact Test . . . . .	251
179	Glass/Acrylic Laminate, High-Temperature Impact Test . . . . .	251

LIST OF ILLUSTRATIONS (Continued)

<u>Figure</u>		<u>Page</u>
180	0.125-Inch Cast Acrylic Specimen, Ambient-Temperature Impact . . . . .	.252
181	Typical Moderate Climate, Annual Diurnal Temperature/Humidity Variation . . . . .	.256
182	Typical Extreme Cold Climate, Annual Temperature/Humidity Variation . . . . .	.256
183	Typical Hot/Dry Climate, Annual Diurnal Temperature/Humidity Variation . . . . .	.257
184	Typical Hot/Wet Climate, Annual Diurnal Temperature/Humidity Variation . . . . .	.257
185	Aerodynamic Pressure Ground-Air-Ground Cycle, UTTAS Helicopter . . . . .	.259
186	Windshield Vibration vs Aircraft Velocity, 1.0 g Level Flight . . . . .	.261
187	Windshield Test Specimens . . . . .	.264
188	Hot and Cold Spot Locations . . . . .	.265
189	Assembly of Windshield, Canopy Structure, and Reinforcing Ring . . . . .	.268
190	Schematic View of Basic Testing Facilities . . . . .	.273
191	View of Edge Loading Attachment Showing 8-Point Load Input and Load Cell . . . . .	.275
192	View of Mechanism for Applying Load to Edge Load System . . . . .	.276
193	Schematic View of Frame Support and Mass Balancing System . . . . .	.277
194	Windshield Installation and Pressure Box . . . . .	.279
195	View of "Bungee" Loops to Restrain Floating Canopy Structure in Neutral Attitude When Pressurized . . . . .	.280
196	Location of Instrumentation . . . . .	.281

LIST OF ILLUSTRATIONS (Continued)

<u>Figure</u>		<u>Page</u>
197	Failure of Glass/Glass (-101) Windshield, Serial No. 7-10-75-4, During Case 21 . . . . .	285
198	Failure of Glass/Acrylic (-102) Windshield, Serial No. 002, During Installation . . . . .	286
199	Strain Gauge Data, Glass/Glass Windshield (-101), Thermal Shock . . . . .	291
200	Time to Cool-Down, Glass/Glass Windshield (-101), Cold Shock . . . . .	292
201	Failure of Polyester/Acrylic (-103) Windshield During Low-Temperature Test Spectrum . . . . .	301
202	Failure of Polyester/Acrylic (-103) Windshield During Low-Temperature Test Spectrum Also Showing Nib Seal Separation . . . . .	302
203	Overall View of Interlayer Bubbling on Polyester/Acrylic (-103) Windshield After Prolonged Humidity Exposure . . . . .	304
204	Close Range View of Interlayer Bubbling on Polyester/Acrylic (-103) Windshield After Prolonged Humidity Exposure . . . . .	305
205	"Dished" Shape of Polyester/Acrylic (-103) Windshield After Prolonged Humidity Exposure . . . . .	306
206	Delamination of Acrylic Edge on Polyester/Acrylic Windshield (-103) . . . . .	306
A-1	Apparatus for Dry Rubbing Abrasion Test . . . . .	314
A-2	Gardner Hazemeter . . . . .	314
A-3	Apparatus for Falling Sand Test . . . . .	315
A-4	Windshield Wiper Test Apparatus . . . . .	316
A-5	Windshield Wiper Locating Mask . . . . .	317
A-6	Wet Rubbing Abrasion Test Setup . . . . .	318
A-7	Digital Readout Hazemeter and Wet Rubbing Abrader . . . . .	319

LIST OF ILLUSTRATIONS (Continued)

<u>Figure</u>		<u>Page</u>
B-1	Temperature Induced Apparent Strain on Stretched Acrylic . . . . .	322
B-2	Temperature Induced Apparent Strain on Polyester . . . . .	323

LIST OF TABLES

<u>Table</u>		<u>Page</u>
1	Materials For Abrasion Tests . . . . .	28
2	Summary of Abrasion Test Results . . . . .	30
3	Results of Dry Rubbing Abrasion Tests . . . . .	31
4	Results of Falling Sand Test . . . . .	34
5	Results of Windshield Wiper Tests . . . . .	36
6	Number of Revolutions Which Produced 30% Haze.	39
7	Material Combinations Used in Structural Adhesion Tests . . . . .	45
8	Structural Adhesion Test Matrix . . . . .	45
9	Results of Bond Tensile Tests . . . . .	50
10	Results of Shear Tests . . . . .	55
11	Results of Cleavage Tests . . . . .	59
12	Strain Gauge Test Results, Polyester-PVB-Stretched Acrylic . . . . .	78
13	Strain Gauge Test Results, Glass-PVB-Stretched Acrylic . . . . .	79
14	Strain Gauge Test Results, Glass-ETP-Polycarbonate . . . . .	80
15	Strain Gauge Test Results, Glass-PVB-Stretched Acrylic (No Coating) . . . . .	81
16	Summary of Flexure Test Results . . . . .	83
17	Section Properties of Side Posts and Sills . .	94
18	Maximum Displacements for Flat Windshields . .	105
19	Stresses and Edge Forces in Windshields, .3 psi Pressure . . . . .	110
20	Edge Forces in Windshields, 1 psi Pressure on Center Windshield . . . . .	116
21	YUH-60A Linear and Angular Accelerations For Two Design Flight Load Conditions . . . . .	118

LIST OF TABLES (Continued)

<u>Table</u>		<u>Page</u>
22	Comparison of Loads in Windshield Support Structure, Vertical Bending Condition . . . . .	119
23	Comparison of Linear Static and Differential Stiffness Solutions, Vertical Bending Condition . . . . .	121
24	Edge Forces in Windshields, Vertical Bending Condition . . . . .	125
25	Deflections and Stresses for Three Loading Conditions . . . . .	126
26	Edge Attachment, Thermal Expansion and Installation Preload Tests . . . . .	129
27	Assembly Test Conditions . . . . .	143
28	Face Ply Materials Used in Residual Visibility Study . . . . .	158
29	Pilot Ratings of Residual Visibility . . . . .	168
30	Scale for Rating Haze Specimens . . . . .	170
31	Light Transmission Measurements for Helicopter Overhead Windows . . . . .	173
32	Pilot Exposure to Aircraft Evaluated in Questionnaire . . . . .	174
33	Material Descriptions for Ballistic Tests . . . . .	203
34	Results of Preliminary Screening Test . . . . .	206
35	Test Conditions for Ballistic Tests . . . . .	210
36	Visibility Data From Ballistic Tests . . . . .	212
37	Dispersion of Penetrations in Witness Sheet . . . . .	219
38	Foam Penetration Data . . . . .	224
39	Total Weight of Spall Fragments . . . . .	226
40	General Description of Spall Fragments . . . . .	227

LIST OF TABLES (Continued)

<u>Table</u>		<u>Page</u>
41	Velocity Necessary to Penetrate Various Combinations of Witness Material, Fragment Mass = 0.05 Gram . . . . .	232
42	Material Description for Low Energy Impact Tests . . . . .	237
43	Test Conditions for Impact Tests . . . . .	238
44	Specimen Appearance After Ambient Temperature Tests . . . . .	239
45	Specimen Appearance After High-Temperature Tests . . . . .	240
46	Specimen Appearance After Low-Temperature Tests . . . . .	241
47	Spall Data, Ambient-Temperature Tests . . . . .	242
48	Spall Data, High-Temperature Tests . . . . .	243
49	Spall Data, Low-Temperature Tests . . . . .	244
50	Summary of Temperature and Relative Humidity, Diurnal Extremes . . . . .	255
51	Cold Climate Temperature Distribution . . . . .	258
52	Hot Climate Temperature Distribution . . . . .	258
53	Flight Load Spectrum for a UTTAS Helicopter . . . . .	260
54	Windshield Vibration Sensitivity to Aircraft Load Factor . . . . .	261
55	Typical Utility Helicopter Loading Spectrum . . . . .	262
56	Part and Serial Numbers of Test Specimens . . . . .	265
57	Windshield Temperature Uniformity Measurements . . . . .	266
58	Loading Parameter Matrix for the Glass/Glass (-101) Windshield . . . . .	270
59	Loading Parameter Matrix for the Glass/Acrylic (-102) Windshield . . . . .	271

LIST OF TABLES (Continued)

<u>Table</u>		<u>Page</u>
60	Loading Parameter Matrix for the Polyester/ Acrylic (-103) Windshield . . . . .	271
61	Summary of Maximum Recorded Stresses . . . . .	288
62	Modulus of Elasticity of Facing Materials . . . . .	289
63	Strain Gauge Data, Glass/Glass Windshield (-101) Aerodynamic Pressure . . . . .	293
64	High-Temperature Endurance Test Spectrum . . . . .	297
65	Low-Temperature Endurance Test Spectrum . . . . .	298
66	Deflection Measurements (Center Relative to Edge) Taken During Low-Temperature Test Spectrum on Specimen Serial Number 007 . . . . .	300

## INTRODUCTION

Helicopter transparencies have a relatively poor service record and represent an exceptionally high percentage of airframe maintenance costs.

The Army, recognizing this deficiency, funded two parallel studies conducted by PPG Industries, Inc., and Goodyear Aerospace Corporation to document the scope of the problem and to recommend action in the form of design, test and acceptance criteria. Results of these studies, published in USAAMRDL Technical Reports TR 73-19<sup>(1)</sup> and TR 73-65,<sup>(2)</sup> showed that windshields were a major source of airframe problems - particularly heated windshields. Some heated windshields had a mean time between failures (MTBF) as low as 200 to 300 hours. Furthermore, many scratches, pits, scores and overall optically degraded transparencies were "lived with" in the field. Thus, the reported time between removals was artificially higher than warranted. Some of these deficiencies persisted well after the helicopter was put into service. These studies also pointed out that no specifications or design guidelines addressing helicopter transparent enclosures as a subsystem exist. Further, for a given type or class of helicopter, there was no generally accepted method for ranking the relative importance of transparency characteristics leading to an effective trade-off of the many conflicting requirements. The necessity for a major effort to develop design, test and acceptance criteria for helicopter transparent enclosures was evident.

The Eustis Directorate, USAAMRDL, awarded a contract in June of 1974 to Sikorsky Aircraft, which was intended to establish validated design, acceptance and test criteria based upon additional research and extensive laboratory and analytical studies. Emphasis was placed on structural substantiation methods and the airframe transparency interface. The effort was accomplished in three major tasks:

- . Establishment of Preliminary Criteria
- . Verification of Criteria by Analysis and Test
- . Preparation of a Design Handbook

---

(1) James, H. C., et al, Goodyear Aerospace Corp., "Design, Test and Acceptance Criteria for Army Helicopter Transparent Enclosures," USAAMRDL-TR-73-19, U. S. Army Air Mobility Research and Development Laboratory, Fort Eustis, Virginia, May 1973, AD 767242.

(2) Cook, L. M., et al, PPG Industries, "Development of Design, Test and Acceptance Criteria for Army Helicopter Transparent Enclosures," USAAMRDL-TR-73-65, U. S. Army Air Mobility Research and Development Laboratory, Fort Eustis, Virginia, September 1973, AD 772936.

Preliminary criteria were established by consolidating the design, acceptance and test criteria from References (1) and (2) into a single document. Subsequent efforts were then directed toward resolving discrepancies and making additions, deletions and changes. The finalized criteria are included in a comprehensive Design Handbook and a General Specification for Helicopter Transparent Enclosures, (3) prepared in conjunction with this report. A system for ranking criteria was also developed for inclusion in the Design Handbook.

---

(3) Kay, B. F., Sikorsky Aircraft Div., "Helicopter Transparent Enclosures," Volume I, Design Handbook, and Volume II, General Specification, USARTL-TR-78-25A&B, Applied Technology Laboratory, US Army Research and Technology Laboratories (AVRADCOM), Ft. Eustis, Va., November 1978.

## ABRASION TESTS

Existing field service has demonstrated that the most prevalent problem experienced with Army helicopter windshields is abrasion resulting in loss of transparency. Thus, the ability of helicopter transparencies to withstand abrasion, with minimal loss of optical quality, is of fundamental interest. Abrasion may be caused by windshield wiper action, impingement of sand or dust particles, and improper cleaning procedures. Figure 1 is an example of the type of abrasive damage caused by windshield wipers.



Figure 1. Windshield Wiper Abrasion Damage.

Laboratory simulation of these conditions is required as part of component qualification so that service performance can be reasonably predicted prior to introduction to service. The series of tests described herein were conducted with this purpose in mind.

The five abrasion tests performed were:

1. Dry Rubbing Abrasion Test
2. Falling Sand Test
3. Windshield Wiper Test
4. Wet Rubbing Abrasion Test
5. Blowing Sand and Dust Test

The tests were performed by Swedlow, Inc., Garden Grove, California, and Gentex Corporation, Carbondale, Pennsylvania, with specific materials as shown in Table 1. Using identical materials, selected abrasion tests were also performed by the Army Materials and Mechanics Research Center (AMMRC), Watertown, Massachusetts, to evaluate repeatability of the test methods.

It should be noted that the intent of these abrasion tests was only to develop means to predict the performance of transparent materials when exposed to abrasive environments, and not to select materials for that purpose. Accordingly, complete qualification testing was not implemented for the hard-coats. Prior to production commitments for any hard-coated plastics, it is recommended that thorough qualification testing be performed. This would include, in addition to the tests described herein, rigorous environmental testing.

The most pronounced effect of abrasion on transparent materials is to increase the surface haze. Haze is generally defined in terms of the percentage of light scattered and therefore lost in passage through the material. To provide a frame of reference, a material with 30% haze would be considered translucent rather than transparent.

Periodic haze measurements were taken at intervals corresponding approximately to each 5% increase in haze during each test until a level of 30% was reached to determine relative tolerance of transparency materials to different types of abrasion.

#### Material

Five specimens of each of seven generic materials were tested to evaluate their comparative performance. The generic materials were:

- Acrylic
- Hard-coated acrylic
- Hard-coated acrylic (artificially weathered)
- Polycarbonate
- Hard-coated polycarbonate
- Hard-coated polycarbonate (artificially weathered)
- Glass

Two different hard coatings were used in these tests, Dupont Abcite and Swedlow SS-6590. In addition, each coating was also tested after artificial weathering that consisted of 250 hours exposure to 100% relative humidity at 160°F. Similar test conditions have shown that typical hard-coats may degrade significantly with respect to adhesion and abrasion resistance after this type of environmental exposure.

TABLE 1. MATERIALS FOR ABRASION TESTS.

TEST CODE	MATERIAL/SPECIFICATION	TEST LABORATORY	TESTS*				
			1	2	3	4	5
A	0.120" soda-lime glass, commercially designated as double-strength window glazing.	Swedlow, Inc.	X	X	X		
B	0.250" biaxially-stretched S-350 material, MIL-P-25690, Swedlow, Inc.	Swedlow, Inc. AMMRC	X	X	X	X	X
C	0.250" Swedlow hard-coated acrylic, SS-6590, a proprietary abrasion resistant coating formulated by Swedlow, Inc.	Swedlow, Inc. AMMRC	X	X	X	X	X
D	0.250" Swedlow hard-coated acrylic material after artificial aging consisting of 250 hours exposure to 100% relative humidity and 160°F temperature environment.	Swedlow, Inc.	X	X	X		
E	0.180" extruded polycarbonate material, MIL-P-33310.	Swedlow, Inc. AMMRC	X	X	X	X	X
F	0.180" Swedlow hard-coated polycarbonate, SS-6590, a proprietary abrasion resistant coating formulated by Swedlow, Inc.	Swedlow, Inc. AMMRC	X	X	X	X	X
G	0.180" hard-coated polycarbonate material after Swedlow, Inc. artificial aging consisting of 250 hours exposure to 100% relative humidity and 160°F temperature environment.	Swedlow, Inc.	X	X	X		
H	0.250" glass (commercial grade) 6 in. x 6 in.	Gentex Corp				X	X
J	0.125" acrylic, MIL-P-8184 6 in. x 6 in.	Gentex Corp				X	X
K	0.125" acrylic with 5 microns of abcite**	Gentex Corp				X	X
L	0.060" polycarbonate, MIL-P-83310, 6 in. x 6 in.	Gentex Corp				X	X
M	0.060" polycarbonate with 5 microns of abcite 6 in. x 6 in.	Gentex Corp				X	X

\*Tests: #1 Dry Rubbing Abrasion Test, #2 Falling Sand Test, #3 Windshield Wiper Test, #4 Wet Rubbing Abrasion Test, #5 Blowing Sand and Dust Test

\*\*A proprietary hardcoat, Trademark of E. I. DuPont de Nemours and Company

## ABRASION TEST METHODS

The following abrasion tests, described in detail in Appendix A, were performed.

Dry rubbing abrasion test: This type of test was performed to evaluate the rubbing abrasion resistance of the different materials to simulated dry wiping or cleaning of dirty transparencies.

Falling sand test: This type of test was performed to evaluate the effect of impingement by falling abrasive particles representative of wind-blown sand and dust.

Windshield wiper test: As the name implies, this type of test was performed to simulate the effect of windshield wiper operation on dirty windshields.

Wet rubbing abrasion test: This type of test was performed to simulate the effects of wiping dirty, wet windshields, wherein the dirt contains abrasive particles.

Blowing sand and dust test: This type of test was performed to simulate the effects of high velocity sand and dust particles impinging on a helicopter transparency characteristic of recirculating downwash of a helicopter operating in a dusty environment.

## ABRASION TEST RESULTS

The tests showed that the tolerance to abrasion of uncoated acrylic or polycarbonate material is very poor as measured by the falling sand, rubbing abrasion, and windshield wiper tests that were conducted. The application of hard coats to acrylic and polycarbonate glazing material imparted a significant increase in the tolerance to abrasion as indicated by the test results. The effect of artificial aging, 250 hours exposure to 100% humidity at 160°F environment was found to severely degrade adhesion of the SS-6590 hard coat to the polycarbonate substrate. Marginal adhesion of unaged SS-6590 hard coat to polycarbonate was also noted during the windshield wiper test. Glass material was found to be vastly superior to the hard-coated materials during the rubbing abrasion and windshield wiper tests, but not as good as the hard-coated materials when subjected to the falling sand impingement tests.

A summary of the results of all four abrasion tests is presented in Table 2, followed by a detailed discussion of the individual test results.

TABLE 2. SUMMARY OF ABRASION TEST RESULTS

Material	Test			
	Falling* Sand	Dry** Rubbing Abrasion	Slurry** Rubbing Abrasion (30% haze)	Wind-** shield Wiper
Polycarbonate	110 gm	15-27%	60	50-30%
Polycarbonate (Hard coated)	5500	600-11%	750	50,000-25%
Aged Polycarbonate (Hard coated)	7500	500-10%	---	500-30%
Acrylic	190	24-30%	70	350-30%
Acrylic (Hard coated)	6500	1500-14%	200	25,000-25%
Aged Acrylic (Hard coated)	7500	1500-11%	---	25,000-25%
Glass	1300	1500-1.5%	3600	50,000-5%

- \* Grams of sand required to produce 30% haze.  
 \*\* Average number of test cycles or revolutions to produce the percent of haze listed.

### Dry Rubbing Abrasion Test Results (Test 1)

Five specimens of each material were tested to evaluate the consistency of the results. The scatter in test measurements was approximately 3% haze throughout the test. This variation is expressed as haze percentage points. For example, a nominal 30% value would have experimental limits of 27% to 33% haze.

Test results are summarized in Table 3 and Figure 2. The dashed lines shown in Figure 2 are the average results from the AMMRC tests. Figure 3 shows a polycarbonate test specimen where the lighter rectangular shaped region is the abraded area.

Some of the differences in the dry rubbing abrasion test results obtained from Swedlow and AMMRC can be attributed to changes in abrasives medium. The AMMRC test used a larger 60 grit abrasive as compared to the 400 grit abrasive used in the Swedlow tests.

The materials tested can be placed in three groups in accordance with their relative resistance to abrasion. The lowest group contains uncoated polycarbonate and acrylic, which showed almost immediate degradation from rubbing abrasion. The next group contained the coated materials which exhibited a definite improvement in abrasion resistance over those which were not coated. Glass was found to be virtually unaffected by the test, and is in a class by itself.

TABLE 3. RESULTS OF DRY RUBBING ABRASION TESTS

Material	Number of Test Cycles	Average Haze (%)	Min	Max
Polycarbonate	15	27	23	32
Polycarbonate (Hard-coated)	600	11	9	14
Aged Polycarbonate (Hard-coated)	500	10**	9	13
Acrylic	24	30*	29	30
Acrylic (Hard-coated)	1500	14	11	16
Aged Acrylic (Hard-coated)	1500	11	9	12
Soda Lime Glass	1500	1.5	1	2

\* Average of 3 specimens

\*\* One specimen developed coating adhesion breakdown, and was not included in average AMMRC test results not included in this table.

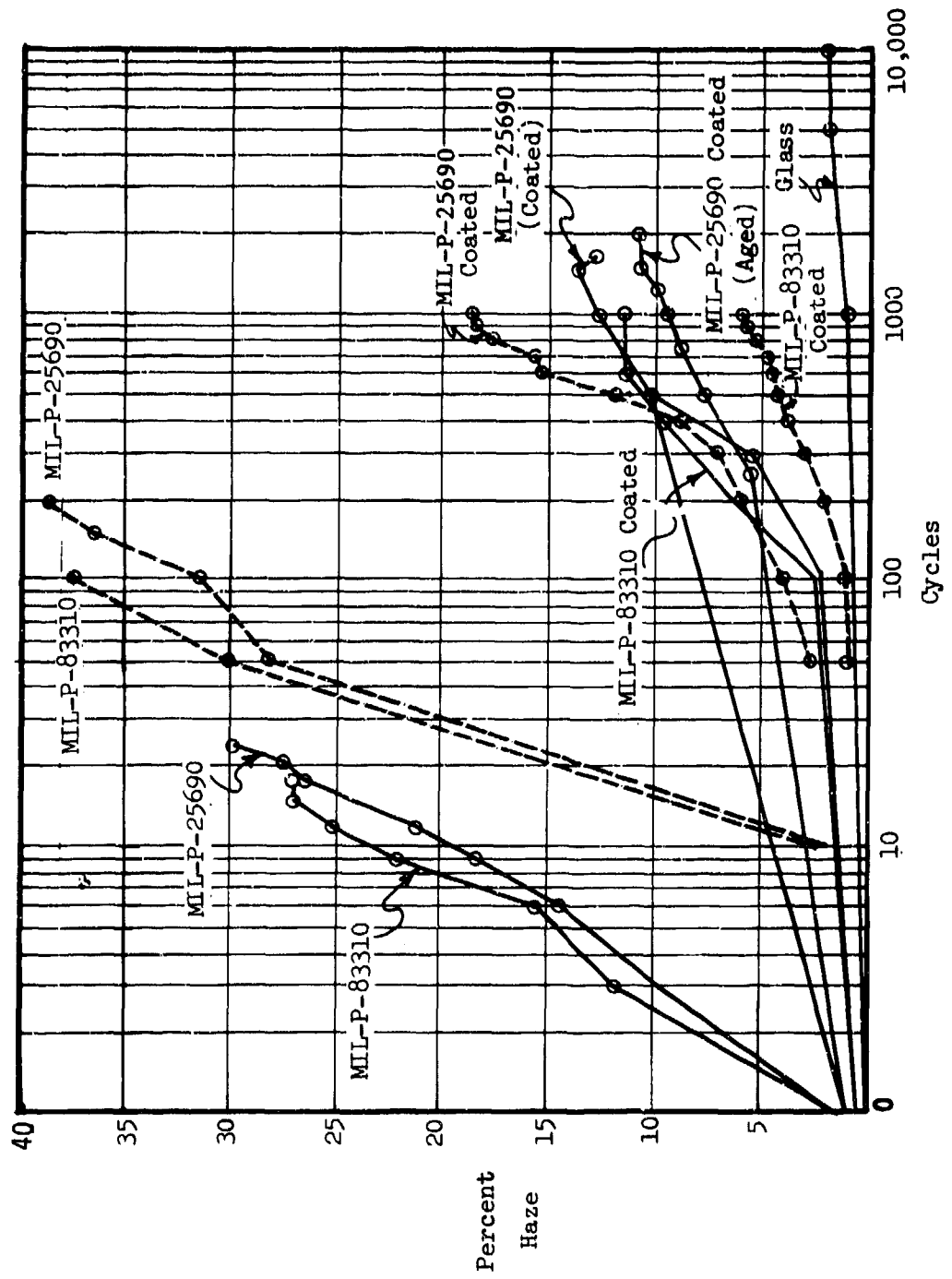


Figure 2. Dry Rubbing Abrasion Test Results.

Artificially aged (250 hours exposure to 100% humidity at 160°F) hard-coated acrylic was more abrasion resistant than the unaged hard-coated acrylic. However, the effect of artificial aging was found to degrade adhesion of the hard coat to the polycarbonate substrate. Massive adhesive failure between the hard coat and the polycarbonate resulted in very high haze values after 1200 cycles.

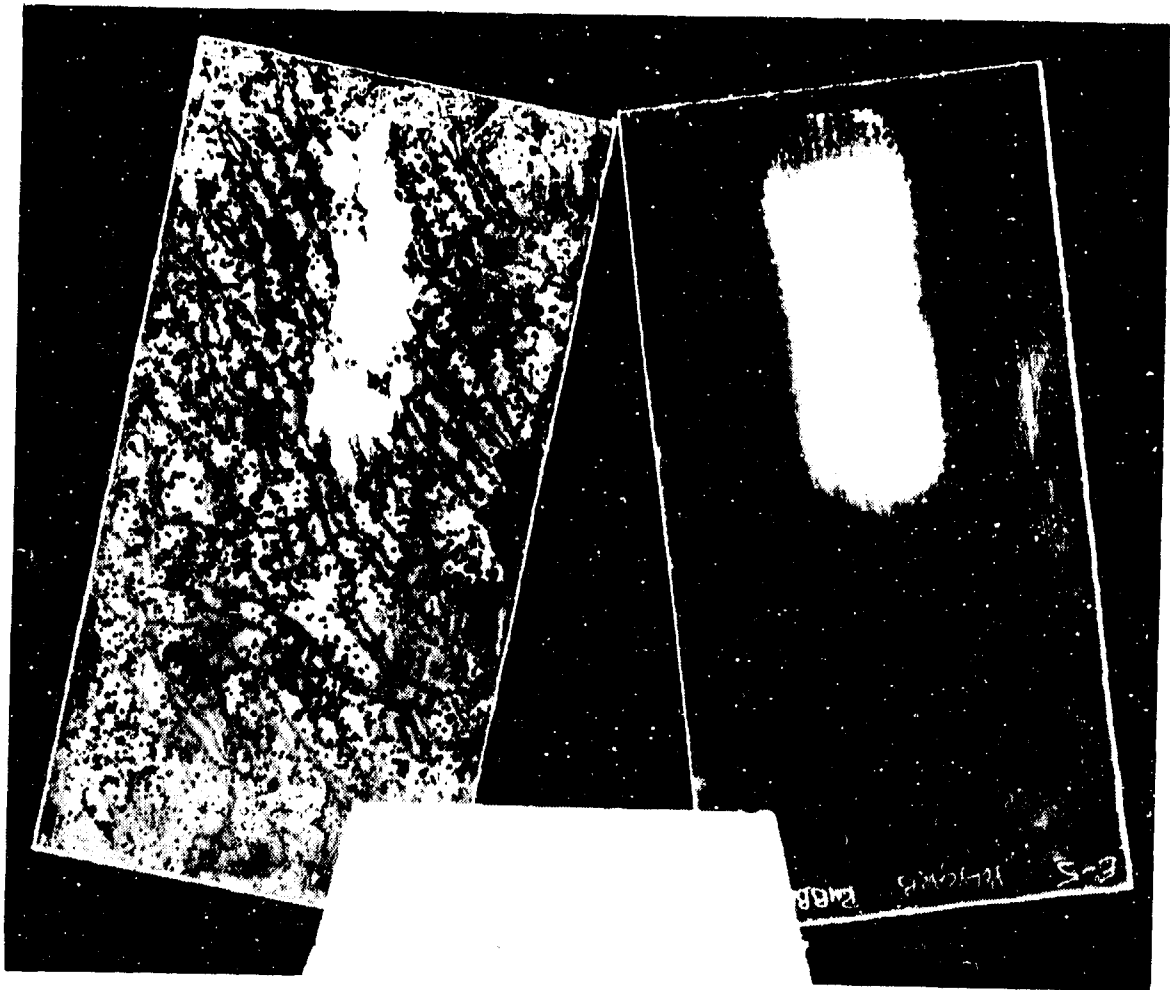


Figure 3. Specimen From Dry Rubbing Abrasion Test.

### Falling Sand Test Results (Test 2)

Test results are summarized in Table 4 and Figure 4 as a function of the amount of sand required to produce a given level of haze.

Hard-coated materials were found to be superior to the uncoated materials and glass in abrasion resistance. The effect of artificial aging did not cause any degradation of the hard coats during the test.

TABLE 4. RESULTS OF FALLING SAND TEST

Material	Quantity of Sand*	Haze**	
	(grams) Average	Min	Max
Polycarbonate	110	26	30
Polycarbonate (Hard coated)	5500	31	32
Aged Polycarbonate (Hard coated)	7500	30	32
Acrylic	190	28	31
Acrylic (Hard coated)	6500	30	31
Aged Acrylic (Hard coated)	7500	29	32
Glass	1300	28	31

\* Quantity of sand required to produce nominal 30% haze level.

\*\* Range of haze readings for number of grams noted.

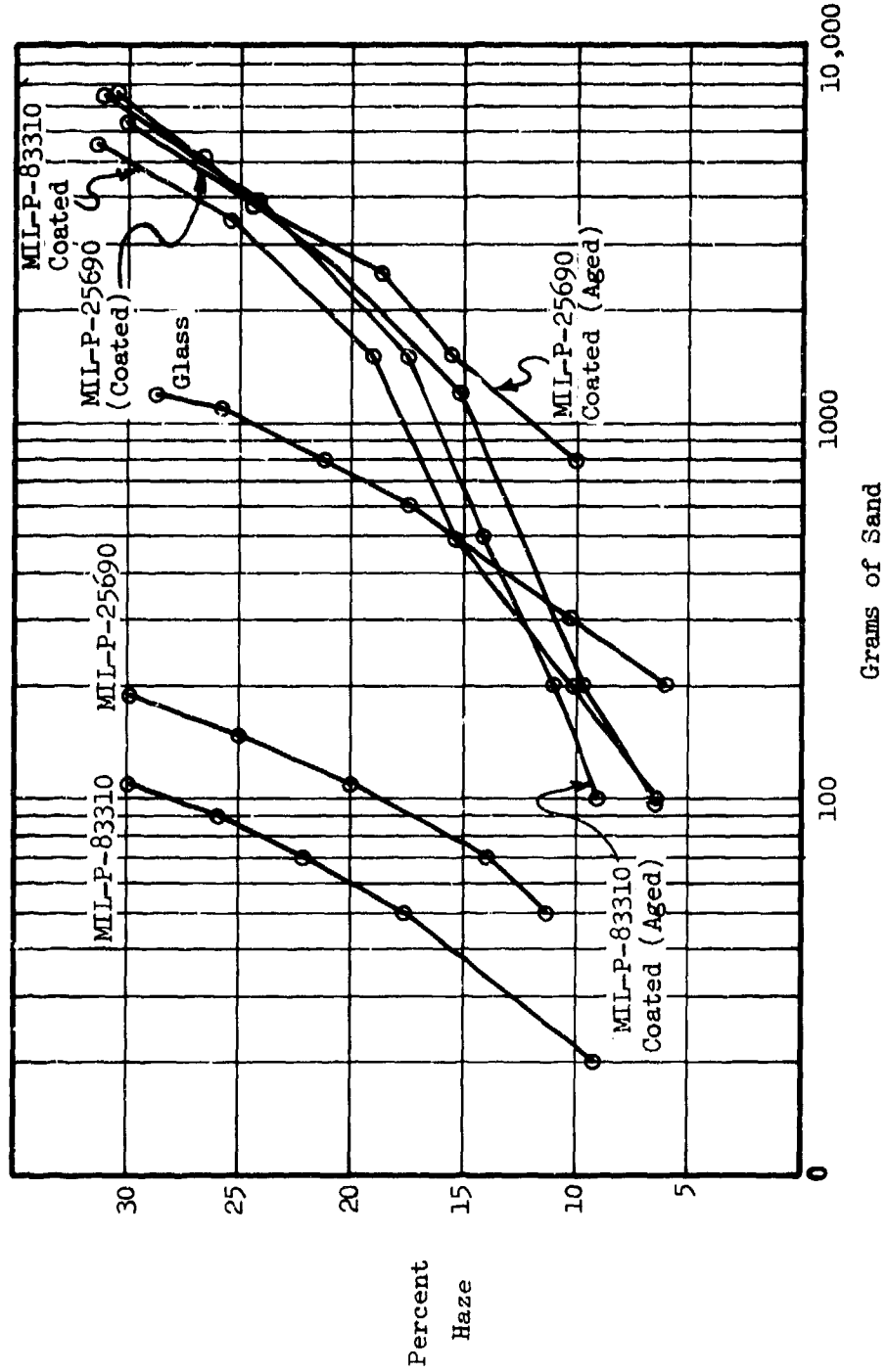


Figure 4. Falling Sand Test Results.

### Windshield Wiper Test Results (Test 3)

Considerable variation in measurements occurred during the windshield wiper test. Fluctuations in readings of over 10% haze were noted for measurements taken from the same specimen, and also from specimen to specimen. (Note, this scatter is expressed as haze percentage points.)

Some of the factors causing the variability are inherent to the type of abrasion, and others are related to the characteristics of the wiper blade, the flatness of the test specimen, and the wetting action of the abrasive slurry on different substrates.

Test results are summarized in Table 5 and Figure 5. The dashed lines shown in Figure 5 are the average results obtained from the AMMRC tests.

Some of the differences in the windshield wiper test results can be attributed to wiper blade angles. In the Swedlow test, the wiper blades were parallel to the wiper arm, while the AMMRC wiper blade was offset approximately 45° to the arm.

TABLE 5. RESULTS OF WINDSHIELD WIPER TESTS

Material	Haze (%)	Min Max		No. of Test Cycles
	Average			
Polycarbonate	30	11	38	50
Polycarbonate (Hard coated)	25	11	51	50,000
Aged Polycarbonate (Hard coated)	30	26	38	500
Stretched Acrylic	30	16	34	350
Stretched Acrylic (Hard coated)	25	16	37	25,000
Aged Acrylic (Hard coated)	25	14	33	25,000
Glass	5	1	16	50,000

AMMRC tests not included in this table.

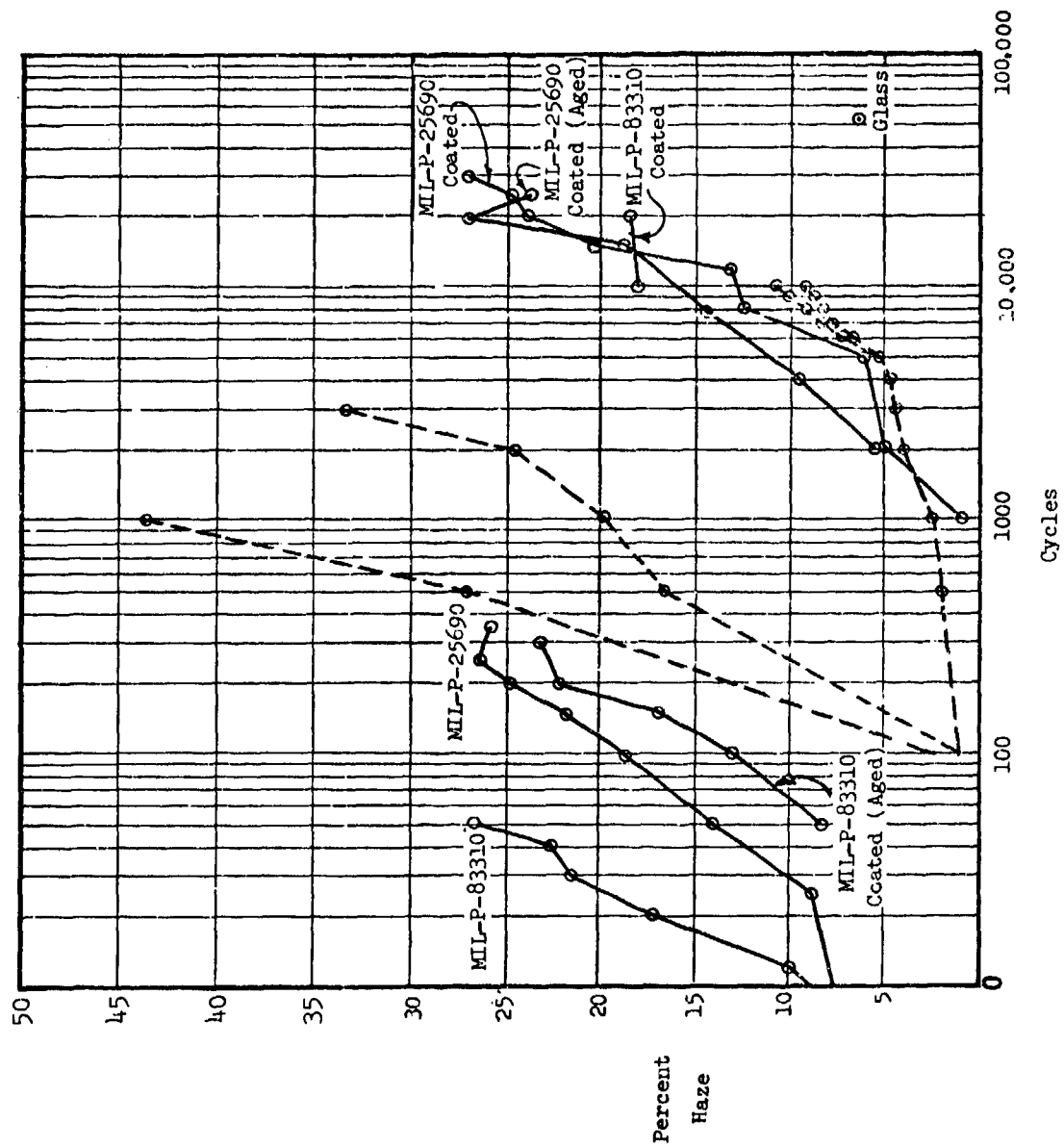


Figure 5. Windshield Wiper Test Results.

Uncoated polycarbonate and stretched acrylic suffered immediate degradation from the wiper actions. The tests showed no significant difference in abrasion resistance between aged or unaged hard-coated acrylic specimens. However, the aging process had an apparent deleterious effect on the hard-coated polycarbonate, as evidenced by marginal adhesion of the coating to the substrate on some specimens. The marginal adhesion of the hard coat adversely affected the testing of two out of five specimens at 10,000 cycles, whereas the other three exhibited high readings only after 50,000 cycles.

Glass was found to be virtually unaffected by the test.

An abraded specimen is shown in Figure 6. The circles on the specimen indicate the locations where haze measurements were taken.

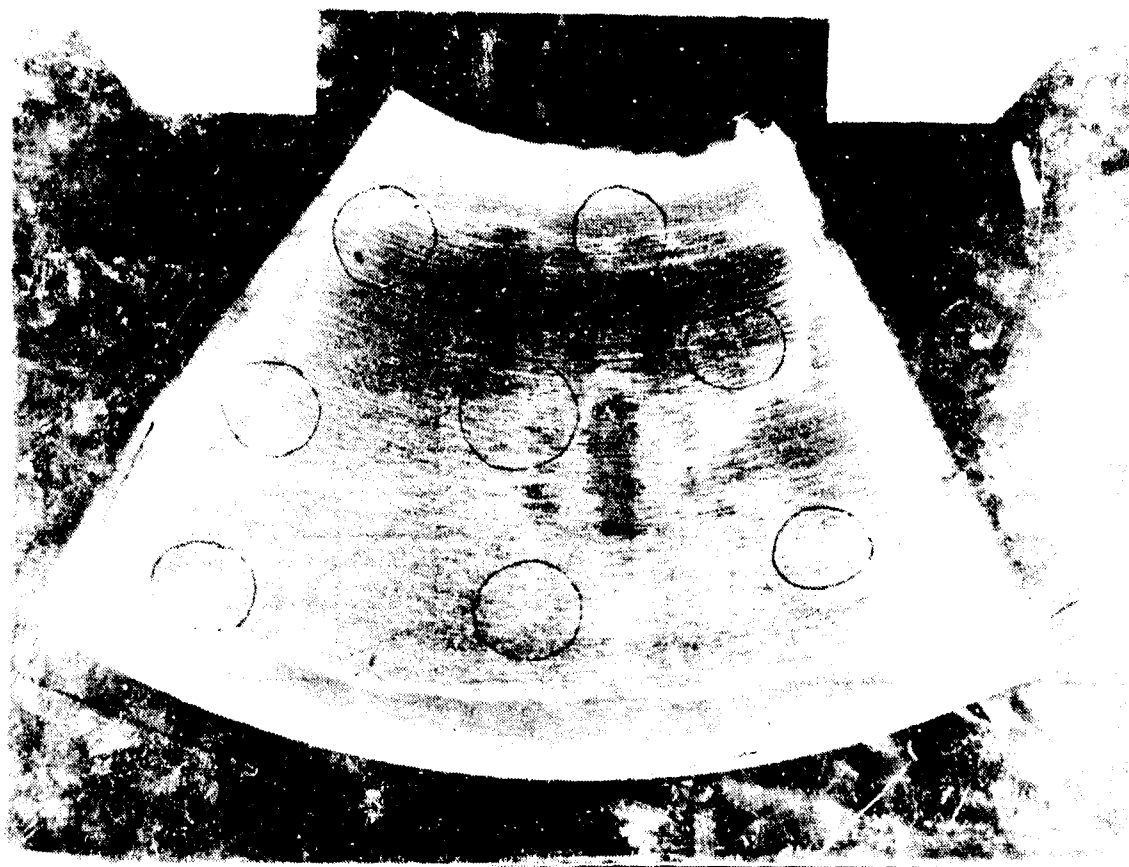


Figure 6. Windshield Wiper Test Abraded Sample.

#### Wet Abrasion Test Results (Test 4)

In this test, inconsistency of abrasion caused deviations greater than 1% haze, and an average deviation of approximately 5% haze. Test results are shown in Table 6 and Figure 7 for each material.

TABLE 6. NUMBER OF REVOLUTIONS WHICH PRODUCED 30% HAZE

Material	No. of Revolutions	Haze* (%)	
		Min	Max
Polycarbonate	60	27	37
Polycarbonate (Hard coat)	750	20	55
Acrylic	70	23	34
Acrylic (Hard coat)	200	11	45
Soda Lime Glass	3600	27	37

\* Range of haze readings for number of revolutions noted.

The relative performance of the coated versus uncoated materials showed that significant benefits were obtained from the hard coats. The hard-coated polycarbonate was found to be superior to the hard-coated acrylic. It is also interesting to note that it was possible to abrade the glass specimen to 30% haze with this test, while the dry rubbing abrasion test could only achieve 2% haze after 10,000 abrasion cycles.

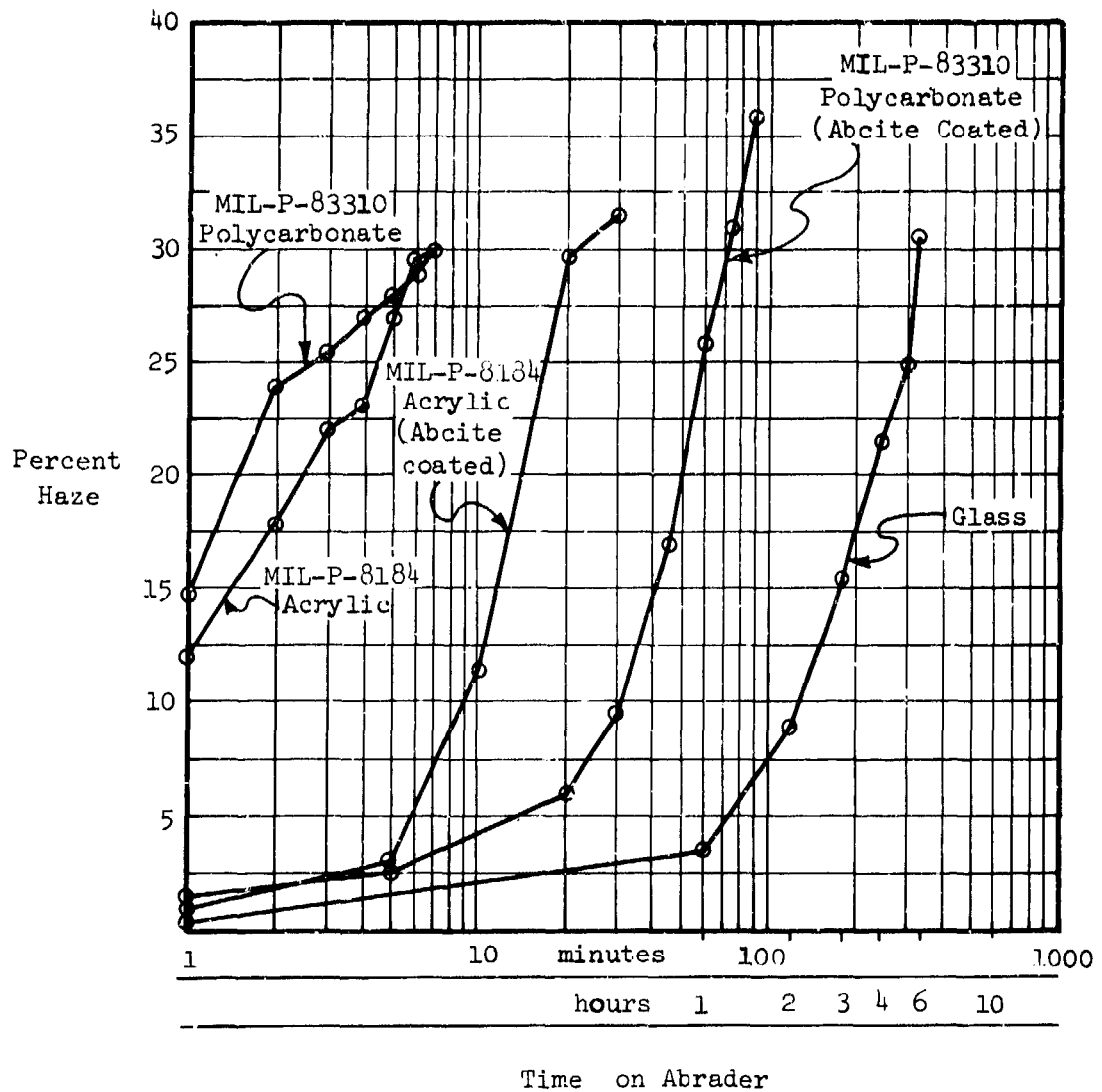


Figure 7. Wet Rubbing Abrasion Test Results.

The characteristic abrasion marks produced by the test are illustrated in Figure 8.



Figure 8. Specimen From Wet Rubbing Abrasion Test.

Blowing Sand and Dust Test Results (Test 5)

After more than 24 hours of exposure, the test was terminated because there was little or no measurable change in haze on any of the specimens.

## CORRELATION OF TEST RESULTS

A realistic correlation between the test methods for rubbing abrasion and windshield wiper abrasion can be made with actual service experience. For example, several cycles of windshield wiper operation on dry or dirty acrylic helicopter windshields will have immediate effect in producing objectionable haze. The windshield wiper test performed duplicated this condition by increasing the original haze level in stretched acrylic by 5% after only 25 cycles of operation. Likewise, the dry rubbing abrasion tests produced an increase in haze of 8% after only 3 cycles and the slurry abrasion test produced 12% haze after 10 cycles on stretched acrylic, which is representative of the damage produced by wiping plastic transparencies with dirty rags.

Correlation of the falling abrasive to field service experience was difficult because this failure mode is rare in comparison to the other forms of abrasion. However, some estimation of the severity of the test can be obtained by calculating the flux of the impinging abrasive particles and comparing it to Army specifications for density of blowing sand which is 0.1 gm/ft<sup>3</sup>. Using this approach, 1 gm of falling abrasive can be roughly equated to 4 minutes exposure to blowing sand at 11 ft/sec or 7.5 mph.

An increase in haze of 10% was measured for the stretched acrylic material after exposure to 50 gm of falling abrasive which might be likened to 3 hours exposure to dense blowing sand. When one considers that sand storms can induce higher impingement velocities, notwithstanding flight through the storm, the potential hazard from impinging sand can be fully appreciated. Note that the kinetic energy of the impinging particles is proportional to the square of their velocities.

It is felt that the reason impingement abrasion damage to helicopter transparencies has not been documented as a serious problem is that there has been only minimal exposure to conducive environments. In addition, the ASTM 673-70 test abrasive, silicon carbide, was used instead of silicon dioxide common sand, although silicon dioxide is a softer material. This possibly increased the amount of abrasion experienced in the test.

## ABRASION TEST CONCLUSIONS

1. The abrasion resistance of uncoated acrylic and polycarbonate was very poor in comparison to the hard-coated materials and glass.
2. Prolonged exposure to heat and high humidity caused a deterioration in adhesive strength of the SS-6590 coated polycarbonate.
3. Glass was vastly superior to the hard-coated materials in the rubbing abrasion tests, and was virtually unaffected by the windshield wiper tests.
4. The Swedlow SS-6590 coated acrylic and polycarbonate materials were superior to glass in resisting impingement abrasion; apparently due to ductility of the coating which minimized spallation.
5. The windshield wiper and rubbing abrasion tests realistically produce failure modes characteristic of field service abrasion damage and the test methods are useful for predicting comparative performance of transparent materials. However, correlation to service life in terms of flight hours or calendar time is not possible due to operational and environmental variables.
6. The MIL-STD-810, Method 510, blowing sand and dust test is unsuitable for evaluating the effects of blowing sand on transparent materials. The fineness of the sand and the agitation created in the test chamber were insufficient to abrade even the soft polycarbonate material.
7. Considerable variations in test results occur during abrasion tests, some of which are inherent to the phenomena, and some of which result from variations in procedure.

## STRUCTURAL ADHESION TESTS

Due to problems with delamination of windshields, it is necessary to perform bond peel, shear and tension tests as part of development and acceptance testing. Therefore, a series of tests was conducted to obtain structural characteristics of laminated transparent coupons and to evaluate standard methods of testing for adhesive properties. Several cross-sectional configurations were tested which represent actual windshield configurations currently in service as well as those planned for the near future and within current state-of-the-art capabilities. The tests conducted and reported herein include bond tension, bond shear, and cleavage strengths as well as flexural characteristics for the selected laminated constructions. Specimens were tested at  $-65^{\circ}\text{F}$ ,  $+70^{\circ}\text{F}$  and  $+125^{\circ}\text{F}$ .

Strains and deflections were measured during the flexural tests and compared to solutions obtained by analytical methods. Separate analyses were performed which considered the interlayer as both coupled and uncoupled.

These tests were performed by Sierracin/Sylmar, Sylmar, California, in accordance with Sikorsky specifications.

### Materials

Test specimens consisted of two basic combinations of materials

- |     |            |     |            |
|-----|------------|-----|------------|
| (a) | Face Ply   | (b) | Face Ply   |
|     | Coating    |     | Interlayer |
|     | Interlayer |     | Face Ply   |
|     | Face Ply   |     |            |

The specific materials used in the specimens are given in Table 7.

TABLE 7. MATERIAL COMBINATIONS USED IN STRUCTURAL ADHESION TESTS

Number	Material Combination	
1	Face Ply --	.062-inch-thick polyester, CR-39 (LP-516a, Class 3)
	Coating --	Standard Sierracote 303 system
	Interlayer--	.075-inch-thick 38 pph DBS (PVB)
	Face Ply --	.150-inch-thick stretched acrylic (MIL-P-25690)
2	Face Ply --	.085-inch-thick Chemcor 0401 glass
	Coating --	Standard Sierracote 303 system
	Interlayer--	.075-inch-thick 38 pph DBS vinyl (PVB)
	Face Ply --	.080-inch-thick stretched acrylic (MIL-P-25690)
3	Face Ply --	.085-inch-thick Chemcor 0401 glass
	Coating --	Standard Sierracote 303 system
	Interlayer--	.075-inch-thick Ethylene Terpolymer (ETP), NOXO78
	Face Ply --	.063-inch-thick polycarbonate 9030-112
4	Face Ply --	.085-inch-thick Chemcor 0401 glass
	Interlayer--	.075-inch-thick 38 pph DBS (PVB)
	Face Ply --	.080-inch-thick stretched acrylic (MIL-P-25690)

Each of the four specimen configurations was subjected to the following test matrix in the quantities indicated (see Table 8). A total of 156 specimens were tested.

TABLE 8. STRUCTURAL ADHESION TEST MATRIX

	No. of Configurations at Each Temperature	No. of Samples of Each Configuration		
		-65°F	Room (70°F)	+125°F
Bond Tensile	4	3	3	3
Bond Shear	4	3	3	3
Bond Cleavage	4	3	3	3
Flexure *	4	4	4	4

\*One specimen at each temperature was instrumented with strain gauges on the upper and lower flexural surfaces; the other three specimens were tested to destruction.

### Test Machine

A BLH Universal Testing Machine, Model PIE12 (Figure 9), was used in all tests. This testing machine was equipped with the necessary drive mechanism for imparting to the crosshead a uniform, controlled velocity with respect to the base. Also, it incorporated a load-indicating mechanism capable of showing the total load carried by the test specimen. This mechanism was essentially free from inertial lag at the specified rate of testing and indicated the load within the specified accuracy of +1.0 percent of the indicated value.

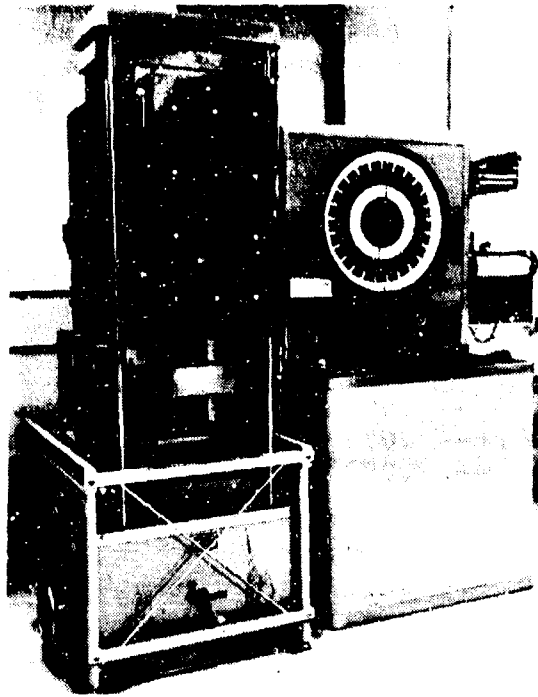


Figure 9. Baldwin Model 3LH PIE-132 Universal Testing Machine.

### Conditioning

The test specimens were conditioned at  $23 \pm 2^{\circ}\text{C}$  ( $73.4^{\circ} \pm 3.6^{\circ}\text{F}$ ) and  $50 \pm 5\%$  relative humidity for a period of 24 hours prior to start of testing. After conditioning, the low-temperature tests were conducted after the temperature had been stabilized at  $-65^{\circ}\text{F} \pm 5^{\circ}\text{F}$ , and the high-temperature tests were conducted after the temperature had stabilized at  $+125^{\circ}\text{F} \pm 5^{\circ}\text{F}$ . Temperatures were monitored using iron/constantan thermocouples and a Doric Model DS-500 indicator.

## BOND TENSILE TEST

This test established the bond tensile strength of laminated coupons. Bond tensile strength is the adhesive or cohesive strength of the bond between the interlayer and outer layer when subjected to a mechanical load in a direction perpendicular to the plane of the bond.

### Apparatus

Metal blocks were made using an aluminum "T" section cut to a 2-inch square. A hole was drilled in the upright section of each "T" block (see Figure 10) to accommodate a metal pin or holding device correlative to the test machine used.

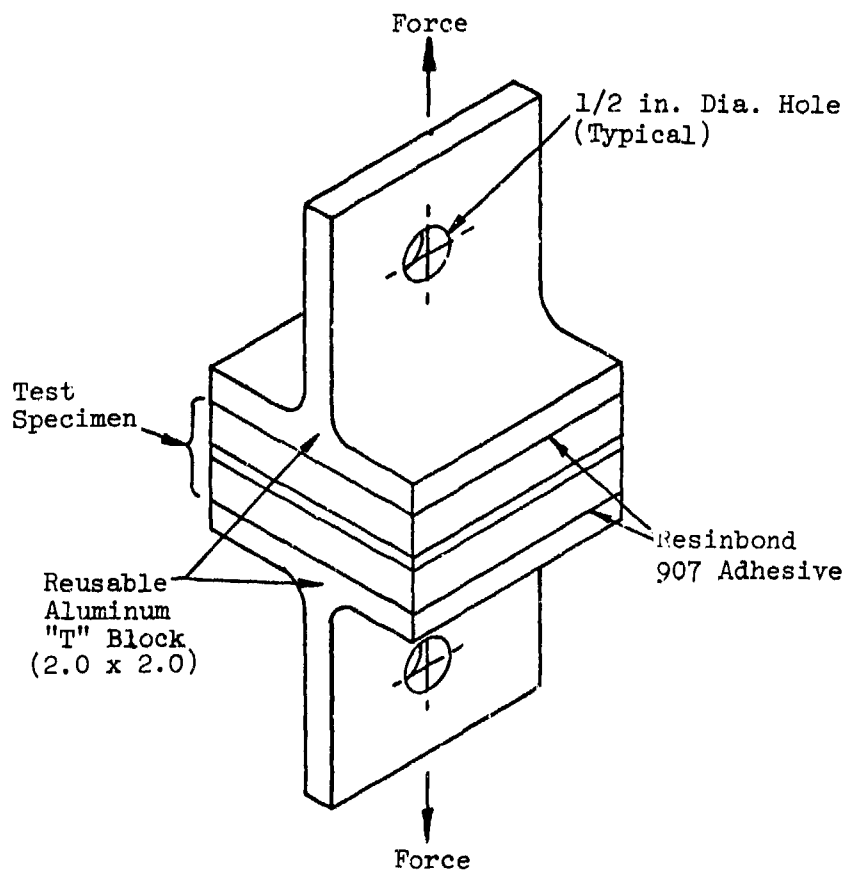


Figure 10. Bond Tensile "T" Blocks.

### Materials

The coupon specimens for this test were fabricated as shown in Figure 11.

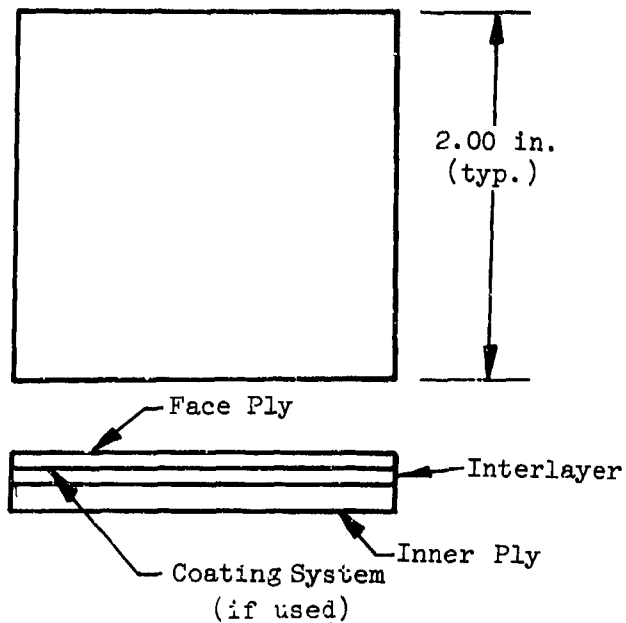


Figure 11. Test Coupon, Tensile Bond.

#### PREPARATION OF TEST ASSEMBLIES

The cross-sectional area of the test specimen was determined in a plane parallel to the surface to within  $\pm 0.01$  in.<sup>2</sup> using Vernier Calipers or similar measuring instruments. The specimens were then assembled to the holding fixture as follows:

Both sides of the specimen and the aluminum metal of the "T" block contact surfaces were roughened by sanding while taking care not to abrade or round the edges and corners of the specimen.

All contact surfaces of the specimens and "T" blocks were cleaned with a soft cloth saturated with isopropyl alcohol. They were untouched afterward. A thin coating of Resinbond Adhesive, Number 907, was applied to both the contact surfaces of the specimen and the blocks with a spatula or similar tool, and all air bubbles were removed from the adhesive. After the specimens were aligned on the blocks, they were clamped in place and allowed to cure for a period of 16 hours.

Procedure (Bond Tensile Test)

1. Three specimens of each configuration were tested at each temperature.
2. The specimens were each placed in the tensile testing machine with self-aligning holders, Figure 12, and loaded to failure at a rate of 0.2 inch/minute.
3. Step 1 was repeated at a temperature of  $-65^{\circ}\text{F} \pm 5^{\circ}\text{F}$ .
4. Step 1 was repeated at a temperature of  $+125^{\circ}\text{F} \pm 5^{\circ}\text{F}$ .

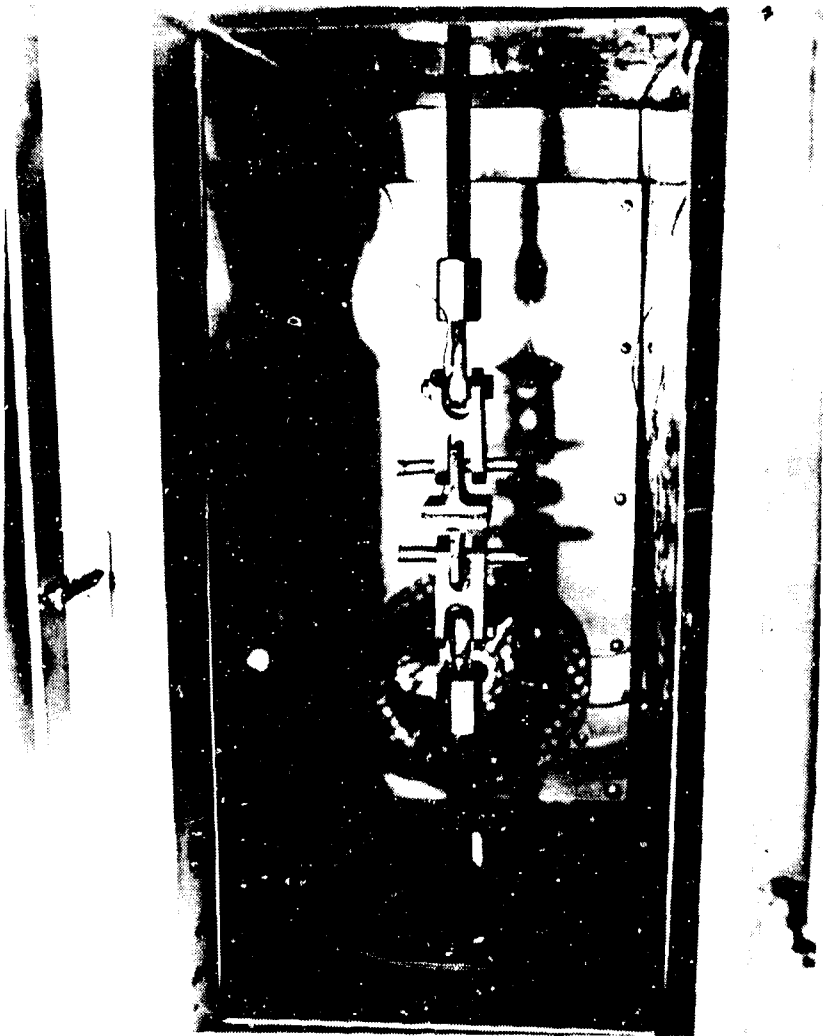


Figure 12. Bond Tensile Test Setup.

## Results

The effect of temperature on polyvinyl butyral was extremely significant. Maximum strength was obtained at  $-65^{\circ}\text{F}$  and minimum strength was obtained at  $+125^{\circ}\text{F}$ . The effect of different substrates was not as significant as temperature, although the presence of a conductive coating tended to reduce strength at room temperature and  $+125^{\circ}\text{F}$ .

The tensile strength of the ethylene terpolymer laminates was relatively constant with respect to temperature.

The results of the bond tensile tests are presented in Table 9.

TABLE 9. RESULTS OF BOND TENSILE TESTS

Material Combination	Average Tensile Strength (psi)		
	$-65^{\circ}\text{F}$	$+72^{\circ}\text{F}$	$+125^{\circ}\text{F}$
Polyester - PVB - Stretched Acrylic with Conductive Coating	870	300	150
Glass - PVB - Stretched Acrylic with Conductive Coating	770	390	150
Glass - PVB - Stretched Acrylic, No Conductive Coating	770	580	240
Glass - ETP - Polycarbonate with Conductive Coating	380	470	480

## BOND SHEAR TEST

This test established the bond shear strength of laminated coupons. Shear strength is the maximum adhesive or cohesive strength of the bond between the interlayer and the outer plies when subjected to mechanical load in the plane of the interlayer.

### Apparatus

The shear test fixture was a sliding type constructed so that it imparted a shearing load on each side of the interlayer directly to the rigid outer plies. A cross section is shown in Figure 13.

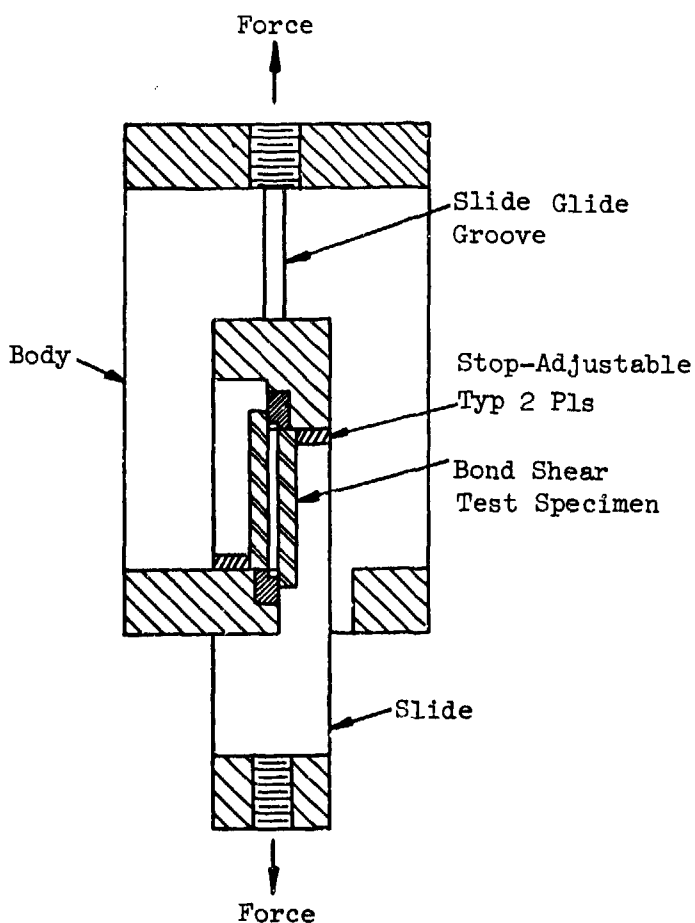


Figure 13. Bond Shear Test Fixture.

## Materials

The coupon specimens for this test were fabricated as shown in Figure 14.

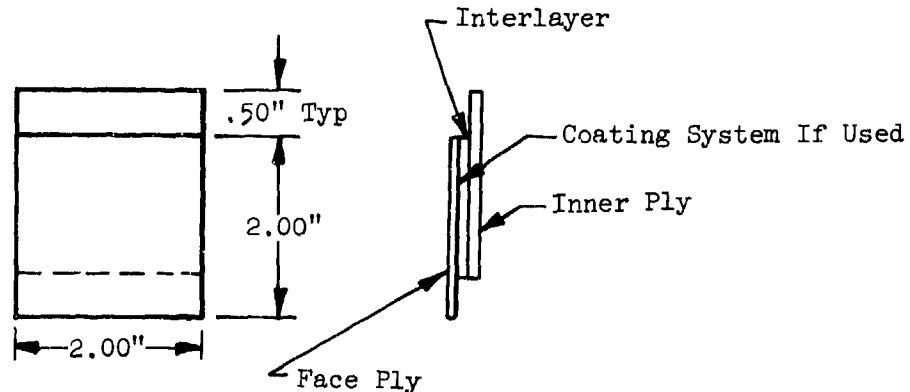


Figure 14. Bond Shear Test Specimen.

## Procedure

1. The length, width, and thickness of the bond area were measured to the nearest 0.001 inch and recorded.
2. The specimen was mounted in the test fixture, Figure 15, by carefully aligning the loaded end of the specimen parallel to the loading bar. A dial indicator, capable of measuring deflections to 0.001 inch, was mounted on the machine to measure crosshead motion.
3. The rate of motion was set at 0.05 inch per minute and the machine was started.
4. The maximum load was applied to the specimen and the deflection of the specimen up to the point of rupture was recorded.
5. The test specimen was removed and examined for evidence of premature failure due to edge chipping or slippage of the specimen in the fixture.
6. The bond strength was calculated by dividing the maximum load by the total bond area.
7. The shear modulus of rigidity was calculated by dividing the shear stress by the shear strain.

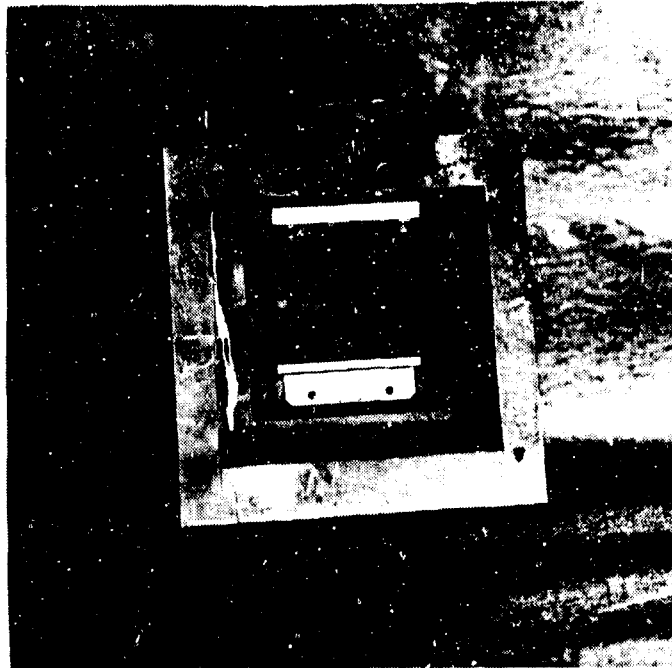


Figure 15. Shear Fixture.

### Results

In all tests, the bond shear strength and modulus of elasticity was substantially reduced at elevated temperatures. The presence of a conductive coating was also shown to reduce the strength of the bond.

The results of the shear tests are presented in Table 10.

It should be noted that the bond shear test results obtained for these small samples include interlayer stress concentrations at the sample edge as shown in Figure 16(a). That is, for small samples such as those tested, the stress concentration region is a much larger portion of the total shear area than it is for full-scale panels. Therefore, the gross shear strength data determined from the small 2-inch-square specimens could be considerably higher.

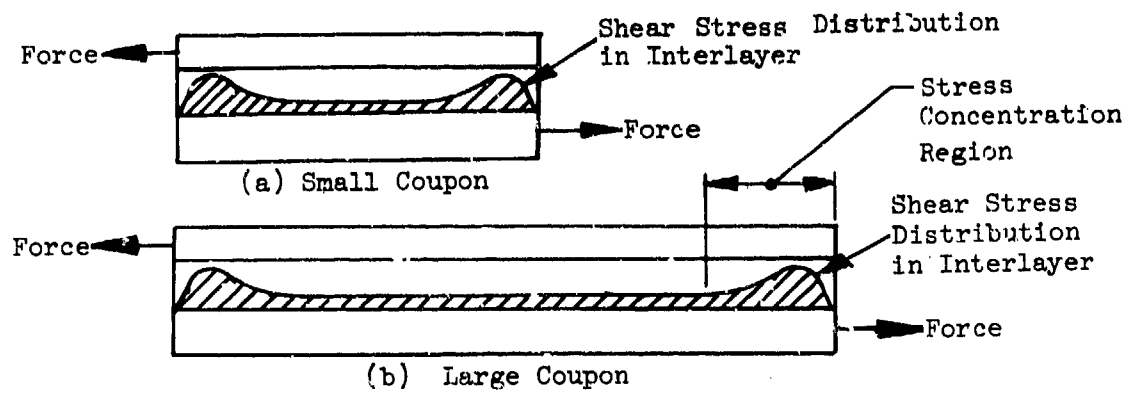


Figure 16. Shear Stress Distribution in Interlayer.

TABLE 10. RESULTS OF SHEAR TESTS

Material Combination	Average Shear Strength (psi)		Average Shear Deflection (in.)		Average Secant Shear Modulus (psi)				
	-65° F	+72° F +125° F	-65° F	+72° F +125° F	-65° F	+72° F +125° F			
Polyester - PVB - Stretched Acrylic with Conductive Coating	643	357	30	.047	.356	.110	1150	260	31
Glass - PVB - Stretched Acrylic with Conductive Coating	517	237	28	.038	.198	.152	1083	196	24
Glass - PVB - Stretched Acrylic, No Conductive Coating	1150	513	27	.066	.126	.151	1580	495	24
Glass - ETP - Polycarbonate with Conductive Coating	217	473	103	.024	.092	.057	705	537	157

### BOND CLEAVAGE TEST

This test established cleavage strength data based on a loading condition similar to that which occurs in designs that contain an unreinforced extended edge attachment.

Bond cleavage strength is the adhesive or cohesive strength of the bond between the interlayer and the facings when subjected to a mechanical load applied to the edge of one face ply in a direction perpendicular and away from the bond. The test measured the load necessary to cause a cleavage failure when the load was applied to an overhanging face ply.

### Apparatus

A test fixture was provided as shown in Figure 17. It was constructed so that one specimen was held rigidly against a stationary metal block while a moveable ram applied a load to the extended edge of the specimen, Figure 18.

### Materials

The coupon specimens for this test were fabricated as shown in Figure 19.

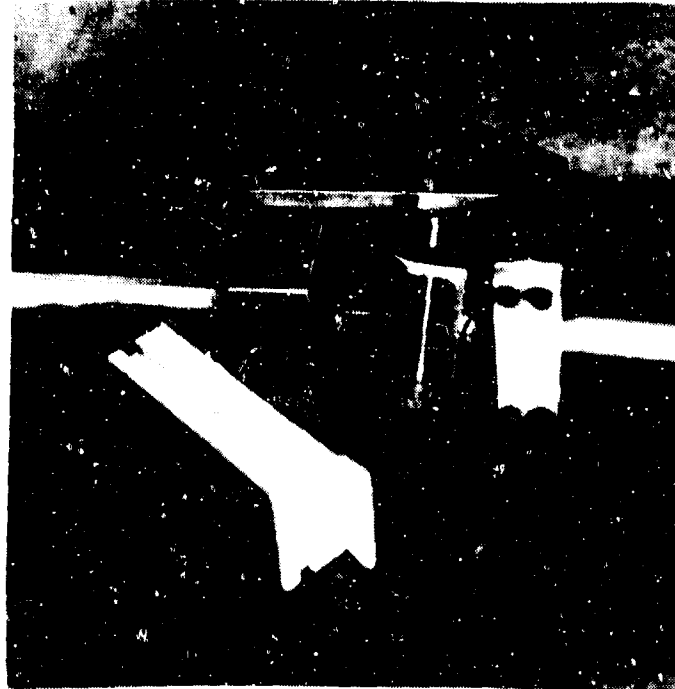


Figure 17. Cleavage Test Fixture With Restrainer to Prevent Loading Pin Deflecting Away From Coupon.

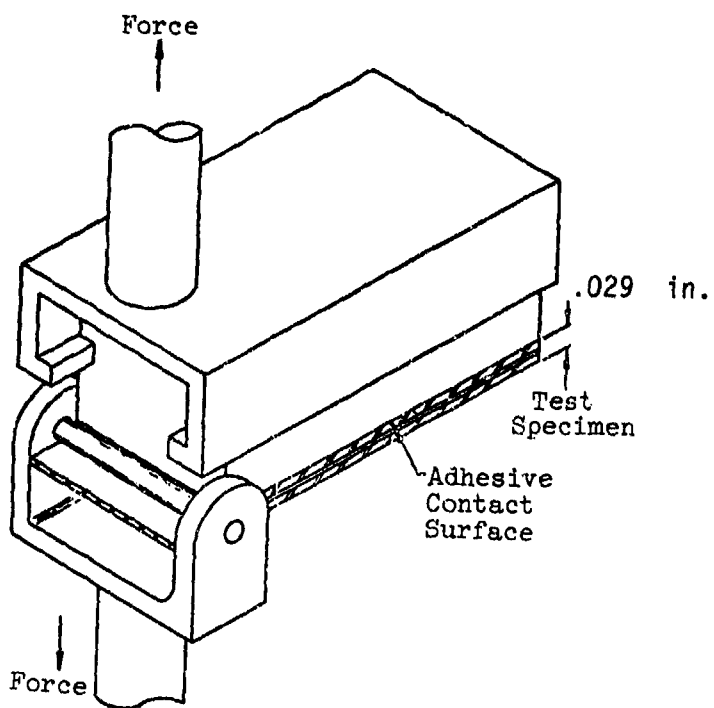


Figure 18. Cleavage Test Fixture.

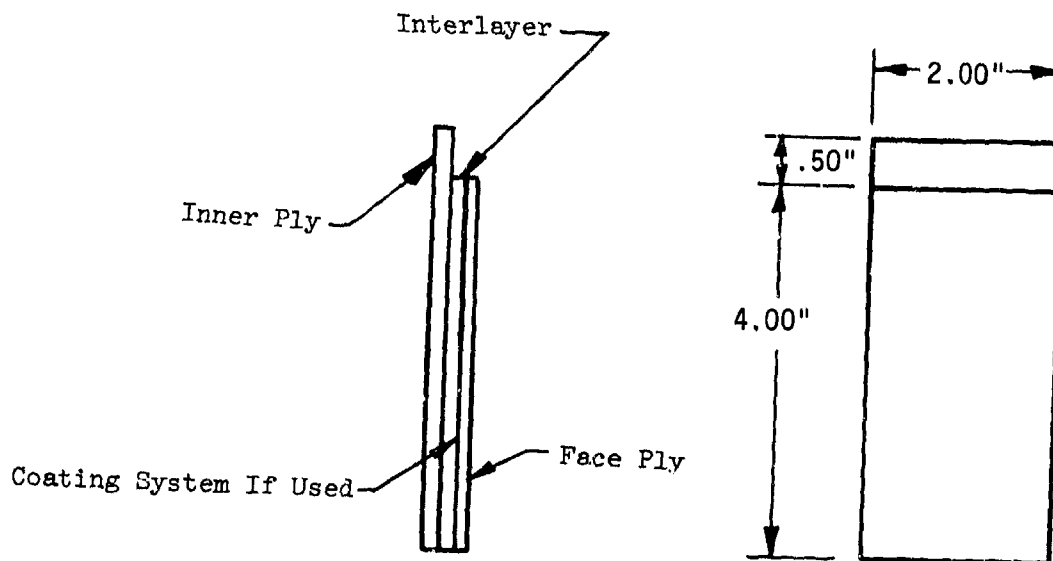


Figure 19. Bond Cleavage Test Specimen.

### Preparation of Test Assemblies

The width of the test specimens and the thickness of the interlayers and extended face plies were all measured to within 0.001 inch. The specimens were then assembled to the holding fixture as follows:

The surface of the shorter facing and the metal block were roughened by sanding. Care was taken not to abrade the edges or to round the corners. The contact surfaces between metal blocks and specimens were cleaned with isopropyl alcohol and thereafter not handled except by mechanical means. Each specimen and block received a thin coating of Resin Bond No. 907 adhesive on faying surfaces. Care was taken to eliminate all air bubbles from the adhesive. After the specimen was aligned on the block, it was held in place by a spring clamp for a minimum of 16 hours while the adhesive cured.

### Procedure (Bond Cleavage Test)

1. The assembly was placed in the test fixture, Figure 20.
2. The testing machine was set at a rate of .05 inch per minute and started.
3. The maximum load carried by the specimen up to the point of rupture was recorded.
4. The test specimen was examined for evidence of premature failure due to edge chipping.
5. Calculations of the bond cleavage strength (lb/in.) were made by dividing the maximum load by the width of the bond.

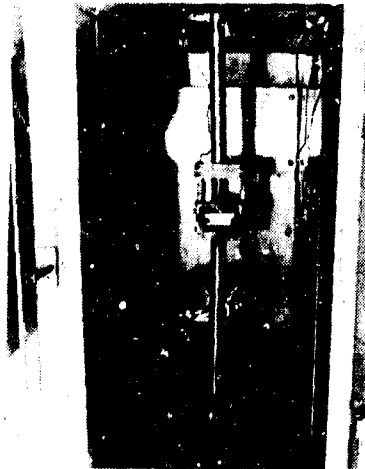


Figure 20. Cleavage Test Setup Shown in the Environmental Chamber on the Baldwin.

6. Steps 1 through 5 were repeated at a temperature of -65°F.
7. Steps 1 through 5 were repeated at a temperature of +125°F.

### Results

Table 11 shows the average cleavage strength for each group of specimens at each of the three test temperatures.

TABLE 11. RESULTS OF CLEAVAGE TESTS

Material Combination	Average Cleavage Strength (lb/in.)		
	-65°F	+72°F	+125°F
Polyester - PVB - Stretched Acrylic with Conductive Coating	33	62	25
Glass - PVB - Stretched Acrylic with Conductive Coating	13	28	14
Glass - PVB - Stretched Acrylic, No Conductive Coating	30	84	35
Glass - ETP - Polycarbonate with Conductive Coating	18	60	47

The low values of cleavage strength obtained in this test indicate that some form of overlapping edge reinforcement is desirable for laminated transparencies to preclude delamination from edge forces.

The polyester/stretched acrylic configuration exhibited substantially higher strength than the glass/stretched acrylic design. This can be attributed in part to differences in base ply thickness (0.150 inch vs 0.080 inch respectively). A stiff inner ply tends to spread the load over a greater area while a thin inner ply concentrates the load as peel forces. However, it should be noted that this was an extremely conservative test since the outer ply was rigidly held to the support fixture. In a typical design, the outer ply is unrestrained and will deflect with the face ply to relieve some of the loading applied to the interlayer.

## FLEXURAL TESTS

This series of tests provided data for the design and analysis of composite transparencies subject to flexural loading. Unique analytical solutions are required to determine deflections and stresses for composite windshields. Composite transparencies, because of their laminated construction, do not resist flexural bending loads as monolithic structures. Instead, the load is distributed to each lamina in proportion to the stiffness,  $EI$ , of each constituent ply. An extreme condition is when the interlayer is very soft relative to the facings. Then the facings carry all the shear and bending loads as two parallel beams with the interlayer behaving as a viscous fluid to space them apart.

Between the extremes of homogeneous beams and laminates containing interlayers of negligible stiffness is the typical composite windshield. The typical composite windshield has an interlayer with sufficient stiffness to provide some coupling between the two face plies, particularly at low temperatures.

Analytical solutions for stress and deflections were determined for composite beam specimens for two cases, coupled and uncoupled. This data was then compared to the results of instrumented tests conducted on similar specimens. Destructive tests were also conducted to determine breaking strength at different temperatures.

### Apparatus

A four-point beam loading setup was provided to load the specimen as shown in Figures 21 and 22. The distance between the lower supports was 8 inches and the distance between the loading bars was 1 inch. All supports were constructed in accordance with the method shown in ASTM D-690.

A Starrett 0 to 1 inch (0.001 inch subdivisions) dial indicator, calibrated to  $\pm 0.001$  inch, was used to measure deflection. A Magnaflux Bridge and Balance Unit, Model GB-100 (Figure 23), with an accuracy of  $\pm 1$  microstrain; a Strain Indicator Model GA-100, accurate to  $\pm 1$  microstrain; and Strain Gauges, Model PA06-250BA-120, accurate to  $\pm 1\%$ , were used to determine strain characteristics during flexural testing.

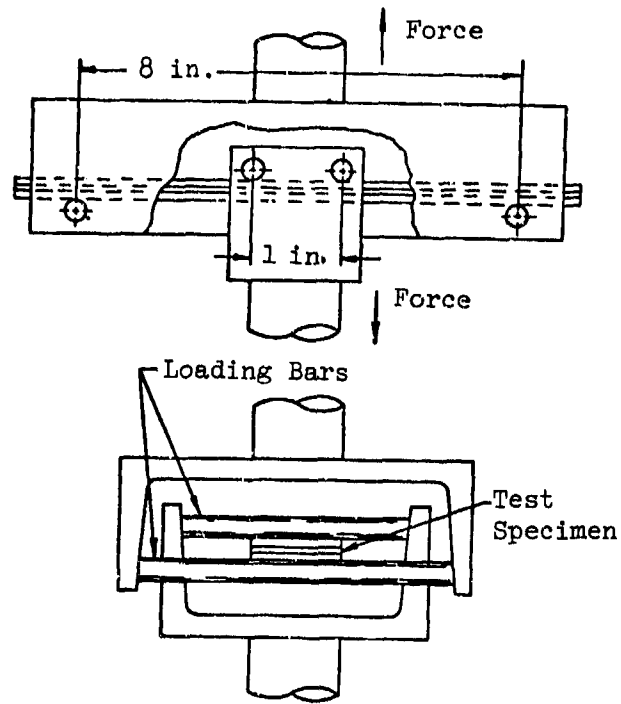


Figure 21. Flexural Test Setup.

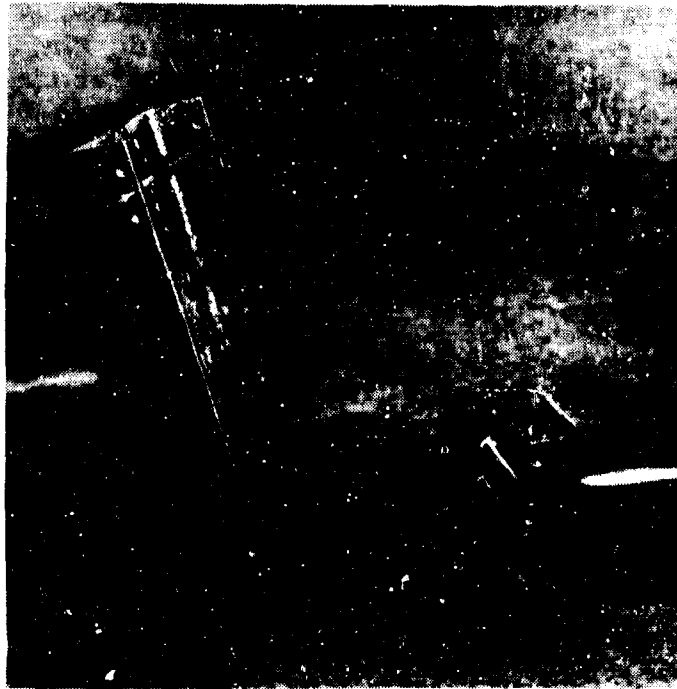


Figure 22. Flexural Test Fixture.

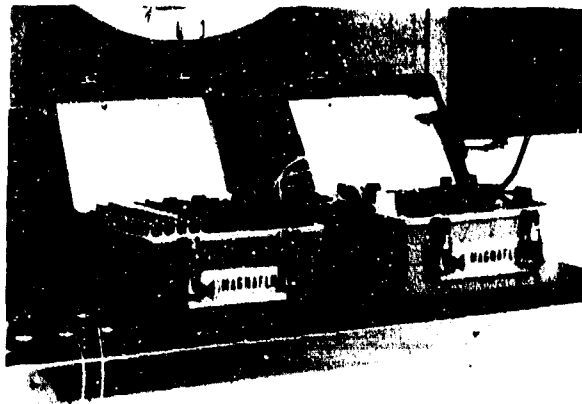


Figure 23. Strain Measuring Equipment.

Strain Gauge Temperature Compensation

To allow for strain gauge thermal compensation, a quarter bridge, three-wire circuit (Figure 24), using the indicator internal dummy, was used; this caused temperature changes to appear equally in adjacent arms of the bridge and resulted in a strain measurement that was unaffected by changes in lead resistance caused by changes in temperature.

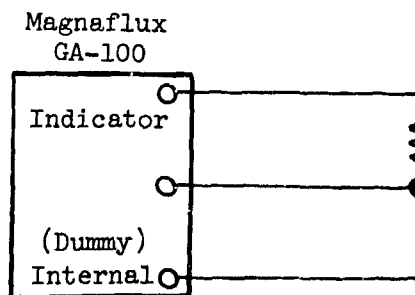


Figure 24. Strain Gauge Thermal Compensation.

Materials

The coupon specimens for this test were fabricated as shown in Figure 25.

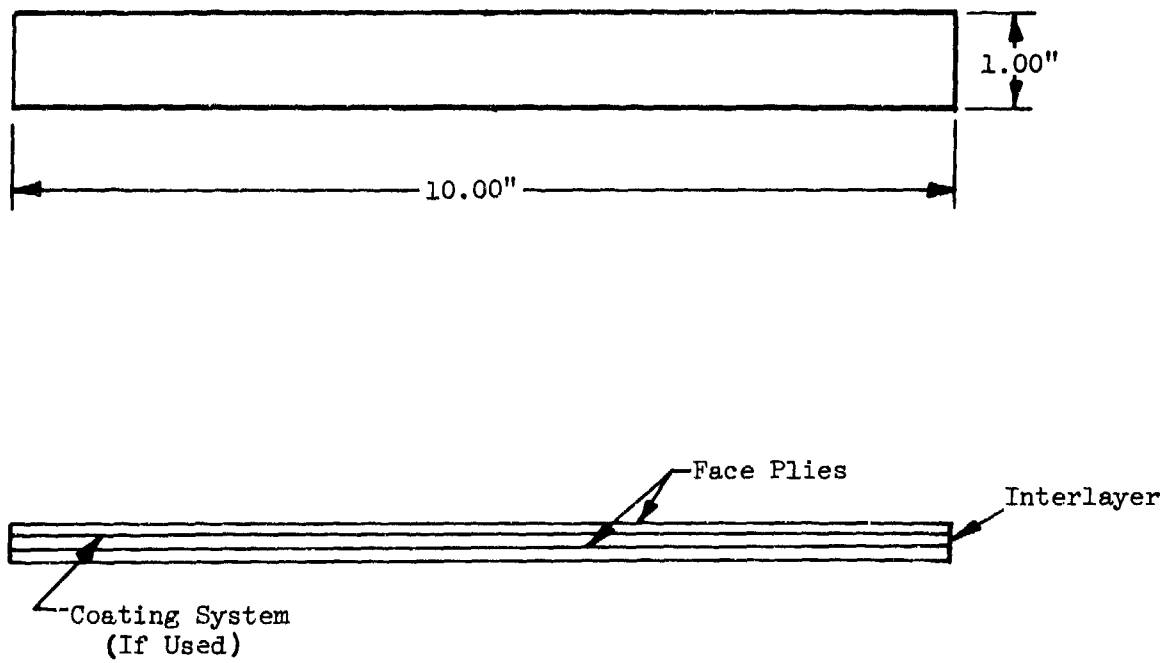


Figure 25. Flexure Test Typical Specimen.

### Procedure

1. The width and individual laminate thicknesses were measured to within  $\pm 0.001$  inch.
2. The testing machine (Figure 26) was started; caution was used not to overload the specimens.
3. The deflection and strain under load was measured at midspan and recorded at increments of 0.025 inch deflection.
4. Steps 2 and 3 were repeated with the temperature at  $+125^{\circ}\text{F}$ .
5. Steps 2 and 3 were repeated with the temperature at  $-65^{\circ}\text{F}$ .
6. With the outer surface of the plastic ply toward the tension side, loading of the specimen was continued until failure. Breaking load and maximum deflection were recorded for each specimen. This test was performed on three specimens of each cross section.
7. Step 6 was repeated with the specimens hot soaked at  $125^{\circ}\text{F}$ .
8. Step 6 was repeated with the specimens cold soaked at  $-65^{\circ}\text{F}$ .



Figure 26. Flexure Test Setup Shown in the Environmental Chamber on the Baldwin.

### Analysis

The analysis was conducted as a two-phased effort calling for:

1. The derivation of analytical solutions to determine deflections and stresses for four types of composite transparency beams subjected to flexural loading.
2. The correlation by test of the derived analytical solutions.

The scope of effort and time for performance of this program was limited and so was the extent to which plausible non-linear relationships based on time-independent and time-dependent theories could be analyzed. It was felt that rigorous applications of such theories to composite windshields would involve complex relationships. In turn, the resulting complicated equations would require accurate nonelastic material properties data such as for creep and relaxation with precise definition of the applied loads and timing involved, a difficult situation at present.

Instead, it was considered that for the present, technical solutions resulting from this program would be based on an empirical approach to the elastic beam theory without consideration of visco-elastic effects. The relationships so developed were based on a constant rate of loading and provide a reasonable representation of these effects without concern for time-dependent phenomena such as creep, relaxation and recovery.

### Analytical Approach

Composite bonded beams frequently encountered in structural practice use engineering materials having well defined elastic properties. The theory of bending of beams is relatively simple, following the classical theory within the elastic range of the constituent materials. Here, such bonded beam plies are considered as fully coupled; that is, each laminate carries its share of the shear and in-plane forces created by the bending loads. In turn, the composite transparencies used in windshield and window applications use materials having both elastic and visco-elastic properties. Here, one set of plies can be considered elastic within the range of deflection and stress of interest with adjacent plies or layers behaving as a viscous material with extremely limited mechanical properties. Such composite beams carry practically all the load in the main plies, with minimum support by the viscous interlayers, and are to be considered as partially uncoupled. A bonded composite beam consisting of parallel spaced plies separated by weak nonfunctional interlayers would be considered as fully uncoupled.

Temperature plays a major role in the analysis since the candidate composite structures consist of a variety of transparent materials, most of which have mechanical properties that vary widely within the range of operating temperatures. As an example, the coupon interlayers tested in this program all varied with temperature to the extent that they provided almost ideal (total) coupling (elastic) at extreme low temperatures to practically no coupling (viscous) at 125°F.

The analytical approach consisted of four elements: (1) the deflection and stress relationships for the four-point beam loading were derived; (2) the characteristics of coupled composite beams of uniform section were developed on the basis of pure bending (here the effort was to develop a means for calculating the position of the neutral axis and the composite beam stiffness,  $EI$ ); (3) the characteristics of "uncoupled" composite beams were defined in terms of the beam test configuration; and (4) the stress relationships for both coupled and uncoupled beams were enumerated. The rationale for these elements is presented in this section of the report.

### Four-Point Beam Loading

The four-point method of beam loading represents a useful test method for determining small strain behavior in beams. This same technique is used to evaluate flexural properties of plastic (ASTM D790-71) and has the advantage of providing a region of the beam undergoing pure bending without shear.

The test fixture used for the tests reported herein had the load points spaced 1 inch apart and thus the stress and deflection equations had to be determined specifically for this test series.

Using the geometry shown in Figure 27, the following relationship was derived:

$$\delta = \frac{10.21 P}{EI} \quad (1)$$

where

- P = total applied load (lb)
- E = modulus of elasticity (psi)
- I = moment of inertia (in.<sup>4</sup>)
- $\delta$  = beam deflection at midspan (in.)

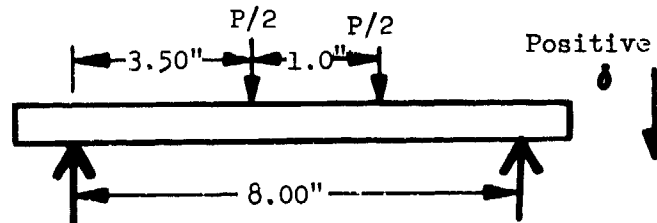


Figure 27. Beam Loading Geometry.

### Beam Stress

For a fully coupled laminated beam, the stress at any point within the beam is given by Equation (2):

$$\sigma_n = \frac{E_n My}{S} \quad (2)$$

where

- $\sigma$  = flexural stress (psi)
- $E$  = modulus of elasticity (psi)
- $M$  = applied moment (in.-lb)
- $y$  = distance from neutral axis to the fiber being strained (in.)
- $n$  = subscript represents the  $n$ th laminate of the beam
- $I$  = moment of inertia (in.<sup>4</sup>)
- $S$  =  $EI$

Based on convention, a negative value of stress represents compressive stress and a positive value represents tensile stress.

### Coupled Beam Flexural Stiffness

The analytical derivation of flexural stiffness ( $EI$ ) of multilayer composite beams can be obtained using either tabular or algebraic techniques. The tabular technique is derived from the parallel axis theorem for moment of inertia.

$$S = EI = \sum E_n I_n + \sum A_n Z_n^2 - \bar{Z} \sum A_n A_n \quad (3)$$

where

- $A_n$  =  $E_n b_n h_n$  (lb-in.<sup>2</sup>)
- $b$  = width of laminate (in.)
- $h$  = thickness of laminate (in.)
- $Z_n$  = distance from base to each element centroid (in.)
- $\bar{Z}$  = distance from the base to the neutral axis of the complete cross section

### Uncoupled Beam Stiffness

The behavior in bending a completely uncoupled composite beam is that of a series of freely stacked plies, the left spring concept. That is, each ply acts independently and slips with respect to its neighbor as it deflects, except that it is assumed to deflect identically as the other plies and

to take up its portion of total load in relation to its stiffness. Thus, the flexural stiffness of the uncoupled beam is merely the sum of the individual stiffnesses:

$$(EI)_g = \sum E_n I_n \quad (4)$$

#### Deflection Test Results - Flexural Loading

A major objective of this task was to develop analytical solutions for deflection and stress distribution and to calculate these characteristics at the various thermal conditions.

The analysis and testing showed both the sensitivity of the data to beam thickness variations and the material modulus of elasticity. In order to minimize the data spread between successive samples of each beam type, the deflection loading and flexural stiffness calculations were normalized to the beam design thickness by the relationship

$$P_{\text{plotted}} = P_{\text{test}} \left( \frac{h_{\text{design}}}{h_{\text{test}}} \right)^3 \left( \frac{b_{\text{design}}}{b_{\text{test}}} \right)$$

The data reduction procedure was to plot the normalized load versus deflection and to determine the slope (m) of the resulting line as

$$m = \frac{P_1 - P_2}{\delta_1 - \delta_2}$$

Calculation of deflection and/or loading for each beam cross-section, considering the beam as coupled and uncoupled, was based on the relationship defined in Equation (1).

$$\delta = 10.21 \frac{P}{EI}$$

This also allowed for determining the beam's apparent stiffness factor, S, by combining both formulas to yield

$$S = (EI) = 10.21m$$

Figures 28 through 31 show the load deflection lines derived from the test data. The slopes, m, and the EI were determined for each test temperature.

Sample Number 3 in Figure 31 showed inordinately high values when tested at -65°F and +125°F. Since these were broken during test, reruns were not possible. Therefore, the slope and stiffness results for this test disregard the data from these samples.

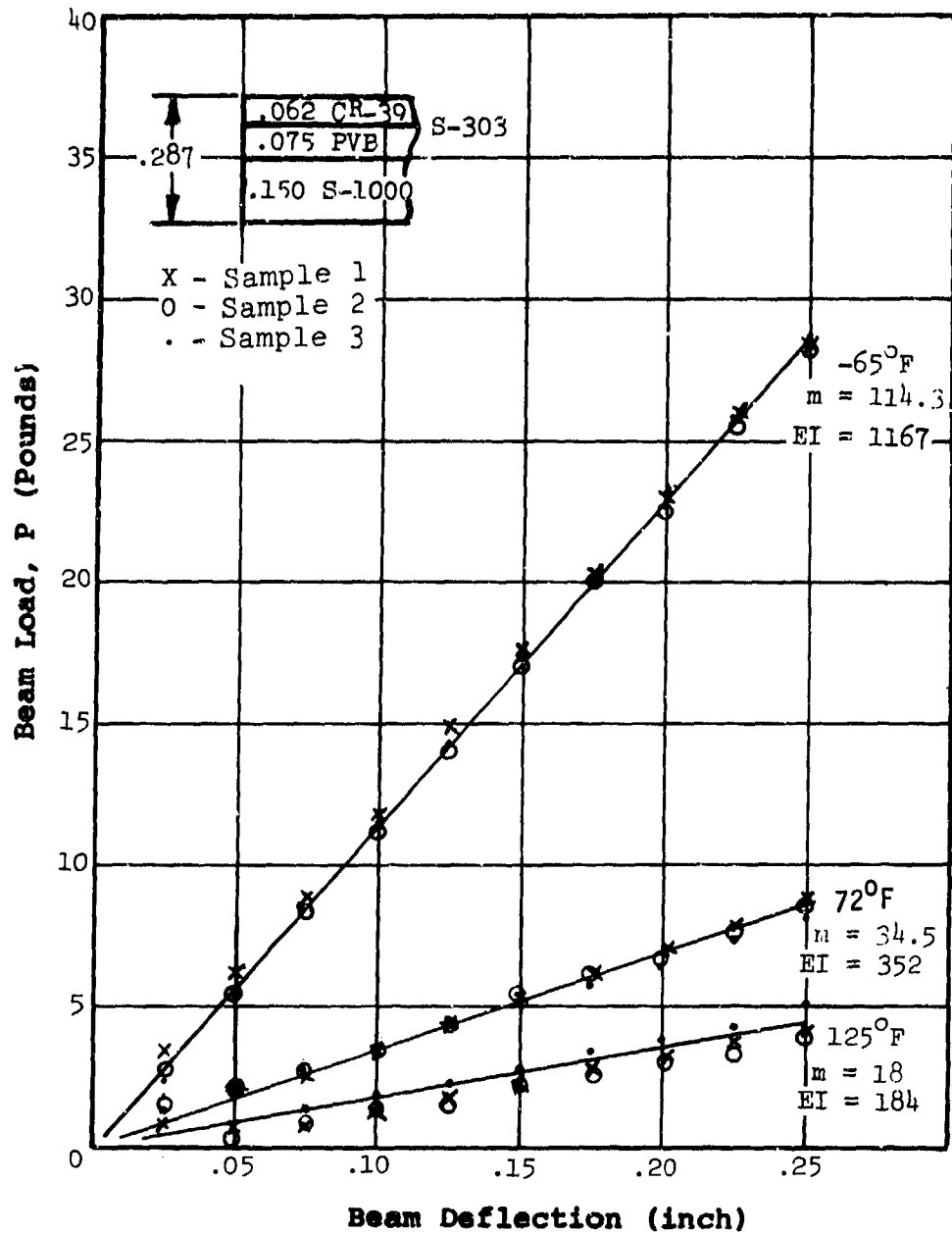


Figure 28. Load Deflection Test Data, Polyester/PVB/Acrylic Laminate with Coating.

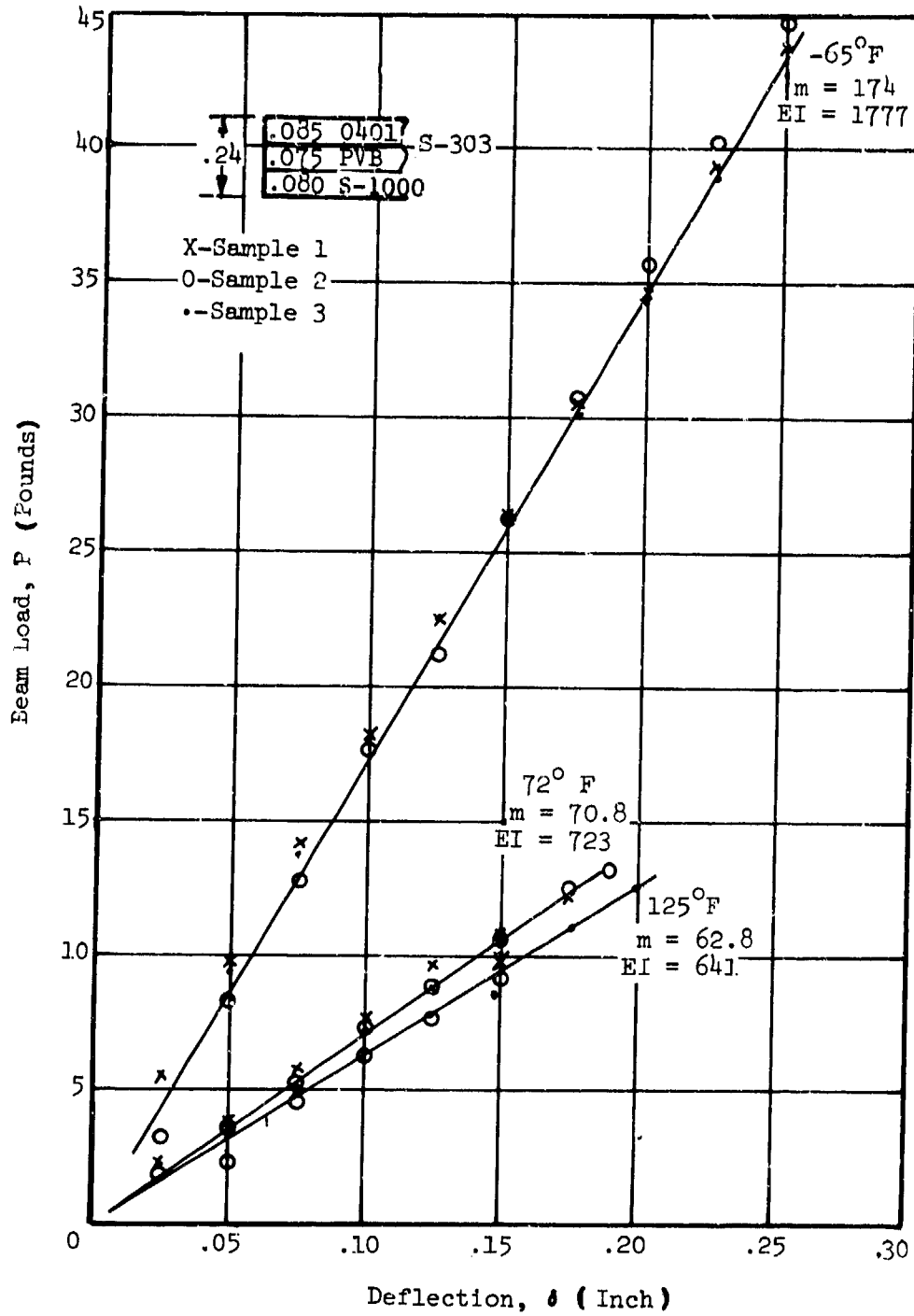


Figure 29. Load Deflection Test Data, Glass/PVB/Acrylic Laminate with Coating.

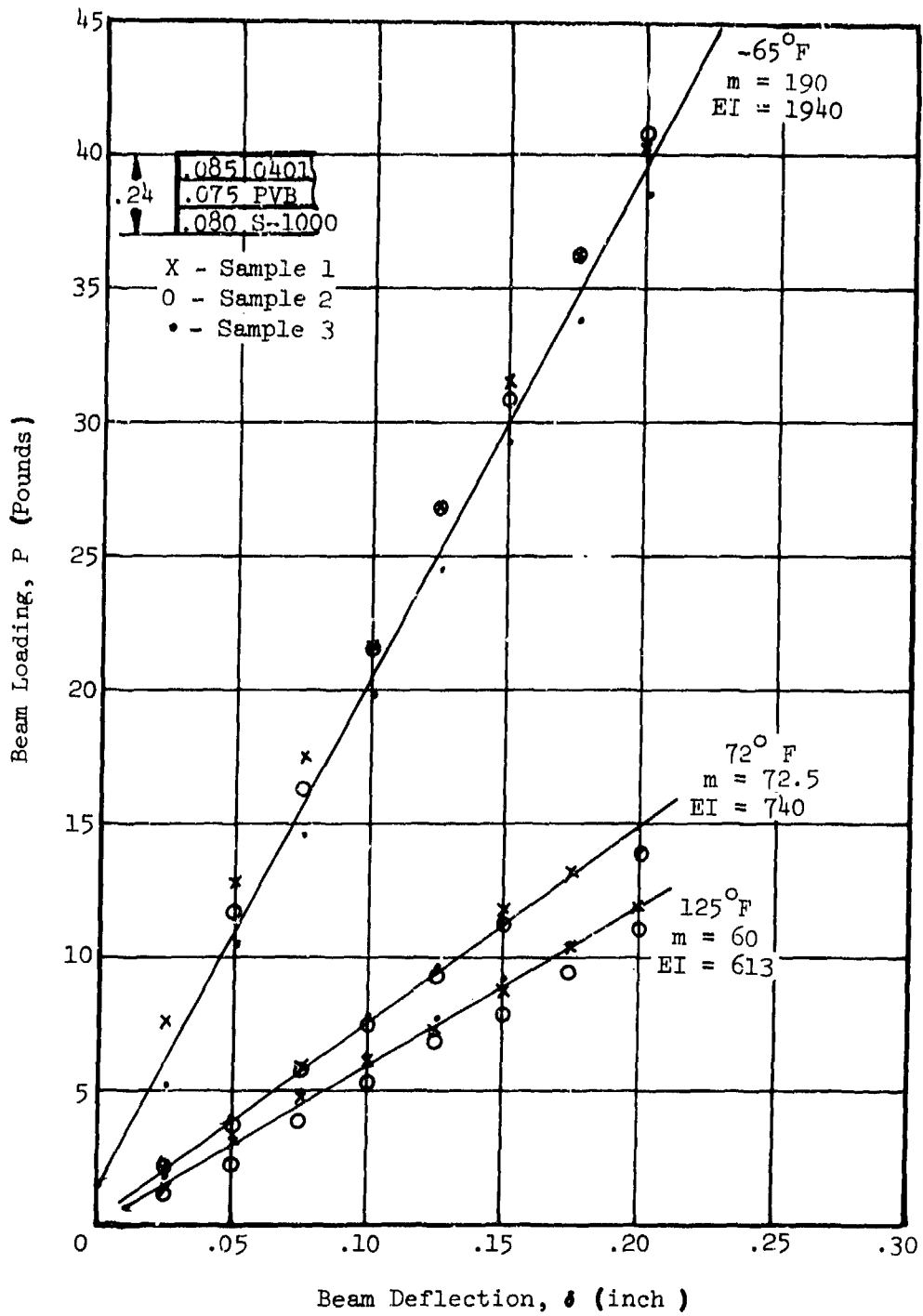


Figure 30. Load Deflection Test Data, Glass/PVB/Acrylic Laminate, No Conductive Coating.

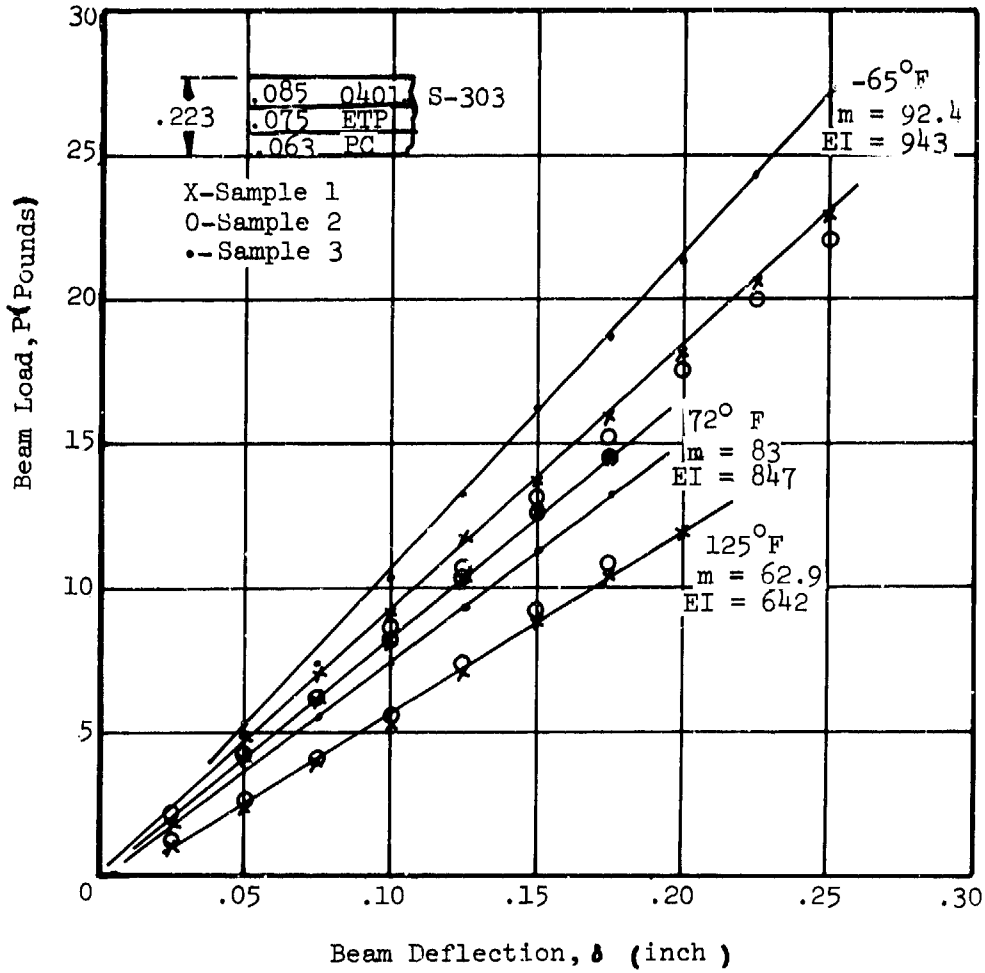


Figure 31. Load Deflection Test Data, Glass/ETP/Polycarbonate Laminate with Coating.

Figures 32, 33 and 34 show curves of the expected stiffnesses for the ideal coupled and uncoupled beams as well as the equivalent stiffnesses derived from the load deflection curves. The glass-PVB-stretched acrylic specimens, with and without conductive coatings, are plotted on the same curve since the coatings do not affect stiffness. The calculations for the theoretical stiffnesses were obtained from Equations (3) and (4).

The material modulus of elasticity with respect to temperature was determined from data in MIL-HDBK-17, Part II, or the manufacturer's data wherever possible.

These curves show that at low temperatures the interlayers provided almost total coupling, while at high temperatures coupling effects were minimal. At room temperature, partial coupling was apparent for all cases.

#### Strain Gauge Results

The theoretical stresses for each beam cross section were calculated using Equations (2), (3) and (4), and are shown in Tables 12 through 15. Each table includes the applied load, calculated facing stresses based on the strain gauge results, the load-stress relationship for fully coupled beams, and the load-stress relationship for uncoupled beams. Each set of loads in the tables corresponds to deflections of 0.10 and 0.15 inch respectively.

The tables show that flexural stresses based on uncoupled section properties were conservative in comparison to measured stresses for equivalent loading conditions. However, the conservatism applied to the dominant (stiffest) structural ply only.

When there is a significant difference in stiffness between the two facings, partial coupling creates a strain distribution similar to that shown in Figure 35. Here the neutral axis remains within the dominant structural facing, and the interlayer coupling induces a higher strain in the softer ply than would occur if it were considered uncoupled.

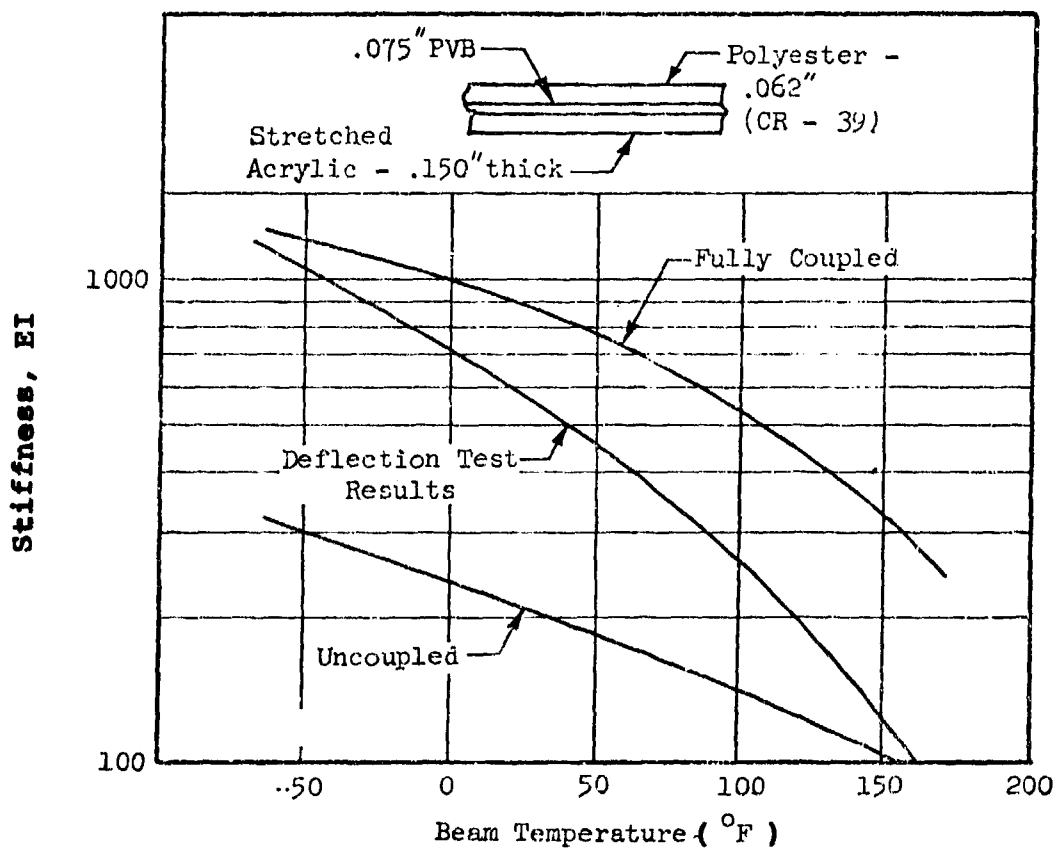


Figure 32. Variation in Stiffness With Temperature, Polyester-PVB-Stretched Acrylic.

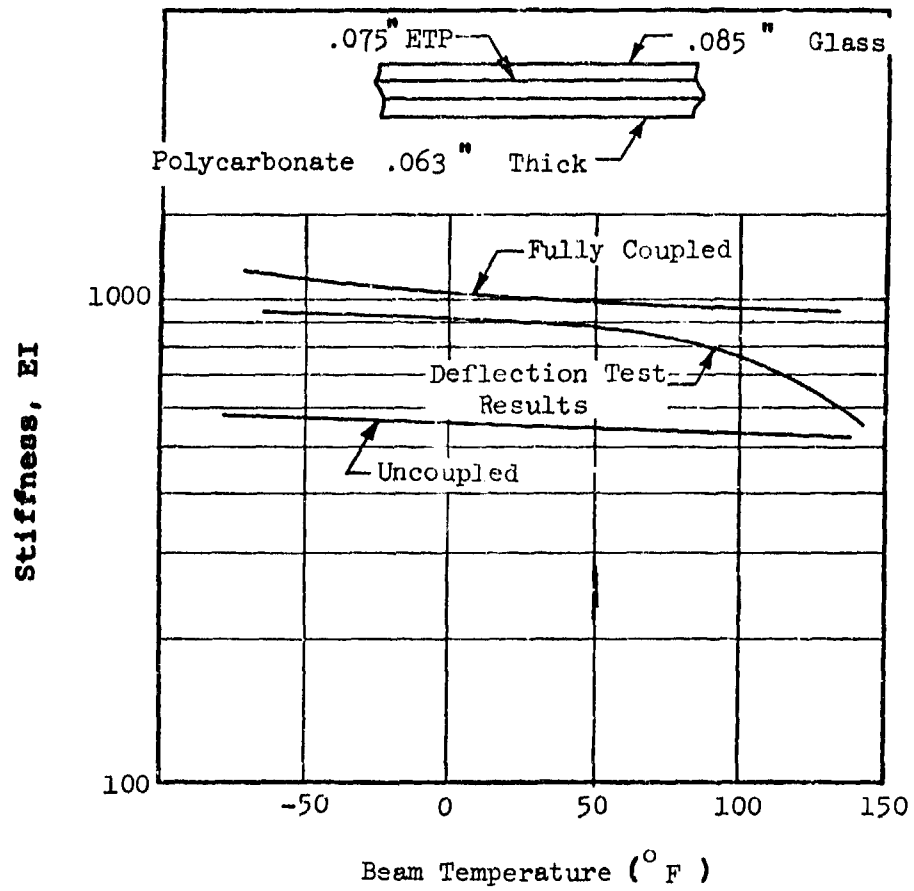


Figure 33. Variation in Stiffness With Temperature, Glass-ETP-Polycarbonate.

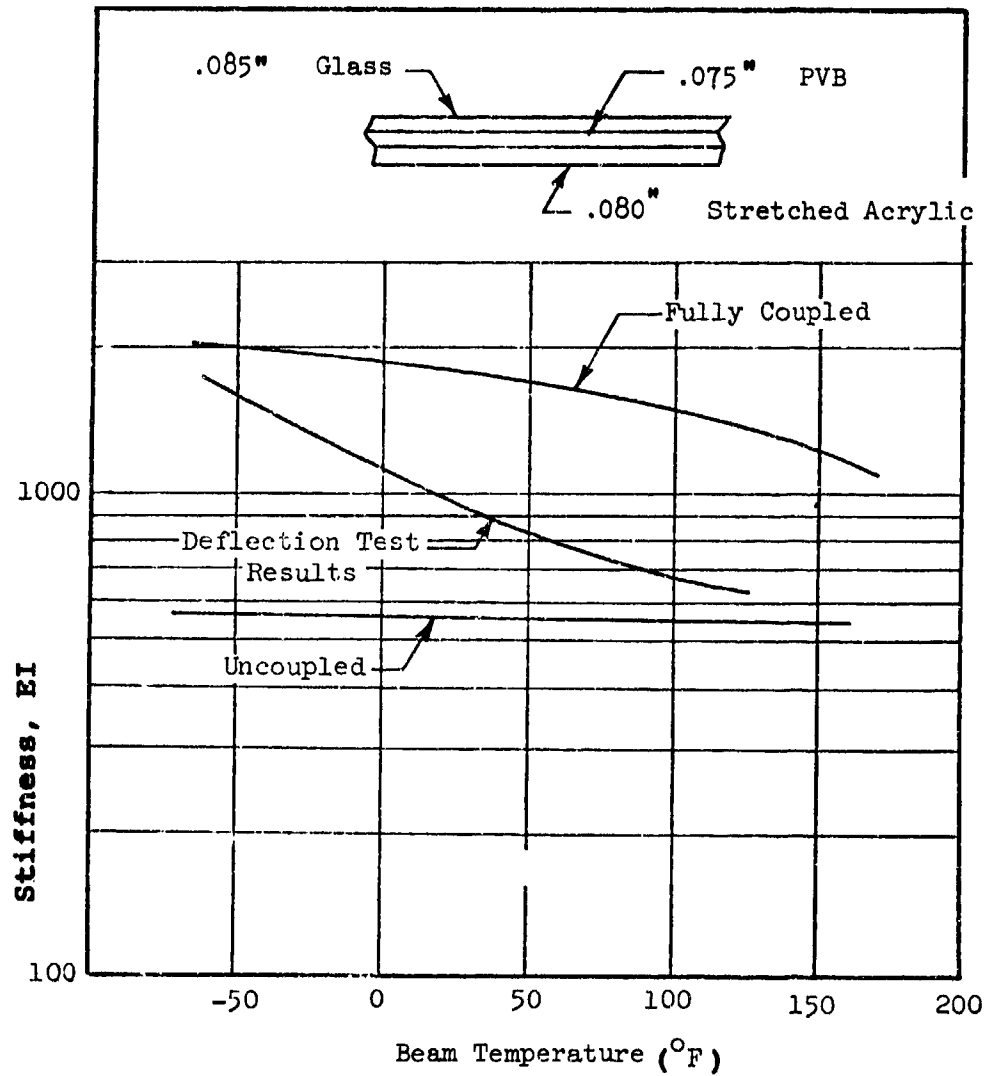


Figure 34. Variation in Stiffness With Temperature, Glass-PVB-Stretched Acrylic.

TABLE 12. STRAIN GAUGE TEST RESULTS  
POLYESTER - PVB - STRETCHED ACRYLIC

Temperature (°F)	Load (lb)	Modulus of Elasticity (psi)	CR-39 Face Ply			Acrylic Face Ply			
			Test Stress (psi)	Coupled Stress (psi)	Uncoupled Stress (psi)	Modulus of Elasticity (psi)	Test Stress (psi)	Coupled Stress (psi)	Uncoupled Stress (psi)
-65	12.4	$5.4 \times 10^5$	-1460	-1560	-1120	$7.5 \times 10^5$	1500	1600	3680
	18.2		-2170	-2290	-1650		2230	2340	5400
70	3.5	$3.0 \times 10^5$	- 540	- 330	- 370	$5.6 \times 10^5$	720	620	1660
	5.3		- 800	- 490	- 550		1070	920	2460
125	1.4	$1.7 \times 10^5$	- 370	- 180	- 110	$4.2 \times 10^5$	580	250	640
	2.0		- 510	- 260	- 150		770	360	910

TABLE 13. STRAIN GAUGE TEST RESULTS  
GLASS - PVB - STRETCHED ACRYLIC,  
WITH CONDUCTIVE COATING

Temperature (°F)	Load (lb)	Glass Face Ply				Acrylic Face Ply			
		Modulus of Elasticity (psi)	Test Stress (psi)	Coupled Stress (psi)	Uncoupled Stress (psi)	Modulus of Elasticity (psi)	Test Stress (psi)	Coupled Stress (psi)	Uncoupled Stress (psi)
-65	16.2	$103 \times 10^5$	-8830	-7190	-21926	$7.3 \times 10^5$	1970	1990	460
	23.5		-12880	-10430	-31810		2980	2880	2120
+70	5.5	$103 \times 10^5$	-6900	-3190	-7640	$5.6 \times 10^5$	440	660	400
	8.3		-10820	-4760	-11540		680	980	590
+125	7.9	$103 \times 10^5$	-7380	-4750	-11100	$4.2 \times 10^5$	300	810	430
	11.5		-11380	-6920	-16160		450	1170	620

TABLE 14. STRAIN GAUGE TEST RESULTS  
GLASS - ETP - POLYCARBONATE

Temperature (°F)	Load (lb)	Modulus of Elasticity (psi)	Glass Face Ply			Polycarbonate Face Ply			
			Test Stress (psi)	Coupled Stress (psi)	Uncoupled Stress (psi)	Modulus of Elasticity (psi)	Test Stress (psi)	Coupled Stress (psi)	Uncoupled Stress (psi)
-65	13.4	$103 \times 10^5$	-9460	-10190	-17790	$3.8 \times 10^5$	1080	1400	490
	19.5		-13770	-14825	-25890		1620	2040	710
+70	7.0	$103 \times 10^5$	-6490	-5680	-10060	$3.4 \times 10^5$	670	750	250
	11.3		-10720	-9160	-16240		1080	1220	400
125	6.1	$103 \times 10^5$	-8480	-5920	-8780	$3.3 \times 10^5$	550	660	210
	9.4		-13240	-9120	-13540		860	1010	320

TABLE 15. STRAIN GAUGE TEST RESULTS  
GLASS - PVB - STRETCHED ACRYLIC (NO COATING)

Temperature (°F)	Load (lb)	Modulus of Elasticity (psi)	Glass Face Ply		Acrylic Face Ply	
			Test Stress (psi)	Coupled Stress (psi)	Test Stress (psi)	Coupled Stress (psi)
-65	16.7	$103 \times 10^5$	- 9310	- 7530	1750	1870
	23.7		-13920	-10680	2750	2650
+70	6.3	$103 \times 10^5$	- 7810	- 3290	560	680
	9.3		-11520	- 4860	810	1000
+125	9.3	$103 \times 10^5$	- 8810	- 6260	370	920
	12.3		-13100	- 8280	540	1220
						1500
						2130
						450
						670
						500
						660

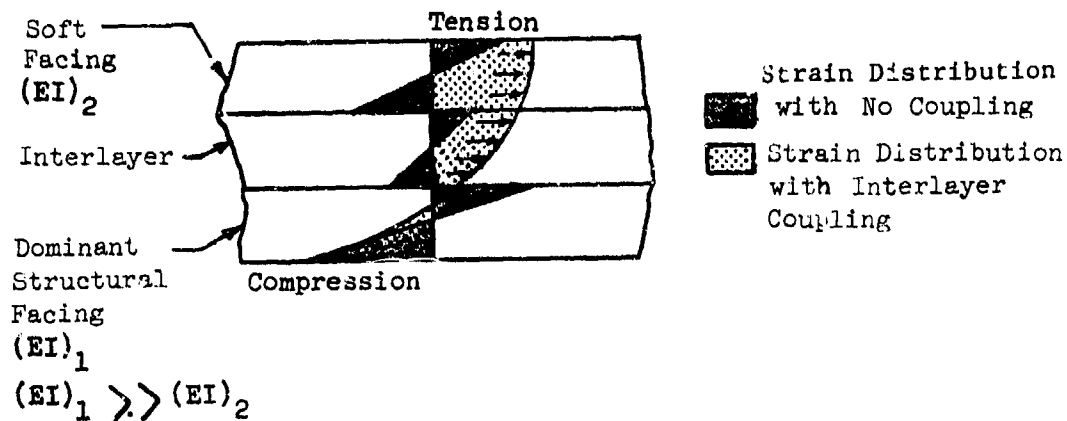


Figure 35. Strain Distribution in Uncoupled and Partially Coupled Composite Beam.

#### Destructive Test Results

The results of the flexure tests that were conducted until failure occurred are presented in Table 16. For each material combination and temperature, the average breaking load and deflection at failure is presented.

The test data indicated that a very substantial increase in flexural strength occurred at low temperatures. Deflection capability was also shown to increase at low temperatures. This can be attributed to interlayer coupling, increased material strengths at lower temperatures and differential thermal contraction. The latter condition occurs because the interlayer contracts more than the facings. This induces a compressive preload in the facings which effectively reduces the magnitude of the tensile stresses from flexure.

TABLE 16. SUMMARY OF FLEXURE TEST RESULTS

Material Combination	Average Breaking Load (lb)		Max Deflection (in.)	
	-65°F	+72°F	+125°F	+125°F
Polyester - PVB - Stretched Acrylic with Conductive Coating	113	*	*	1.38
Glass - PVB - Stretched Acrylic with Conductive Coating	*	11	9	0.183
Glass - PVE - Stretched Acrylic - No Conductive Coating	130	12	11	0.192
Glass - ETP - Polycarbonate with Conductive Coating	58	17	14	0.208

\*Excessive deflection, did not break.

### STRUCTURAL ADHESION TEST CONCLUSIONS

1. Temperature had a very significant effect on interlayer adhesion. Maximum strength occurs at low temperatures and minimum strength occurs at high temperatures.
2. Interlayer adhesion was also shown to be sensitive to substrate material. Electrically conductive coatings caused a reduction in shear and tensile strengths.
3. The shear and tensile test procedures are suitable for comparative and quality control purposes although they do not correspond to actual transparency loading conditions due to differences in stress concentration effects.
4. The cleavage tests demonstrated, in a conservative manner, how low magnitude transverse loads applied to an unreinforced edge of an extended base ply laminate can promote delamination.
5. The flexure tests showed that at low temperature, laminates using PVB and ETP interlayers were structurally coupled, and at high temperatures there was only slight coupling.
6. Flexural stresses will be conservative when calculated on the basis of uncoupled section properties. However, if the face plies differ greatly in stiffness, the conservatism applies only to the stiffer ply.
7. Load and deflection capabilities of the laminated coupon specimens increased substantially at low temperatures.

## NASTRAN FINITE ELEMENT ANALYSIS

The study described herein was conducted to investigate the suitability and limitations of the NASTRAN (NASA Structural Analysis) finite element analysis for calculating stresses and displacements in helicopter transparent enclosures.

The expansive transparent areas found on most helicopters offer potentially significant savings in weight when aerial densities are minimized. In order to achieve this objective, while maintaining structural integrity, the magnitude of the design operating stresses in the transparent enclosure must be reliably known. Conventional "hand" methods of rigid body stress analysis have significant deficiencies when applied to typical helicopter transparencies. Also, in the past, canopies for helicopters have been considered secondary structure, and analyzed only for local airloads and inertia loads. Influence on overall cockpit bending was assumed negligible, and usually ignored during structural analysis. However, since canopies are rigidly fastened to the primary structure, secondary loads can be induced as a result of primary structure deflections from application of flight loads.

With the advent of computer capabilities, the analysis of complex loading conditions and interactions in structures has become more efficient and reliable. Use of finite element analyses has shown weight savings in the design of airframe structures because it has been possible to investigate additional cases in more detail than has hitherto been possible. Therefore, a NASTRAN finite element analysis is a potential tool for saving weight while maintaining structural integrity in the transparency and its supporting structure.

### INVESTIGATIVE STUDY

Specific factors that were investigated in this study are enumerated below:

Effects of large displacements on analytical accuracy

Effects of elastic supports on windshield stress

Interaction between membrane and bending stresses due to transparency curvature

Effect of fuselage deformation on windshield stress

The state of stress in any transparency, plate or membrane type, is strongly influenced by the elasticity of its supports. When windshield or window edge members are loaded, they deflect, with the result that support constraints for the transparency are shifted. It was shown that this condition had significant effects on the internal stress distribution for helicopter windshields.

Helicopter cockpits can undergo severe deflections during flight maneuvers. Depending upon the helicopter configuration and specific loading case, vertical bending, lateral bending, or torsion, or any combination thereof, can be applied to the transparent enclosure. Using the Sikorsky YUH-60A as a case study, the effect of maneuver loads on windshield stress was evaluated.

Many helicopter cockpit transparencies have second-degree curvature, either compound or conic. When subjected to pressure loading, these structures support loads partially by membrane action, and partially by bending. Classical handbook equations do not apply to these shapes, and unique analytical solutions are required to determine stresses. Frequently, however, the mean radius of curvature is used in conjunction with circular or hemispherical pressure vessel equations, or equivalent flat plate analogies are used to calculate stresses. This study showed how the NASTRAN finite element analysis can be used to obtain both in-plane membrane loads and bending loads in a curved second-degree conic windshield subject to uniform pressure loading.

Nonuniform aerodynamic pressure distributions generally apply to helicopter cockpits. In order to facilitate stress analysis idealized uniform pressures are frequently used in calculations, which can introduce errors. The NASTRAN format readily accepts discrete pressure loadings applied to each finite element with no compromise in distribution. However, to accomplish the objectives of this study which were primarily concerned with windshield/airframe interactions and analytical accuracy, only the simpler case of uniform pressure was studied.

A NASTRAN differential stiffness approach was used to evaluate the effects of large displacements on the analytical determination of internal stresses and deflection for typical helicopter windshields. Bennet has shown in Reference 5 that the changes in geometry of an aircraft canopy cross-section greatly affect the internal member loads within the structure. In order to obtain correct design operating stresses within a canopy, deformation of the canopy under loading must be accounted for.

- (5) Bennet, R. D., LTV Aerospace Corp, "NASTRAN Differential Stiffness Analysis of an Aircraft Canopy," NASA TM-X-2378, National Aeronautics and Space Administration, Washington, D.C., September 1971.

## NASTRAN FINITE ELEMENT THEORY

NASTRAN uses the displacement or stiffness method to calculate the forces in the structural elements. This method consists of modeling a structure as a collection of finite elements that are mathematically considered to have the elastic properties of the structure they represent. These elements are connected at joints or nodes called grid points. The force-displacement equations for the various connected elements are compiled in matrix form.

$$(F) = (K) (\delta)$$

where

- (K) = stiffness matrix
- ( $\delta$ ) = displacements at node points
- (F) = forces applied at the node points

The nodal displacements are the unknowns in this problem, so the stiffness matrix must be inverted and multiplied by the applied load vector to yield

$$(\delta) = (K)^{-1}(F)$$

When the displacements are known, the extensions of each finite element can be found and the stresses determined from the stress/strain relationships for the elements.

In the development of this finite element method for the analysis of linearly elastic structures, it is assumed that:

1. Displacements and strains developed in the structure are small. Physically, this means that during the loading process, the geometry of the structure remains basically unchanged, so that the infinitesimal, first-order linear strain-displacement relations may be used, and the equations of equilibrium written for the undeformed structure remain valid.
2. Stress/strain relationships for the material are linear. This assumption, loosely speaking, can be thought of as following from the first, since the stress/strain relations for most engineering materials can be considered linear when the stresses are below the elastic limit and the displacements are small.

In many instances, these assumptions may fail, even though the actual strains and displacements may be small and the elastic limits of the structural material are not exceeded. For example, stresses due to membrane action which are usually neglected in plate bending may cause a considerable decrease in displacement when compared to the linear solution even though the displacements are small. Thus, in order to accurately determine the stresses and displacements, nonlinear effects may have to be considered in the analysis of the structure.

From the above discussions, it is seen that there are two basic types of nonlinear static effects occurring in structural problems:

Material nonlinearities  
Geometric nonlinearities

Material nonlinearity effects occur because the stresses are nonlinear functions of the strain resulting from the nonlinear elastic or plastic behavior of the structural material.

Geometric nonlinearity effects occur because the strains and/or displacements at the points of applied loading are nonlinear functions of the degrees of freedom used to describe the motion of the structure. That is, geometric nonlinearities occur when the loads applied to the structure are large enough to give rise to relatively large displacements. When the deflections are large, they cause significant changes in the geometry of the structure, and in this case, the equations of equilibriums must be formulated for the deformed configuration.

#### NASTRAN FINITE ELEMENT CAPABILITIES FOR NONLINEAR PROBLEMS

In addition to a linear static analysis (Format 1), NASTRAN also offers:

Differential Stiffness Analysis (Format 4)  
Piecewise Linear Analysis (Format 6).

These capabilities have not been combined.

The differential stiffness capability (Rigid Format 4) includes the stiffening or softening effects of static in-plane loads. Thus, the differential stiffness matrix may be interpreted as an effective stiffness created by the internal stresses existing in the structure, which is added to the standard elastic element stiffness matrix. This added stiffness is calculated from the geometry and internal loads existing in the element, and is assumed to be proportional to the magnitude of the applied loads. The total stiffness of the structure is the sum of the elastic stiffness matrix and the geometric stiffness matrix.

In the NASTRAN differential stiffness approach, the nonlinear solution is obtained in the following manner:

1. The linear elastic stiffness matrix ( $K_E$ ) is formed for the entire structure.
2. Using ( $K_E$ ), the solution for the linear response of the structure is obtained, and the internal forces for the elements are calculated.
3. Knowing the internal forces for the elements and the displacements at the grid points, the geometric stiffness matrix ( $K_G$ ) for the structure is formed.
4. ( $K_G$ ) is added to ( $K_E$ ) to obtain a total stiffness matrix which is used to calculate the final nonlinear solution.

This two-step approach is not iterative and because of this, the differential stiffness approach can only be expected to give reasonably accurate answers for those problems where the effects of geometric nonlinearities are not too severe.

Finally, it should be noted that for the BAR (NASTRAN beam element) and TRIAL (Plate Bending element), the geometric stiffness matrices for these elements are functions of only the axial or in-plane loads determined from the linear solution. The changes in the axial and in-plane strains due to transverse loads are considered as higher order effects and are ignored in the geometric stiffness matrix formulation. Physically, this means that in the case of perfectly flat plates with no prescribed in-plane loading, membrane effects arising from transverse pressure loads cannot be predicted.

The piecewise linear analysis option is available in NASTRAN as Rigid Format 6 and is used to solve problems involving material plasticity. In this approach, the nonlinearity of the materials is defined in the program in the form of a tabular stress/strain curve. The load is applied in increments such that the stiffness properties of the elements can be assumed to be constant over each increment. The stiffness matrix for each increment is dependent on the current states of stress in the elements, and displacement increments and stresses are accumulated to produce the final nonlinear result.

The piecewise structural stiffness matrix must be reformulated and decomposed for each load increment. From the analysis standpoint, however, the most serious drawback is the fact that for each load increment, the coordinates of the grid points in the undeformed state are used to calculate the element stiffness matrix. Because of this, many piecewise linear solutions are only gross approximations of the true response of the structure. However, it should be pointed out that even if the coordinates of the grid points were updated,

the solution would still be only an approximate (albeit a much better one) of the true response unless the effects of differential stiffness were included.

Detailed instructions for the use of NASTRAN are given in the NASTRAN Users' Manual<sup>6</sup>. Extensive explanation of the theoretical aspects of NASTRAN is provided in the NASTRAN Theoretical Manual<sup>7</sup> and the NASTRAN Applications Manual<sup>8</sup>. Manuals are available from NASA and the MacNeal Schwendler Corporation.

#### STRUCTURAL DESCRIPTION

The aircraft selected for this study was the Sikorsky YUH-60A Utility Tactical Transport Aircraft System (UTTAS). UTTAS represents the newest generation of Army helicopters, has relatively large windshields supported by slender posts (Figure 36), and is subjected to high aerodynamic pressure and maneuver loads.



Figure 36. Sikorsky YUH-60A UTTAS.

- (6) McCormick, C.W., "NASTRAN Users' Manual," MSR-39, The Mac Neal Schwendler Corp., Los Angeles, Calif., March 1974.
- (7) MacNeal, R.H. "The NASTRAN Theoretical Manual," MSR-40, The MacNeal Schwendler Corp., Los Angeles, Calif., May 1974.
- (8) Joseph, J.A. "MSC/NASTRAN Application Manual," MSR-35, The MacNeal Schwendler Corp., Los Angeles, Calif., Nov. 1972.

The primary area of concern was the windshield and its immediate surrounding support structure. However, to properly consider the influence of airframe stiffness on the behavior of the canopy structure, the analysis was expanded to include the lower cockpit and the forward mid-cabin section as shown in Figure 37.

The windshield was constructed in three sections; the center section, between B.L. +10, was a flat plate; and the outboard sections, between B.L. -10 and the outboard posts, were loft conic shapes. Three different types of laminated windshields were considered in the analyses:

- a. two layers of glass, 0.095 inch in thickness
- b. a face ply of glass, 0.085 inch in thickness with a 0.060-inch-thick stretched acrylic base ply
- c. a base ply of stretched acrylic, 0.160 inch in thickness with a 0.060-inch polyester face ply.

All three configurations were laminated with a polyvinyl butyral interlayer.

The principal structural components of the canopy shown in Figure 37 were the canted bulkhead at Station 184.75, the fore and aft "A" frames at butt line +10, the Station 205 box frame above water line 215, the windshield, the windshield sills and posts and the canopy roof structure. The lower windshield sill was a reinforced fiberglass "Z" section, while the upper sill, the B.L. 10 posts, and the outboard posts were fiberglass box beams.

The canopy roof structure was covered with fiberglass skin and contained an aluminum frame at Station 241, and deep fiberglass beams at B.L. +10, running fore and aft from the upper sill to the frame at F.S. 247. The window area between the upper sill, the B.L. 10 beams, and the Station 241 frame was not modeled since its stiffness was negligible.

The lower cockpit was that section of the aircraft between Stations 162 and 247 and below W.L. 215. The lower cockpit was essentially cantilevered from Station 247 and provided the main support for the canopy. It consisted of four main longitudinal beams at B.L. +10 and +30 and transverse bulkheads.

The mid-cabin structure was that section of the aircraft aft of Station 247. For analytical purposes, the structure was terminated at F.S. 308, since the remaining cabin structure had little influence on the canopy load-deflection characteristics. The forward cabin was a conventional semi-monocoque construction utilizing frames, beams, skin and stringers as primary structure.

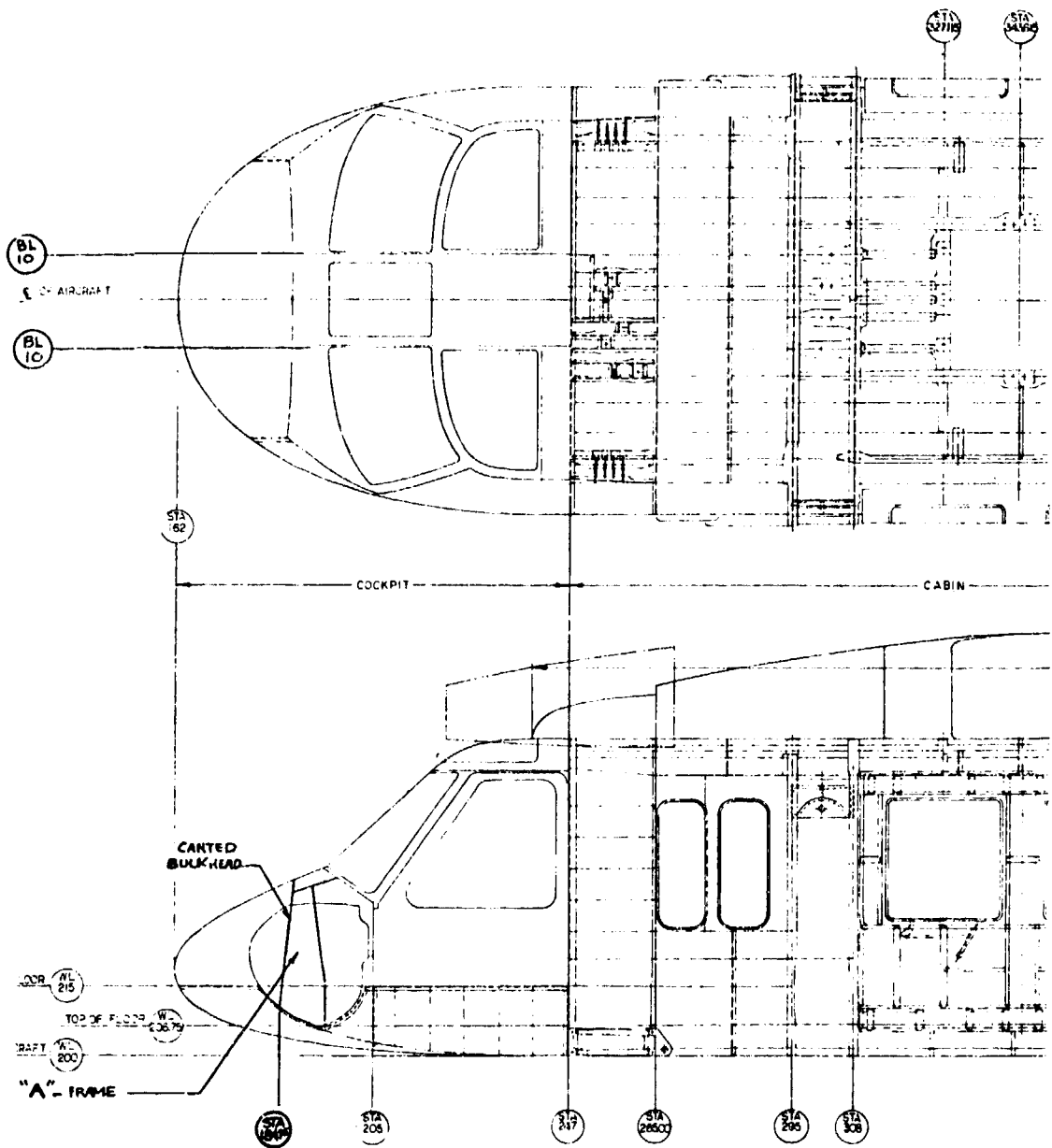


Figure 37. Sikorsky YUH-60A Structural Arrangement.

### NASTRAN MODELS DESCRIPTION

Three separate NASTRAN models were constructed which varied in size and degree of refinement. The basic model contained the upper cockpit, laminated glass windshields, lower cockpit, and forward cabin up to Station 308. This model is shown in Figures 38 and 39. Note that although the cockpit and cabin sections are shown separately in the photographs, they are both part of the same model.

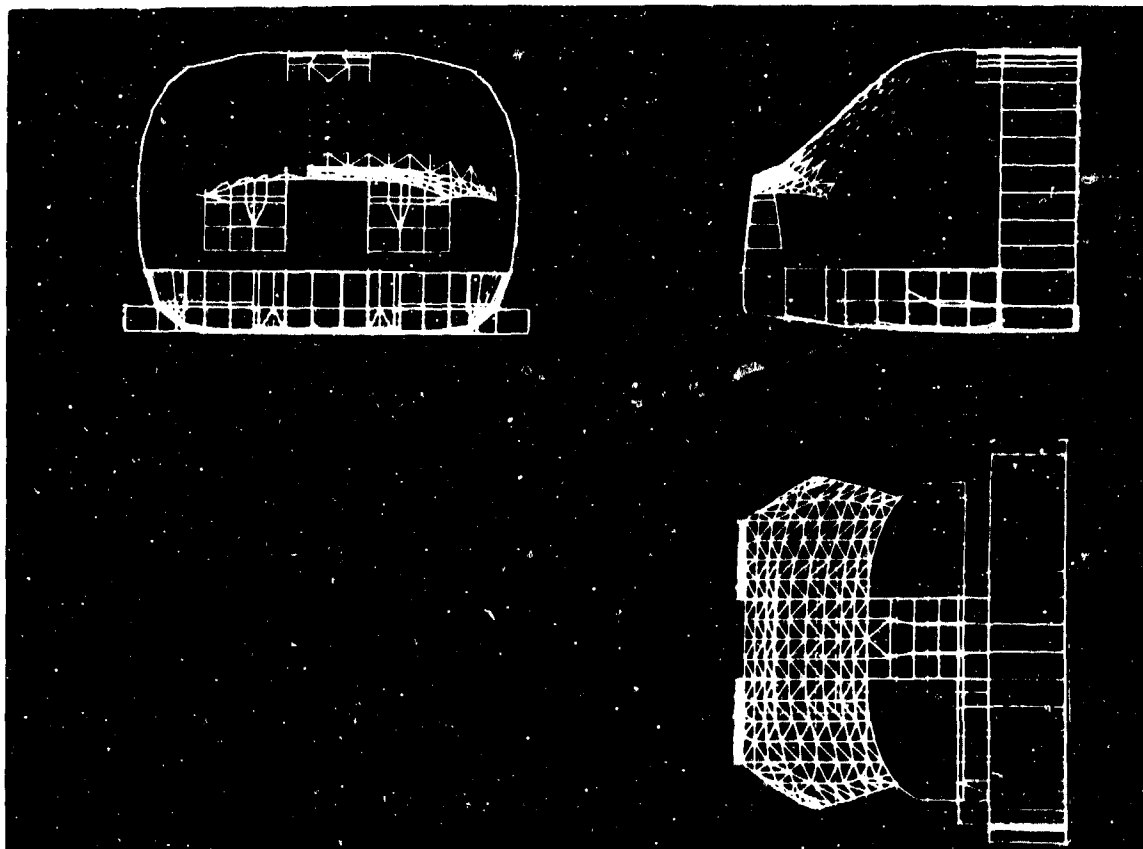


Figure 38. Cockpit NASTRAN Model.

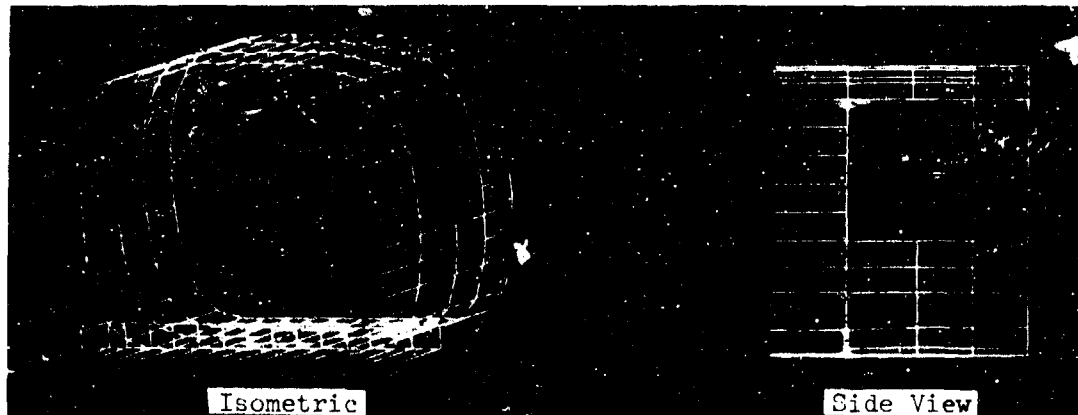


Figure 39. Cabin NASTRAN Model.

The sills and the posts were constructed of fiberglass having an elastic modulus of  $2.0 \times 10^6$  psi and a Poisson's Ratio of 0.4. Typical section properties used in the analysis for these members are summarized in Table 17. In this table, the moment of inertia  $I_2$  corresponds to bending about an axis in the plane of the windshield, and  $I_1$  corresponds to bending about an axis perpendicular to this plane.

TABLE 17. SECTION PROPERTIES OF SIDE POSTS AND SILLS

	Area (in. <sup>2</sup> )	Moment of Inertia $I_1$ (in. <sup>4</sup> )	Moment of Inertia $I_2$ (in. <sup>4</sup> )	Torsional Moment of Inertia (in. <sup>4</sup> )
Upper Sill	.525	.5667	.2004	.140
Lower Sill	.339	.0625	.2516	.050
B.L. 10 Posts	.510	.1947	.3176	.066
Outboard Post	.490	.440	.078	.082

Another model, identical in all respects to the basic model except for omission of the windshields, was constructed to obtain displacements of the windshield support structure. This model is shown in Figure 40.

The third model, shown in Figure 41, was a refined version of the center windshield and the surrounding portion of the upper and lower sills and butt line 10 posts. Restraint was provided by pin supports at the four corners. This model was used for correlating the NASTRAN results with those of instrumented tests performed on a section of the same structure represented by the model. The composite and plastic windshields, as well as the glass windshield, were analyzed with this model.

#### NASTRAN Finite Elements

The finite elements used to model the canopy and its surrounding structure were the CONROD, BAR, SHEAR, TRMEM and TRIAL elements. The CONROD is a line element capable of carrying axial and torsional loads. It is used to model stringers and stiffeners. The BAR is also a line element, which in addition to carrying axial and torsional loads, can react bending and shear loads in its principal and secondary planes. The BAR element was used to model all of the main bending members in the upper cockpit and cabin. Other members modeled with BAR elements were the windshield sills and posts, the outboard intercostals between the canted bulkhead and the lower sill, the B.L. 10 beams and the frames in the main cabin.

The SHEAR is a quadrilateral membrane element defined by four coplanar grid points. It is able to react in-plane tension, compression and shear loads. SHEAR elements were used to model the sheet metal panels in the Station 184.75 canted cabin. The main fore-and-aft members in the cabin structure were modeled as SHEAR panels framed by CONRODS.

The TRMEM is a triangular membrane element which can take in-plane tension, compression, and shear loads. The TRMEM was useful in modeling curved skins because it can be defined by any three nodal points. TRMEMS were used to model areas of the canted bulkhead and the fiberglass skin below the windshield.

The TRIAL is a triangular plate bending element which allows for independent specification of membrane and bending properties. The windshield in the basic model was composed of 200 TRIAL triangular plate bending elements having six degrees of freedom. The outboard curved windshields contained 76 TRIAL elements each and the center flat windshield contained 48 elements. 1020 TRIAL elements were used in the refined model of the center windshield. The numbering sequence for the basic windshield model is shown in Figure 42.

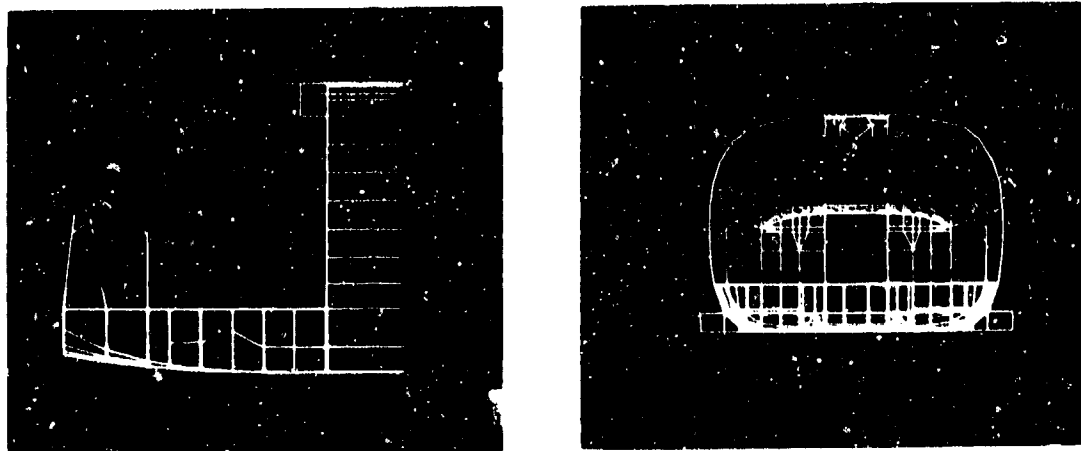


Figure 40. Cockpit NASTRAN Model Without Windshields.

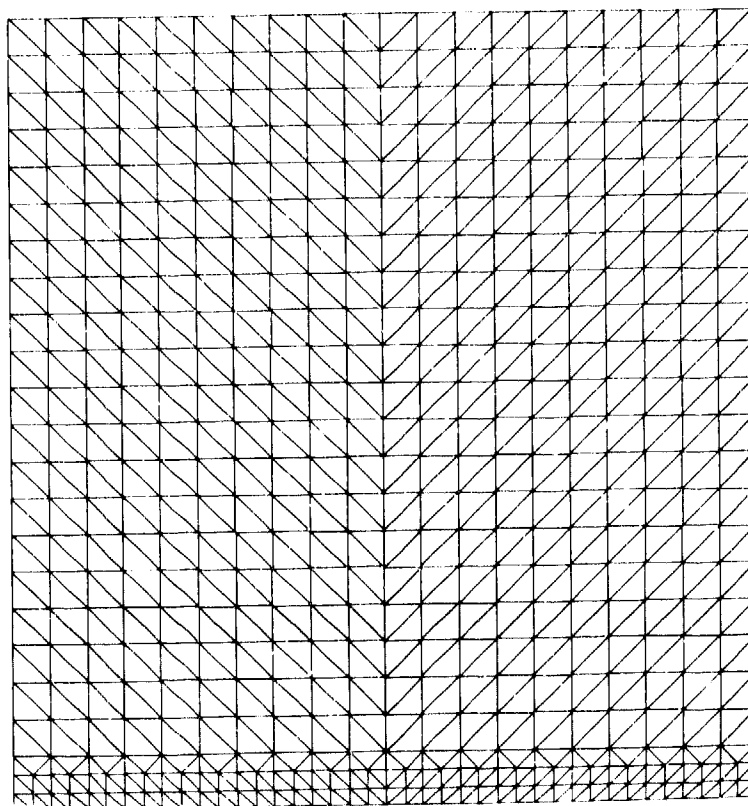


Figure 41. Refined Model Center Windshield.

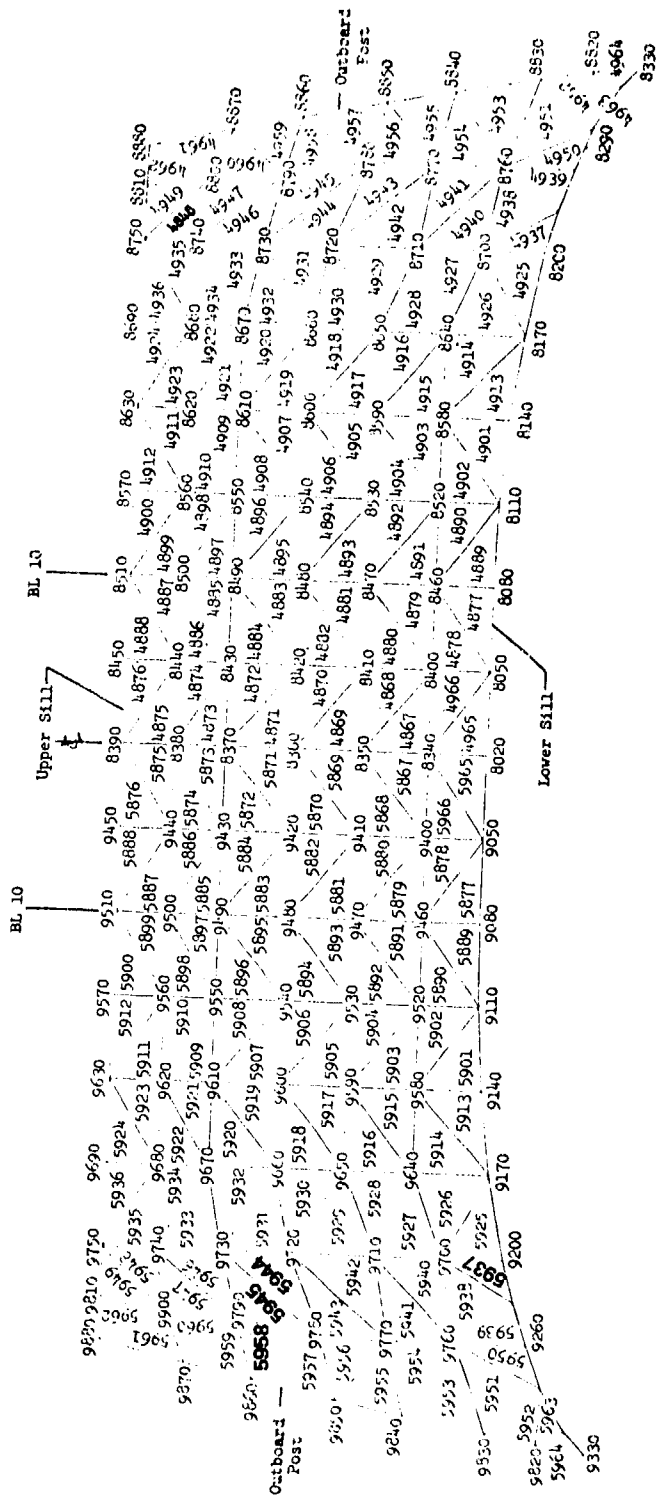


Figure 42. NASTRAN Numbering Sequence for Windshields.

### Modeling Assumptions

The laminated glass windshields were idealized as monolithic structures. At room temperature, the polyvinyl butyral interlayer bonding the two face plies together is highly elastic and acts as a viscous fluid, serving only to separate the facings, and hence provides only minimal structural coupling. This causes the two plates that comprise the windshield to act together in reacting in-plane loads but separately in reacting bending loads. For the all-glass laminate, the properties input into the NASTRAN model were 0.19 inch for membrane thickness, which was the combined thickness of the two plates, and  $1.428 \times 10^{-4}$  in.<sup>4</sup>/in. for the moment of inertia, twice the inertia of a single .095-inch plate.

The composite glass/stretched acrylic and stretched acrylic/polyester windshields were idealized as monolithic glass, and monolithic stretched acrylic, respectively. These assumptions were made because in the glass/plastic configuration, the stiffness of the plastic ply was small in comparison to the glass, and in the case of stretched acrylic/polyester, the polyester stiffness was small in comparison to the stretched acrylic structural base ply. Omission of the nonstructural plies and interlayer coupling effect created a built-in conservatism for stress and deflection computations.

It was assumed that the windshield perimeter plate elements were rigidly clamped to the BAR elements used to represent the supporting sills and posts. The neutral axes of the BAR elements were located on the outside mold line surface of the aircraft for simplicity of analysis. Techniques are available within NASTRAN to simulate flexible edge restraint and structural offsets if their effects are expected to be significant, based on the structural configuration being evaluated.

### Model Development Procedure

Coordinates used to describe model geometry were obtained from an Automatically Programmed Tool (APT) computerized definition of the YUH-60A basic contour lines. Analytic geometry definition by computer was an extremely efficient and rapid method for tabulating the large number of data points required. Total computer time required to generate the approximately 1200 coordinates for the windshields was only 19 minutes using a UNIVAC 1110 computer. Accuracies to five decimal places were also routinely achieved with this procedure.

Prior to running the model with applied loads, the geometry inputs were verified. A CRT, cathode ray tube display, was used to aid in this process. As shown in Figure 43, the analyst used a light pen to identify specific elements and coordinates of the model. By rotating the model about any axis on the display, missing elements, improperly connected elements, and erroneous coordinates were readily detected. For example, Figure 44 shows a CRT display with a missing element on the right side, outboard of the forward cockpit bulkhead.

The final step in debugging was to run a unit load condition to verify the internal load distribution of the structure. After making any necessary final adjustments, the model was then ready to be used for the more complex loading cases.

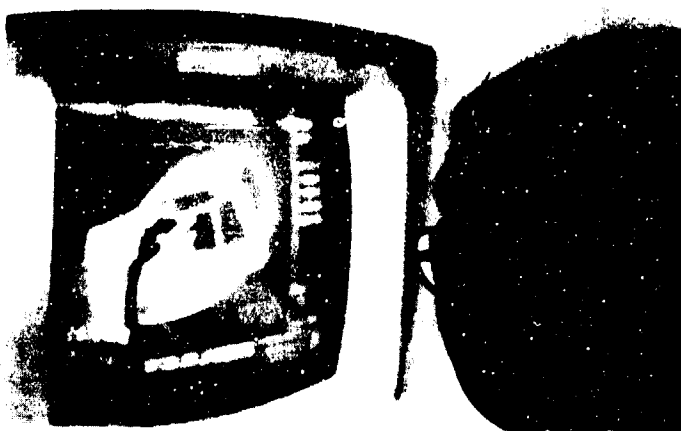


Figure 43. Cathode Ray Tube Display.

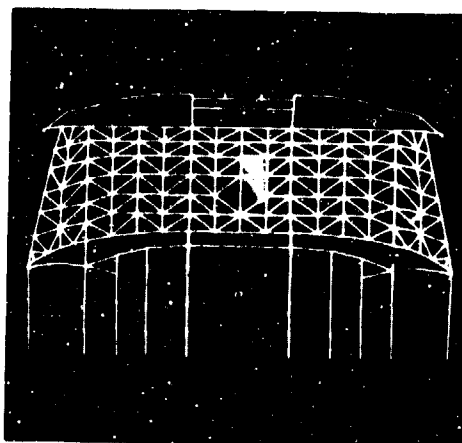


Figure 44. Missing Element Detection by CRT.

## NASTRAN OUTPUT FORMAT

Results from the NASTRAN analysis were output in three main subdivisions:

Displacements  
Forces in Elements  
Stresses in Elements.

Three translational and three rotational components of displacement were output for each grid point. Translational displacements were tabulated in the aircraft coordinate system, measured relative to model support points at Station 308, as illustrated in Figure 45. Rotational displacements for each model element were tabulated as slopes, measured relative to the element's initial orientation.

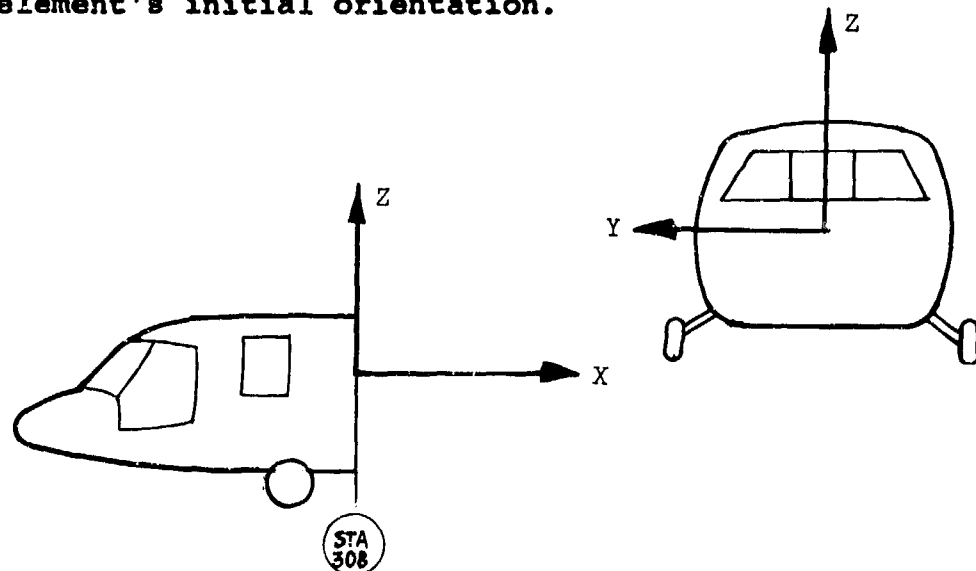


Figure 45. Reference Coordinate System.

The forces output for each element varied between element types. For the BAR elements, used to model the sills and posts, bending moments in the primary and secondary planes at both ends of the element were listed. Average horizontal and vertical shear, average axial load and twisting torque were also output. A positive sign designates a tension load or stress, and a negative sign indicates compression. The positive and negative conventions for bending moments are shown in Figure 46.

For the TRIAL plate element, bending moment per unit length on the x and y faces, twisting moment per unit length and shear force per unit length on the x and y faces were output.

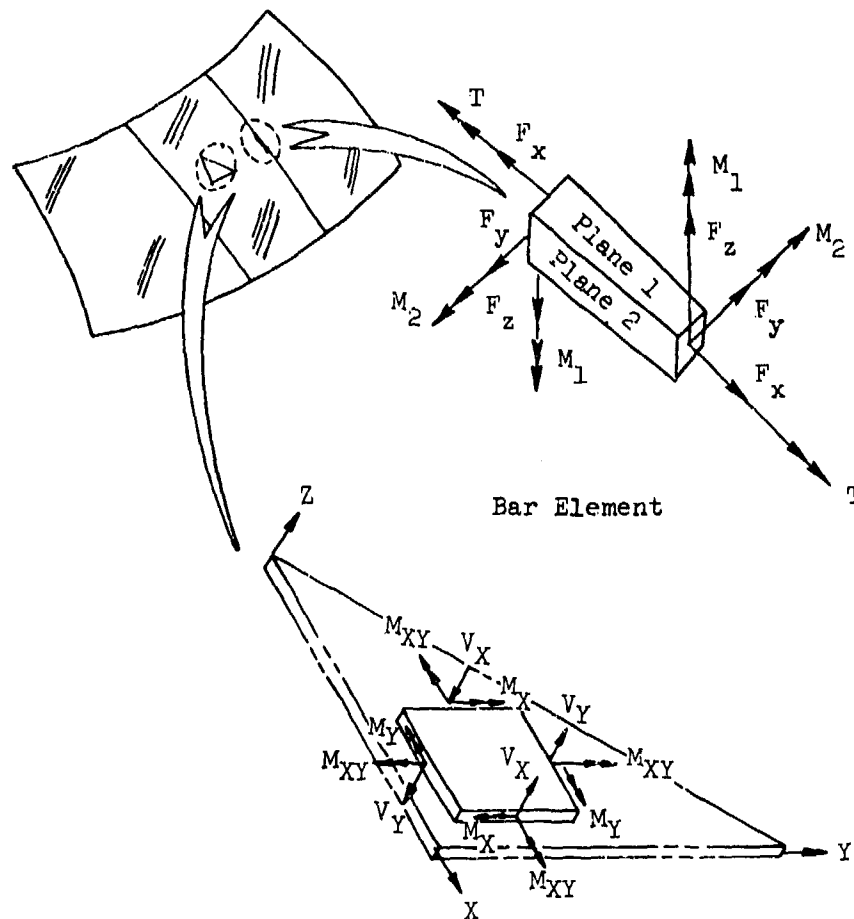


Figure 46. Force Output for BAR and Plate Elements.

In the "stresses in element" section of the NASTRAN output, normal and shear stresses for both the upper and lower surfaces were listed for each TRIAL element, as shown in Figure 47. Resolution of these stresses into bending and in-plane stresses was possible since the normal stress at each surface is equal to the algebraic sum of its in-plane component plus its bending component at each surface as shown in Figure 48. Therefore

$$f_1 = f_m - f_b \text{ and} \quad (1)$$

$$f_2 = f_m + f_b \quad (2)$$

where

$f_1$  = normal stress, top surface  
 $f_2$  = normal stress, bottom surface

Combining equations (1) and (2), a solution for the in-plane stress,  $f_m$ , is obtained:

$$f_m = 1/2 (f_1 + f_2) \quad (3)$$

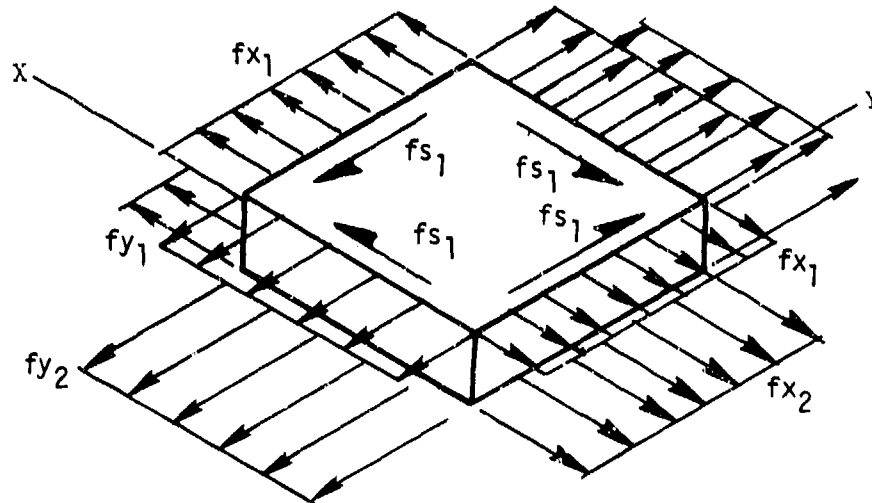


Figure 47. Stress Output for Plate Elements.

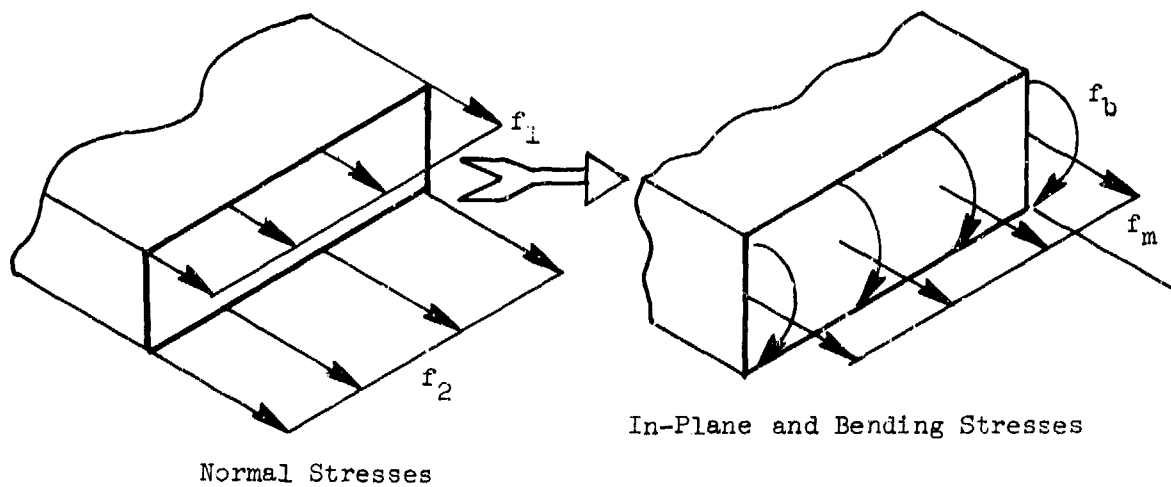


Figure 48. Resolution of Normal Stresses into Bending and In-plane Stresses.

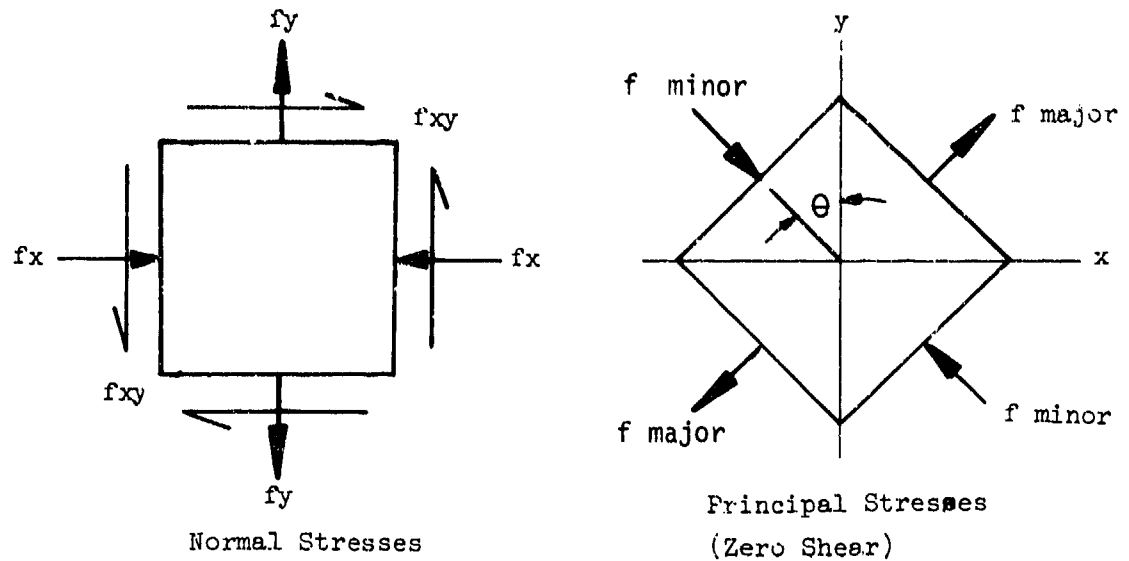


Figure 49. Distinction Between Normal and Principal Stresses.

In addition to normal and shear stresses, the major and minor principal stresses were tabulated for each element (see Figure 49). Strength analyses for glass windshields are based purely on material tensile strengths, whereas most other materials can be analyzed with combined shear and normal stress loadings. This anomaly occurs because the shear strength of glass is very difficult to measure, and is seldom used.

#### LOADING CONDITIONS

Five loading conditions were analyzed using the forward fuselage model. Both linear static and differential stiffness approaches were used in each analysis.

1. Flight inertia loading (windshield omitted from model)
2. Flight inertia loading (windshield installed)
3. 1 psi aerodynamic pressure on center windshield only
4. 0.3 psi aerodynamic pressure applied to windshields
5. Condition 2 (vertical bending) & condition 4 (pressure) combined.

In addition, three refined center windshield models representing the all-glass laminate, composite glass/plastic laminate, and all-plastic laminate were analyzed with 1 psi pressure loading. A differential stiffness analysis was not performed on this model because in the absence of in-plane loads and the flatness of the plate, the differential stiffness solution would produce results identical to those of the static solution.

## RESULTS

Results of these analyses have been grouped according to their relationships to the factors of interest.

### Large Displacement Effects on Analytical Accuracy

The effects of large displacements on analytical accuracy were checked with the flat center windshield models.

In order for the results of the NASTRAN analysis to be valid, it is necessary that the deflections satisfy the assumptions used in the thin plate theory: (1) the deflections are small in comparison with the thickness of the plate, or (2) the deflections are small in comparison to the width of the plate. These assumptions are based on the mid-plane of the part being free of strain. That is, there are no membrane stresses, and only bending stresses are present.

To determine whether the NASTRAN analysis was valid, the three center flat windshield configurations (glass/acrylic, acrylic/polyester, and glass/glass) were analyzed for a pressure loading of 1 psi. In addition, the glass/glass windshield was analyzed under 0.3 psi pressure. These constructions and pressures covered a range of conditions that were considered generic to helicopter windshields.

Pressure was applied to the NASTRAN finite element model using PLØAD bulk data cards. This feature of NASTRAN takes a uniform pressure for an element, calculates the total force, and distributes the force to the nodal points that define the element.

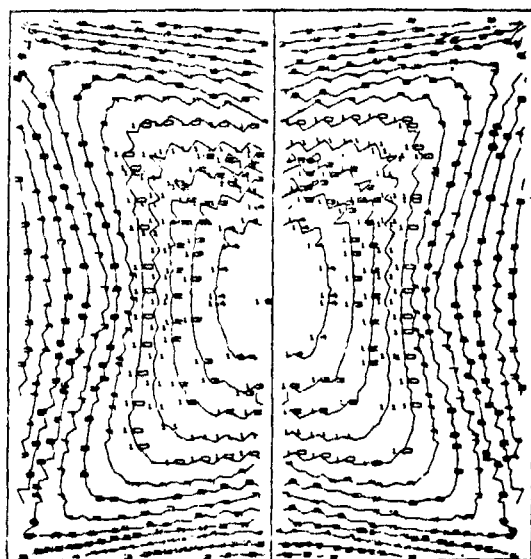
The maximum principal stresses and displacements for the flat windshields are given in Table 18, along with the value of the ratio of deflection to thickness and the ratio of deflection to width. Examination of Table 18 reveals that the calculated deflection to thickness ratios were much greater than one, and the NASTRAN analysis must be considered invalid. These flat windshield configurations support the pressure load by combined membrane-bending action which the NASTRAN program, as presently structured, cannot analyze.

TABLE 18. MAXIMUM DISPLACEMENTS FOR FLAT WINDSHIELDS

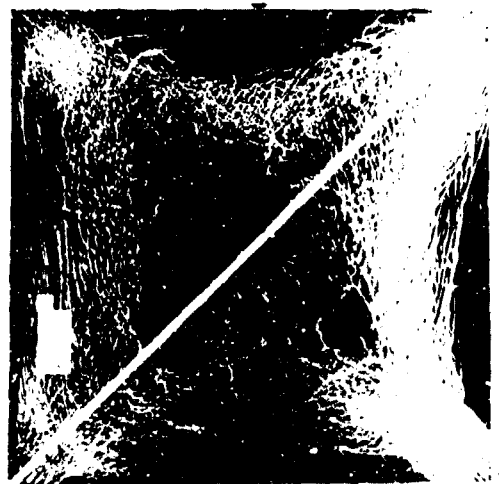
Windshield Type	Pressure (psi)	Max Principal Stress (psi)	Effective Thickness (in.)	Max Deflection (in.)	Deflection to Thickness Ratio	Deflection to Width Ratio
2 Layers of Glass	0.3	1347	.120	0.238	1.98	.011
2 Layers of Glass	1.0	6843	.120	0.623	5.20	.031
Composite Glass/ Stretched Acrylic	1.0	14428	.085	1.118	13.16	.056
Stretched Acrylic/ Polyester	1.0	3842	.160	2.330	14.57	.116

The presence of membrane stresses was confirmed during instrumented windshield tests conducted on a laminated glass windshield identical to that used in the NASTRAN analyses. In these tests, membrane stresses of approximately 180 psi were noted, along with principal stresses and deflections that were significantly lower than the NASTRAN values. For the 1 psi pressure load case, the maximum principal stresses from the instrumented tests were 2300 psi versus 6843 from the NASTRAN analysis, and the maximum test deflection was .098 inch measured relative to the center of the horizontal supports versus a calculated deflection of .623 inch.

The instrumented windshield tests are described in a subsequent section of this report. Also, using test results, a visual correlation of stress patterns can be observed in Figure 50, which compares a NASTRAN generated stress contour plot and a glass fracture pattern from a test conducted on a specimen loaded under similar conditions.



Fracture Pattern  
from Pressure Test



Computer Generated  
Stress Contour Plot

Figure 50. Stress Pattern in Flat Windshield.

A simple method that may be used to determine whether or not an analysis is valid is to check the mid-plane stress. If the mid-plane stress is low in comparison to the NASTRAN computed element stresses, the analysis is valid. Mid-plane stress can be calculated by first calculating the strain between elements based on their relative deflections and spacing and then multiplying that value by the modulus of elasticity for the material.

When the mid-plane stresses are high in relation to the NASTRAN calculated values, the results are invalid and other means must be used for analysis. This was shown to be the case for typical helicopter flat windshields.

#### Effects of Elastic Supports

Conventional structural analyses of plates are based on the assumption that the plate is supported along its perimeter by a rigid member. The plate edges may be considered either simply supported or clamped. However, helicopter windshields are actually supported by structures having considerable elasticity as shown in Figure 51. In the extreme case, a rigid plate mounted to a flexible substructure is supported only at its corners.

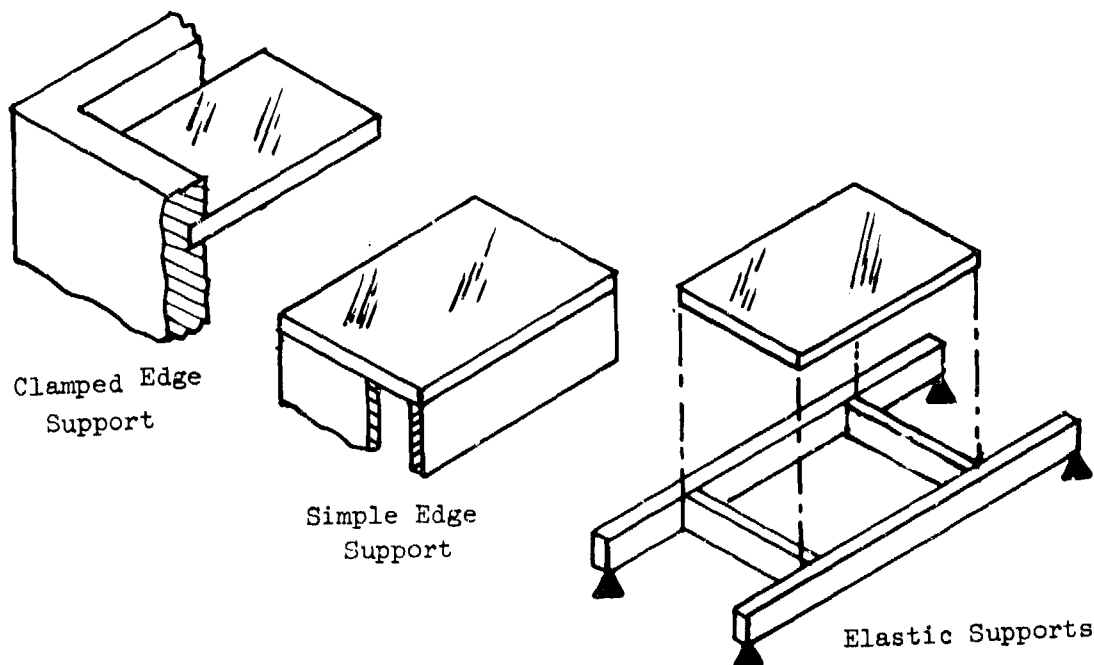


Figure 51. Support Constraints for Plate Analysis.

To gain perspective on how windshield loading and substructure elasticity interact, the analysis of the flat laminated glass/glass windshield under 1 psi pressure is reviewed. Even though NASTRAN could not accurately predict stresses and deflections for the windshield, the effect of the pressure loads on the structure supporting the windshield are within NASTRAN's capability. The structure supports windshield pressure loads as beams in bending, a structural condition for which NASTRAN analyses are considered to be reliable.

Two structural effects of elastic windshield supports are readily detectable in the computer generated displacement plot shown in Figure 52. In the illustration, the total deflection is divided into 14 equal increments, with each increment, or iso-displacement, represented by one line forming a contour plot of the deflected windshield. First, it may be observed that several iso-displacement lines intersect each edge of the windshield, indicating a pronounced sagging of the supports. For example, the maximum displacement midspan on the long edges is 0.178 inch, a value which by itself exceeds the thickness of the windshield, and would therefore be suspected to have a significant effect on analyses based on rigid supports.

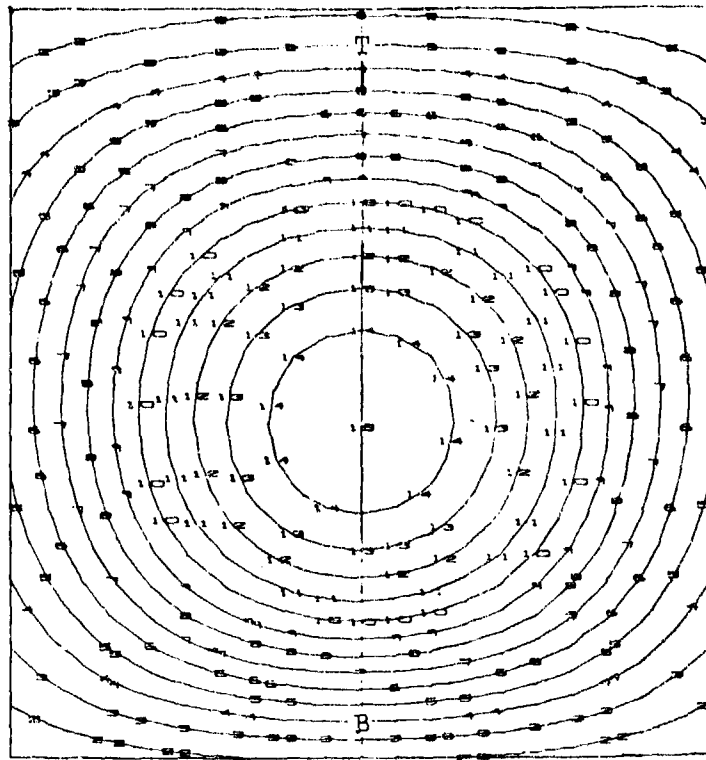
The second observation, of less significance, is that the maximum displacement is not at the center of the windshield, but more towards the lower sill. This is due to the bottom sill having a lower stiffness than the upper sill.

#### Transparency Curvature Effects

The effects of transparency curvature on windshield stresses were evaluated by examining the 0.3 psi aerodynamic pressure load analysis of the laminated glass/glass center and outboard windshield panels.

Table 19 summarizes maximum windshield deflections, stresses, and edge forces from this analysis. The edge forces are the in-plane edge loads perpendicular to the windshield edge, and the shear forces are parallel to the edge of the windshield. They are used to establish fastener and edge reinforcement requirements.

Peak stresses for this condition occurred at the approximate geometric center of the flat center windshield. Since the aerodynamic pressure loading was assumed to be inward acting, the highest stresses for this condition were compressive. The maximum compressive stress in the center windshield was 2345 psi, while the maximum compressive stress in the outboard curved windshields was only 942 psi, despite the outboard panels having approximately twice the area of the center panel. To bring these values further into perspective, the ratio of normalized bending stresses for flat windshields having plan-form areas equivalent to the center and outboard panels,



Symbol	Deflection (in.)
1	.000
2	.044
3	.089
4	.133
5	.178
6	.222
7	.267
8	.311
9	.356
10	.400
11	.445
12	.489
13	.534
14	.579
15	.623

Figure 52. Deflections, 1 psi Pressure Load, Glass/Glass Windshield.

TABLE 19. STRESSES AND EDGE FORCES IN WINDSHIELDS - 0.3 PSI PRESSURE

Parameter	Center Windshield		Outboard Windshield	
	Linear Static Solution	Differential Stiffness Solution	Linear Static Solution	Differential Stiffness Solution
Max Major Principal Stress (psi)				
Outboard Surface	-1007 (4871)	-1311 (4871)	558 (4889)	97 (5912)
Inboard Surface	1347 (4871)	1824 (4871)	505 (4889)	686 (5912)
Max Minor Principal Stress (psi)				
Outboard Surface	-1869 (4871)	-2345 (4871)	86 (5892)	149 (5892)
Inboard Surface	1063 (4871)	1356 (4871)	-799 (5892)	-942 (5892)
Max Normal Edge Load (lb/in.)				
Lower Sill	-19 (4877)	-19 (4877)	-48 (4964)	-48 (4964)
B.L. 10 Post	80 (4877)	79 (4877)	84 (4889)	80 (4889)
Upper Sill	-8 (4876)	-9 (4876)	-21 (4962)	-21 (4962)
Outboard Post	-	-	-43 (4964)	-42 (4964)
Max Edge Shear Flow (lb/in.)				
Lower Sill	6 (4877)	4 (4877)	41 (4964)	41 (4964)
B.L. 10 Post	6 (4877)	25 (4887)	28 (4897)	30 (4897)
Upper Sill	9 (4876)	9 (4876)	25 (4923)	27 (4923)
Outboard Post	-	-	52 (4961)	52 (4961)

NOTE - Second number in parenthesis is element location.

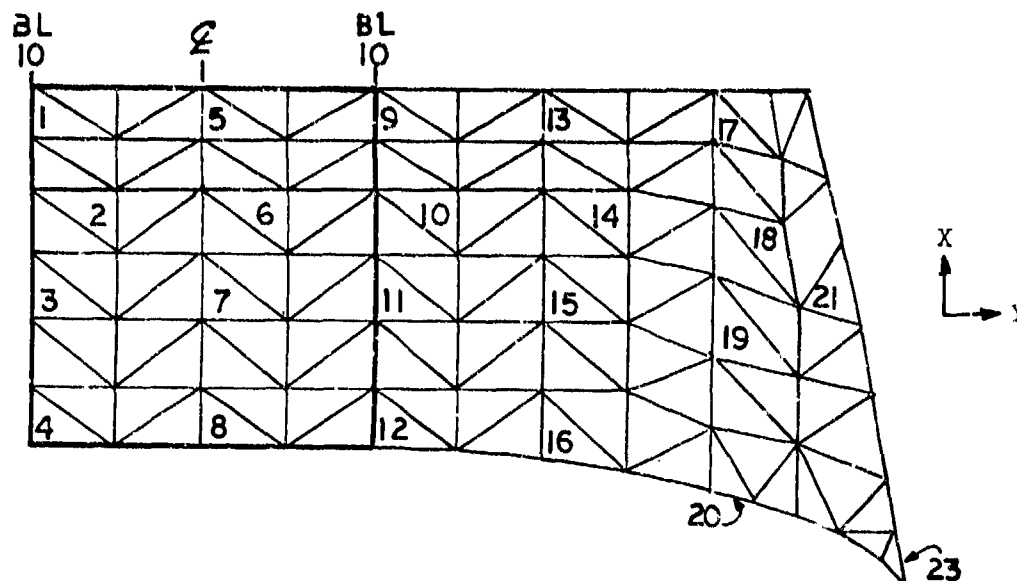
was calculated. The bending stresses were considered to be proportional to  $Kb^2$ , where  $b$  is the shortside length of the panel, and  $K$  is a shape factor, equal to 0.482 for the rectangular center windshield, and 0.297 for the square outboard panel. Using these relationships, the bending stresses in the larger outboard panel would have been approximately 20% higher than those in the center panel were it not for the effects of curvature.

Curvature has the effect of creating in-plane forces that tend to relieve bending stresses. This effect can be seen in Figure 53, which shows a distribution of normal stresses for selected elements of the windshields. The numbered "points" in the figure refer to triangular plate elements, and the stresses reported are the average stresses occurring in each. Bending and in-plane components of the normal stress are also given. The illustration shows that the stresses in the outboard panel were predominantly in-plane, while the stresses in the center panel were predominantly bending. It is interesting to note that the YUH-60A windshield used in this example has mild curvature, transitioning from a flat shape at B.L. 10 to a 16-inch radius of curvature tangent to the outboard post.

Figure 54 shows corner and center deflections for the outboard windshield. The relative displacement between the center of the windshield and each corner is also shown in the illustration. The maximum deflection measured relative to a corner (lower left) was 0.048 inch, which is less than half the panel thickness, and therefore within the limits of acceptability for thin plate stress analysis.

The effects of the complex geometry and structural elasticity on the windshield stress distribution can be seen in Figure 55, which shows windshield in-plane loads normal to the B.L. 10 posts.

Differential stiffness showed only slight changes for the stresses in the outboard area of the windshield, but significant increases for the center panel. This occurred because the large displacements and stresses in the center region had a greater effect on altering geometry than the small loads and displacements in the outboard region, as shown in Figure 56.



Point	NASTRAN Element No.	Normal Stress, Y Direction (psi)		In-Plane Component (psi)	Bending Component (psi)
		Outer Surface	Inner Surface		
1	5887	-152	92	30	-122
2	5884	-570	510	-30	-540
3	5881	-240	-232	-236	4
4	5877	-28	-170	-99	71
5	4875	759	-769	-5	764
6	4872	-866	809	-28	-837
7	4869	-1220	1300	40	-1260
8	4965	801	-788	6	794
9	4899	-126	41	-42	-83
10	4896	91	-148	-28	119
11	4893	-260	-191	-225	-34
12	4889	-26	-170	-98	72
13	4923	-231	296	32	-263
14	4920	27	52	39	-12
15	4917	166	91	128	37
16	4913	-143	120	-11	-131
17	4948	-46	50	2	-48
18	4945	-104	-148	-126	22
19	4942	-84	-4	-44	-40
20	4937	-	-	-	-
21	4957	-21	10	-5	-15
22	4953	108	-133	-12	120
23	4964	-51	-450	-250	199

Figure 53. Stress Distribution, 0.3 psi Pressure Condition, Glass/Glass Windshield.

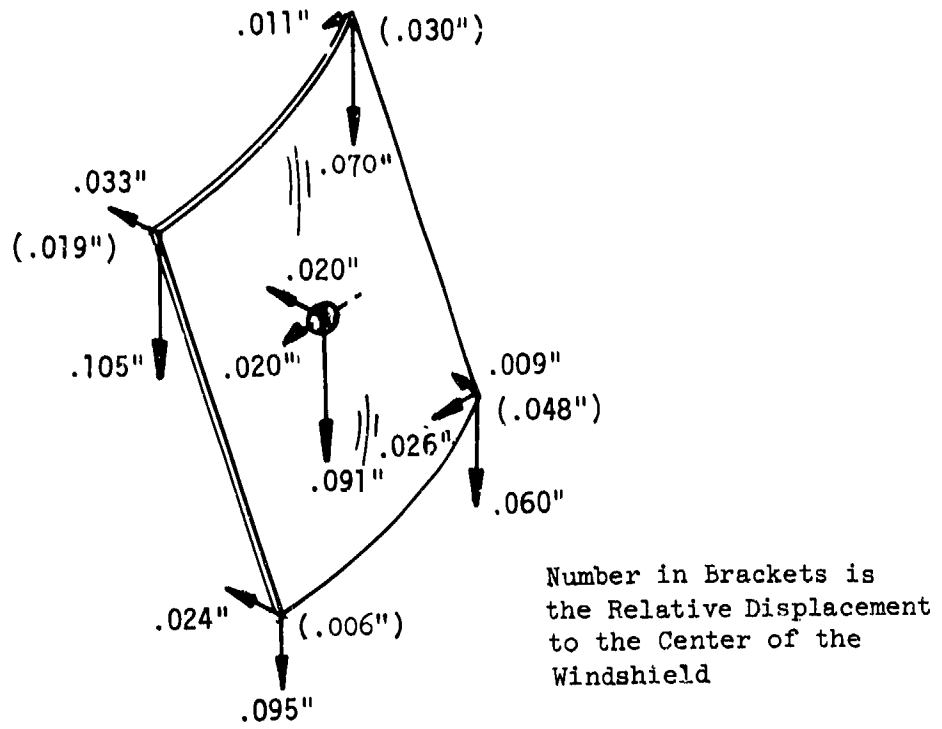


Figure 54. Windshield Deflections Under 0.3 psi Pressure, Outboard Glass/Glass Panel.

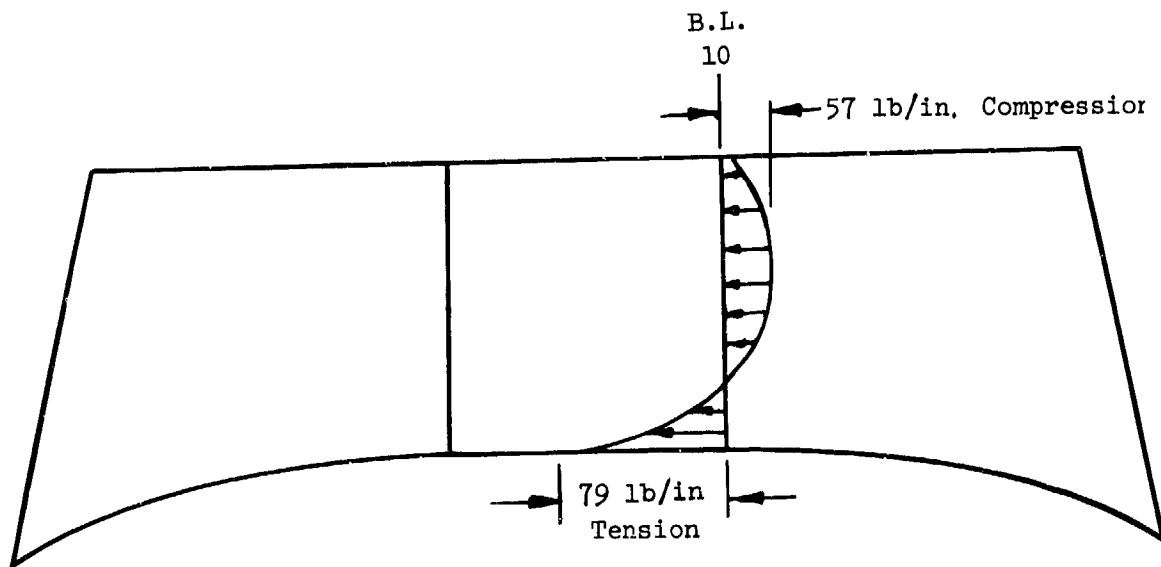
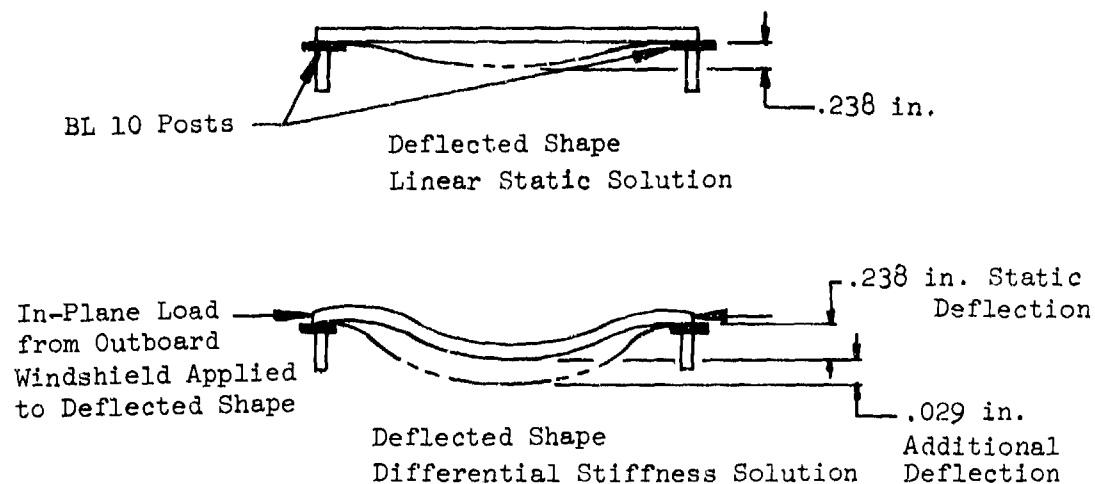


Figure 55. In-Plane Forces Normal to B.L. 10 Post, 0.3 psi Pressure Loading Condition.



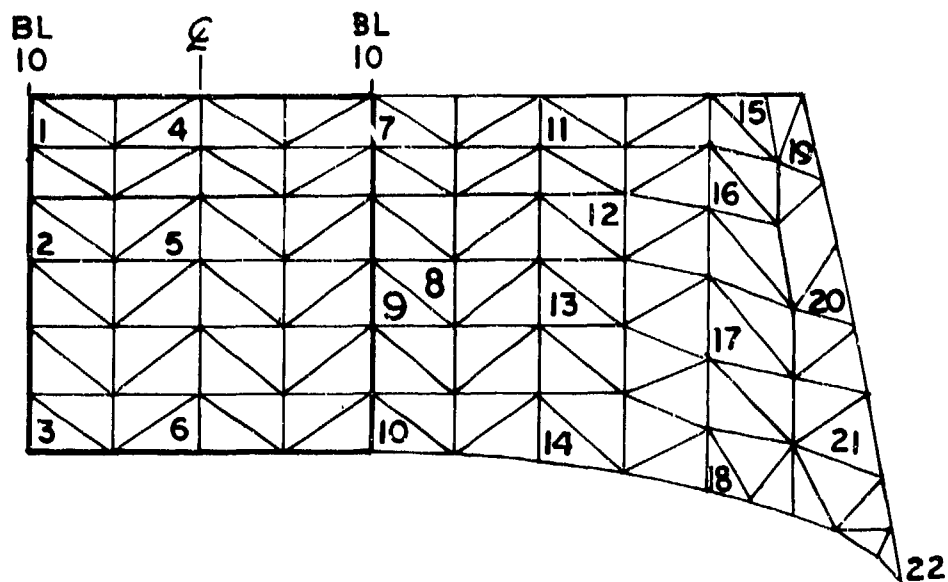
**Figure 56. Differential Stiffness Effects on Center Windshield Deflections.**

#### Panel Interaction/Load Sharing Effects

The entire cockpit structure was analyzed for a 1.0 psi pressure applied to the laminated glass/glass center windshield only to show panel interaction or load sharing effects. Although the calculated stresses in the center windshield were known to be unreliable, for reasons discussed earlier, load sharing trends between the center and outboard windshields were clearly discernable. For this case, the outboard windshields, like the center windshield, were also glass/glass laminates.

Figure 57 shows the distribution of major principal stresses in both windshields. The maximum stress calculated for this condition was 7807 psi located approximately in the middle of the center windshield. The effect of panel interactions was evident by the presence of stresses of up to 2757 psi in the unloaded outboard windshields. The stresses in the outboard panel diminished as the distance from the center panel increased.

Maximum and average windshield edge forces are presented in Table 20. These are the forces that are transmitted from the loaded center windshield to the adjacent outboard windshield and structure.



**Major Principal Stress  
(psi)**

Point	NASTRAN Element No.	Outer Surface	Inner Surface
1	5887	1973	1547
2	5883	3018	-762
3	5877	1784	1562
4	5875	3260	1532
5	5871	-5166	7807
6	5965	2729	637
7	4899	1560	942
8	4894	2141	-383
9	4893	2757	-507
10	4889	1021	1003
11	4923	-22	423
12	4920	215	213
13	4917	510	359
14	4913	-7	268
15	4948	48	-14
16	4946	75	30
17	4942	3	12
18	4937	522	-179
19	4961	110	288
20	4957	165	-80
21	4953	99	-78
22	4964	175	-11

**Figure 57. Major Principal Stress, 1 psi Pressure  
On Center Windshield, Differential  
Stiffness Solution.**

TABLE 20. EDGE FORCES IN WINDSHIELDS, 1 PSI PRESSURE ON CENTER WINDSHIELD (DIFFERENTIAL STIFFNESS SOLUTION)

Parameter	Center Windshield		Outboard Windshield	
	Maximum Value	Average Value	Maximum Value	Average Value
Normal Edge Load (lb/in.)				
Lower Sill	157	152	92	91
B.L. 10 Post	-109	65	103	63
Upper Sill	-85	76	-69	31
Outboard Post	-	-	-54	21
Edge Shear Flow (lb/in.)				
Lower Sill	-19	10	49	13
B.L. 10 Post	-23	18	87	57
Upper Sill	-10	9	39	18
Outboard Post	-	-	19	10

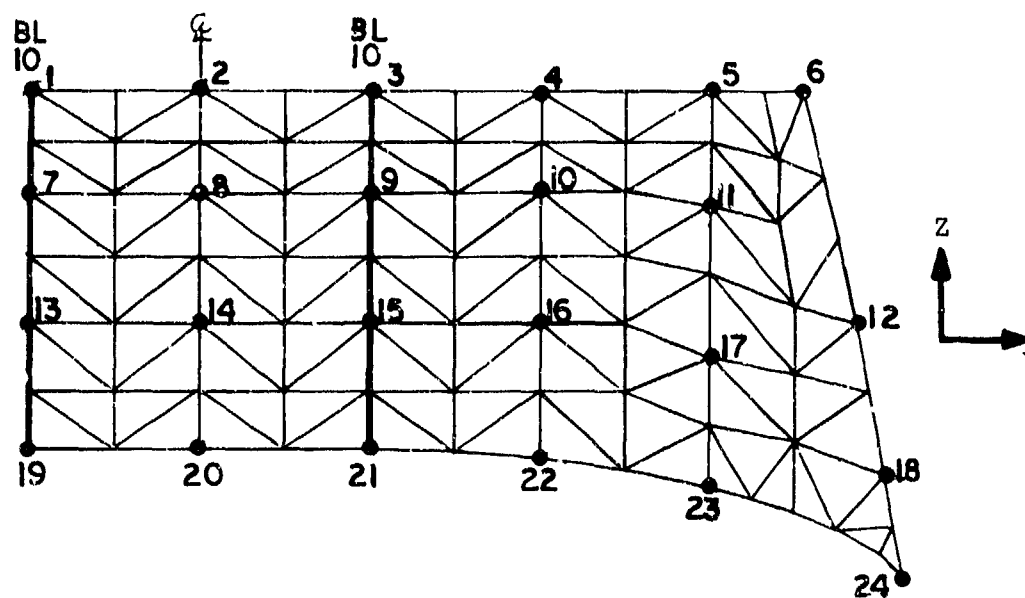
The distribution of displacements for selected points on the windshields are shown in Figure 58. This distribution shows how pressure applied to the center windshield caused the entire structure to deform, thereby causing adjacent transparencies to share the load.

#### Fuselage Deformation Effects

To evaluate the effects of fuselage structural deformation on windshield stress, a NASTRAN analysis of the airframe undergoing a severe flight maneuver, with and without windshields installed, was conducted.

Two flight conditions for the YUH-60A were initially investigated. The first condition represented the inertial loading on the airframe during a symmetrical pullout maneuver. This condition produced critical down-bending loads in the area of the cockpit. The second condition was for the aircraft performing a rolling pullout to the right. This condition produced critical side-bending loads in the cockpit.

Table 21 shows the accelerations on the airframe under these conditions.



Point	NASTRAN Grid No.	Displacements (in.)		
		x	y	z
1	9510	.061	.000	-.149
2	8390	.085	.000	-.175
3	8510	.060	.000	-.149
4	8630	.017	-.003	-.102
5	8750	-.008	-.010	-.075
6	8800	-.010	-.011	-.073
7	9490	.110	.000	-.202
8	8370	.361	.000	-.471
9	8490	.110	.000	-.202
10	8610	.003	-.006	-.088
11	8730	-.008	-.010	-.076
12	8850	-.023	-.023	-.062
13	9470	.102	.000	-.193
14	8350	.394	.000	-.507
15	8470	.102	.000	-.193
16	8590	.000	-.007	-.084
17	8710	-.009	.011	-.074
18	8830	-.028	-.027	-.057
19	9080	.038	.001	-.123
20	8020	.062	.000	-.150
21	8080	.030	-.000	-.124
22	8140	.008	-.004	-.093
23	8200	-.014	-.013	-.069
24	8330	-.025	-.022	-.060

Figure 58. Displacements, 1 psi Pressure on Center Windshield, Differential Stiffness Solution.

TABLE 21. YUH-60A LINEAR AND ANGULAR ACCELERATIONS FOR TWO DESIGN FLIGHT LOAD CONDITIONS

Linear Accelerations on Aircraft (g's)			
Condition	$N_x$	$N_y$	$N_z$
Symmetrical Pullout Maneuver	0.77	0.069	2.514
Rolling Pullout to Right	0.255	0.650	0.235

Angular Accelerations on Aircraft (Rad/Sec <sup>2</sup> )			
Condition	$a_x$	$a_y$	$a_z$
Symmetrical Pullout Maneuver	1.96	1.89	-0.2786
Rolling Pullout to Right	-0.7044	-0.3542	1.3646

Preliminary analysis of canopy displacements resulting from these two loading conditions indicated that vertical bending produced the most critical loading for the windshields. As a result, only the symmetrical pullout condition was used in subsequent analyses. The symmetrical pullout maneuver is schematically depicted in Figure 59.

Vertical and horizontal shears, drag loads and bending moments were obtained for this condition at stations along the aircraft from computerized load calculations. These loads were resolved into components that were applied at grid points corresponding to the panel points of the aircraft. A panel point is a mass center of gravity at a specified station.

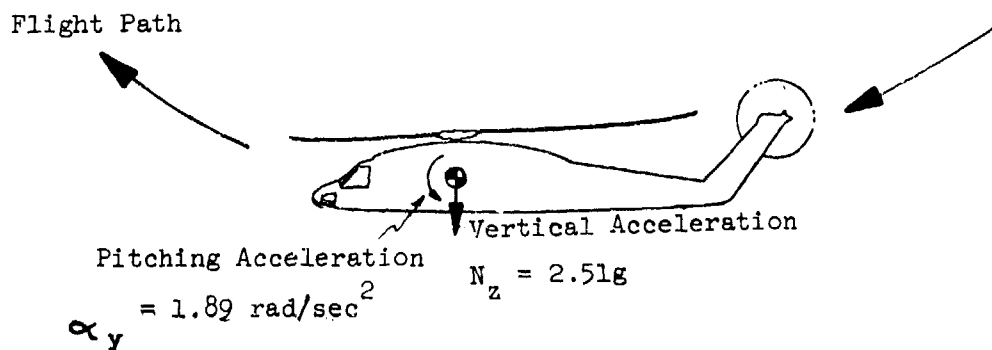


Figure 59. Symmetrical Pullout Maneuver.

Table 22 compares the maximum internal loads in the windshield support structure from cockpit vertical bending for two cases, with and without a windshield. For the with-windshield situation, the glass/glass laminated construction was assumed. These cases are shown schematically in Figure 60. Two moments are listed for each element. The primary value is for bending in the plane of the deepest dimensions, and the secondary value is for bending in the plane of the shortest dimensions, as shown in Figure 61. These results show that significant redistribution of internal loading occurred, which can only be attributed to the stiffening effect of the windshield on the overall structure.

TABLE 22. COMPARISON OF LOADS IN WINDSHIELD SUPPORT STRUCTURE, VERTICAL BENDING CONDITION (DIFFERENTIAL STIFFNESS SOLUTION)

	Load With Windshield	Load Without Windshield
Axial Load (lb)		
Lower Sill	95	1443
B.L. 10 Post	51	520
Upper Sill	-124	112
Outboard Post	-217	19
Moments (in.-lb)		
Lower Sill*	94	-5053
Lower Sill**	1203	640
B.L. 10 Post*	19	897
B.L. 10 Post**	946	2078
Upper Sill*	1653	1031
Upper Sill**	1024	492
Outboard Post*	721	380
Outboard Post**	799	905

\* Bending moment about smallest bending section.

\*\* Bending moment about largest bending section.

Table 23 compares the differential stiffness solution and linear static solution for maximum axial loads and bending moments in the windshield supports for the no-windshield loading case.

The differential stiffness analysis showed moderate changes in all loads as compared to the linear static solution, except at the lower sill. The loads in the lower sill were shown to increase substantially when differential stiffness was used, with displacements also drastically changed. The reason for this was because the lower sill was located on a contour crease line and was basically unstable without support from the windshield.

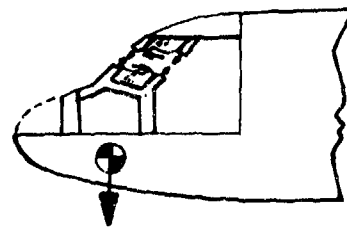
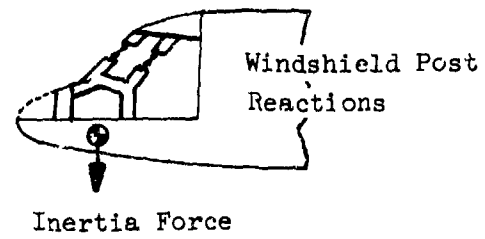


Figure 60. Schematic Representation of Windshield Structure Reaction to Inertia Loading.

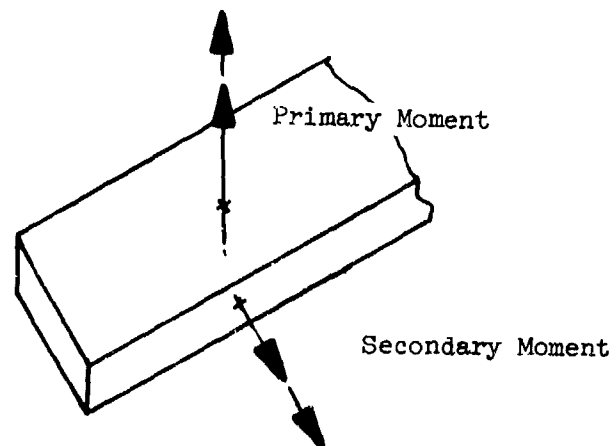


Figure 61. Moment Definition for Posts and Sills.

TABLE 23. COMPARISON OF LINEAR STATIC AND DIFFERENTIAL STIFFNESS SOLUTIONS, VERTICAL BENDING CONDITION (WINDSHIELD OMITTED FROM MODEL)

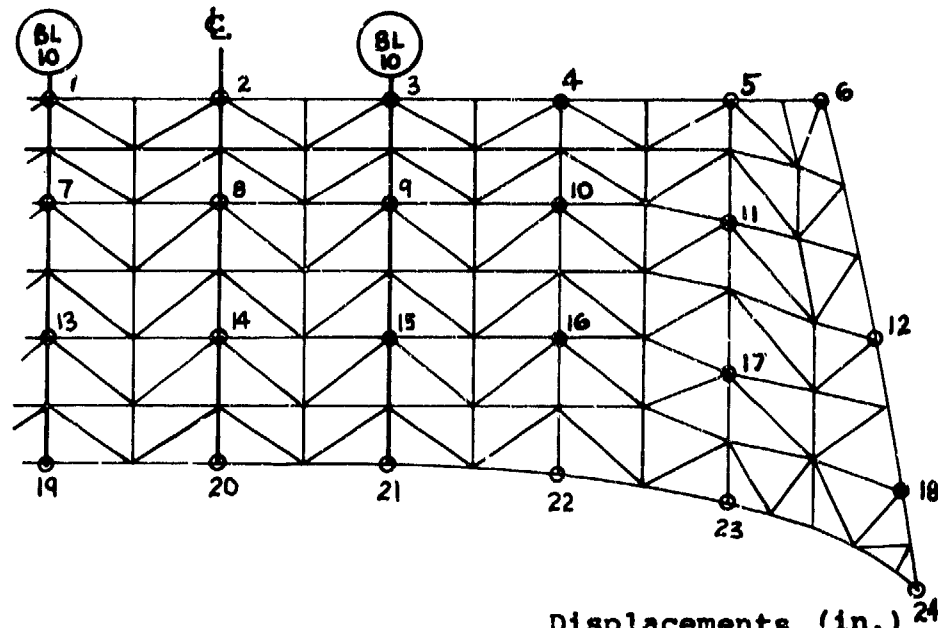
Location	Linear Static Solution		Differential Stiffness Solution	
	Maximum Moment (in.-lb)	Maximum Axial Load (lb)	Maximum Moment (in.-lb)	Maximum Axial Load (lb)
Lower Sill	491	-293	640	1443
B.L. 10 Post	2525	588	2078	520
Upper Sill	1094	-253	1031	112
Outboard Post	822	163	905	19

While the loads induced in the canopy structural elements were small in relation to the overall cockpit loading, they were significant with respect to the individual members. More important, however, were the displacements that occurred around the perimeter of the windshields. Figure 62 compares displacements for the same flight condition, with and without the windshields installed.

Insight as to the significance of these displacements can be gained by observing the deflection modes of the structure. Figure 63 shows the deformed outboard windshield structure superimposed on the undeformed shape. This illustration shows graphically how fuselage racking tended to warp and twist the windshield's cavity. Although windshields are normally mounted with a certain degree of flexibility via oversize holes and gaskets, for the conditions analyzed, the displacements and loads were large, and could not be absorbed entirely by edge attachment flexibility.

Figure 64 is a profile view of the center post deflected shape. Note that the post had a maximum camber of approximately 1/16 inch. Since the post was stiffer than the windshield, this camber was certain to induce windshield stresses, and when the vertical bending condition was reanalyzed with the windshield in the model, maximum tensile stresses in the windshield were calculated to be approximately 2000 psi. The highest stresses were located at, and adjacent to, the edges, which was to be expected since the loads are applied at the edges. The distribution of major principal stresses for this case is shown in Figure 65.

The distribution of in-plane windshield forces normal to the center posts is plotted in Figure 66. Additional edge force data is presented in Table 24. These distributions are indicative of how cockpit deflections induced in-plane bending loads in the windshields.



Point	NASTRAN Grid No.	Displacements (in.)					
		Without Windshield			With Windshield		
		x	y	z	x	y	z
1	9510	.125	.000	-1.144	.084	-.006	-.889
2	8390	.104	.000	-1.198	.135	-.006	-.945
3	8510	.128	.001	-1.158	.088	-.006	-.996
4	8630	.030	-.004	-1.034	-.033	-.015	.766
5	8750	-.062	-.029	-0.855	-.109	-.032	-.675
6	8800	-.082	-.034	-0.718			
7	9490	.097	.028	-1.119	.095	-.006	-.902
8	8370	-	-	-	.169	-.005	-.982
9	8490	.102	-.041	-1.135	.101	-.005	-.910
10	8610	-	-	-	-.041	-.017	-.758
11	8730	-	-	-	-.101	-.037	-.692
12	8850	.009	-.064	-0.779	-.134	-.078	-.648
13	9470	-.057	.050	-0.963	.061	-.005	-.864
14	8350	-	-	-	.112	-.005	-.921
15	8470	-.051	-.109	-0.981	.068	-.005	-.874
16	8590	-	-	-	-.030	-.015	-.770
17	8710	-	-	-	-.086	-.038	-.707
18	8830	-.127	-.062	-0.688	-.144	-.106	-.635
19	9080	-.158	-.039	-0.863	.013	-.003	-.814
20	8020	.231	-.043	-0.498	.049	-.004	-.852
21	8080	-.152	-.047	-0.879	.021	-.005	-.824
22	8140	-.183	-.040	-0.854	-.014	-.011	-.788
23	8200	-.197	-.053	-0.787	-.070	-.041	-.715
24	8330	-.142	-.053	-0.681	-.126	-.091	-.648

Figure 62. Displacements, Vertical Bending, Differential Stiffness Solution.

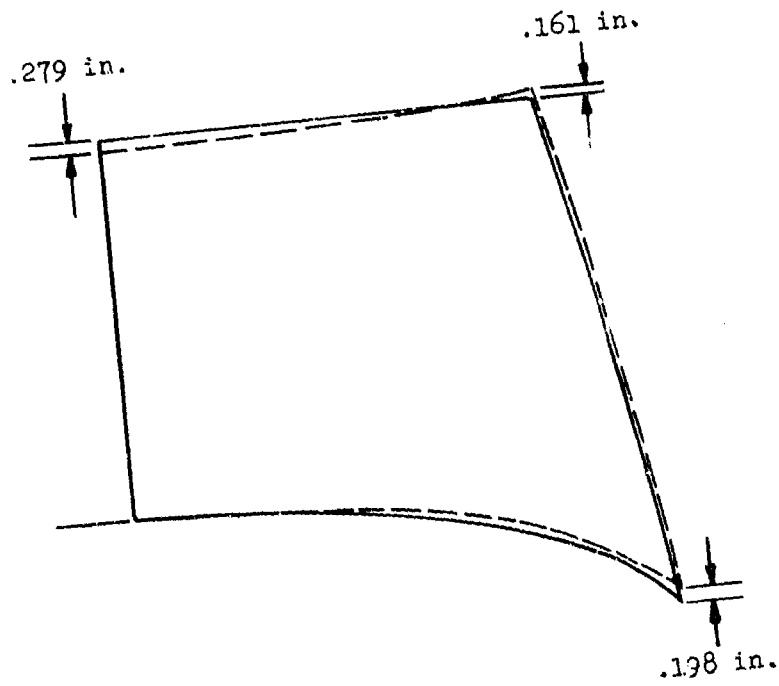


Figure 63. Deformed Shape of Windshield Cavity.

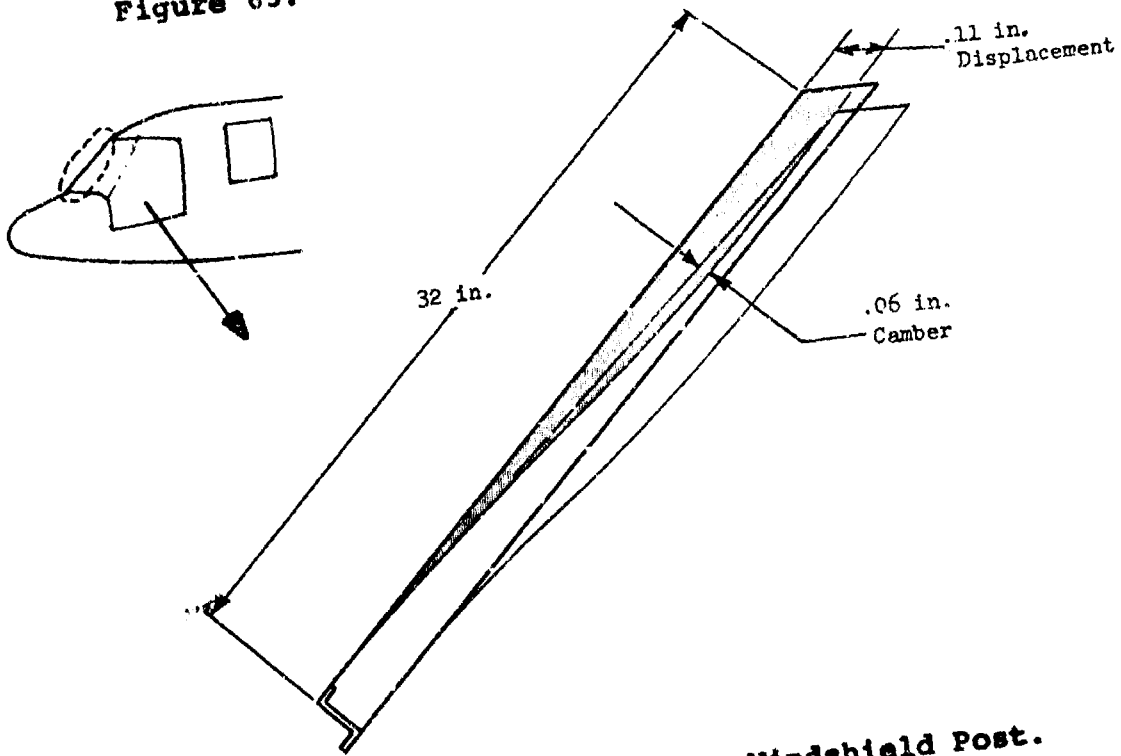
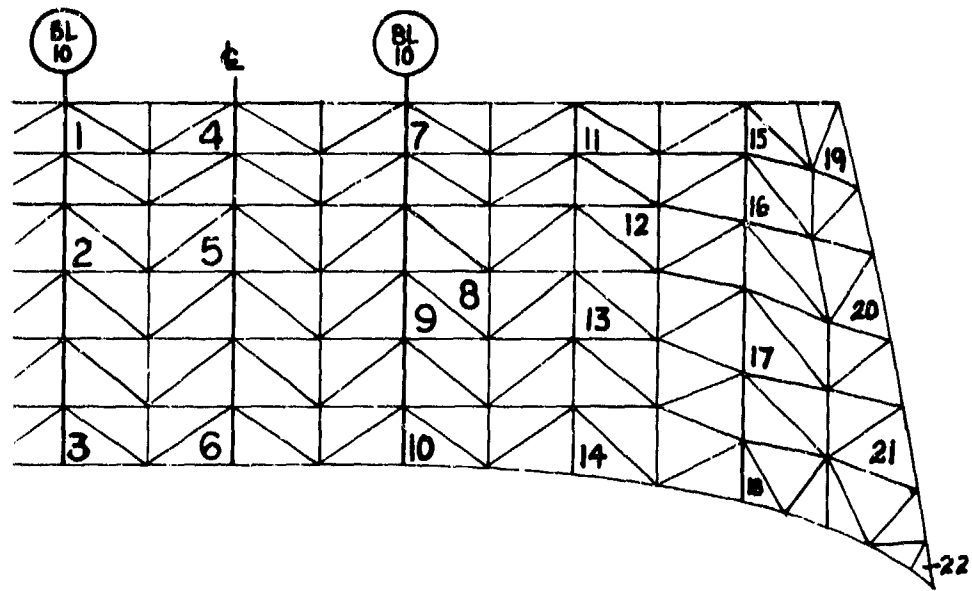


Figure 64. Deflection Mode for Windshield Post.



Point	NASTRAN Element No.	Major Principal Stress (psi)	
		Outer Surface	Inner Surface
1	5887	-269	1047
2	5883	-375	505
3	5877	1765	1392
4	5875	-459	494
5	5871	-852	1039
6	5965	546	1738
7	4899	-404	1528
8	4894	-174	418
9	4893	-87	1055
10	4889	1654	2132
11	4923	202	146
12	4920	604	239
13	4917	606	228
14	4913	767	1387
15	4948	36	128
16	4946	425	281
17	4942	339	326
18	4937	225	-28
19	4961	491	1848
20	4957	724	-226
21	4953	800	-482
22	4964	1145	-289

Figure 65. Major Principal Stresses, Vertical Bending Condition, Differential Stiffness Solution.

TABLE 24. EDGE FORCES IN WINDSHIELDS, VERTICAL BENDING  
CONDITION (DIFFERENTIAL STIFFNESS SOLUTION)

Parameter	Center Windshield		Outboard Windshield	
	Maximum Value	Average Value	Maximum Value	Average Value
Normal Edge Load (lb/in.)				
Lower Sill	147	198	299	118
B.L. 10 Post	140	52	153	52
Upper Sill	-74	40	-195	134
Outboard Post	-	-	346	143
Edge Shear Flow (lb/in.)				
Lower Sill	150	129	263	59
B.L. 10 Post	108	97	102	61
Upper Sill	29	22	200	64
Outboard Post	-	-	144	75

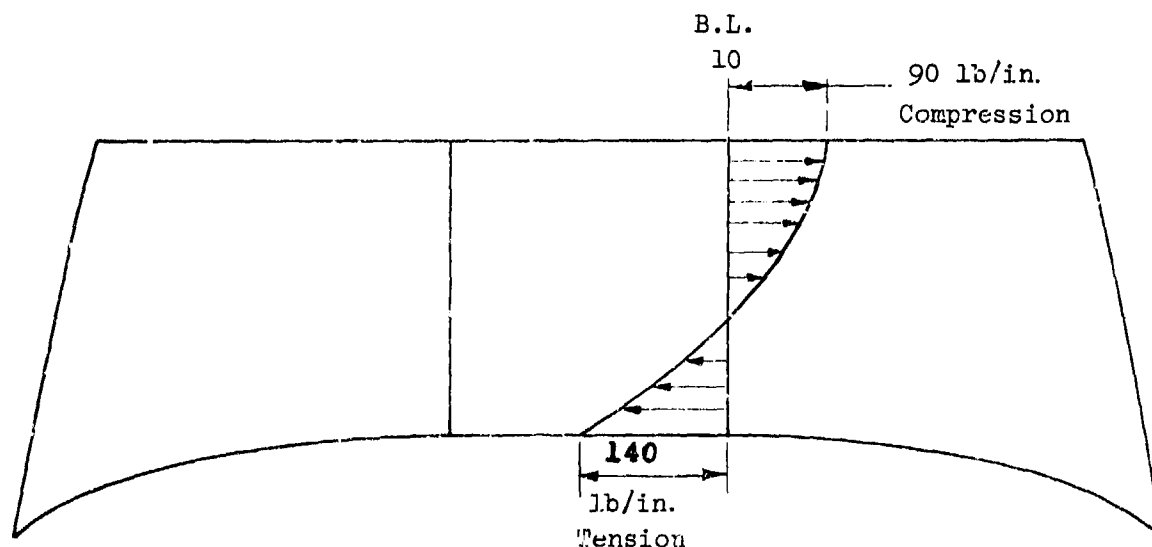


Figure 66. In-Plane Forces Normal to B.L. 10 Post,  
Vertical Bending Condition.

#### Interactive Effects of Combined Loading

As would be expected, when the pressure loading and vertical bending cases were combined, the resultant stresses were higher than for either case alone. The highest tensile stress, 4231 psi, for this condition again occurred in the center flat panel. A comparison of stresses for the three conditions is given in Table 25. However, it should be kept in mind that the calculated stresses in the center windshield for 0.3 psi pressure were inaccurate, and the information is therefore useful only for trending purposes.

TABLE 25. DEFLECTIONS AND STRESSES FOR THREE LOADING CONDITIONS

	Center Windshield			Outboard Windshield		
	(1)	(2)	(3)	(1)	(2)	(3)
	0.3 psi Pressure	Vertical Bending	Vertical Bending Combined	0.3 psi Pressure	Vertical Bending	Vertical Bending Combined
Total Deflection (in.)	0.267	1.064	1.283	0.100	0.835	.927
x component	0.195	0.109	0.348	0.025	0.030	0.060
y component	0.000	-0.006	-0.010	0.000	-0.008	-0.012
z component	-0.225	-0.982	-1.235	-0.097	-0.834	-0.925
Max Major Principal Stress (psi)						
Outboard Surface	801	1813	2584	97	2510	1948
Inboard Surface	1824	1469	4231	686	118	2576
Max Minor Principal Stress (psi)						
Outboard Surface	-2345	-1708	-5228	149	1560	-1560
Inboard Surface	1356	877	3414	-942	3698	-3698

## NASTRAN CONCLUSIONS

1. The NASTRAN finite element analysis was found to be suitable for the analysis of homogeneous transparencies of the following types:
  - a. Flat plates and curved shells where the transverse deflections are small in comparison to the thickness of the part.
  - b. Curved shells where the pressure loads are resisted by in-plane forces (similar to hoop tension or compressive arch).
2. It was found that the NASTRAN analysis was not suitable for the analysis of transversely loaded flat plates where the load is carried partially or entirely by membrane effects. Flat helicopter transparencies generally fall into this category.
3. The NASTRAN analyses conclusively showed how fuselage racking can and does induce loads into transparencies. For the specific loading and airframe stiffnesses analyzed, these loads were found to be approximately the same magnitude as the primary pressure loads.
4. The effect of complex geometry and elastic support constraints on transparency stresses and deflections were readily analyzed by NASTRAN.
5. It is essential to use differential stiffness in the analysis of helicopter transparent enclosures because of the relatively large displacements that occur. These displacements significantly alter the geometric matrices used for computing stresses and deflections, and must be compensated for to obtain accurate results. It was shown that differential stiffness solutions can alter the results of a linear static analysis by over 100%.
6. It is essential to have a very accurate model representation of the stiffness of the windshield's backup structure. This is necessary because windshield stresses and deflections calculated by NASTRAN are sensitive to structural support constraints.

## THERMAL EXPANSION, INSTALLATION PRELOAD AND ASSEMBLY TESTS

The purpose of this series of tests was to measure the stress levels induced in three different windshield design configurations from:

Differential thermal expansion between windshield material and support structure

Loading of the windshield attachment supports

Contour mismatch on installation

A typical composite windshield is generally composed of three plies, including a glass facing, an interlayer, and a glass or plastic facing, which are attached to the airframe by an edge reinforcement. The thermal expansion coefficient and the modulus of elasticity of each of these laminate materials are significantly different from each other and result in different rates of expansion with temperature variation. The edge reinforcement introduces still another component influencing thermal expansion. The thermal expansion stresses in such configurations are not readily determined by analysis, and a series of tests were conducted to measure them.

Axial loads applied to transparency support structures can induce secondary loads in the transparency when tight-fitting fasteners are used for installation. The series of tests described herein were performed to determine the amount of structural isolation provided by typical laminated edge reinforcements.

During assembly, windshields do not exactly match the contour of the canopy structure because of manufacturing tolerances. The effects of induced stresses due to various degrees of contour mismatch between windshields and structure were also evaluated to provide data for establishing installation tolerances.

Table 26 lists the different tests that were performed.

TABLE 26. EDGE ATTACHMENT, THERMAL EXPANSION AND  
INSTALLATION PRELOAD TESTS

Number	Description	Parameters
1	Tensile Stiffness	Measure axial spring rate of edge attachment
2	Cold Soak	Determine facing stresses at -65°F
3	Hot Soak	Determine facing stresses at +160°F
4	Installation Pre-load	Determine facing stresses as a function of contour mismatch
5	Assembly Test	Compare facing strain with support strain when axial load is applied to support (tight fitting fasteners, neoprene gasket, 30 in.-lb torque)
6	Assembly Test	Determine facing stresses at -65°F (fastened to post)
7	Assembly Test	Determine facing stresses at +160°F (fastened to post)
8	Assembly Test	Same as 5 except loose fitting fasteners, 30 in.-lb torque
9	Assembly Test	Same as 8 except wet sealant used between transparency and support
10	Assembly Test	Same as 8 except 10 in.-lb torque on fasteners

## Materials

Three different 24-inch-square laminated sample windshield configurations (Figure 67) were tested. The first configuration consisted of a glass outer surface, a polyvinyl butyral (PVB) interlayer, a plastic (stretched acrylic) inner surface, with a bonded Acrylonitrile Butadiene Styrene (ABS) edge reinforcement. The second configuration had glass inner and outer surfaces, a PVB interlayer and a bonded fiberglass edge reinforcement. The third configuration was the same as the second except for a bonded flexible impregnated fabric edge reinforcement.

## TENSILE STIFFNESS TEST

Tensile stiffness tests were conducted on each of the three specimens by application of incremental tensile loads to one edge of each specimen using a hydraulic cylinder. A calibrated load cell in series with the cylinder and the test article was used to measure applied load. 500-lb incremental loads were applied to a maximum of either 5000-lb load, 0.010-inch specimen elongation or 3000 psi resultant stress in the windshield. Resultant strains and specimen elongation between points 10 inches apart were measured at each load increment. Figure 68 shows the test setup.

## Results (Tensile Stiffness Test)

The laminated glass with rigid fiberglass edge reinforcement, the second configuration in Figure 67, was found to be the stiffest design and exhibited a spring rate of approximately 233,000 lb/in. The composite glass/plastic design had a spring rate equal to 7700 lb/in. and the laminated glass panel with flexible edging had a spring rate of only 2100 lb/in. The spring rates are compared in Figure 69.

Figure 70 presents plots of resultant stress vs load for each configuration. Testing of the glass/acrylic configuration was stopped at 500-lb load when the deflection limit was reached. The initial compression stresses in the glass in this configuration were attributed to a warped condition of the specimen prior to loading. In the free state, the glass/acrylic panels were slightly bowed, and the initial tensile loading caused the panels to straighten out, which induced a compressive stress in the glass facing. The effect of straightening was more pronounced for the glass ply because of its higher modulus, which is an order of magnitude greater than that for stretched acrylic.

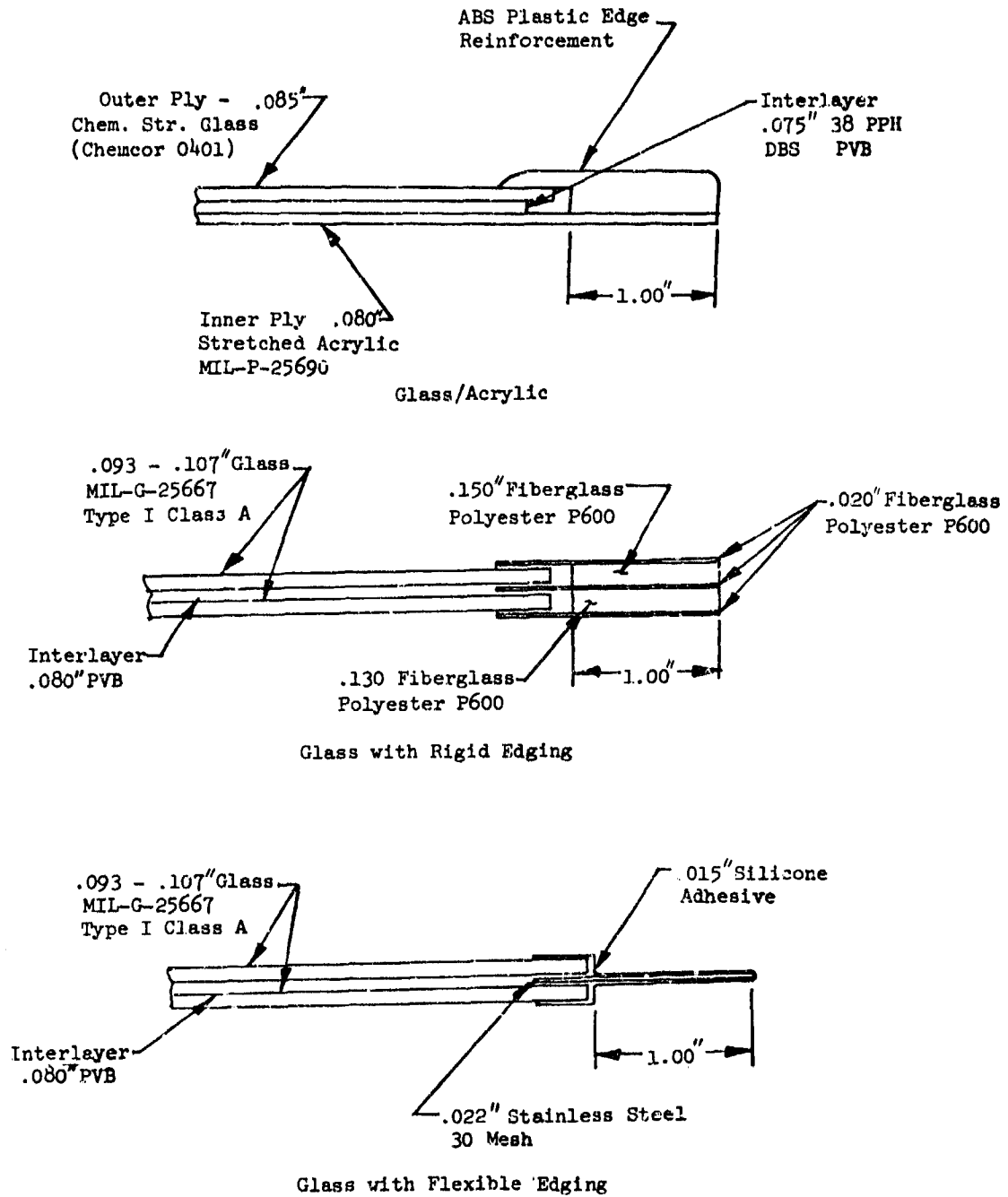


Figure 67. Laminated Test Specimen Edge Configurations.

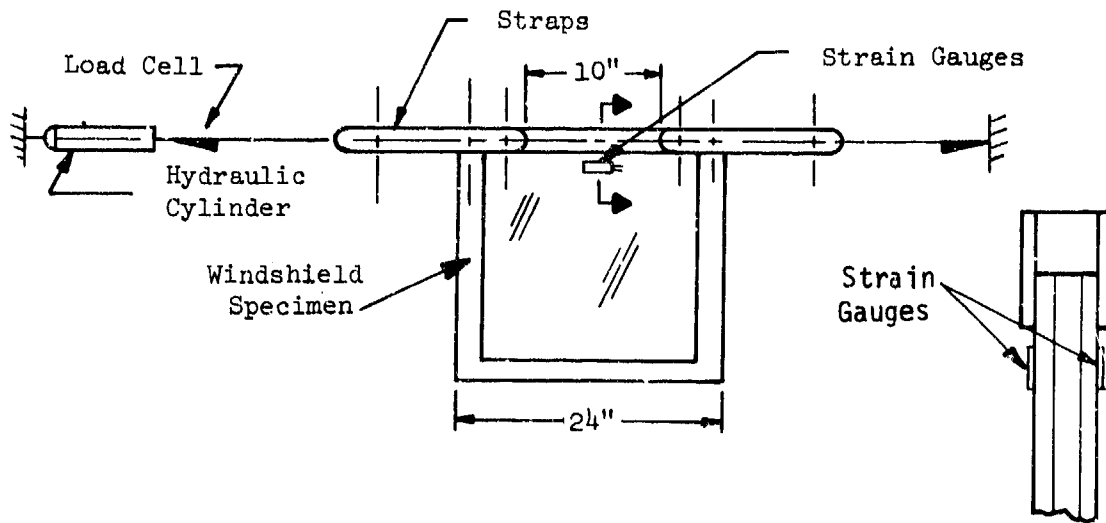


Figure 68. Stiffness Test Setup.

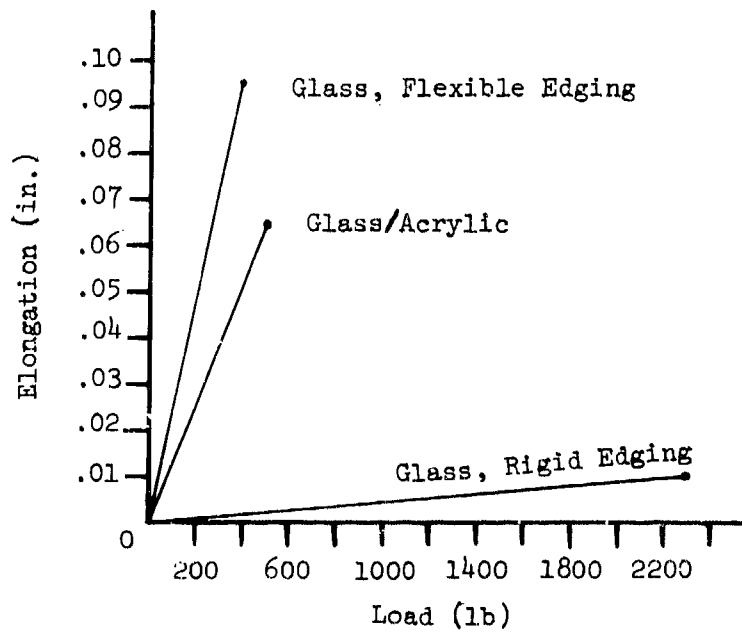


Figure 69. Spring Rate Test Data.

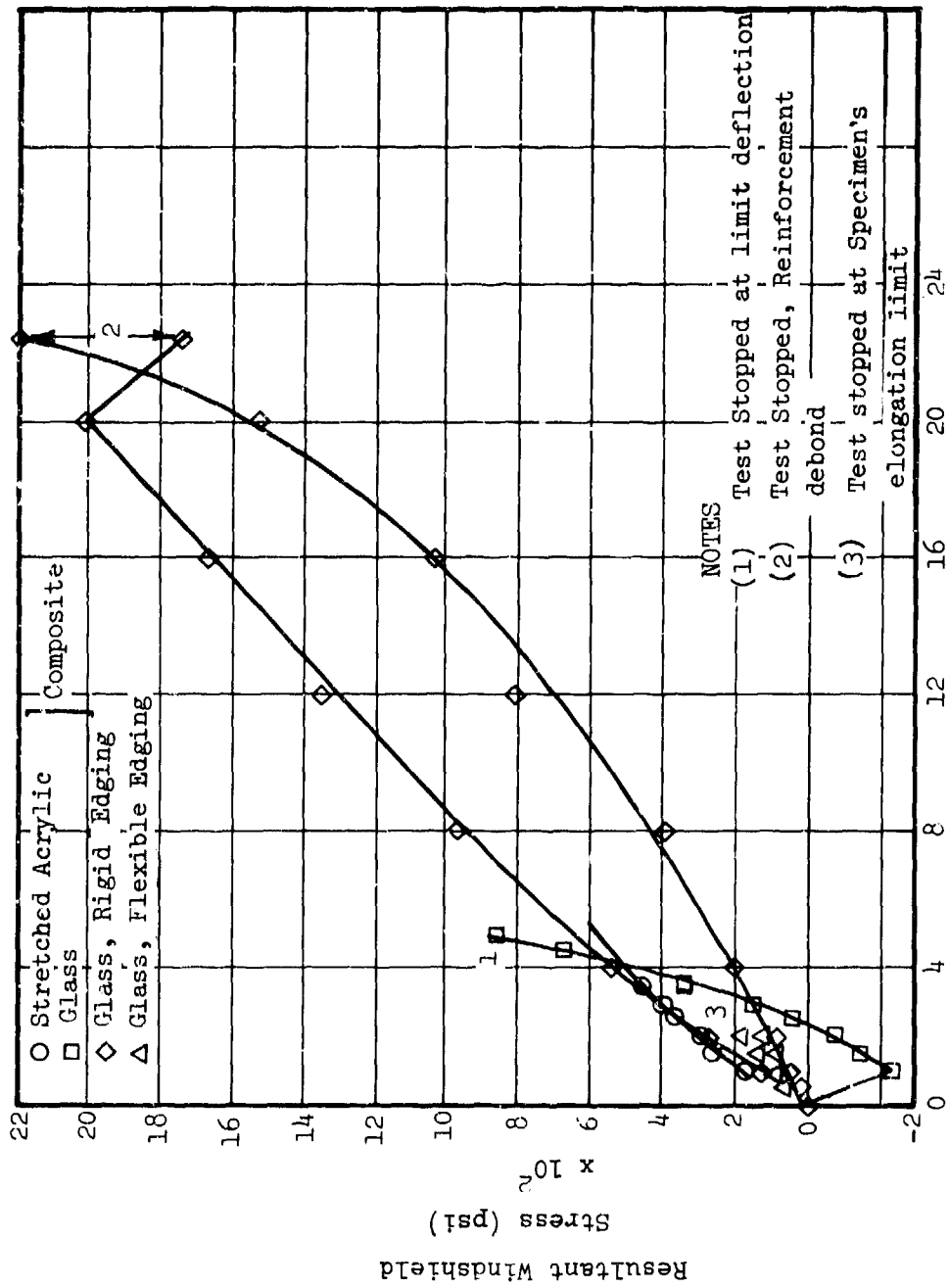


Figure 70. Load vs Stress Test Data.

Testing was stopped at 2230-lb load on the glass with rigid edging when there were indications of debonding of the fiberglass edge reinforcement. The two plots for this configuration represent data from gauges on each side of the specimen. The uneven load sharing between the two glass plies was attributed to slight eccentricities in the test setup. Although these effects were significant in comparison to overall strains, the magnitude of the deviations was about 0.001 microinch, which is considered to be small.

Testing of the glass with flexible edging was stopped at 200-lb load because of excessive elongation of the flexible impregnated fabric reinforcement.

#### THERMAL TESTS

Samples of each type windshield construction were placed in an environmental chamber at room temperature and subjected to incremental changes in temperature from  $-65^{\circ}\text{F}$  to  $+160^{\circ}\text{F}$ . Resultant thermal strains were measured after the specimen had stabilized at each temperature level. The test setup is shown in Figure 71. Note that the flexibility of the edging on one of the glass panels is apparent by its waviness as seen in the right-hand side of the photograph.

#### Results (Thermal Tests)

The most significant effects observed were for the composite glass/plastic specimen. The glass/plastic specimen is an unsymmetrical laminate and when heated or cooled, differential thermal expansion creates a severe bow in the unrestrained part. This condition is apparent in Figure 71. At both temperature extremes, the facing stresses were relatively high (about  $-9500$  psi) for the glass, but low (about  $1000$  psi) for the plastic.

Positive stresses are tension, and negative stresses are compression.



Figure 71. Laminated Windshield Thermal Test at Low Temperature.

When temperatures were increased, glass stresses increased to a maximum of approximately 1200 psi at 120°F and were observed to drop off with increasing temperature to 160°F, as shown by the solid line in Figure 72. When the specimen was cooled back to room temperature, residual stresses of -660 psi and 60 psi were recorded for the glass and acrylic. The decrease in stress with increasing temperature above 120°F was attributed to softening of the PVP interlayer. The residual stresses were attributed to relieving of built-in manufacturing stresses in each facing.

A second specimen was tested; it exhibited similar decreases in glass stress at temperatures above 120°F. Residual stresses for the second specimen were -1220 psi and 20 psi for the glass and plastic, respectively. Each specimen was tested again to 160°F, and glass stresses of approximately 1700 psi were achieved at 120°F to 130°F. These runs are shown (dashed line) in Figure 72.

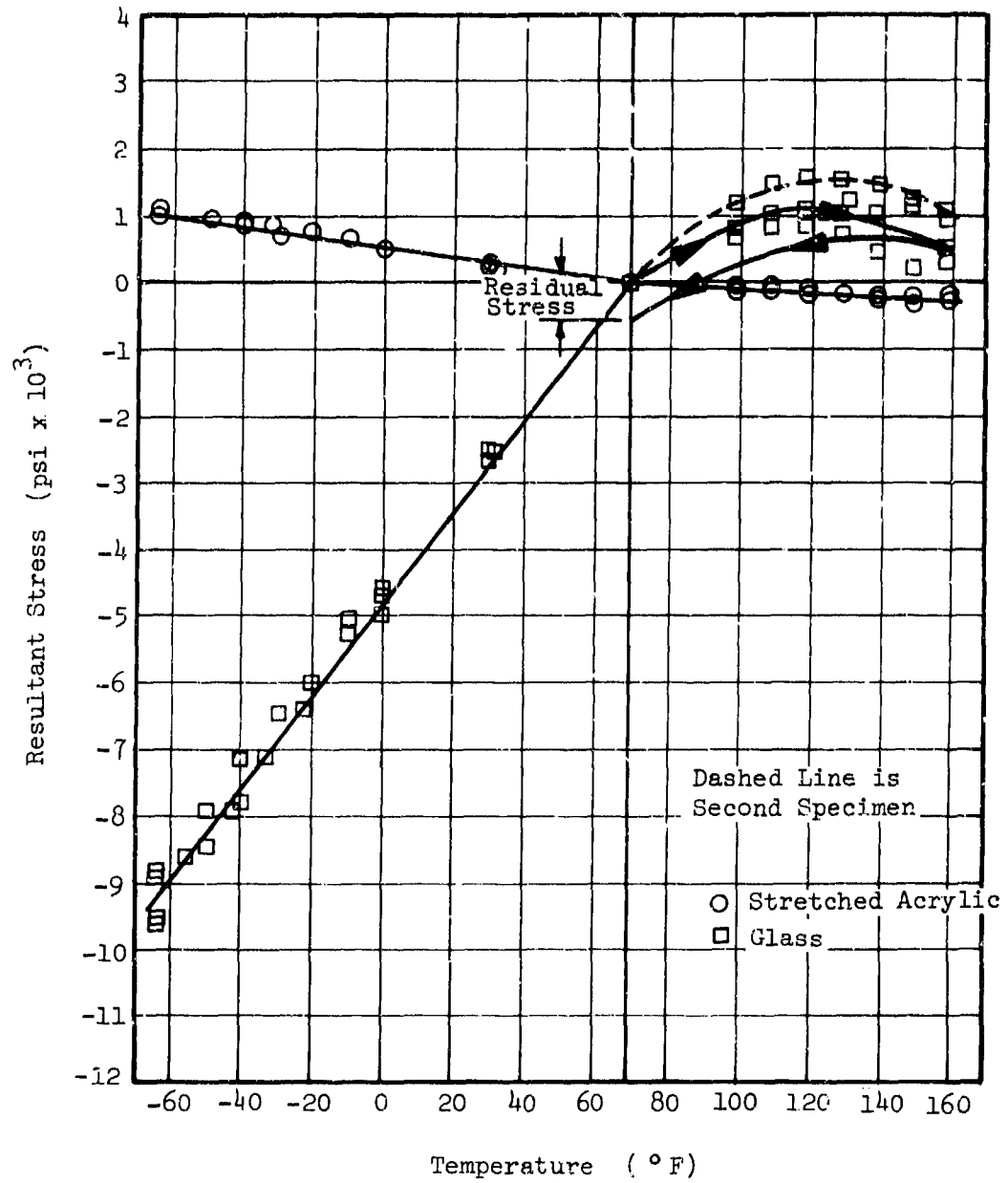


Figure 72. Thermal Test Data, Temperature vs Stress, Glass/Acrylic Specimen.

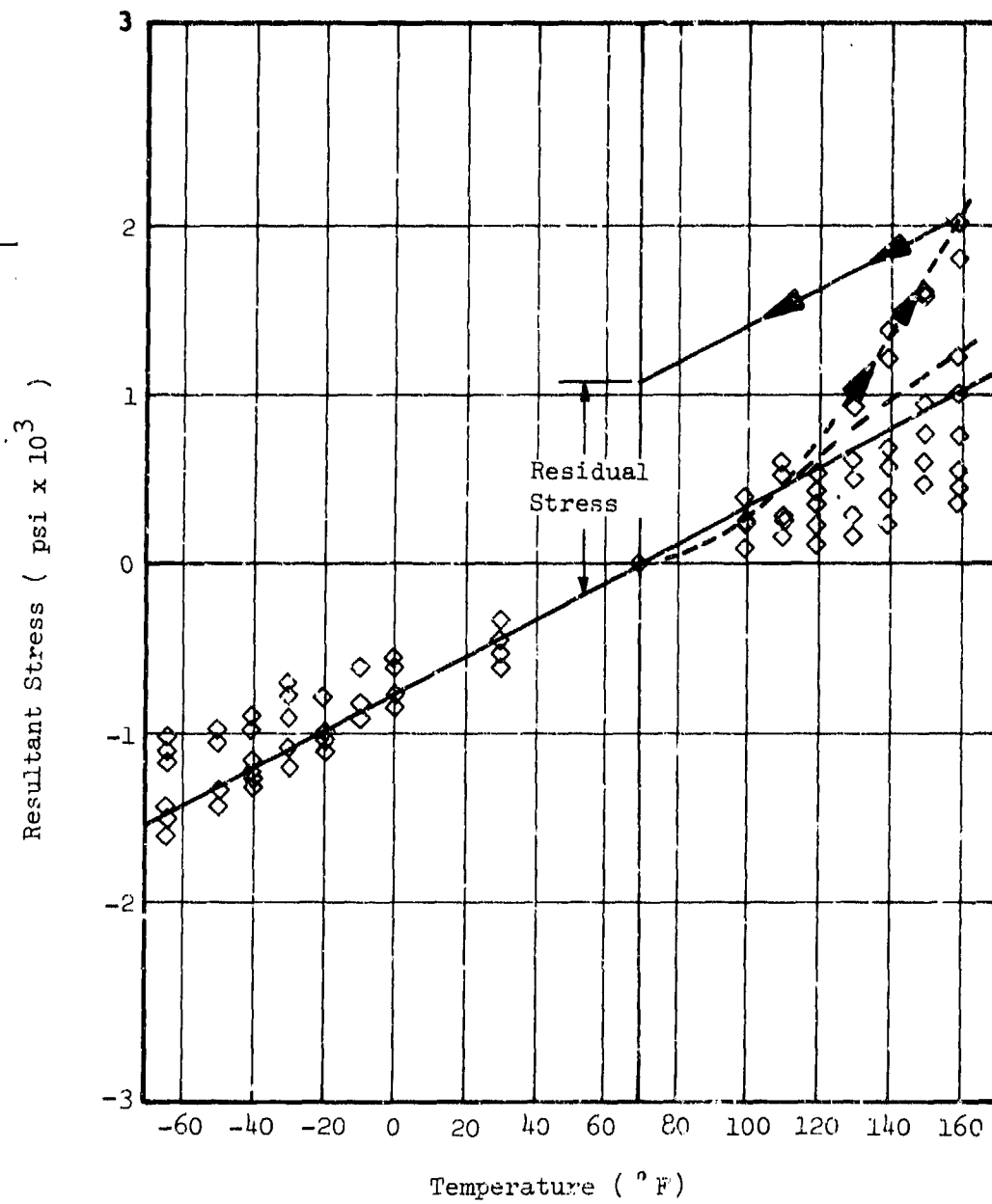
In the glass panel with rigid edging, temperatures to  $-65^{\circ}\text{F}$  resulted in glass facing stresses of  $-1600$  psi. Initial runs to  $160^{\circ}\text{F}$  resulted in glass facing stresses to  $2000$  psi as shown by the dashed lines in Figure 73. Manufacturing residual stresses were  $1100$  psi during the first run to  $160^{\circ}\text{F}$ . Subsequent tests to  $160^{\circ}\text{F}$  (solid line, Figure 72) resulted in glass stresses of approximately  $1050$  psi.

Temperatures to  $-65^{\circ}\text{F}$  resulted in glass stresses of approximately  $-1000$  psi on the glass panel with flexible edging. During initial runs to  $160^{\circ}\text{F}$  (dashed lines) manufacturing residual stresses were  $2900$  psi. Subsequent tests resulted in stresses to  $500$  psi as shown in Figure 74 (solid line).

#### INSTALLATION PRELOAD TEST

Installation preload tests were conducted to determine a method for establishing recommended windshield dimensional manufacturing tolerances based on induced stresses resulting from windshield/airframe contour mismatch. A cambering test fixture, shown schematically in Figure 75, was fabricated with an adjustable surface contour to simulate various degrees of contour mismatch. Strain gauges installed on opposite sides of the test specimens at the flexed edge were used to measure flexural stress.

Each specimen was attached to the test fixture shown in Figure 76, and strains were recorded to provide a reference position. After each specimen was removed, the test fixture was adjusted to provide a smooth curvature and to produce a  $1/16$ -inch camber. The test specimen was torqued to the fixture for each camber configuration following the torque sequence of Figure 77, and the resultant strains were recorded at increments of  $1/16$  inch camber until the camber was  $0.5$  inch, or  $3000$  psi was measured on the glass material. Micrometer measurements were also taken to measure the change in laminate thickness at the unflexed edge as shown in Figure 77.



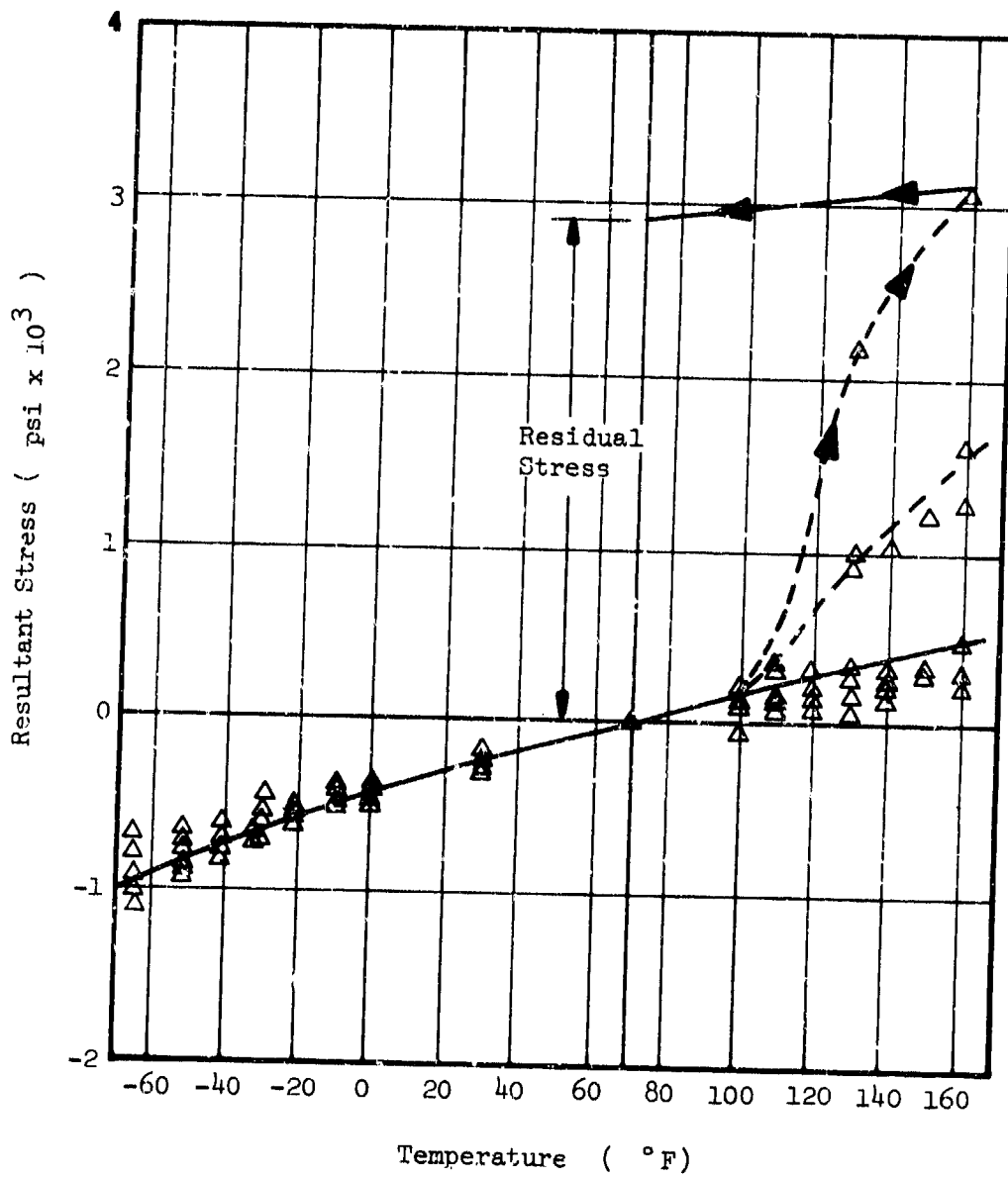


Figure 74. Thermal Test Data, Temperature vs Stress, Glass Panel With Flexible Edging.

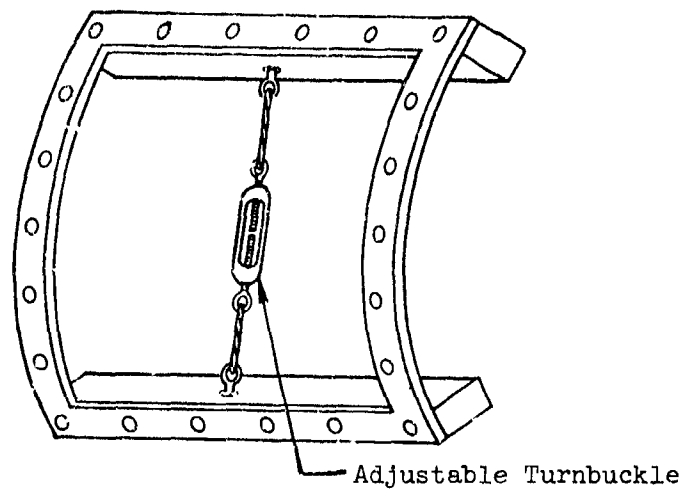


Figure 75. Schematic Representation of Cambering Fixture.

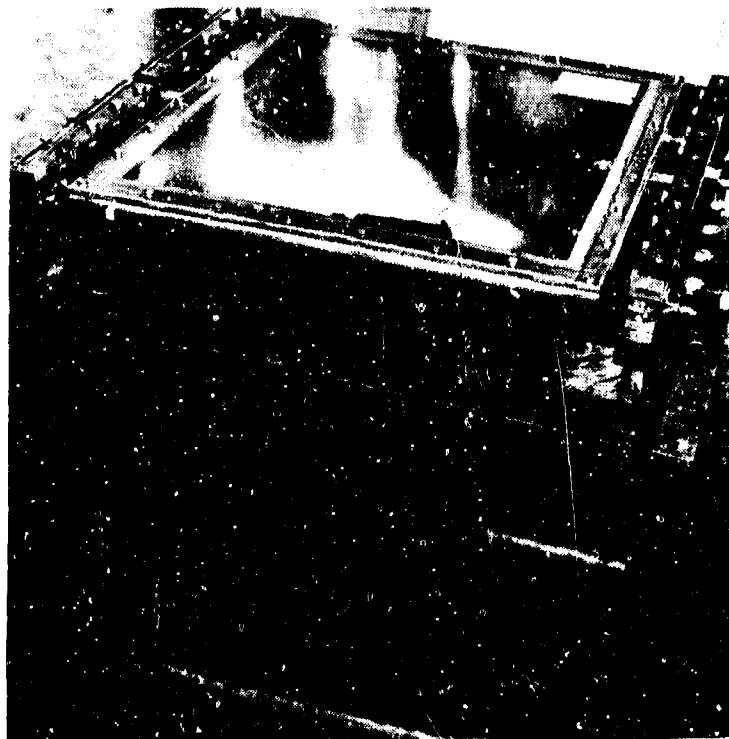


Figure 76. Contour Mismatch Test Setup.

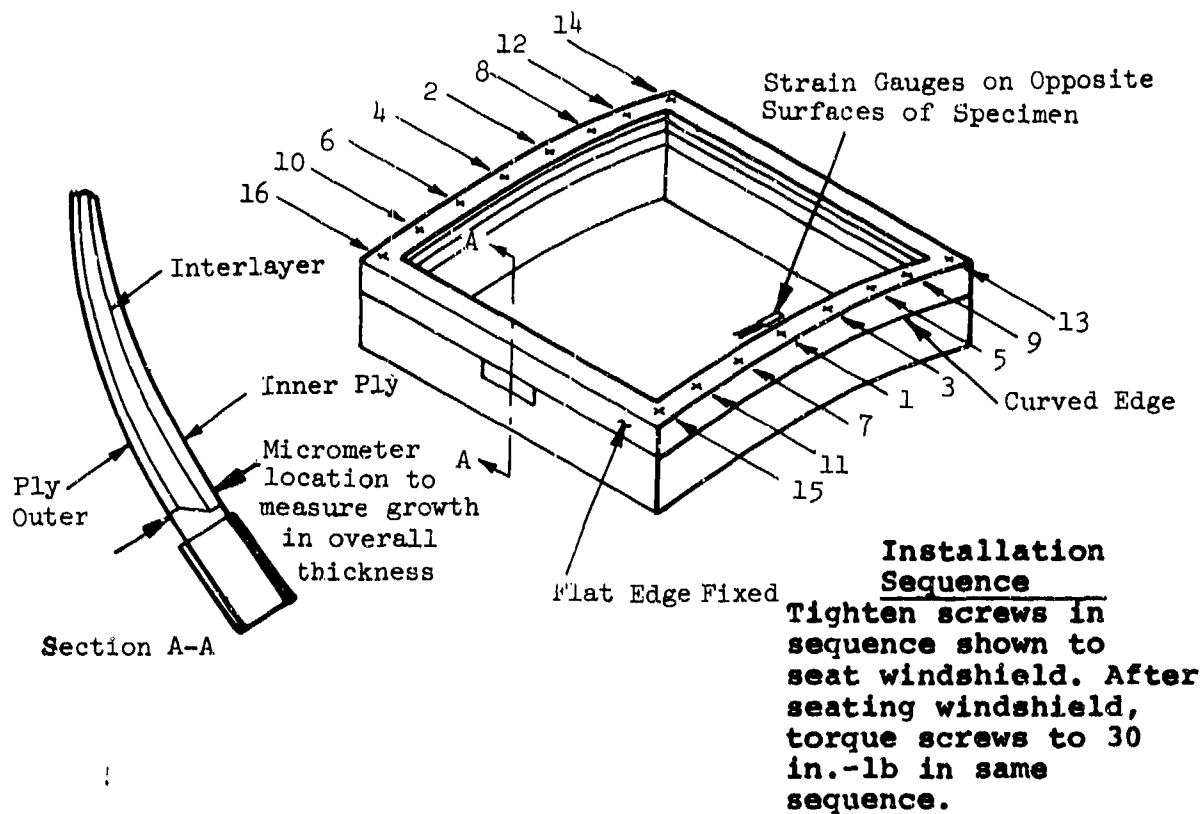


Figure 77. Torquing Sequence.

#### Results (Installation Preload Tests)

Figure 78 shows plots of stress vs camber for each configuration. The abscissa also shows the normalized ratios of camber to panel length. Testing of the glass/acrylic specimen, which had a built-in  $3/16$  inch camber from manufacture, was discontinued at  $3/8$  inch camber when limit stress was reached in the glass. Testing of the glass panel with rigid edging configuration was discontinued at  $1/16$  inch camber when limit stress was reached in the glass. Testing of the glass panel with flexible edging configuration was started at  $3/8$  inch camber due to the flexibility of the fabric edge reinforcement. Testing of this configuration was discontinued at  $7/16$  inch camber when the attachment bolts tore through the fabric edge reinforcement. There were no measurable changes in laminate thickness in any windshield configuration.

These tests showed that the more rigid the edge reinforcement, the higher the facing stresses would be for a given contour mismatch.

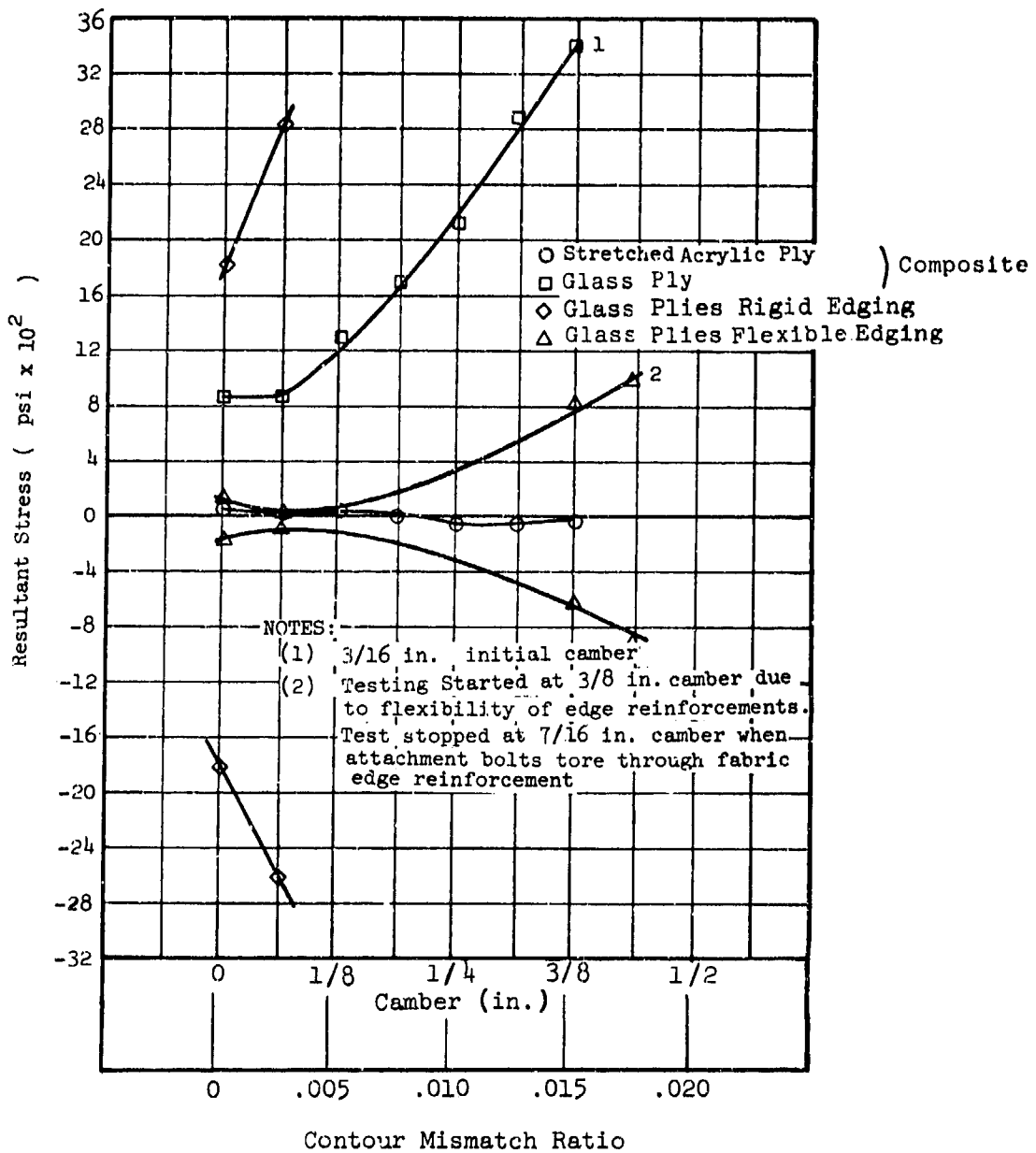


Figure 78. Windshield Installation Preload Tests, Induced Stress vs Camber.

## ASSEMBLY TESTS

Each of the test specimens was assembled in turn to a representative aluminum post configuration, Figure 79. The posts were 1.00 inch x 1.00 inch x 0.125 inch 2024-T3 aluminum angle extrusions that are similar in cross-sectional area to typical helicopter transparency support structures. The specimens were assembled with AN-3 bolts torqued to 30 in.-lb, except as noted. Hole size was 0.190 +.002/-.001 inch and the gasket material was 0.125 inch neoprene sponge rubber except where noted otherwise.

Following assembly, each specimen was subjected to axial loadings and temperature tests to measure the strains induced by tensile and thermal loads. Axial loads were applied to each post to develop a maximum windshield stress of 3000 psi or an applied load of 5000 lb, whichever was lower. Strain gauge readings were obtained at each 500-lb increment of load.

Following this, each specimen was subjected to temperature environmental tests with strain gauge measurements taken at stabilized temperature increments to -65°F and +160°F.

In order to evaluate the effect of hole size, fastener torque and sealant, each assembly was also tensile tested after the configuration variables were changed as follows:

1. Hole size: 0.190-in.-dia holes increased to 0.310-in.-dia.
2. Fastener Torque: 30 in.-lb torque loosened to 10 in.-lb
3. Gasket: Neoprene rubber replaced with EC1675 polysulfide sealant.

A matrix of the assembly test configuration is shown in Table 27.

TABLE 27. ASSEMBLY TEST CONDITIONS

Condition	Hole Size (in.)	Temperature (°F)	Torque (in.-lb)	Gasket	Axial Load
1	0.190	70	30	Rubber	Yes
2	0.190	-65	30	Rubber	No
3	0.190	160	30	Rubber	No
4	0.310	70	30	Rubber	Yes
5	0.310	70	30	EC1675	Yes
6	0.310	70	10	EC1675	Yes

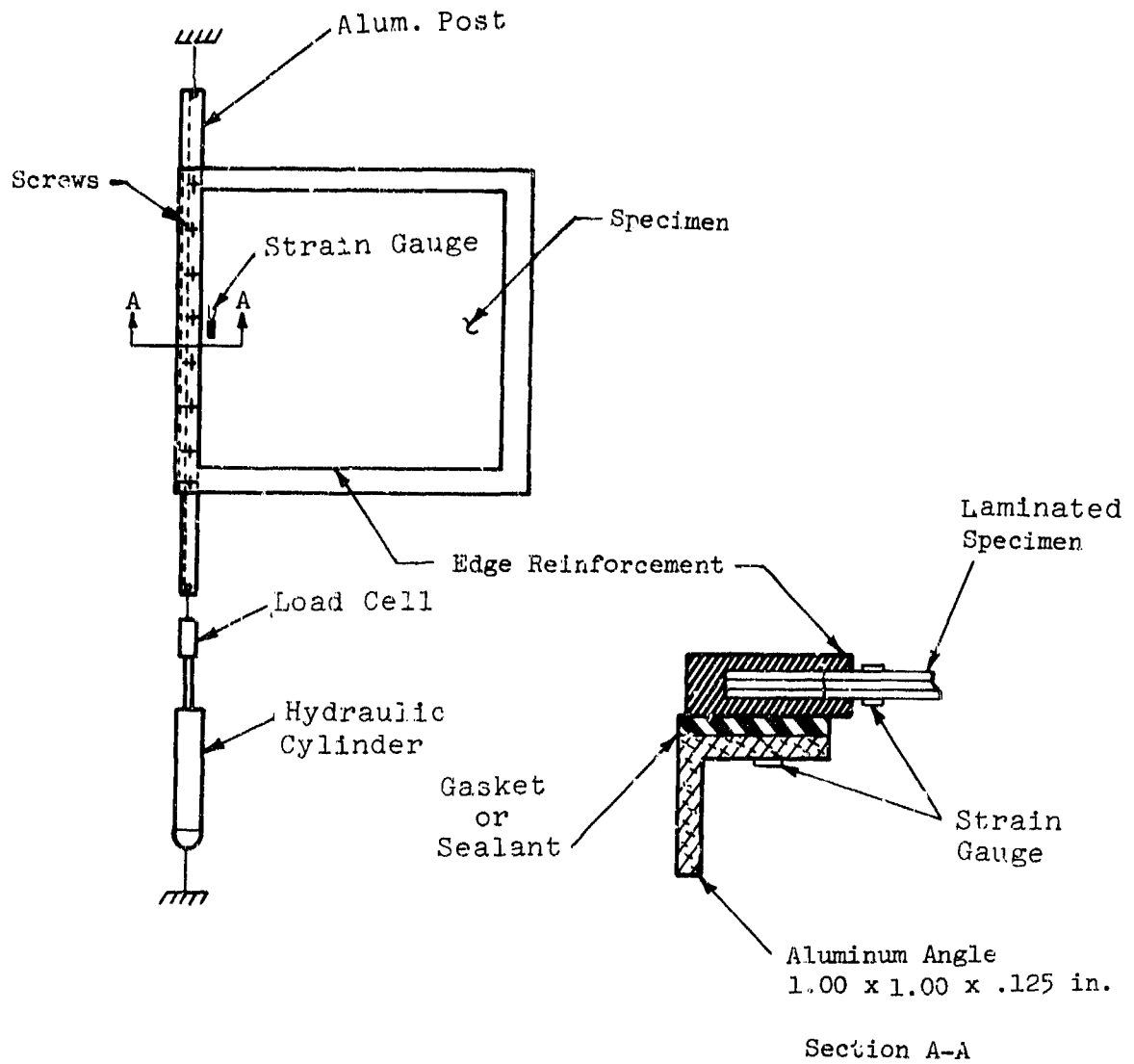


Figure 79. Windshield Assembly Test Setup.

## Results (Assembly Test)

Condition 1 - 0.190 inch holes, 30 in.-lb torque. Figures 80 and 81 present plots of applied load vs resultant stress for each configuration. Testing of the glass/acrylic configuration was stopped at 4500 lb when limit stress was reached in the glass. Testing of the all-glass specimens was limited to 5000-lb load.

The all-glass laminate with flexible edging offered virtually complete isolation from axial loads that were applied to the posts. Glass facing stresses remained exceptionally low (<100 psi) for all loading conditions up to the maximum post load of 5000 lb.

Facing stresses measured in the all-glass laminate with rigid edge treatment were approximately 1100 psi when a 5000-lb load was applied to the post section. Comparison of the strain measured in the glass (120  $\mu$ -in./in.) with the strain measured at an adjacent point on the post (1700  $\mu$ -in.-in.) indicates that the rate of strain for the glass was only 7% of that for the post. Thus, a high degree of structural isolation against axial loads was present even in a so-called rigid edge attachment.

For the glass-plastic composite design, the most pronounced effect was the appearance of preload stresses in the facings when the specimen was torqued to the post. This condition occurred because of two reasons:

1. The panels were initially bowed and became prestressed when they were fastened to the straight post.
2. Local preload stresses were induced from uneven torquing of fasteners. In a subsequent series of ballistic tests, this condition actually caused the glass to fracture. The magnitudes of these stresses are highly variable and can be either tension or compression depending on individual fastener preloads. The condition can be seen in Figure 82 as a waviness along the edge of the panel.

As a result, the stresses induced from applying a load to the post appear less significant than the initial stresses induced during assembly.

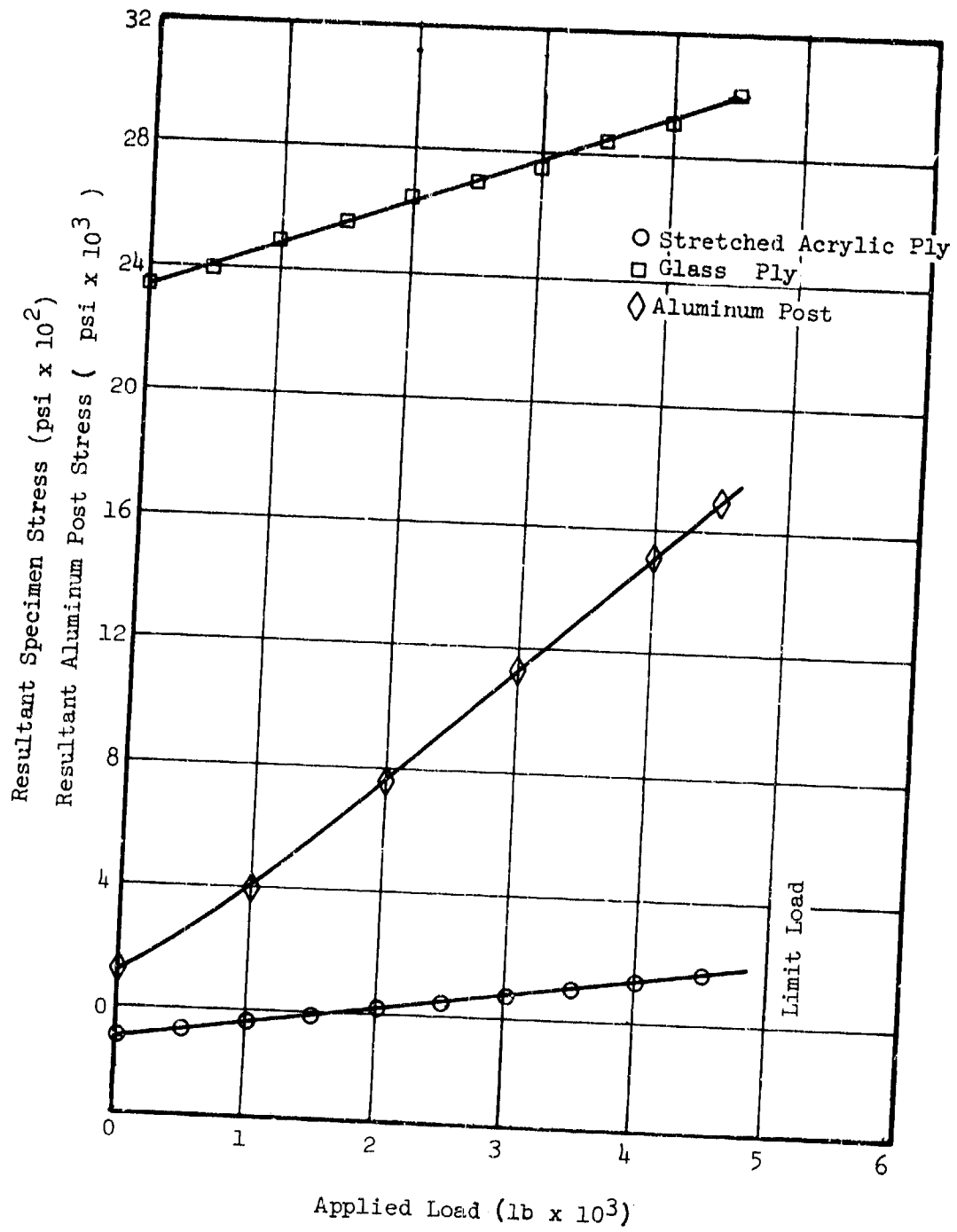


Figure 80. Assembly Tensile Test, 1/8 Inch Neoprene Gasket, 0.190-Inch-Dia Holes, 30-in.-lb Torque, Glass/Acrylic Specimen.

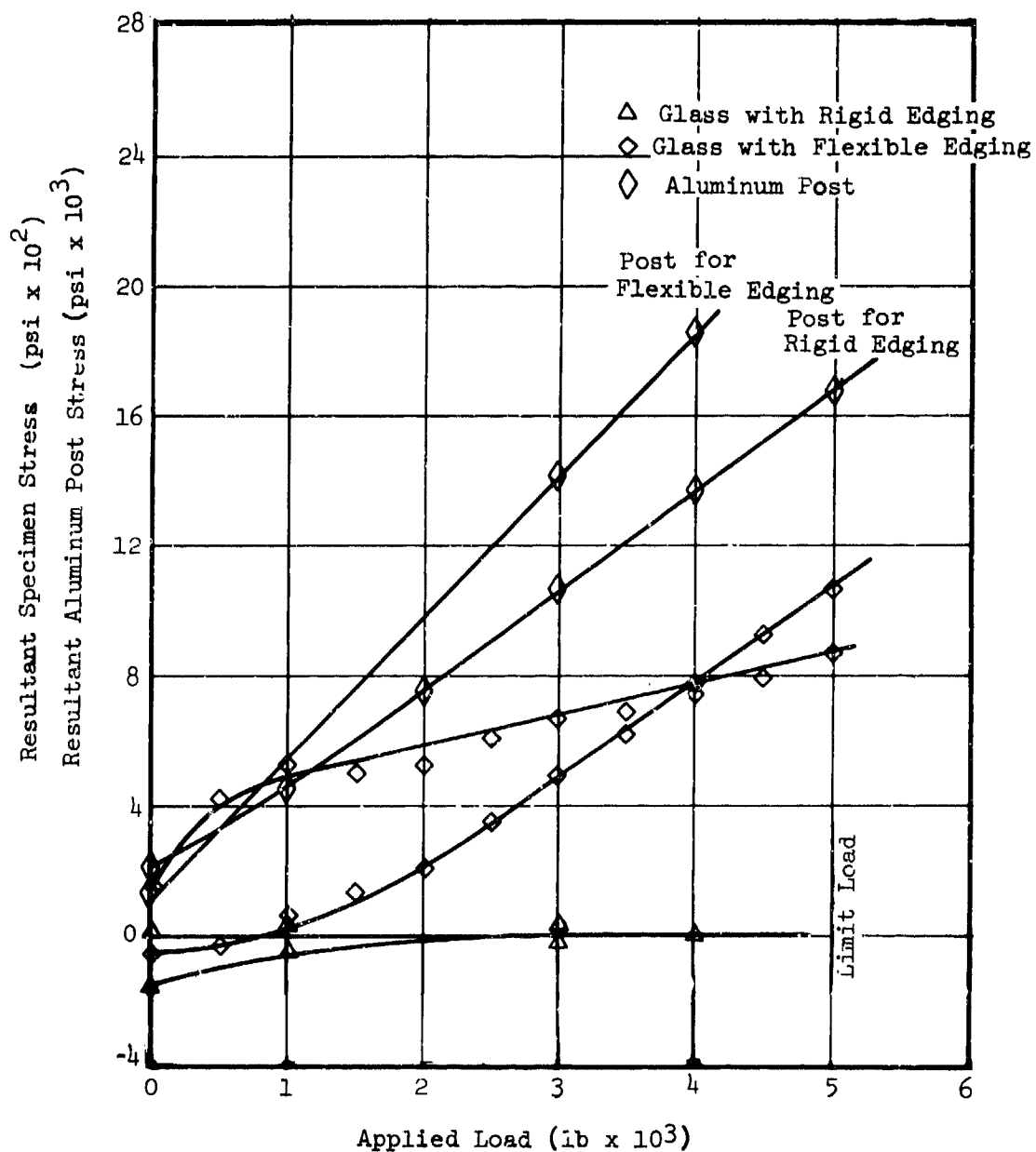


Figure 81. Assembly Tensile Test, 1/8 Inch Neoprene Gasket, 0.190-Inch-Dia Holes, 30 in.-lb Torque, All-Glass Laminated Specimens.

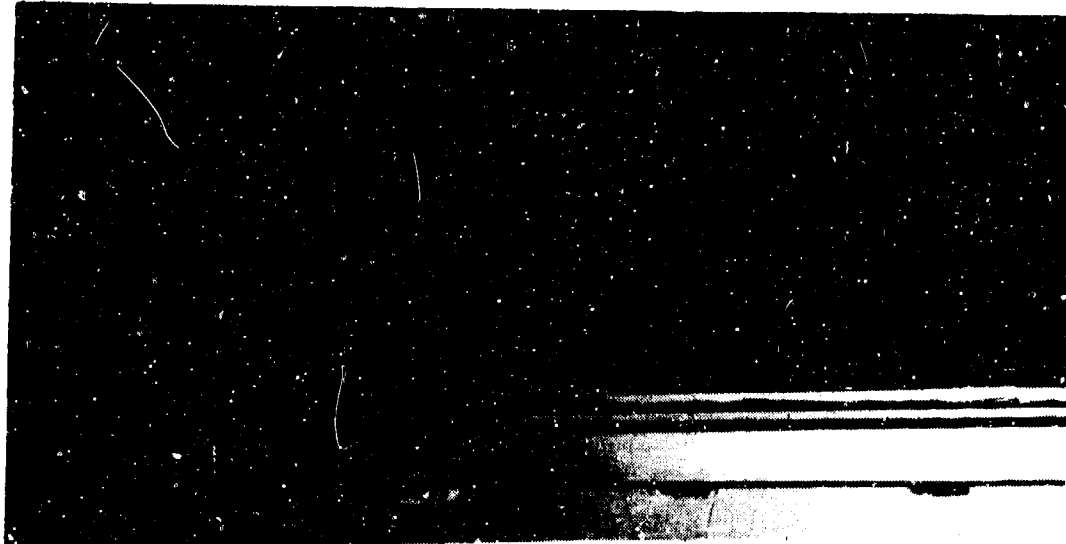


Figure 82. Uneven Torquing of Bolts.

Conditions 2 and 3 - Thermal Test, 0.190-inch-dia Holes, 30-in.-lb torque. Figure 83 presents plots of temperature vs resultant stress for the glass/acrylic specimen. Preload effects of the bowed specimen were observed when the specimen was torqued to the post and resulted in stresses of 2700 psi and 1800 psi in the glass and aluminum post, respectively. Thermal effects of the post were significant at low temperatures when smaller stresses were noted in the glass ply of the restrained specimen as compared to stresses in the unrestrained specimen previously tested.

Figure 84 presents plots of temperature vs resultant stress for the all-glass specimens. Resultant stress magnitudes for both configurations were similar to the results of thermal tests without aluminum posts within the limits of hysteresis and experimental error.

Conditions 4, 5 and 6 - Hole Size, Fastener Torque and Sealant Material. The results of these tests, plotted in Figures 85 through 90, indicate that a high degree of isolation from axial loads is present with each type of post attachment.

The effects of hole size, fastener torque, and sealant material were evaluated, and the following observations were noted. Axial loads transmitted from the post to the facings diminished with increasing hole size. After the holes had been enlarged, fastener torque and sealant material had negligible effect on facing stresses.

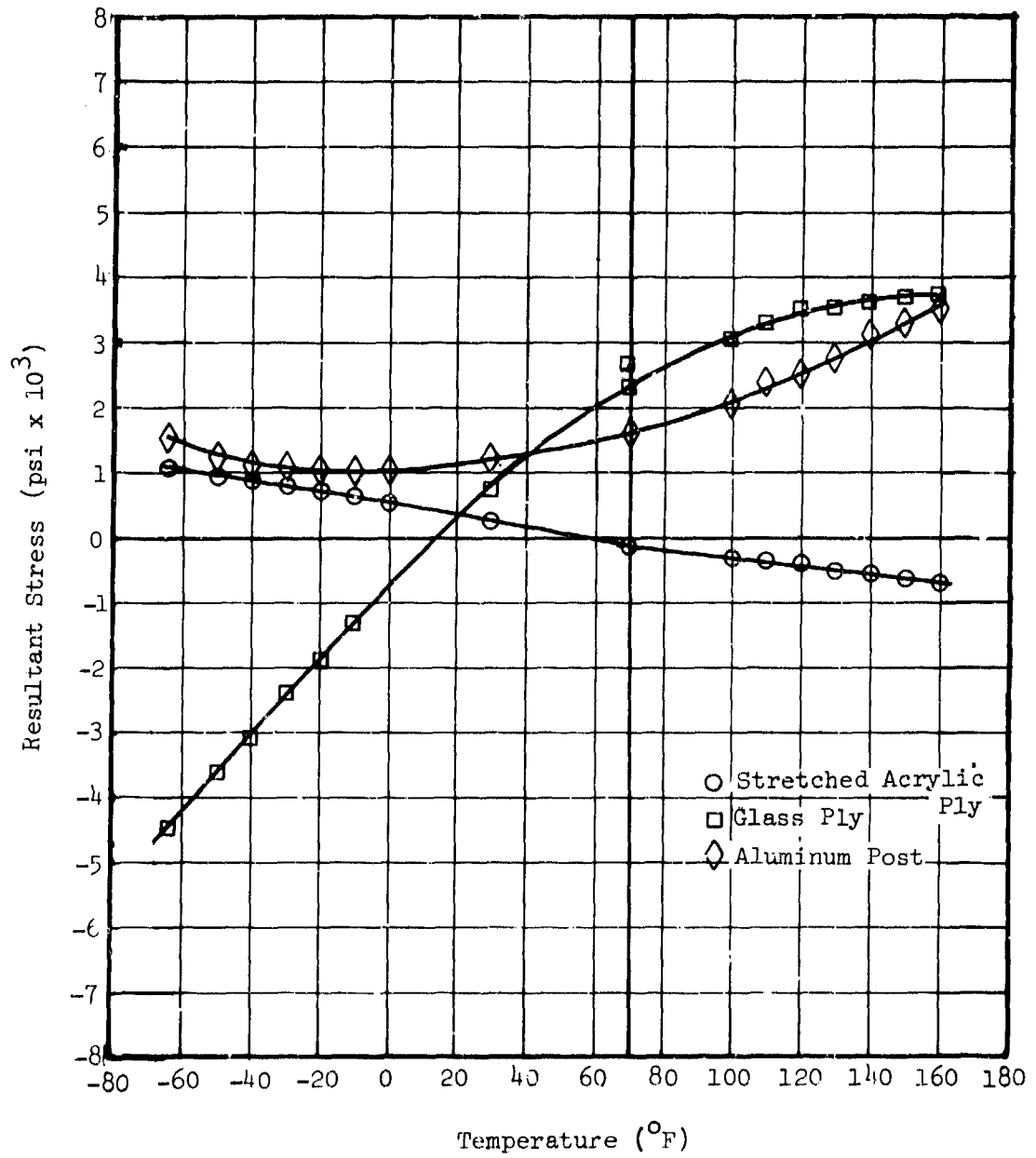
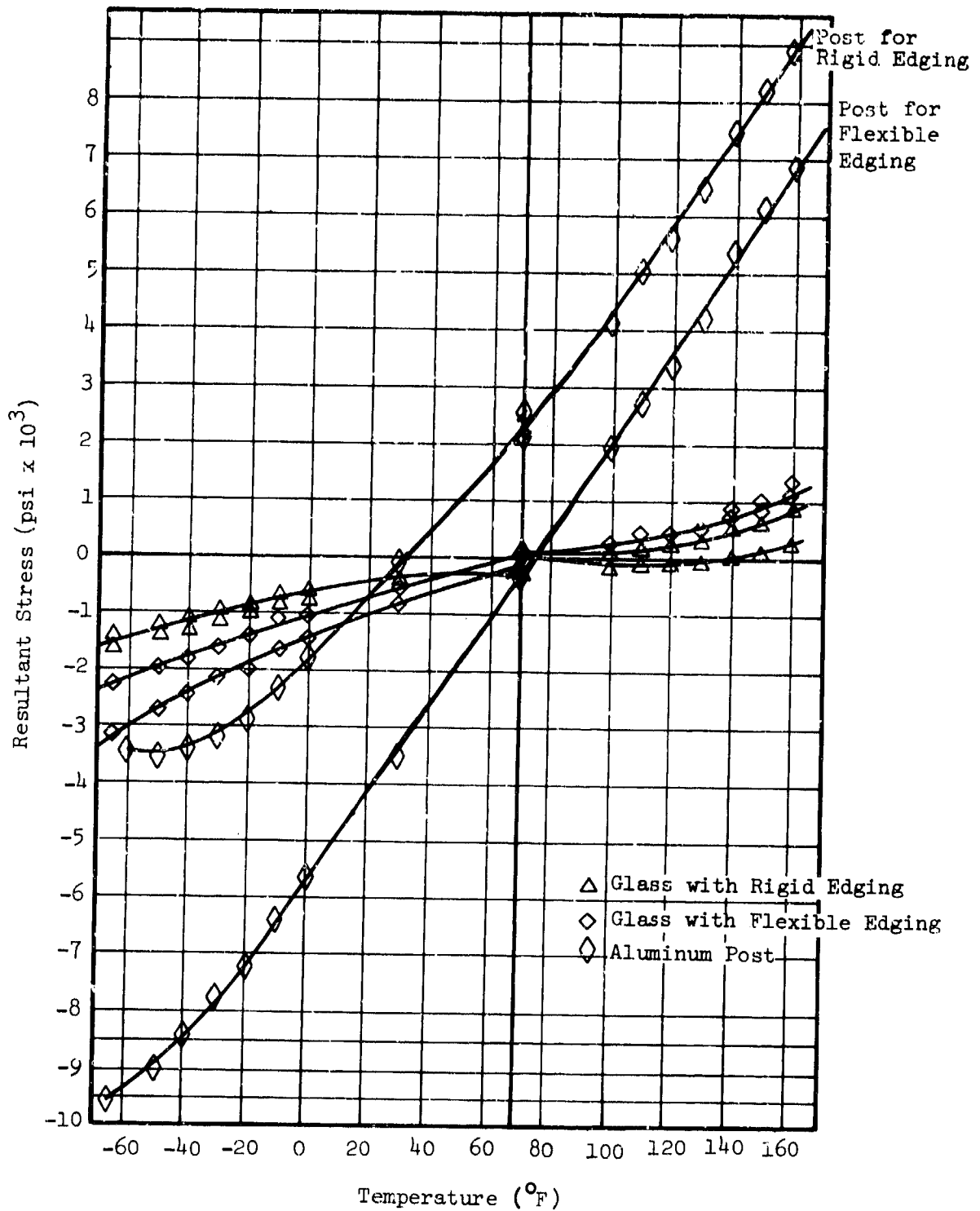


Figure 83. Assembly Thermal Tests, 1/8-Inch Neoprene Gasket, 0.190-Inch-Dia Holes, 30-in.-lb Torque, Glass/Acrylic Specimen.



**Figure 84. Assembly Thermal Tests, 1/8-Inch Neoprene Gasket, 0.190-Inch-Dia Holes, 30-in.-lb Torque, All-Glass Laminated Specimens.**

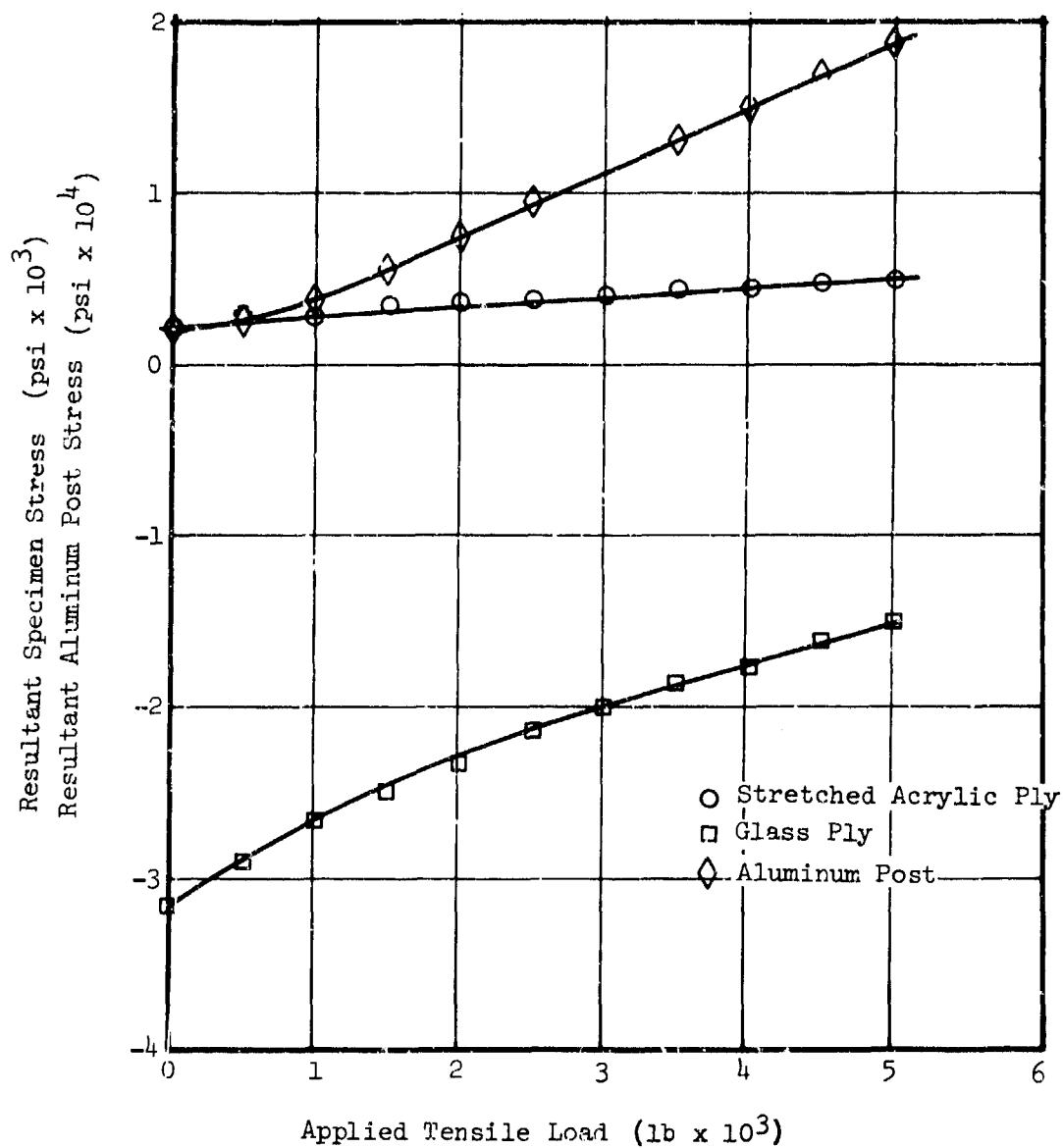
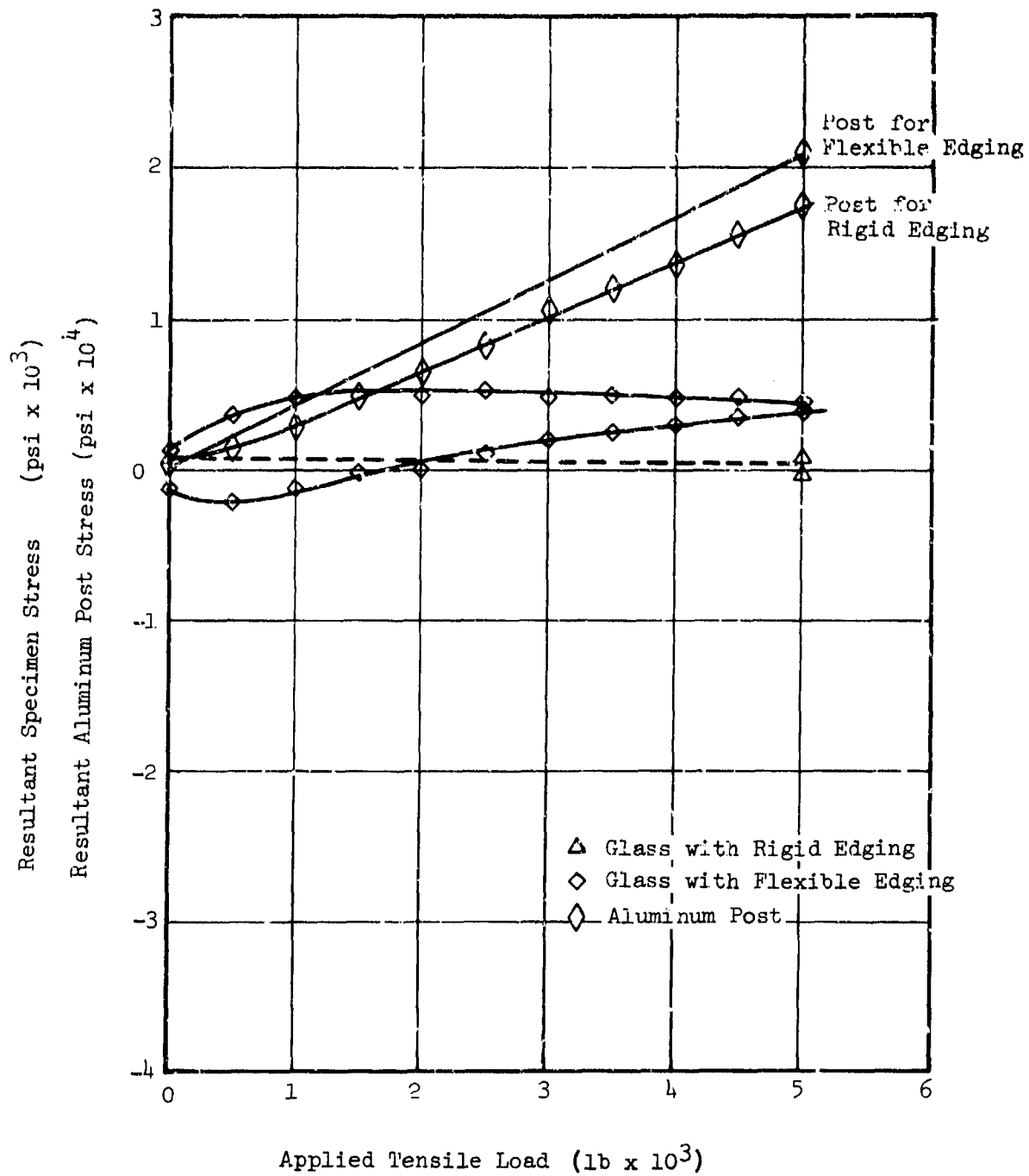


Figure 85. Assembly Tensile Tests, 1/8-Inch Neoprene Gasket, 0.310-Inch-Dia Holes, 30-in.-lb Torque, Glass/Acrylic Specimen.



**Figure 86. Assembly Tensile Tests, 1/8-Inch Neoprene Gasket, 0.310-Inch-Dia Holes, 30-in.-lb Torque, All-Glass Laminates.**

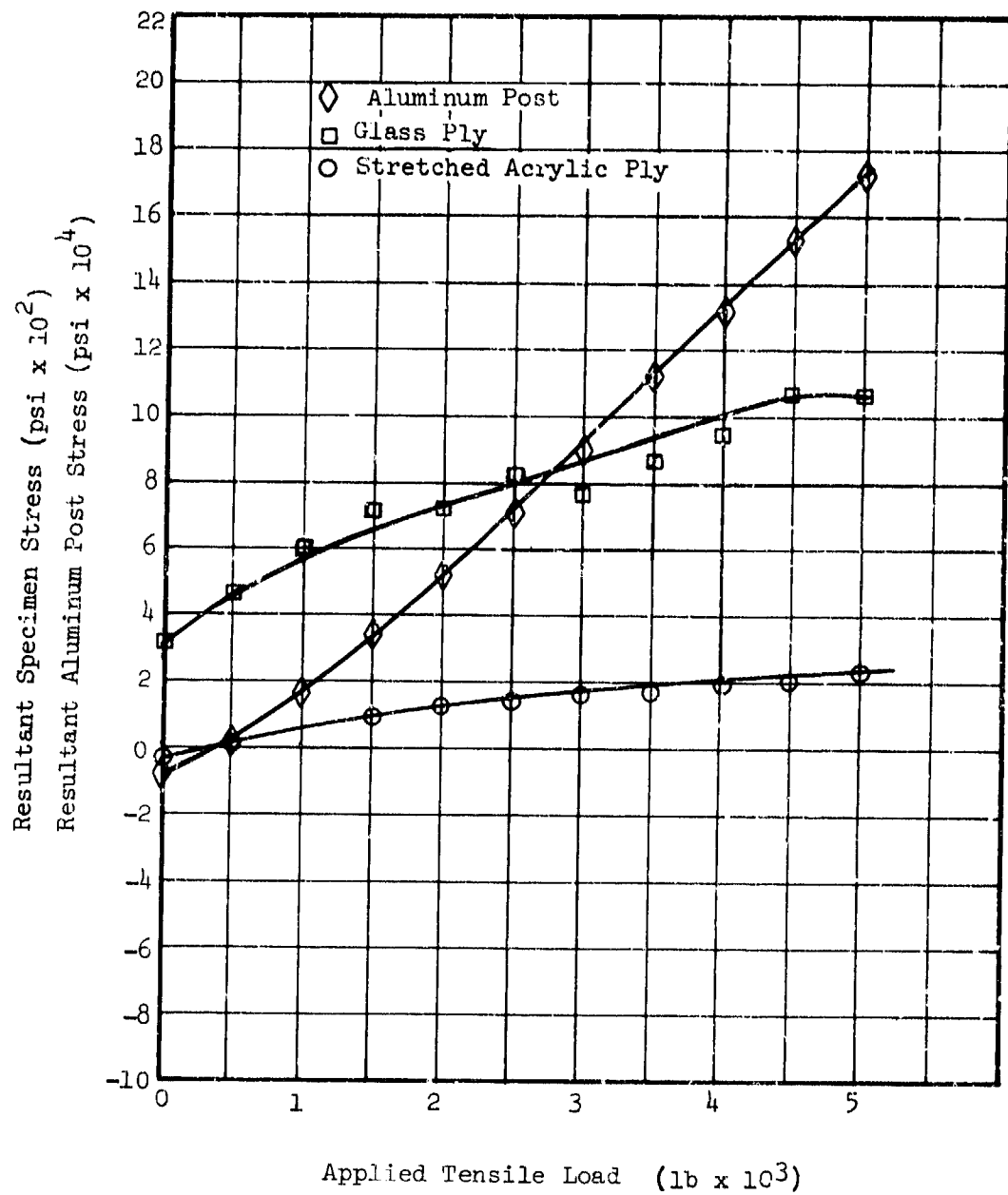


Figure 87. Assembly Tensile Test, EC-1675 Wet Sealant, 0.310-Inch-Dia Holes, 30-in.-lb Torque, Glass/Acrylic Specimen.

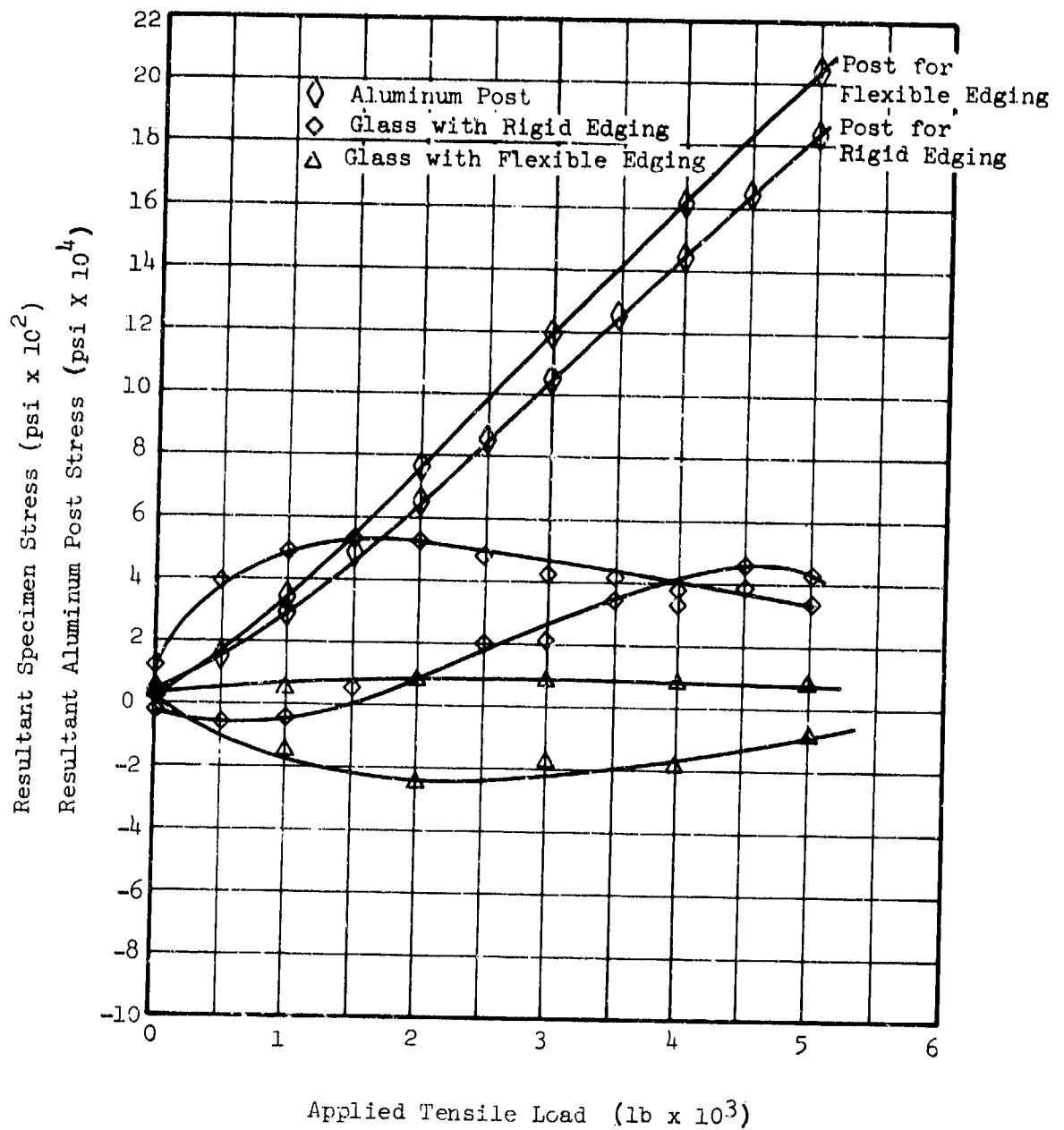
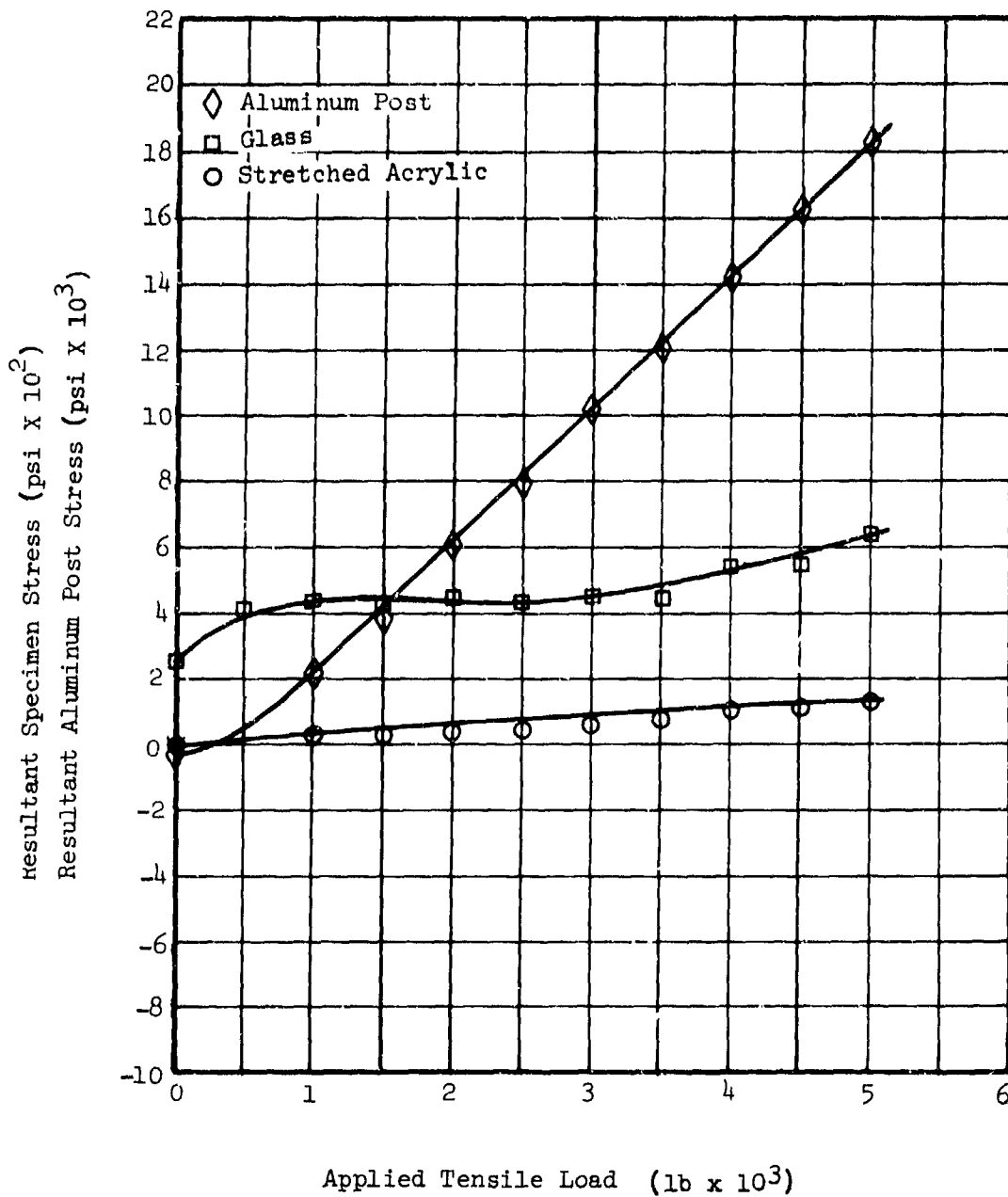


Figure 88. Assembly Tensile Test, EC-1675 Wet Sealant, 0.310-Inch-Dia Holes, 30-in.-lb Torque, All-Glass Laminates.



**Figure 89. Assembly Tensile Test, EC-1675 Wet Sealant, 0.310-Inch-Dia Holes, 10-in.-lb Torque, Glass/Acrylic Specimen.**

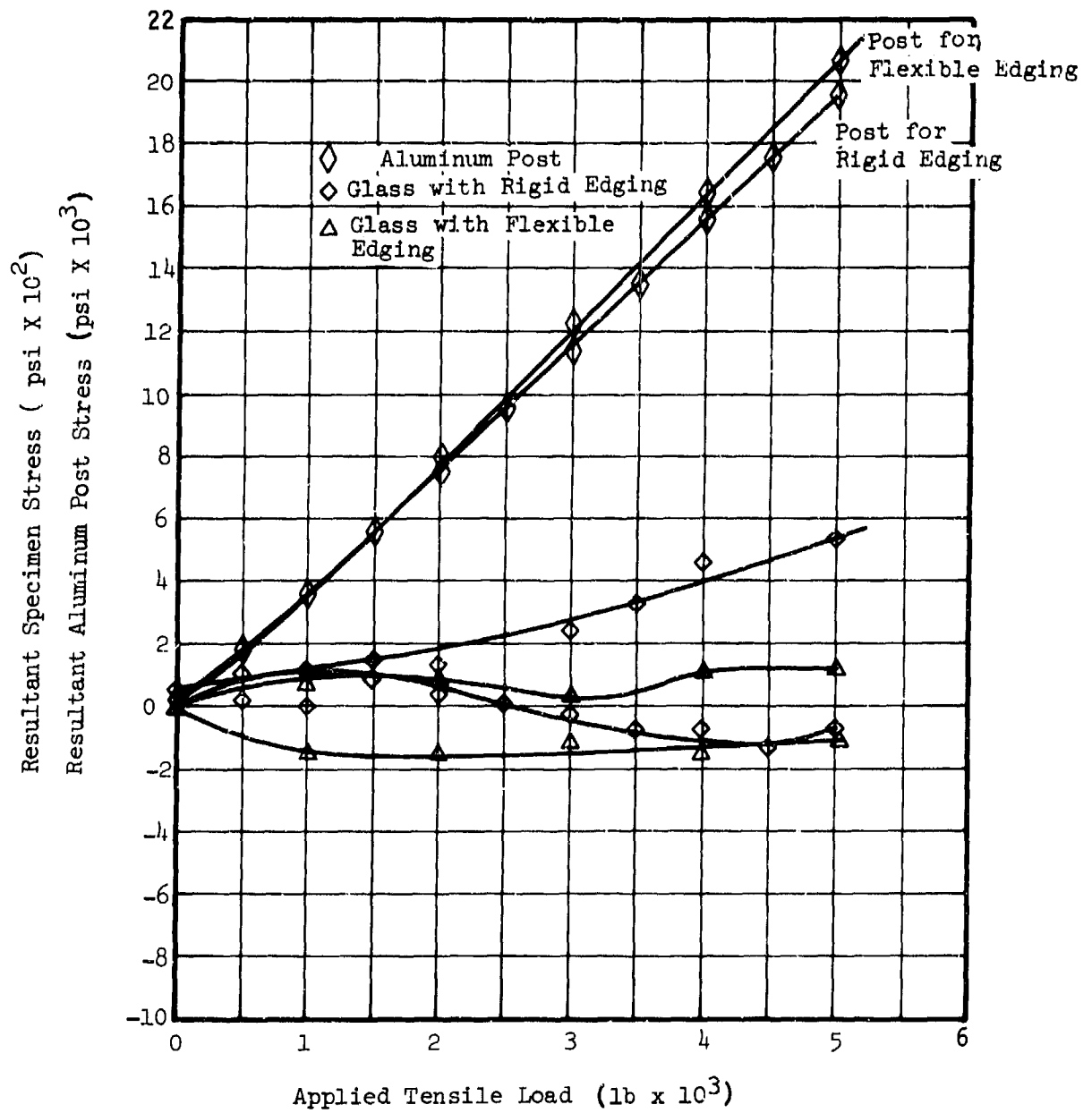


Figure 90. Assembly Tensile Test, EC-1675 Wet Sealant, 0.310-Inch-Dia Holes, 10-in-lb Torque, All-Glass Laminated Specimens.

**THERMAL EXPANSION, INSTALLATION PRELOAD AND ASSEMBLY TEST**  
**CONCLUSIONS**

1. Stresses resulting from differential thermal expansion in laminated transparencies are significant and must be considered during design and structural substantiation.
2. Significant residual stresses are present in laminated transparent assemblies as a result of manufacturing processes.
3. Installation preload forces can create critical loading conditions for certain types of laminated transparencies, particularly those containing glass plies. The stresses can be induced from mismatch of contours between the panel and the airframe, or from uneven torquing of fasteners. These conditions are highly sensitive to edge attachment design.
4. All of the edge attachment configurations evaluated provided good isolation from axial loads applied to the support structure.

## ASSESSMENT OF RESIDUAL VISIBILITY THROUGH FRACTURED GLASS PANELS

Transparencies that are designed with redundant load paths or materials possessing good fracture toughness can suffer cracking and still maintain structural integrity. In such cases, the decision on whether or not to abort a mission is based on residual visibility through the cracks, assuming the fear of imminent cave-in does not take precedence. This study was conducted to establish a threshold crack density for use in selecting materials that will provide adequate post fracture residual visibility. During the study, two types of data were collected: subjective (pilot opinion), and objective (visual acuity).

### Materials Evaluated

The problem of dense crack patterns restricting vision is inherent to certain types of tempered glass. The amount of dicing is a function of tempering, thickness and state of stress existing in the part during fracture. Therefore, in order to obtain a variety of crack patterns for study, five different laminated glass panels were procured from PPG Industries. All panels were 24 inches square with 0.250-inch-thick annealed glass base plies. The face ply materials varied as shown in Table 28 and were laminated with a 0.100-inch-thick polyvinyl butyral interlayer.

TABLE 28. FACE PLY MATERIALS USED IN RESIDUAL VISIBILITY STUDY

Material	Thickness (in.)	Modulus of Rupture (psi)
Chemically Tempered Glass	0.085	50,000
Chemically Tempered Glass	0.109	40,000
Thermally Tempered Glass	0.110	16,000
Thermally Tempered Glass	0.109	20,000
Annealed Glass	0.110	-

The five specimens were mechanically fractured by striking the center of each panel with a center punch. The resultant fracture patterns are shown in Figures 91 through 94. The annealed glass and 16,000 psi thermally tempered glass panels developed identical chips at the point of impact. Therefore, in order to obtain a reasonable variation between specimens, an additional specimen was added to the lot. The additional

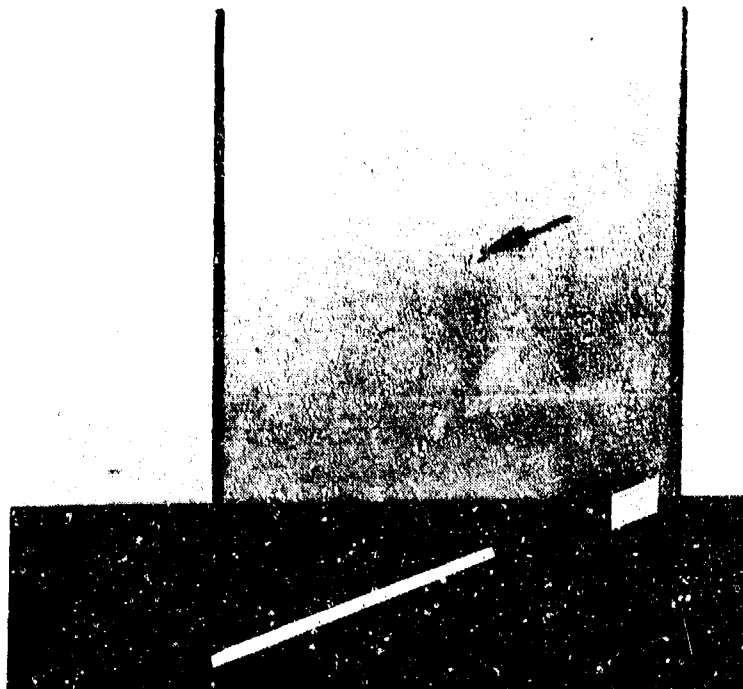


Figure 91. Thermally Tempered Glass (16,000 psi MOR)  
Fracture Pattern.

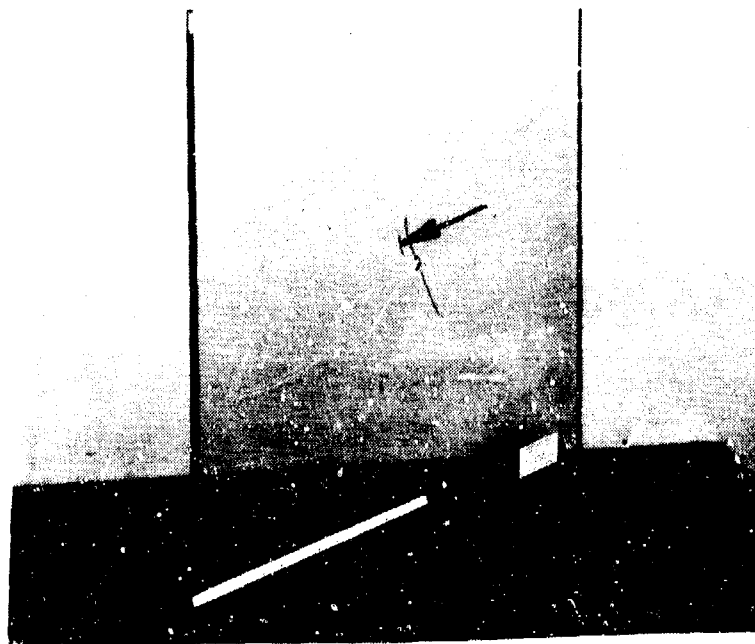


Figure 92. Thermally Tempered Glass (20,000 psi MOR)  
Fracture Pattern.

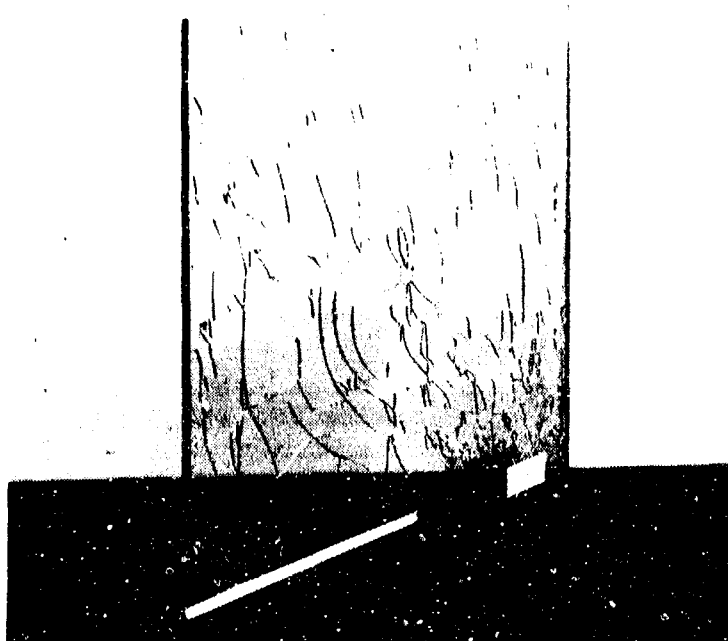


Figure 93. Chemically Tempered Glass (40,000 psi MOR)  
Fracture Pattern - 250 Particles/Ft<sup>2</sup>.

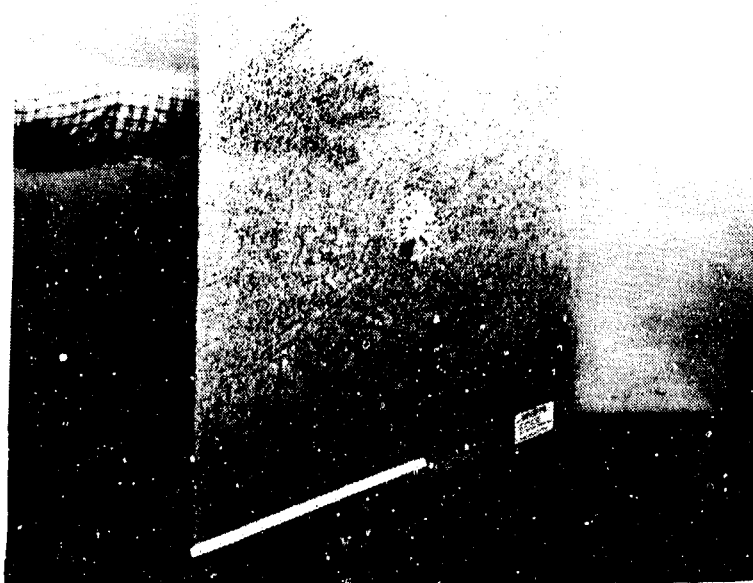


Figure 94. Chemically Tempered Glass (50,000 psi MOR)  
Fracture Pattern - 30,000 Particles/Ft<sup>2</sup>.

specimen consisted of two plies of 0.095-inch soda lime glass laminated with a PVB interlayer, which fractured as a result of an ultimate pressure loading test. The fracture pattern was moderately dense and was divided into graded zones as shown in Figure 95.

Each specimen was classified relative to the fracture density in particles per square foot, as shown in Figures 96 through 101.

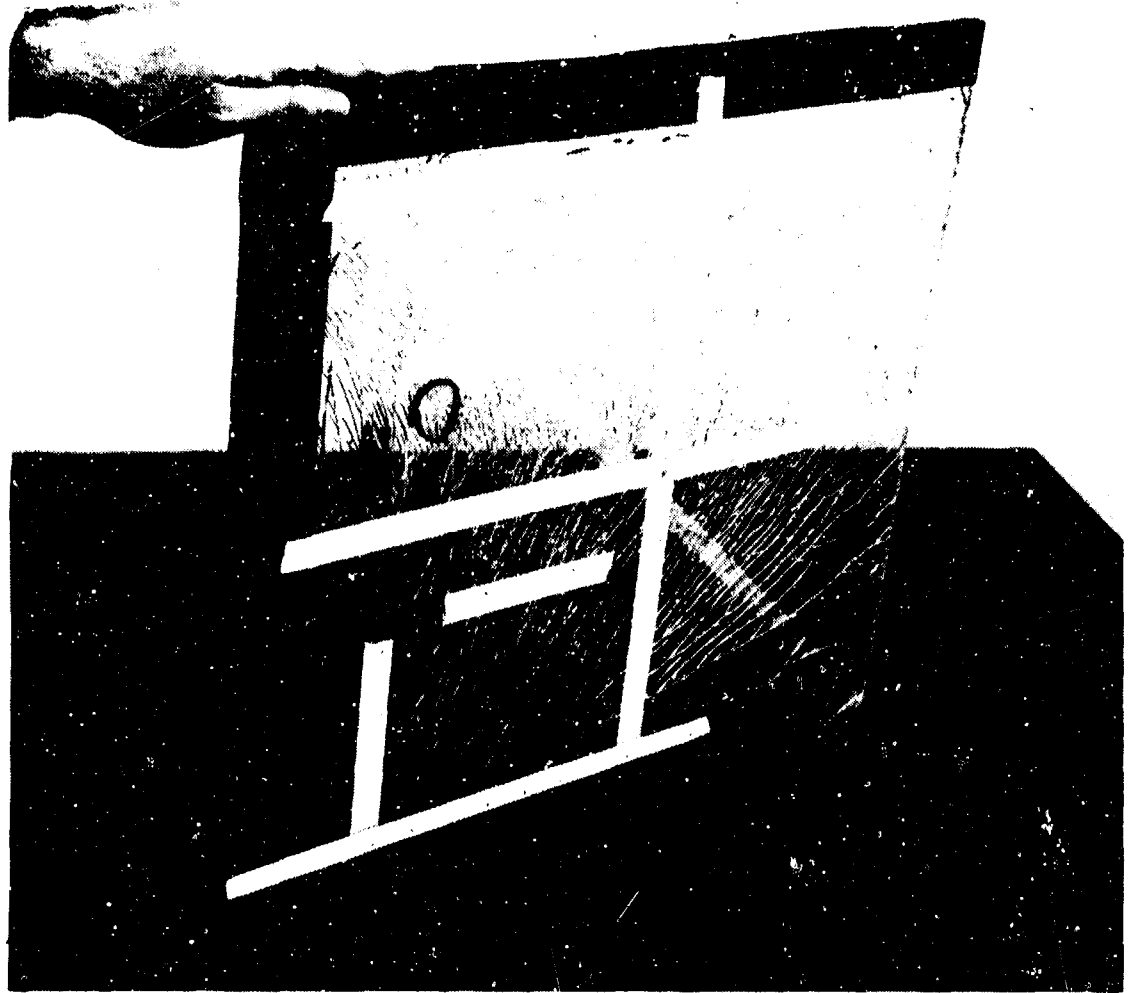


Figure 95. Fracture Pattern From Pressure Test.

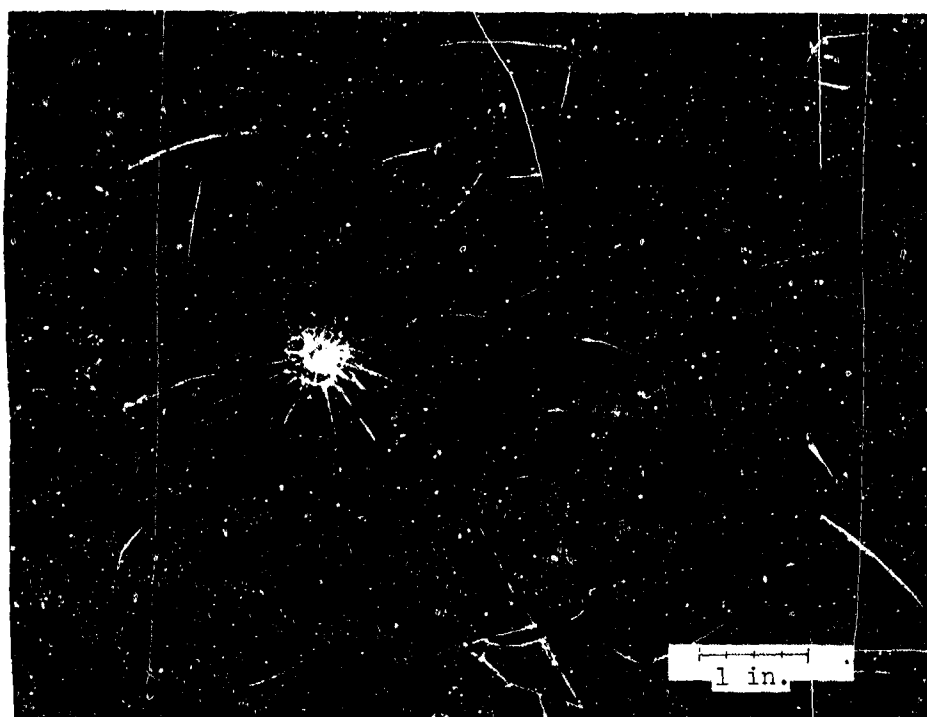


Figure 96. Particle Density, 250 Per Square Foot.

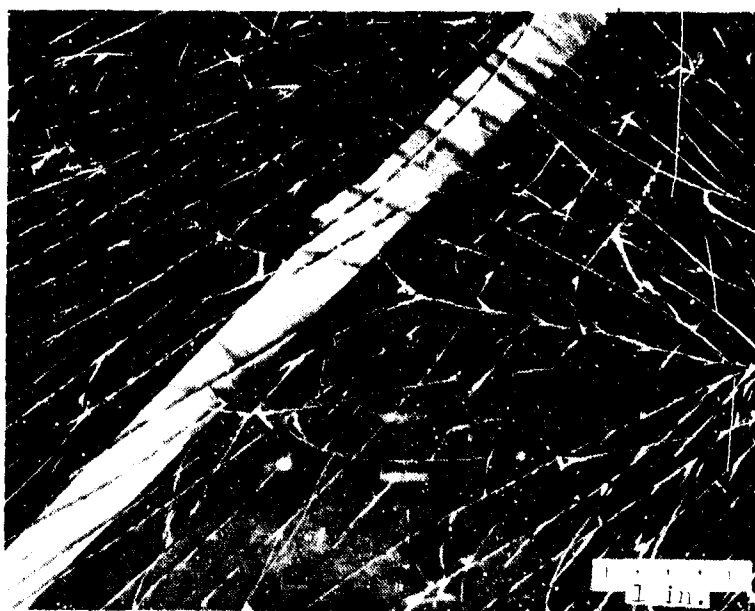


Figure 97. Particle Density, 1600 Per Square Foot.

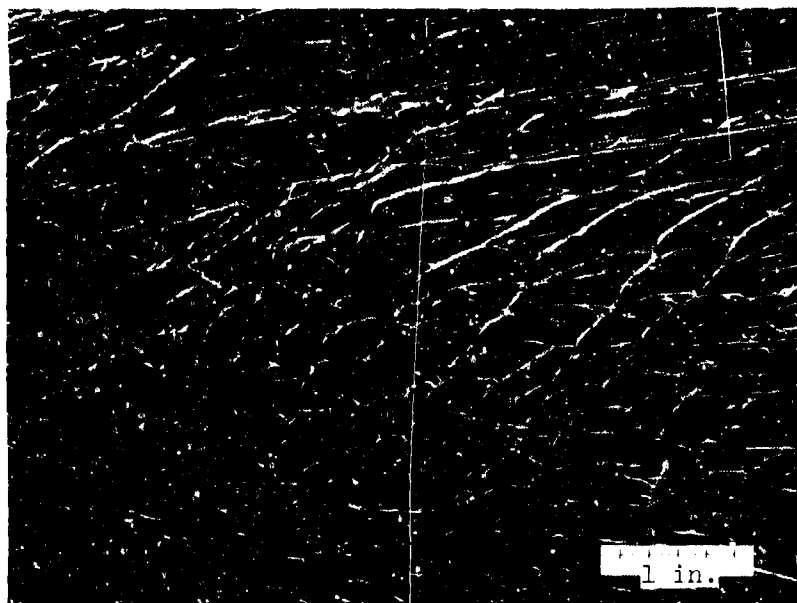


Figure 98. Horizontal Cracks, Particle Density, 4300 Per Square Foot.

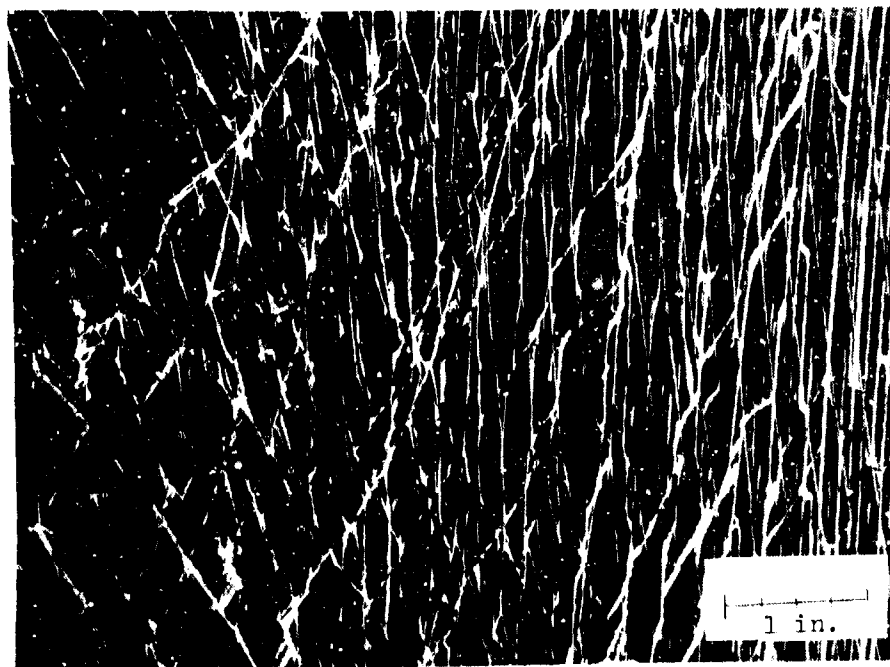


Figure 99. Vertical Cracks, Particle Density, 5200 Per Square Foot.

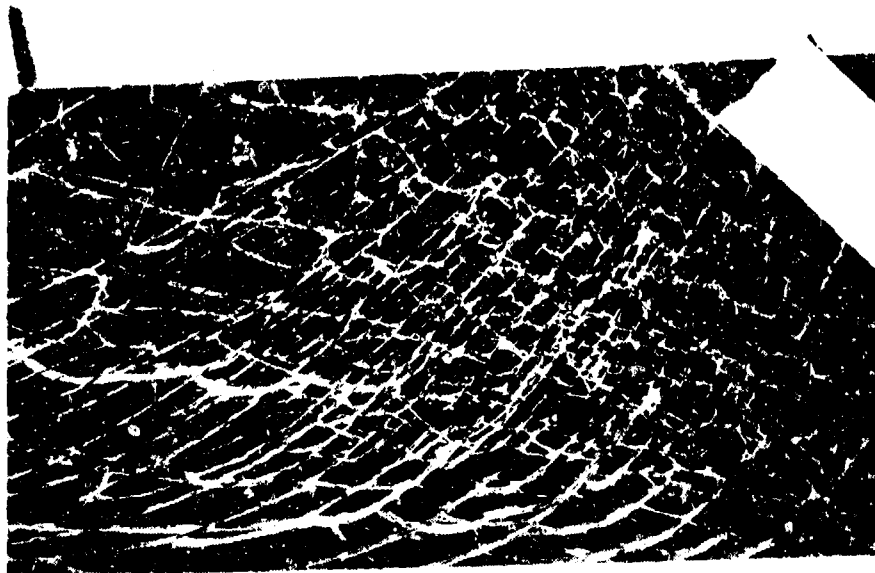


Figure 100. Particle Density, 18,000 Per Square Foot.

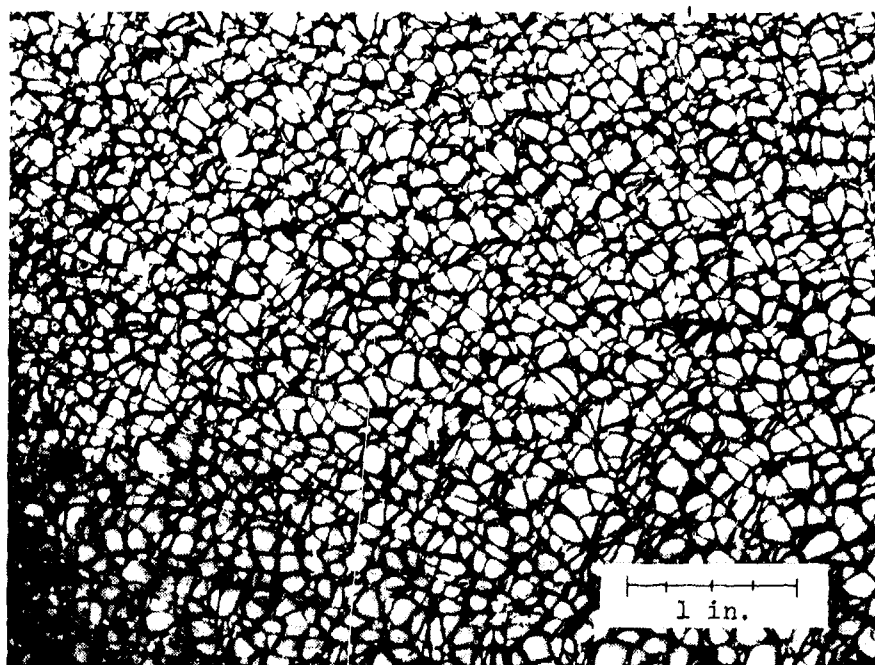


Figure 101. Particle Density, 30,000 Per Square Foot.

## OBJECTIVE MEASURES

In the objective test, data was collected by having subjects view a target through each of the specimens held at specific angles of incidence to the viewer. The viewer errors and time to read the chart were the scoring factors.

### Targets

Seven eye charts containing five lines of random letters on each, similar to that shown in Figure 102, were used in this test. The size of the characters corresponded to acuity levels for 20/10 through 20/40 eyesight.

C D T L F P O E  
T C P D O E F L  
H L E F O D P C T  
E O L T C D F P  
D L F E T C P O

Figure 102. Typical Target Card.

### Procedure for Objective Measures

1. The charts were placed about 14 feet from the viewer's head and perpendicular to the line of sight.
2. The subject read the charts, and his performance was recorded on the basis of errors in reading the letters and the time it took to complete the chart.
3. The specimens were then placed in front of the subject perpendicular to the line of sight and the process was repeated. Different starting points were used on each trial to minimize learning effects.
4. Step 3 was repeated twice with the specimen tilted 30° and 45° to the vertical.

## SUBJECTIVE MEASURES

Subjective measures were taken by having five test pilots view an outside scene through each of the test panels. As in the objective measures, the panels were tilted at 30° and 45° to the line of sight as well as perpendicular to it. Subjects were asked to rate visibility through the panels according to the following set of instructions:

"Rate your confidence in your ability to fly back to an airfield and make a satisfactory landing if you had to look through the windscreen in front of you. Do this by selecting a number from 0 to 10 indicating the confidence you have. Below are word descriptions of various ratings to give you a standard on which to base your ratings."

<u>Rating</u>	<u>Description</u>
10	Can fly home easily with not much more effort than normal flight.
7.5	I can see well enough to fly. I would not declare an emergency.
5	Safe flight would be difficult, I <u>would</u> declare an emergency.
2.5	Safe flight is very difficult, I'm not sure I could land safely.
0	Safe flight is impossible.

## RESULTS

A comparison of time scores for untilted and tilted glass is shown in Figure 103. Examination of the data showed that as the angle of incidence increased, the subjects took longer to read the chart. For the vertical case, it can be seen that time to read the charts increased with particle count. In the tilted column, the results still varied in a predictable manner except for the case in which the fractures formed a horizontal pattern. Horizontal fractures are particularly sensitive to window tilt because the action of tilting the window increases the visual angle obscured by each fracture. Crack patterns, especially horizontal ones, tend to obscure targets rather than to reduce the acuity of vision through the glass. Those areas not crossed by fractures have the same acuity as unfractured glass. This condition is shown in Figure 104.

Scores based strictly on the number of errors in reading the resolution chart had no meaningful relationship with angle of incidence of fracture pattern. This was probably due to the effects of learning. That is, subjects were able to find a clear facet in the fracture pattern and move their heads in a way that allowed them to view the letter they were trying to read through the spot.

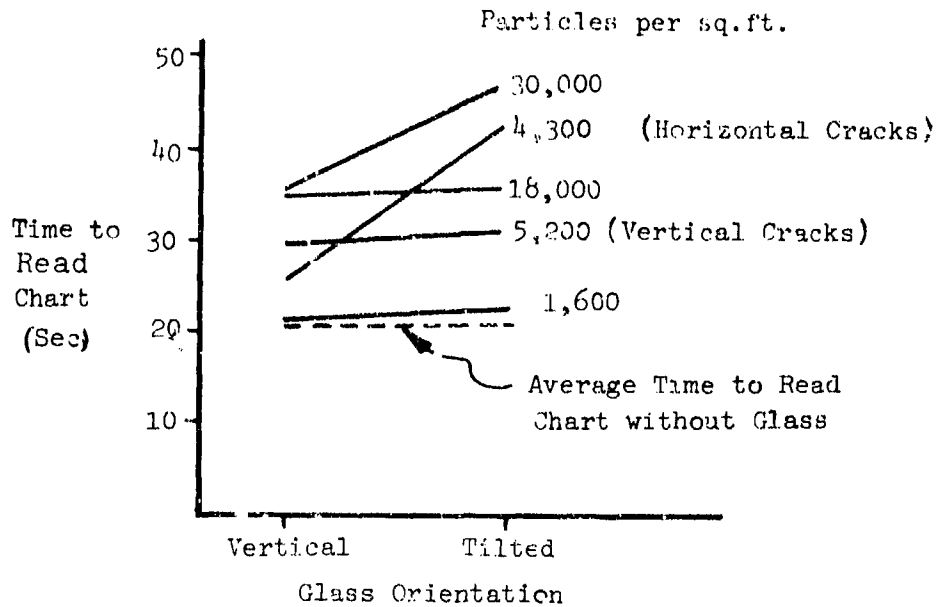


Figure 103. Effect of Crack Density on Visual Response Time.

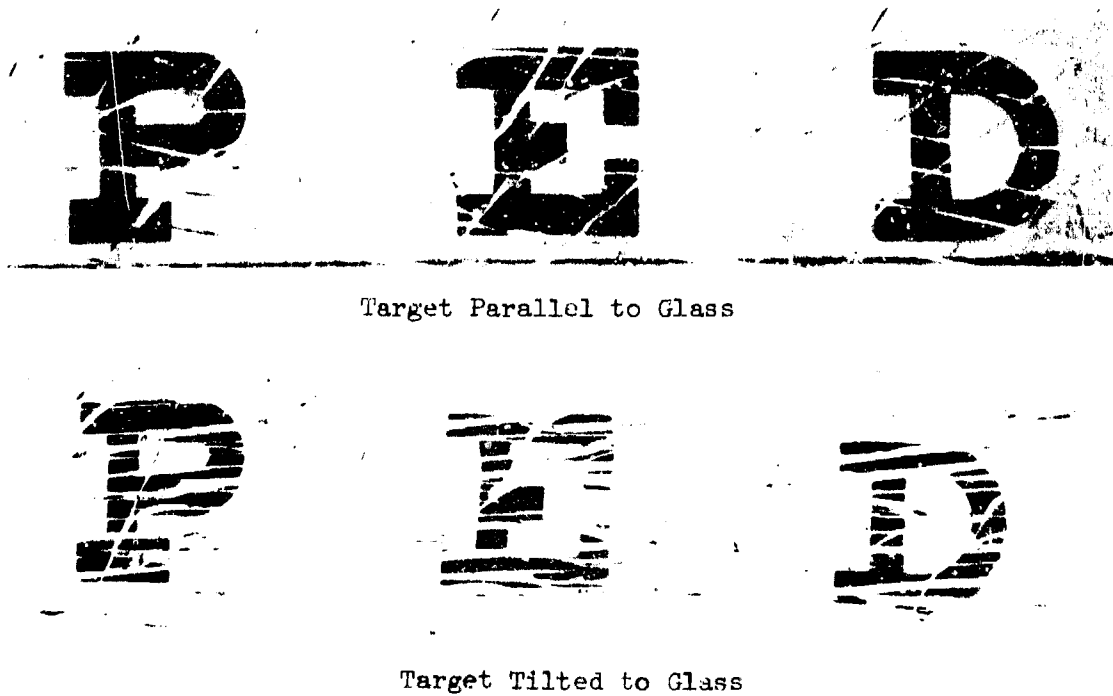


Figure 104. Lateral Crack Pattern vs Angle of Incidence (Effect on Residual Visibility).

After examining the pilot subjective data, it was decided that the most meaningful way to categorize pilot reactions was to divide them into groups: Satisfactory and Unsatisfactory. This was done because it was felt that a transparency specification should call out materials that will not cause pilots to declare an emergency after a fracture pattern propagates across their primary viewing area. Thus, all pilot ratings of 5 and below were classified as unsatisfactory, and those above 5 as satisfactory.

The data in Table 29 show the percentage of pilots giving a satisfactory rating. Ratings of 100% and 0% show total agreement. Data between these values show the percentage of pilots giving a satisfactory rating. In general, the ratings became more unsatisfactory as the angle of incidence increased. As the number of particles per square foot increased, the number of pilots rating the glass as unsatisfactory increased until at about 20,000 particles per square foot, all of the pilots judged the glass to be unsatisfactory. It is assumed that the fracture patterns on which pilots did not agree represent borderline areas.

TABLE 29. PILOT RATINGS OF RESIDUAL VISIBILITY

Particle Count	Angle of Incidence			Comments
	90°	30°	45°	
0	100%	100%	100%	
2	100%	100%	100%	
250	100%	100%	100%	
1,600	100%	80%	40%	
4,300	80%	0%	0%	Horizontal Cracks
5,200	100%	100%	100%	Vertical Cracks
18,000	80%	0%	0%	
30,000	0%	0%	0%	

100%-All Agree Window is Satisfactory

0%-All Agree Window is Unsatisfactory

#### RESIDUAL VISIBILITY CONCLUSIONS

The results of this effort showed that glass with fracture patterns of less than 1,000 particles per square foot are judged to have satisfactory residual visibility. A satisfactory panel was defined as one which cracks but does not cause the declaration of an emergency.

## FIELD STUDY OF ARMY HELICOPTER TRANSPARENCIES

Army helicopter transparencies under actual service conditions were studied at Fort Rucker, Alabama. Four types of data were collected: pilot ratings of haze in sample specimens, measurements of light transmitted through tinted windows, photographs of optical distortions caused by transparencies, and pilot responses to a questionnaire. In addition, informal discussions were held with pilots and maintenance personnel to discover problems and techniques used to maintain windshields.

### PILOT HAZE RATINGS

The amount of haze in transparencies can be measured very accurately, but the point at which haze starts to interfere with pilot function is not known. To determine this level, a standardized measure of pilot opinion was needed. This was accomplished as follows:

A set of eight abraded acrylic specimens with varying degrees of scratch intensity, ranging from clear (0.4% haze) to almost opaque (52% haze), were prepared. Specimen haze was measured by the U. S. Army Aeromedical Research Laboratory at Fort Rucker. The scratches were produced by pulling steel wool across the surface of the specimen under a constant pressure. A viewer consisting of a flat black tube with a holder to support the specimen at a fixed distance from the eye was constructed (Figure 105). Pilots were asked to look through the device at external scenes and were given the following instructions to rate the haze specimens.

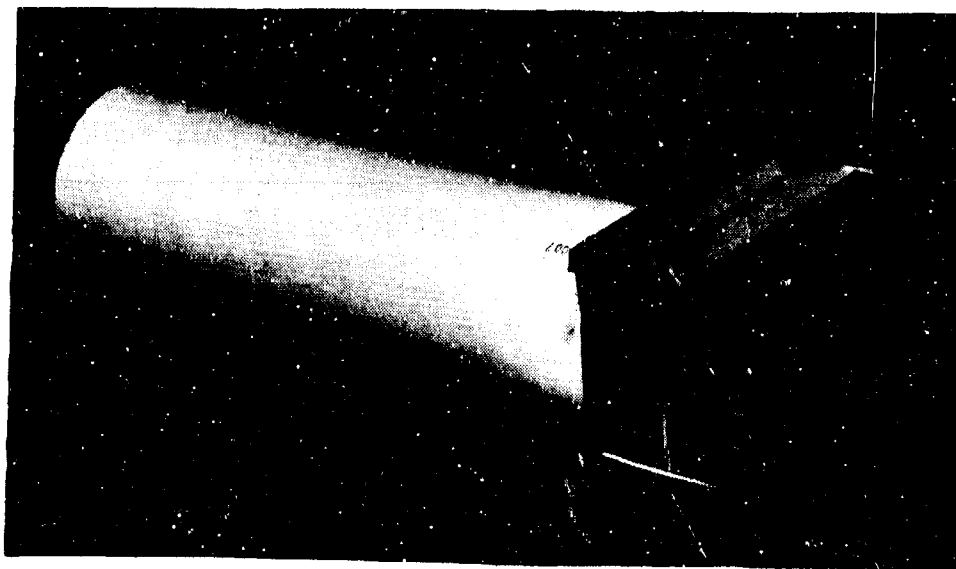


Figure 105. Viewer for Rating Haze Levels.

"As part of a study of windshield criteria, we would like your reaction to various amounts of surface scratches on glass. To do this, we will show you eight samples of glass and ask you to rate them on a scale of one to nine. In assigning your rating to each piece, use the table below (Table 30) as a guide. While judging, move the tube to look at varying light levels."

TABLE 30. SCALE FOR RATING HAZE SPECIMENS

Rating	Description
1	<u>Good</u> : Unaware of glass scratches.
2	
3	<u>Satisfactory</u> : I am aware of scratches but they are not annoying.
4	
5	<u>Poor</u> : The scratches are annoying but do not prevent seeing.
6	
7	<u>Marginal</u> : Very annoying, can still fly but would crab the glass after the flight.
8	
9	<u>Unsatisfactory</u> : I would not take off with a windshield this bad.

Data was collected from thirty-eight helicopter pilots. Although the data was divided between three types of aviators (single engine, multi-engine and test pilots), only the results of the test pilots were different from those of the group as a whole. As a group, test pilots were more tolerant of haze than others.

Since the goal of the study was to determine the level at which haze would cause pilots to request corrective action, the ratings were divided into two groups. Ratings of 1 through 6 were considered satisfactory and ratings 7 through 9 were unsatisfactory. Figure 106 is a plot of the percent of unsatisfactory ratings against the percentage of haze in the chips.

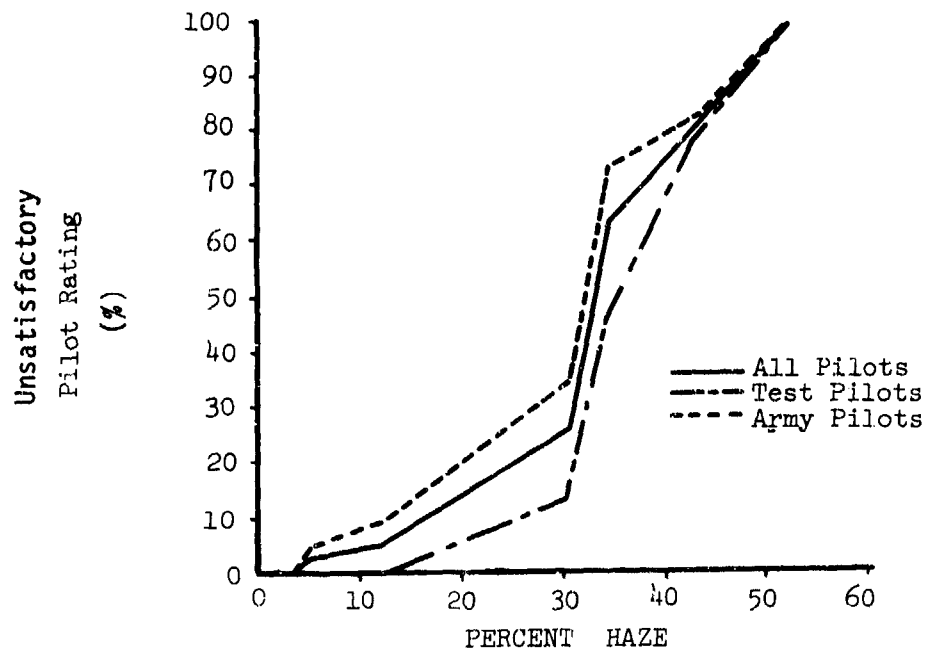


Figure 106. Plot of Unsatisfactory Pilot Ratings vs Haze.

The point at which the curve begins to rise rapidly is indicative of how much haze will be tolerated by flight personnel before a removal is effected. The data collected showed that a level of haze between 15% and 20% was accepted by at least 80% of the Army pilots tested. Comparison of the test chips with helicopter windows at Fort Rucker showed that almost all windows exhibited haze levels of less than 12%.

Figure 107 is a plot of pilot ratings against percentage of haze in the samples. It is provided to show the consistency with which pilots reacted. The vertical bars show the range between the 10th percentile and the 90th percentile for each sample.

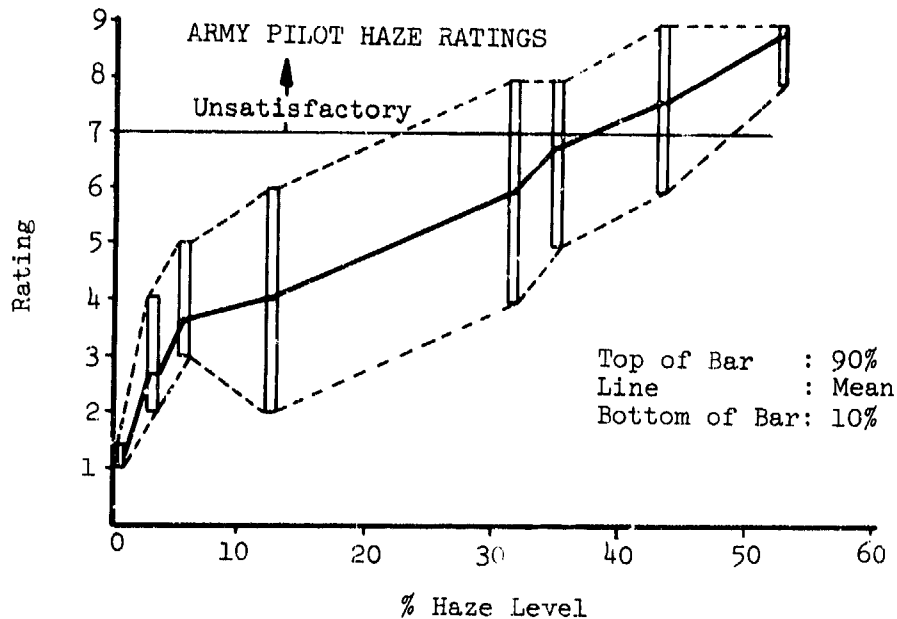


Figure 107. Army Pilot Haze Ratings.

#### TINTED WINDOW LIGHT TRANSMISSION

Specifications for tinting the helicopter overhead windows have not been controlled by the government. As a result, considerable variation in light transmission and color exists on Army helicopters. In order to evaluate the acceptance of tinting, light transmission measurements were taken through tinted windows on nine different helicopter models.

The method of measurement involved using a modified flashlight as a standard light source and a photographic light meter as a sensor. Both the flashlight and the meter were mounted on cardboard tubes to isolate them from ambient light. Measurements were taken with the light held directly against the sensor and then repeated with a window placed between the light source and the sensor. The difference between the two readings represented the loss in light transmitted through the window. The light from the flashlight was defused and reduced in brightness to coincide with the most accurate portion of the light meter's range. In tests made prior to field measurements, the system was shown to be accurate within 3% of the true value of the samples tested.

The average light transmittance measured through the tinted roof windows of Army helicopters and some Sikorsky Navy helicopters is shown in Table 31. The amount of light transmitted ranged from 15% to 85%. The darkest tinting was in the OH-6, where the glass was so dark that it was difficult to see through except in bright environments. The lightest tint was in cobra cockpits.

TABLE 31. LIGHT TRANSMISSION MEASUREMENTS FOR HELICOPTER OVERHEAD WINDOWS

Aircraft	Location	Average Light Transmittance
AF-1	Whole Canopy	85.5%
UH-1	Roof	66.3%
OH-5b	Roof	76.3%
OH-6	Roof	15.8%
TH-55	Roof	27.4%
CH-47	Center Windshield	77.4%
CH-3	Roof	29.2%
CH-54	Roof	30.3%
CH-53	Roof	28.9%

#### PILOT QUESTIONNAIRE

The objective of this effort was to obtain information on pilot reactions to transparencies in present Army helicopters. This was done by obtaining responses to a questionnaire on five aspects of cockpit transparencies:

- distortion
- haze
- small imperfections
- tinted windows and reaction to cockpit windows in general.

Forty-six aviators were involved, representing a cumulative flight experience of 130,000 hours, approximately 16,000 hours of which were night flight.

It was also desired to categorize some of the information by specific helicopter models. To do this, pilot experience with each type of helicopter had to be taken into account. This was done by using the number of hours flown in various types of helicopters. A pilot was considered to be exposed to a specific helicopter only if he had at least 70 hours flight time in that vehicle.

The data was roughly divided into four categories: high exposure/high complaint, high exposure/medium complaint, high exposure/low complaint, and low exposure/no complaints, as shown in Table 32. It was felt that conclusions could be

drawn from the first three categories, while the last group could only be used with caution. One might conclude that the aircraft in the last group had very good windows or one might conclude that not enough exposure was involved to elicit any comments.

TABLE 32. PILOT EXPOSURE TO AIRCRAFT EVALUATED IN QUESTIONNAIRE

Category	Aircraft Type	No. of Pilots Exposed	Total Flt Time by Model (hrs)	Percent Complaining (%)
High Exposure/ High Complaint	OH-58	10	7055	90
	AH-1	10	12040	90
	CH-47	11	8491	82
	UH-1	43	53435	70
High Exposure/ Medium Complaint	OH-6	4	1250	25
	OH-3	12	5415	25
	CH-53	12	4390	25
	H-34	14	6220	14
High Exposure/ Low Complaint	OH-13	12	6130	8
	TH-55	13	3475	8
	OH-23	15	3285	7
Low Exposure/ No Complaint	CH-19	8	3725	0
	CH-54	6	3300	0
	CH-21	4	3236	0
	CH-37	2	800	0

It should be noted that the UH-1 was a dominant factor in pilot experience. Almost all pilots reported UH-1 experience, and the number of flight hours of the pilots as a group showed more than four times as many hours in the UH-1 as in the next nearest helicopter (AH-1). The resulting comments were therefore heavily influenced by UH-1 experience.

A summary of the replies obtained for each question is included in the appropriate spaces following the question in the sample questionnaire which follows. The percentages noted represent the fraction of pilots responding affirmatively to the particular question.

"COCKPIT WINDOW QUESTIONNAIRE"

I. As you view objects through helicopter windows, do they change shape or become wavy due to distortions in the glass or plastic?

A. YES 70% NO    

B. If they do, please check the location, severity, and helicopter model in the below matrix.

Helicopter Model	Window	Severity			Location		
		Slight	Moderate	Major	Edge	Center	Random Throughout
*	Main Windshield	20%	14%	2%	27%	2%	11%
*	Side	10%	16%	4%	2%	4%	23%
*	Roof	6%	6%	2%	4%	0	7%
*	Chin	6%	10%	6%	7%	0	11%
<b>Total</b>		<b>41%</b>	<b>45%</b>	<b>14%</b>	<b>40%</b>	<b>7%</b>	<b>52%</b>

\*Response to this question was distributed by helicopter models as shown below.

Window	Helicopter Model								
Main Windshield	AH-1	-	10%	CH-47	-	3%	CH-3	-	10%
	UH-1	-	34%	OH-13	-	3%	CH-53	-	14%
	OH-58	-	17%	CH-34	-	7%			
Side Windshield	AH-1	-	13%	CH-34	-	7%			
	UH-1	-	60%						
	OH-58	-	20%						
Roof Windows	AH-1	-	12%	CH-34	-	12%			
	UH-1	-	50%						
	OH-58	-	25%						
Chin Window	UH-1	-	53%	CH-47	-	7%			
	OH-6	-	7%	CH-3	-	7%			
	OH-58	-	20%	CH-53	-	7%			

C. Have these distortions affected your performance?

YES 32% NO         

D. If they have, please fill out the matrix below.

Difficulty	Effect		
	Slight	Moderate	Severe
Takeoff	11%	2%	2%
Landing	9%	11%	4%
Reconnaissance	11%	4%	2%
Navigation	9%	2%	2%
Formation	6%	6%	2%
Weapon Use	9%	0	0
Other			
Total	54%	28%	17%

E. Has this type of distortion caused you any personal discomfort such as:

Airsickness	<u>0</u>
Fatigue	<u>8%</u>
Headache	<u>8%</u>
Annoyance	<u>40%</u>
No Effects	<u>32%</u>
Other	<u>10%</u>

(Please describe briefly in the space below)

*About one pilot in four made a comment in this section. About half of those had to do with autorotations, landings or depth perception. This indicated that distortions caused most problems when the vehicle was near another object (ground aircraft, etc.).*

F. Have you had any problems looking through electrically heated windshields?

YES 7% NO          WHICH MODEL AIRCRAFT CH-47

If yes, briefly describe the problem.

*Only two pilots commented on the anti-ice system effects. Both concerned delaminations of the windshield.*

G. Have you had any vision problems with windows deflecting due to wind pressure in flight?

YES 3% NO     

If yes, which model aircraft OH-6

Briefly describe in the space below.

*One pilot indicated that he had problems at high speeds in the OH-6.*

H. Do you have any general comments on window distortions?

*Thirty-two percent of the pilots made negative responses. Of these, over half commented on wipers scratching the windscreen. In addition, two pilots commented on problems during night flight and reflections caused by lights from the ground. All of the other comments were on different aspects of distortion with no two the same.*

II Have you flown vehicles with tinted windows?

A. YES 75% NO     

B. If yes, which vehicle AH-1, CH-47, UH-1, OH-58, CH-34, SH-3, CH-54.

C. Which windows were tinted?

Windshield 32%

What Color? Blue, Gold, Green

Roof 53%

Other 15%

D. Has the tinting adversely affected your performance?

YES 21% NO     

E. If yes, please fill out the matrix below.

Difficulty	Effect			Time of Day			
	Slight	Moderate	Major	Twilight	Sunlight	Overcast	Night
Recognizing Objects	12%	12%	12%	7%	7%	7%	11%
See Colors	12%	0	12%	7%	7%	7%	7%
Range of Vision	0	0	25%	7%	7%	7%	11%
Other (describe)			12%	3%	3%		
Total	25%	12%	62%	25%	25%	21%	28%

F. General comments on tinted windows.

30% of the comments received on tinted windows were positive in nature, i.e., compliments rather than complaints. Thus, when combined with the pilots who did not respond to this question, one can say that about three-quarters of the pilots either felt that tinted glass was a good thing or had a neutral attitude toward it.

Of the 21% who complained about the tinted windows, most complaints concerned the tendency for tinted windows to interfere with night vision and a tendency to detect dirt and scratches more readily on tinted windows.

III Defects on the surface or within windows sometimes cause windows to become hazy or foggy in appearance. Have you ever noticed this in the vehicles you have flown?

A. YES 76% NO     

B. If yes, describe the location and severity below:

Helicopter Model	Window	Severity		
		Slight	Moderate	Major
*	Main Windshield	7%	27%	7%
*	Side	5%	11%	9%
*	Roof	5%	7%	7%
*	Chin	3%	7%	3%
Total		20%	52%	26%

\*Response to this question was distributed by helicopter models as shown below.

Window

Helicopter Model

Main Windshield	UH-1 - 50%	AH-1 - 15%	CH-34 - 9%
	OH-58 - 12%	CH-47 - 3%	CH-53 - 6%
	TH-55 - 3%	CH-3 - 6%	
Side Windshield	UH-1 - 43%	AH-1 - 26%	
	OH-58 - 14%	CH-3 - 5%	
	TH-55 - 5%	CH-34 - 5%	
Roof Window	UH-1 - 60%		
	OH-58 - 30%		
	AH-1 - 10%		
Chin Window	UH-1 - 67%		
	OH-58 - 25%		
	TH-55 - 8%		

C. Has the occurrence of haze or fog in windows affected your performance?

YES 65% NO \_\_\_\_\_

D. If yes, please fill out the matrix below.

Difficulty	Effect			Time of Day			
	Slight	Moderate	Major	Twilight	Sunlight	Overcast	Night
Glare	6%	16%	16%	6%	11%	3%	8%
Identifying Objects	12%	14%	4%	6%	9%	6%	8%
General Annoyance	8%	16%	10%	11%	13%	7%	10%
Other							
Total	26%	46%	30%	23%	33%	16%	26%

E. Is the haze worse with the sun in certain locations?

YES 75% NO \_\_\_\_\_

Where?

No replies.

F. What in your opinion is the cause of hazy windows?

Poor Window Materials	19%
Lack of Cleaning	27%
Too Much Cleaning	7%
Windshield Wipers	23%
Old Age	19%
Don't Know	6%
Other	7%

G. General comments on haze in windows:

About one pilot in three made general comments on haze. Most of these comments concerned the importance of haze free windows in permitting pilots to see for Nap-of-the-earth and night flying. The remaining comments were divided between complaints about window maintenance and observations that better wipers or harder windshield materials are needed.

IV. Sometimes aircraft windows have small imperfections within the glass (bubbles, scratches, discolorations, etc.). Have you ever noticed such imperfections in ships you have flown?

A. YES 76% NO     

B. If you have, indicate the severity and location below:

Helicopter Model	Window	Severity		
		Slight	Moderate	Major
*	Main Windshield	20%	22%	6%
*	Side	13%	11%	0
*	Roof	7%	4%	2%
*	Chin	7%	6%	2%
Total		47%	43%	10%

\*Responses to this question were distributed by helicopter model as shown below.

<u>Window</u>	<u>Helicopter Model</u>		
Main Windscreen	OH-58 -	19%	AH-1 - 16%
	UH-1 -	51%	CH-53 - 8%
	CH-47 -	13%	CH-34 - 3%
Side Windshield	OH-58 -	14%	AH-1 - 24%
	UH-1 -	48%	CH-3 - 5%
	CH-47 -	9%	
Roof Window	OH-58 -	18%	AH-1 - 15%
	UH-1 -	55%	
	CH-47 -	9%	
Chin Window	OH-58 -	23%	
	UH-1 -	69%	
	CH-47 -	7%	

C. Has this type of imperfection ever affected your flight performance?

YES 26% NO     

D. If yes, briefly describe the defect and problem.

*About one pilot in four made a comment. The following window defects were mentioned: delaminations, scratches, dirt, craze, bubbles.*

*The following tasks were affected: formation, NOE, night flight, autorotations, forced landings, take offs, depth perception, flight in marginal weather.*

V. How would you rate helicopter windows in general?

A. Good	<u>23%</u>
Satisfactory	<u>34%</u>
Adequate	<u>17%</u>
Poor	<u>17%</u>
Unsatisfactory	<u>9%</u>

B. Do you have any general complaints about helicopter windows?

*Over 70% of the pilots responded to this question. Almost all of the responses had to do with scratches or cleaning of the transparency to improve visibility through the windshield.*

C. What improvements would you like to see in the future?

*Most of the pilots responded to this question with requests for scratch free materials or easier cleaning materials or better wipers, etc. These responses were mainly the result of UH-1 experience.*

PHOTOGRAPHIC DATA

A series of photographs were taken at Fort Rucker to document the condition of existing transparencies in an operational environment. The photographs showed flaws such as cracks, delaminations, scratches and distortions resulting from optical imperfections.

A portable grid for evaluating optical distortion, shown in Figure 108, was used to locate and quantify optical distortion. Considerable experimentation was required to develop a technique for producing photographs with resolution adequate for measuring grid slope variation. The procedure finally adopted was to place the grid board approximately ten feet from the transparency with the camera at the pilot's eye position. A 4x telephoto lens was used to enable the grid to completely fill the picture. High-speed film with a shutter speed of 1/250th of a second was found to be necessary to prevent blurring lines due to motion of the grid or camera.



Figure 108. Test Grid Used to Measure Distortion.

The survey examined six types of helicopters at Fort Rucker and one type at Sikorsky, as follows:

CH-53: Prior to the visit to Fort Rucker, photographs of Sikorsky helicopters located at the factory were taken, both for practice and to examine distortions exhibited by cargo helicopters. Since most of the Sikorsky helicopters were new and had not been used in the field, little in the way of scratches or flaws was seen, although minor amounts of edge distortion were found in most helicopters photographed.

However, Figure 109 shows a delamination in the left front canopy of a CH-53A that was in for overhaul. The photograph shows that delaminations do not cause distortions, but increase opacity of the window. The picture also shows some edge distortion next to the delamination spot. Figure 110 is an external view of the aircraft showing the location of the delaminations.

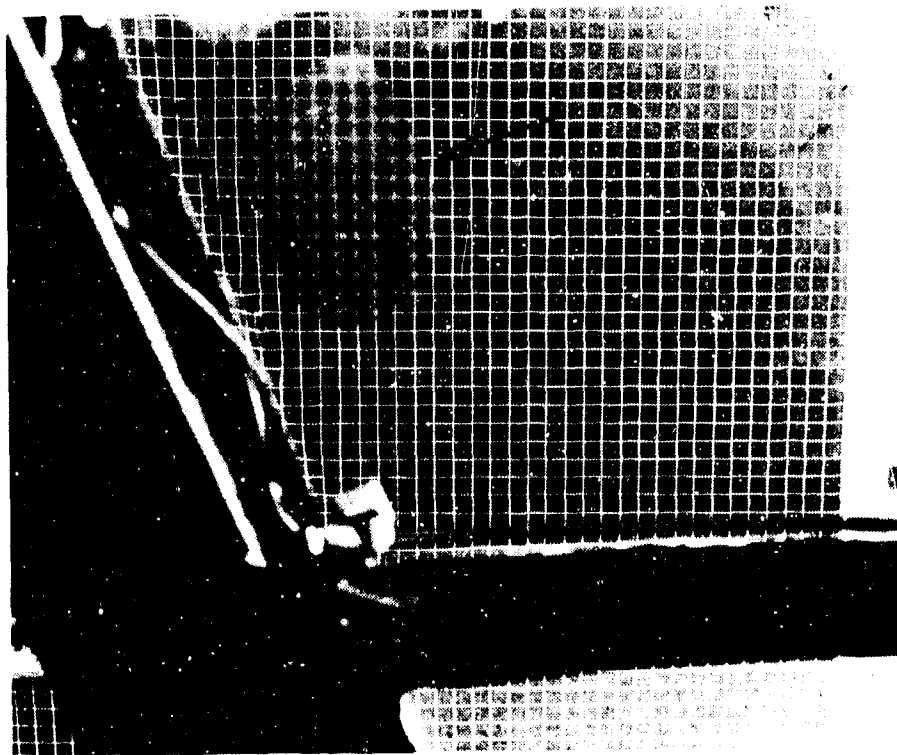


Figure 109. CH-53 Windshield Delamination.



Figure 110. CH-53, External View of Delaminations.

AH-1: Figure 111 is a photograph of the entire aircraft.

Pictures taken through the canopy showed little distortion except around the window edges as seen in Figure 112. The photograph, taken from the aft seat, looks out the left side of the helicopter and shows distortion on the front edge of the canopy. The lighter spots on the grid are caused by dirt and abrasions on the canopy surface.

Impact by a hard object on the canopy surface caused a bull's eye distortion as shown in Figure 113. The physical appearance of the defect was a small dent with a white spot in the center.

In addition to optical defects, Cobra canopies were characterized by many small scratches that tended to increase the haze level of the canopy. This is shown in Figure 114.



Figure 111. AH-1 Cobra, Overall View.

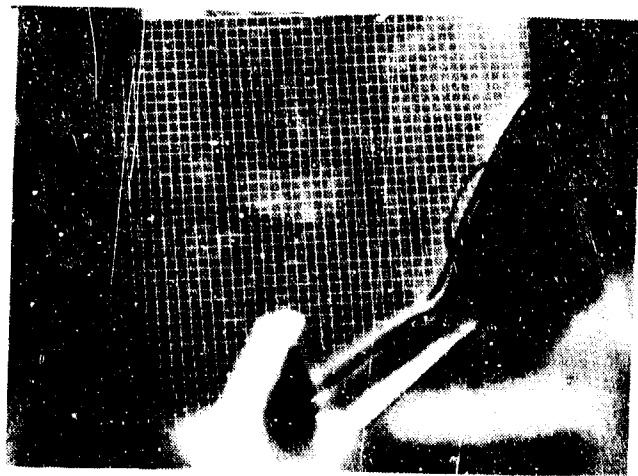


Figure 112. Cobra, Left Side Window.

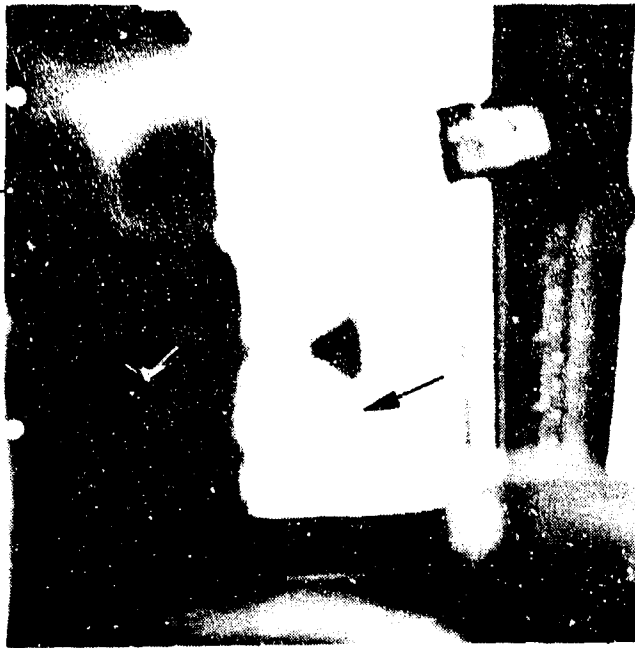


Figure 113. AH-1 Front Windshield, Bulb's Eye Distortion.



Figure 114. AH-1 Windshield Scratches.

UH-1 (Huey): The most frequent complaint voiced by pilots and maintenance officers was the tendency of the UH-1 windshield wipers to scratch the window when used. Most of the helicopters observed, however, showed no evidence of this problem. The reason for this was that the wiper switches at Fort Rucker are safety wired to prevent use except when absolutely required. Two instances were observed in which the wipers had scratched the plastic simply from vibratory motion (Figure 115).

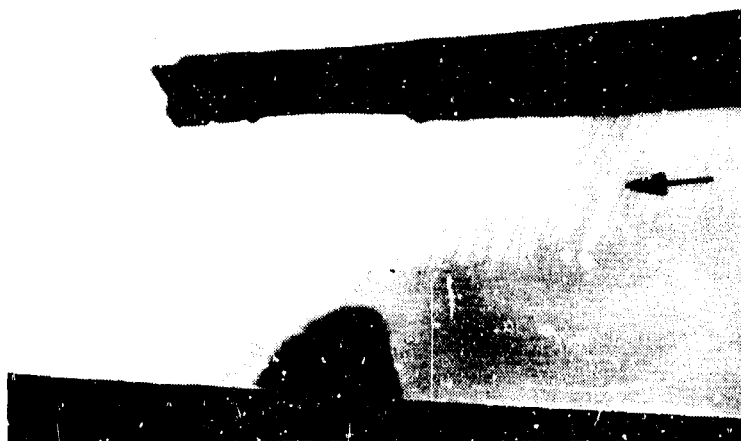


Figure 115. UH-1, Wiper Scratches From Vibration.

As in the Cobra, optical distortion could be found around the edges of the canopies. Figure 116 shows a typical situation at the edge of the front window in the UH-1 door. Measurements of the distortion showed a slope of about 1:10, which meets existing criteria for door windows.

A common observation of the UH-1 at Fort Rucker was a series of scratches on the side door windows. This window opens by sliding down into the door structure. Figure 117 is a view from inside the aircraft and shows translucent bands due to the scratches. Some of the pilots complained about side vision through this window. This defect was uncorrected in most aircraft because repair of the window requires replacement of the entire door since the window is not removable.

Figure 118 shows the entire vehicle and the relative locations of cockpit windows.

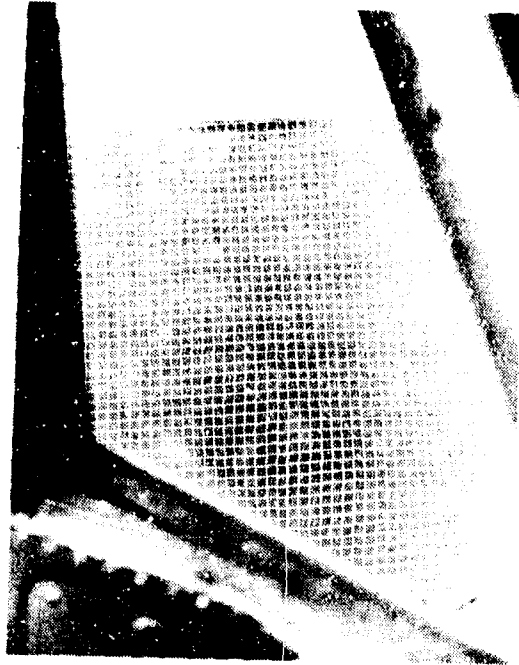


Figure 116. UH-1, Front Door Window, Wave Distortion.

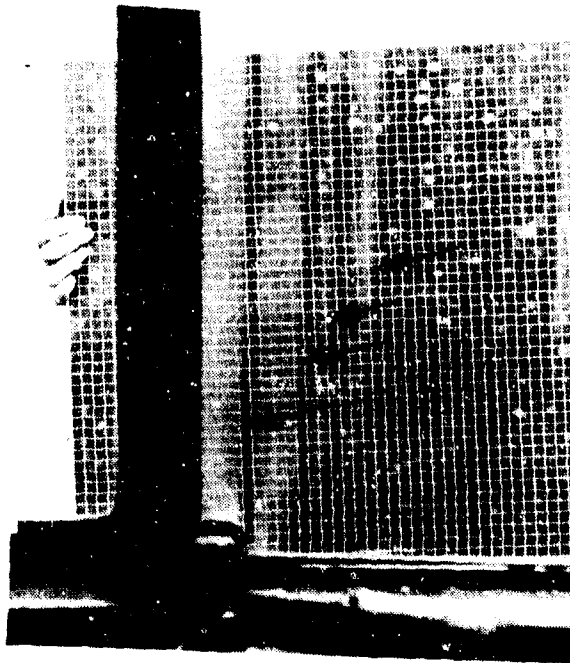


Figure 117. UH-1, Crew Door Window Abrasion.



Figure 118. UH-1, Overall View.

OH-58: An overall view of the OH-58 is shown in Figure 119.

Examination of the OH-58's at Fort Rucker showed edge distortion, as was found in all vehicles (see Figure 120). Figures 121 and 122 show the results of an impact by a hard object on the lower surface of the right window. As can be seen, the effect is one of localized distortion and an obscuring of the view.



Figure 119. OH-58, Overall View.

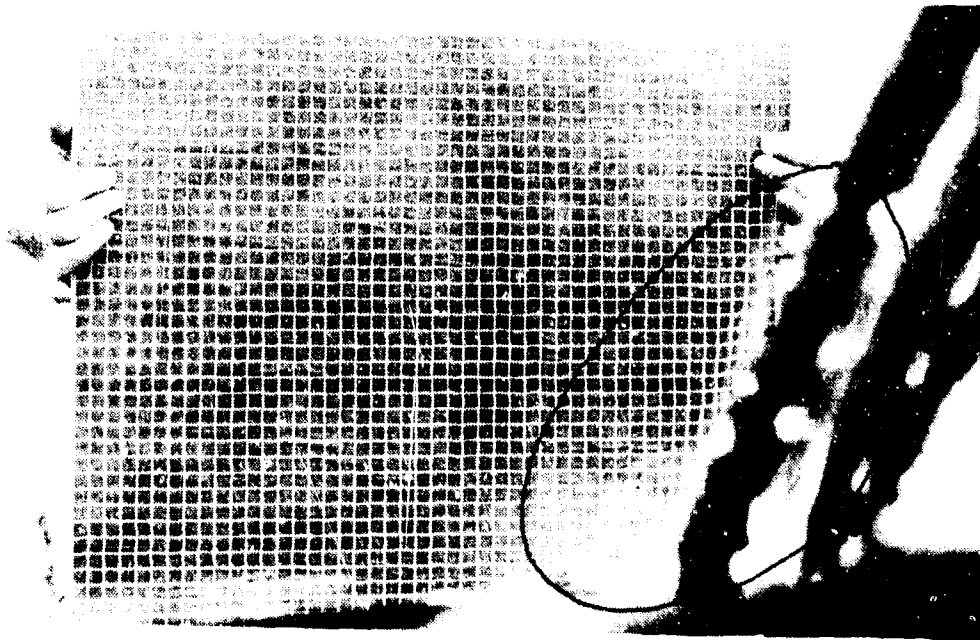


Figure 120. OH-58, Bottom Front Window, Edge Distortion.

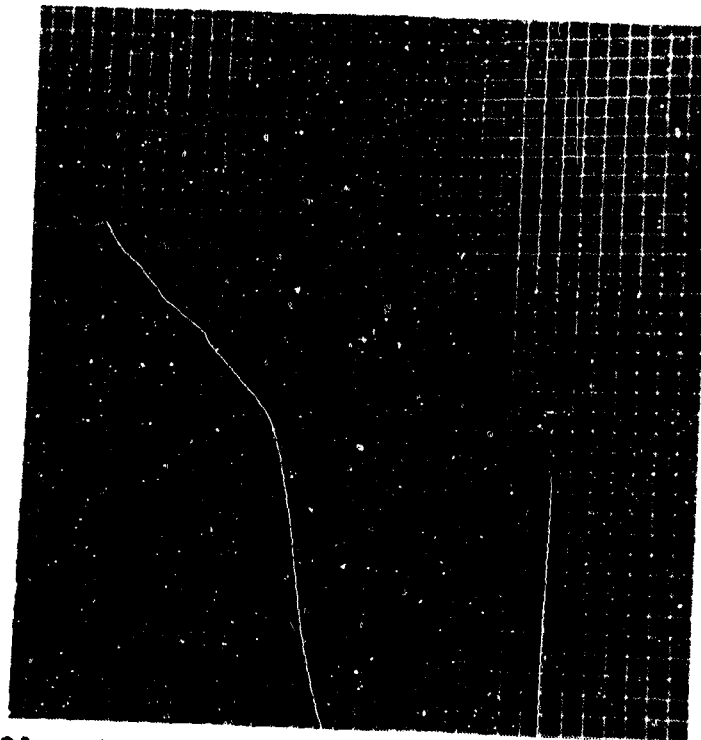


Figure 121. OH-58, Stone Strike, Grid Distortion.



Figure 122. OH-58, Stone Strike, Outside View.

CH-47: The windshield anti-icing systems in the CH-47's at Fort Rucker have been deactivated due to delamination problems. Figure 123 shows an example of front window delamination found in the CH-47. In the vehicles observed, center windshields were usually in relatively poor condition. The defects seen were scratches, edge distortions and wave-like imperfections in the center of the window. Figure 124 shows typical results. The distortions along the edges were measured to be 1:4 or worse. The wave-like distortions in the central part of the grid were 1:10. Apparently these distortions were not considered unsatisfactory since only about 5% of the main windshield distortion complaints were from CH-47 pilots.

Figure 125 shows the effects of scratches on vision through the center window. The scratches in this window were compared with the haze chips evaluated by pilots, and it was estimated that this window had a haze level of about 12%.

Figure 126 shows the appearance of the deletion line in the center windshield of a CH-47. This is an area where the windshield coating has been left off for electrical reasons. As can be seen, it caused little or no distortion. Figure 127 is an overall view of the CH-47 nose section.

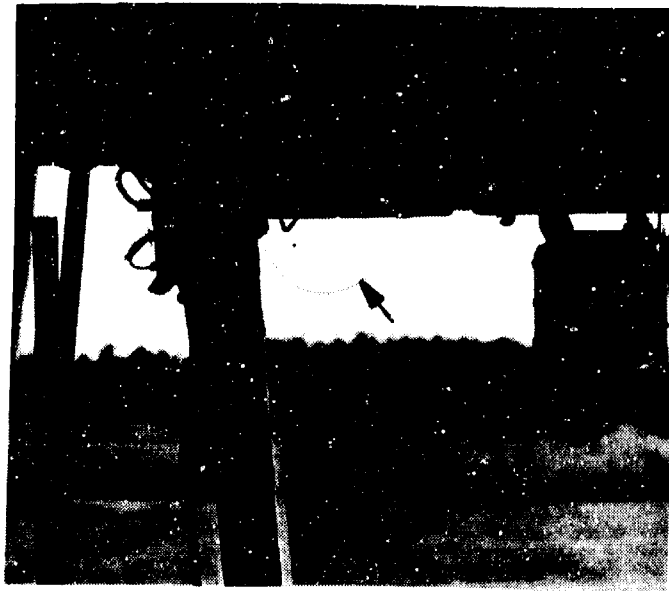


Figure 123. CH-47, Windshield Delamination.

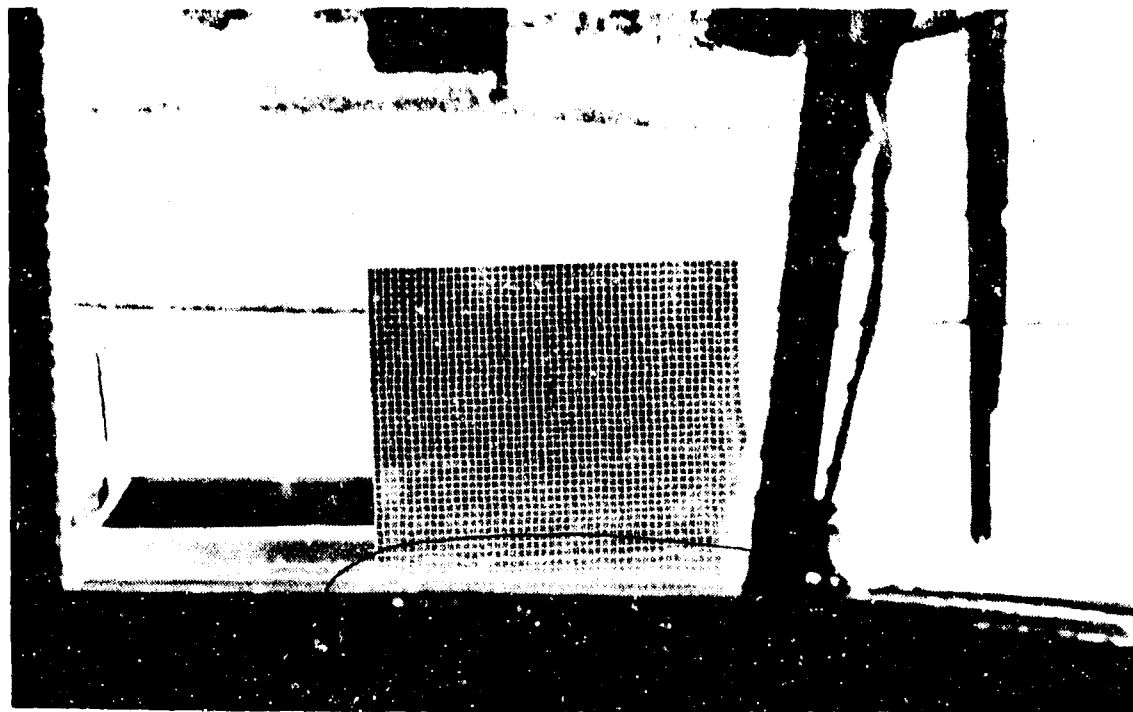


Figure 124. CH-45, Center Windshield Distortions.

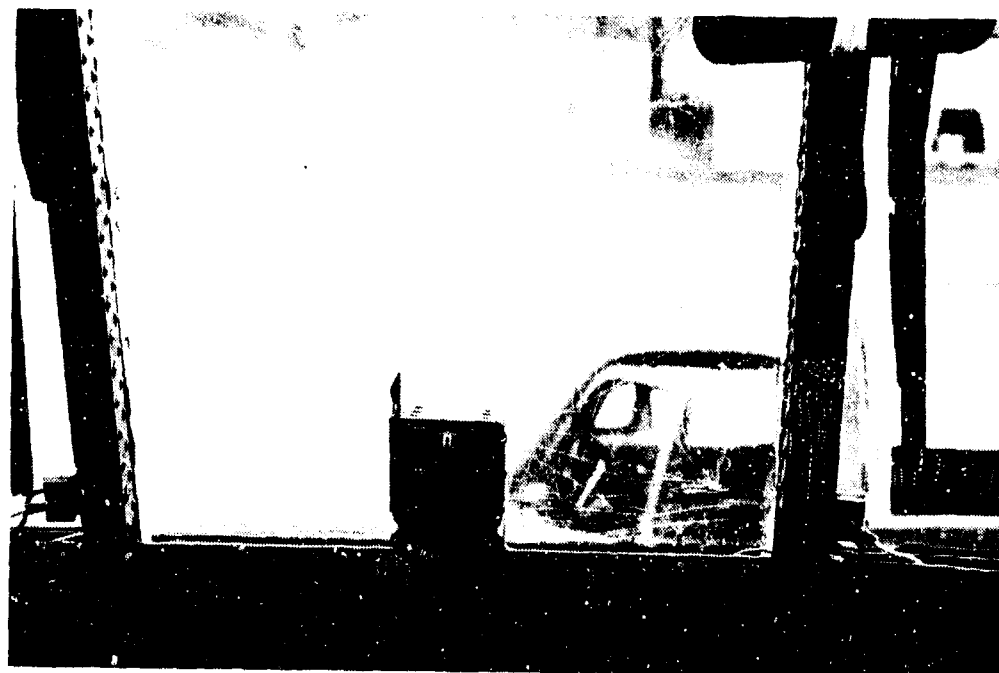


Figure 125. CH-47, Center Windshield Scratches.

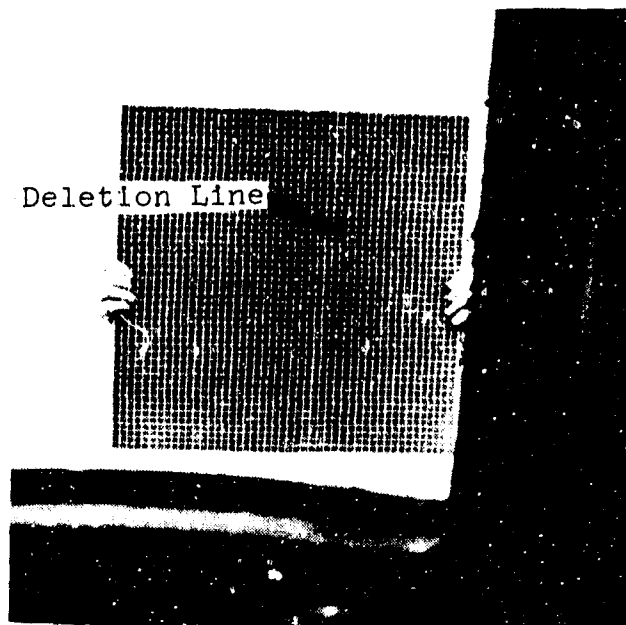


Figure 126. CH-47, Windshield Deletion Line.

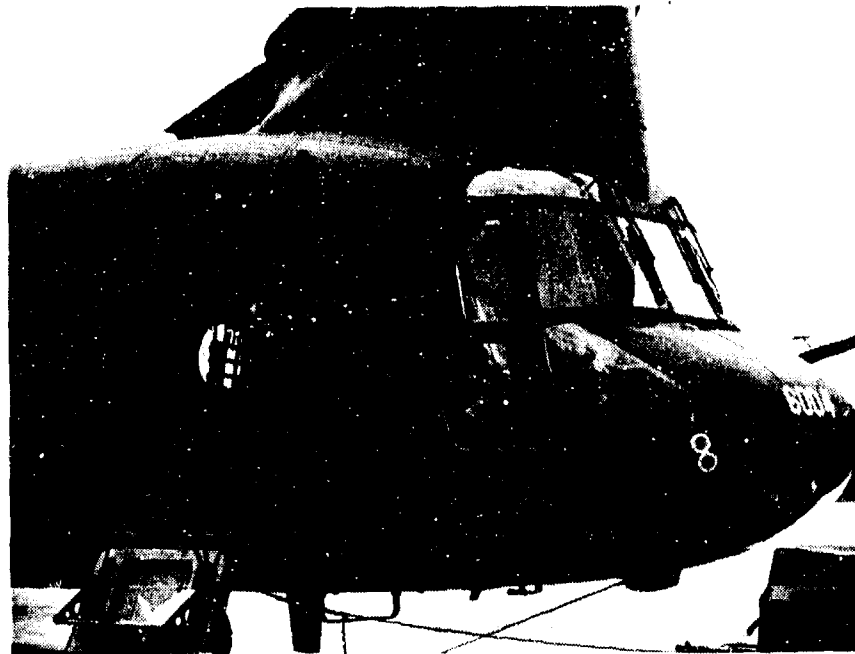


Figure 127. CH-47, Overall View.

TH-55: The TH-55 (Figure 128) is used as a training aircraft and has a windshield made of relatively thin plastic. Figure 124 shows the appearance of the test grid through the front windshield. The grid does not show large distortions, but careful observation shows many small bends in the grid pattern throughout the entire window. This was typical of the TH-55's at Fort Rucker. In all other aircraft types, the central portion of the windshield usually showed no distortions at all. Measurement of the local distortion grid slopes in Figure 129 showed them to be 1:8. However, examination of the questionnaire data showed that no TH-55 pilots complained about windshield distortion.

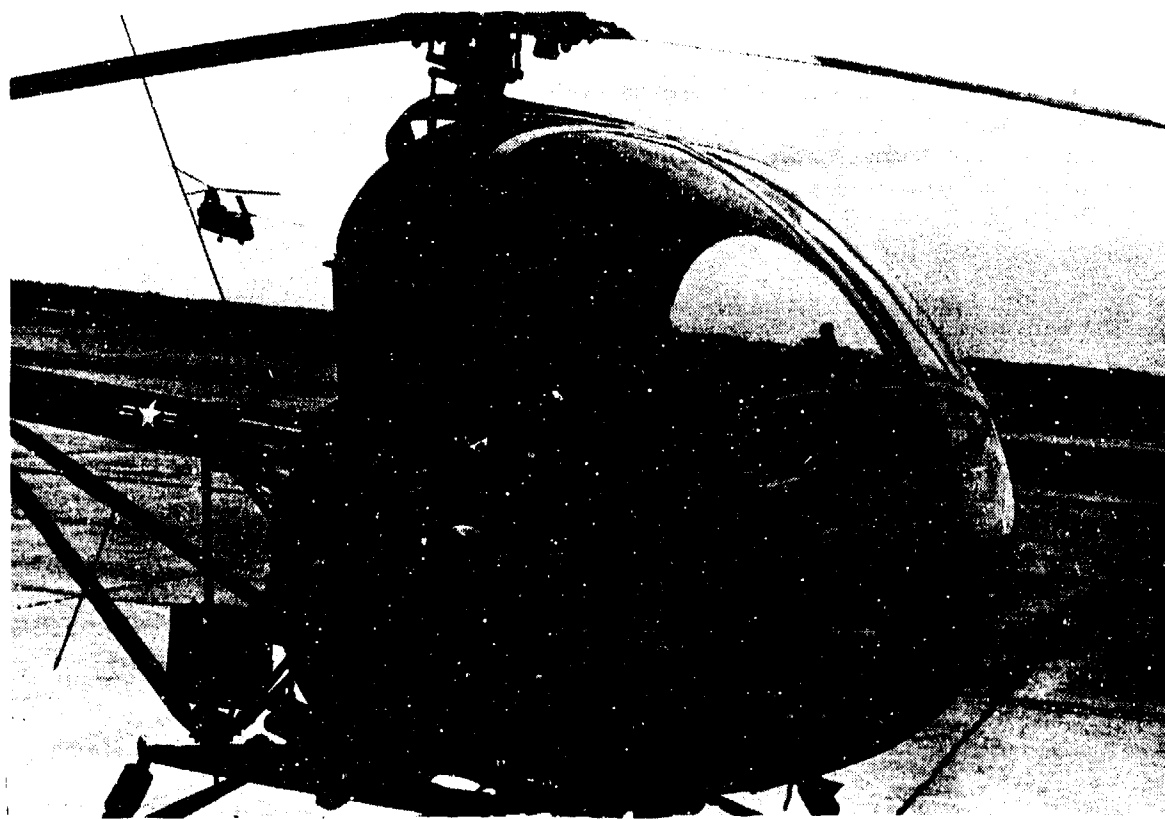


Figure 128. TH-55, Overall View.

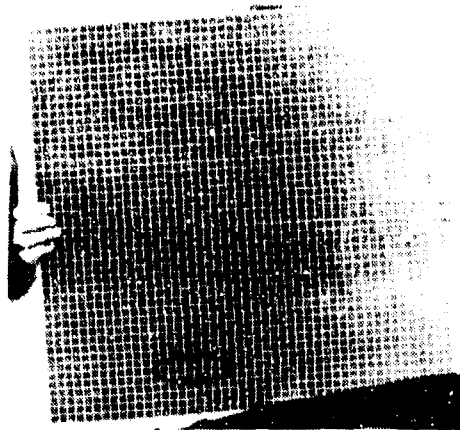


Figure 129. TH-55, Front Windshield Distortions.

Many cracked windshields on the TH-55's were repaired by bonding thin plastic sheets on either side of the surface (Figure 130). As can be seen in Figure 131, this process both obscured and distorted vision through the panel.

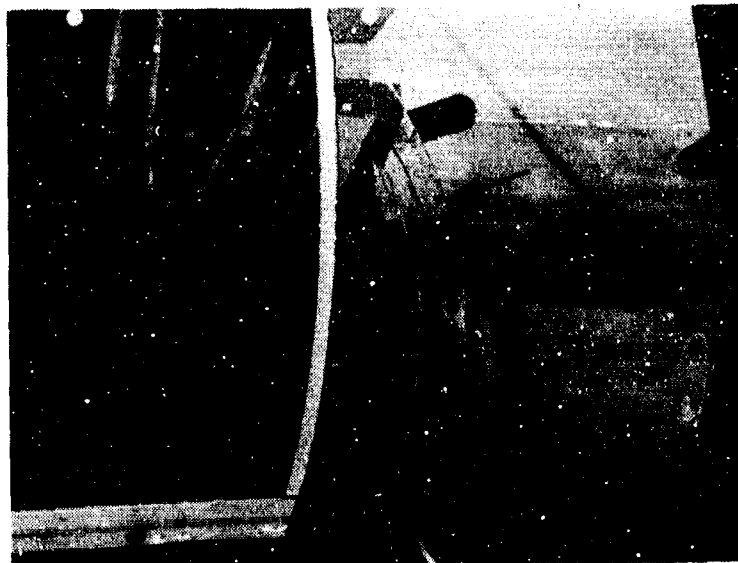


Figure 130. TH-55, Repaired Cracks.

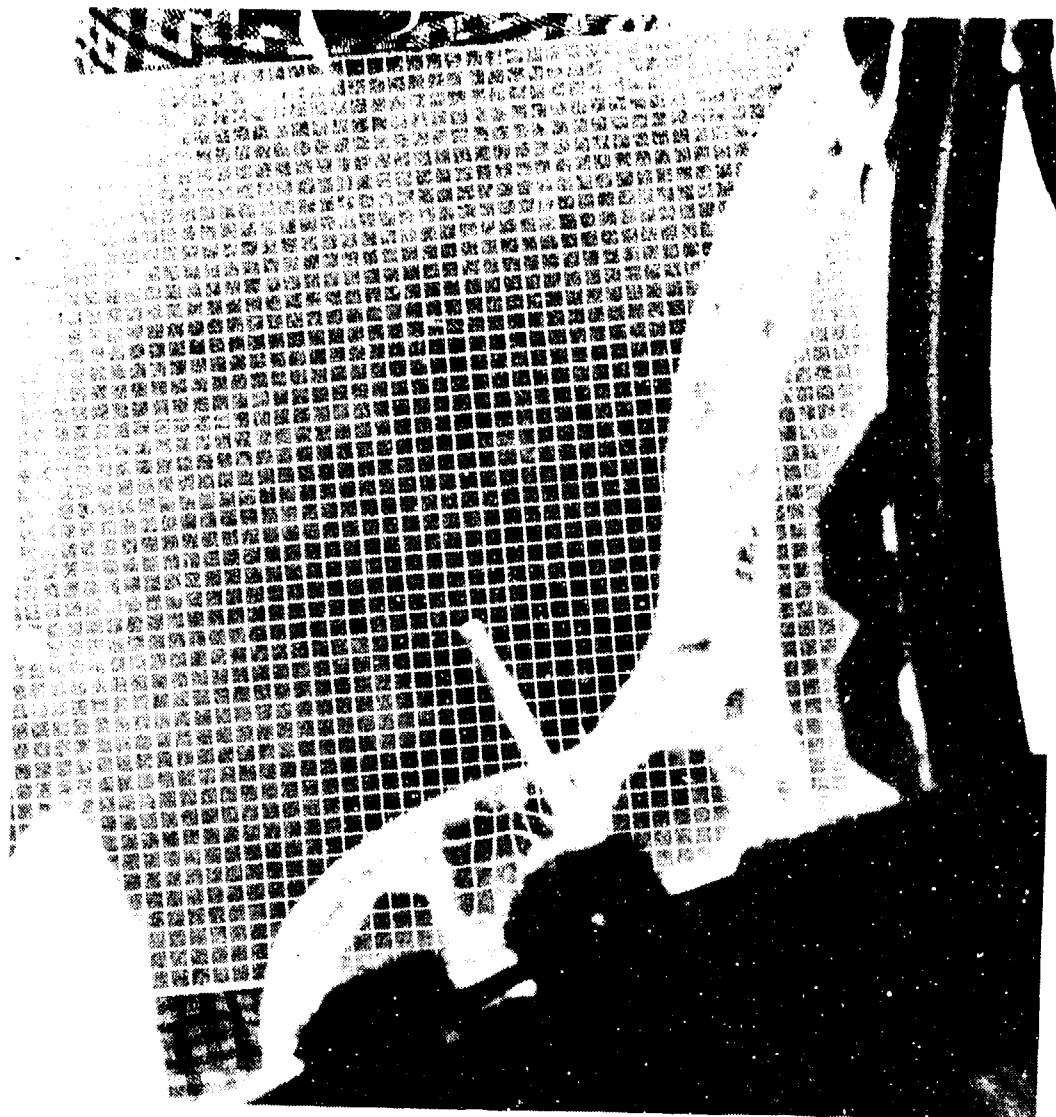


Figure 131. TH-55, Repaired Cracks, Grid Distortion.

OH-6: Only one OH-6 could be located at Fort Rucker. In this helicopter some distortion (1:10) was observed in the lower front window, as shown in Figure 132. The side door window, Figure 133, is made of very thin material that is reinforced with three ridges of plastic. The ridges are translucent and obstruct vision, as shown in Figure 134.

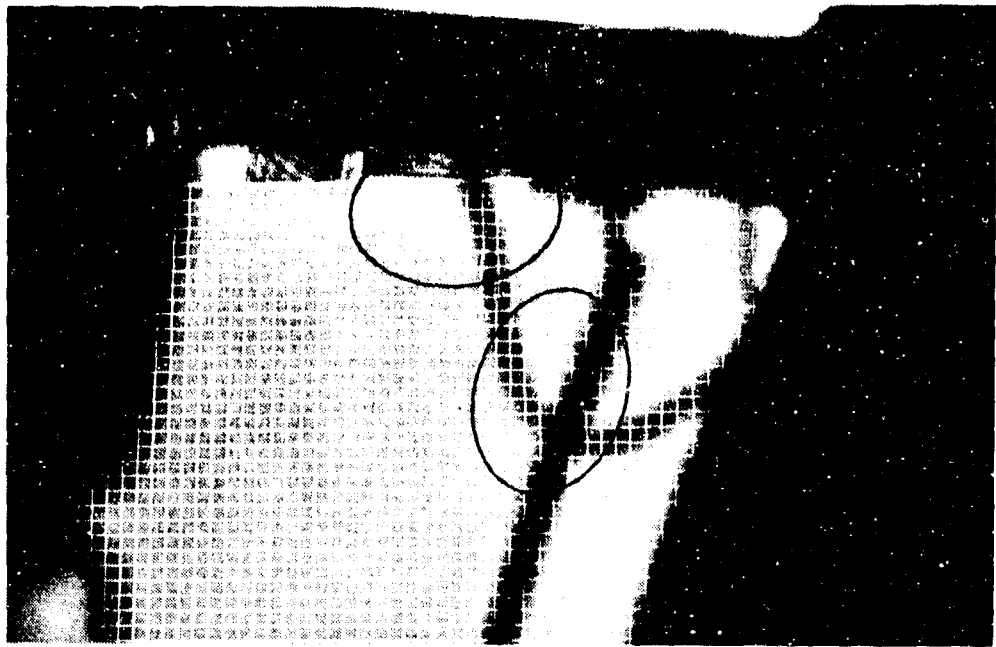


Figure 132. OH-6, Bottom Window Distortions.



Figure 133. OH-6, Overall View.

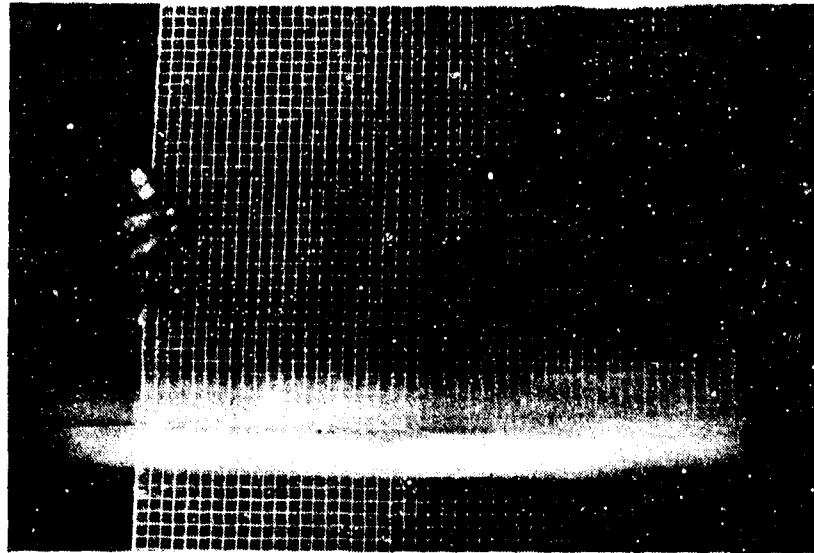


Figure 134. OH-6, Side Window Obstruction, Plastic Stiffeners.

#### DISCUSSION AND OBSERVATIONS

During data collection, several informal discussions were held with maintenance and flight personnel to assess their feelings and practices with regard to cockpit windows. The following information emerged:

1. Only a few passes of a UH-1 wiper over dry plastic will scratch the window so badly that it has to be replaced. To prevent this, wiper switches are safety wired in the off position. If wipers are needed in flight, the pilot must cut the safety wire to activate them.
2. Scratched windshields are repaired by buffing the scratches out. This can be done only once because the process results in distortions in the plastic which become unacceptable after the second time.
3. Windshield replacement required 8 to 14 man-hours and takes at least one day to accomplish.
4. To reduce the need for wiper use, a silicone and alcohol mixture called "Repcon" (FSN-6850-136-5297) is applied to all Huey and Cobra windows. This must be removed and reapplied every 50 hours. This material acts as a rain repellent and surface conditioner. It covers scratches and permits rain drops to run off the windshield in flight without use of the wiper.

5. The officer in charge of maintenance at Fort Rucker indicated that most of the vehicles at the base had been there only for about one year. The aircraft were in very good shape because of the decision to safety wire the UH-1 wipers. If the base were visited the previous year, the UH-1 windshields would have appeared much worse.
6. The method of repairing cracks in plastic windshields has been to glue a patch over the crack as shown in Figure 135. These patches are translucent but not transparent. Patches such as this were found in the OH-58, TH-55 and CH-47. This type of repair solved maintenance problems but tended to degrade operational use of the vehicle.
7. The windshield heating system in the CH-47 has caused delamination malfunctions. To prevent this, the systems have been disconnected at Fort Rucker. A CH-47 was observed with a delamination in the center windshield of about 3 inches in diameter. The inspector indicated that the cost of replacing the window was about \$800 and he was not going to incur that cost until it was absolutely necessary.

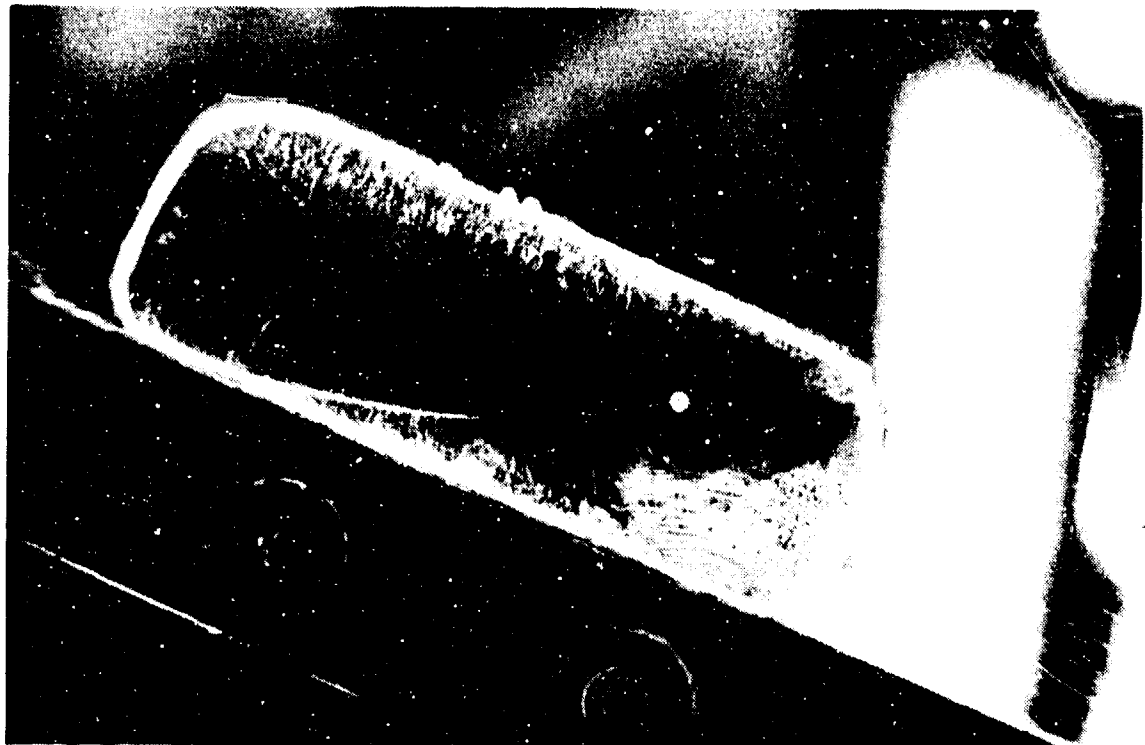


Figure 135. Patch Method of Repair.

## FIELD STUDY CONCLUSIONS

1. The majority of the pilots interviewed complained about excessive haze in transparencies, and 65% of them felt that it affected their performance. The major problems causing this reaction were scratching of the windshield by its wipers and poor cleaning of the windshields by maintenance personnel.
2. Subjective evaluation by helicopter pilots indicated that abraded transparencies containing 15% to 20% haze will be "lived with" before transparency replacements are ordered.
3. Tinted overhead windows currently installed in Army helicopters have visible light transmittance ranging from 16% to 85%. In general, tinting was found to be comforting during operations under a bright sun. However, problems were encountered during reduced light conditions.
4. Most pilots have noticed some optical distortions when looking through helicopter transparencies, although only about 35% of the pilots interviewed said that the distortions caused any performance effects, most of which were rated as slight or annoying in character.
5. The grid line slope for distortions occurring in the central regions of transparencies were generally better than 1:10. Objectionable distortions were primarily confined to the panel edges and local imperfections or reworks.
6. Most pilots noticed small imperfections in transparencies, but only about one-fourth of them felt that their performance was affected. The reasons given for degradation were diverse in nature, but the one mentioned most was delamination.
7. When asked for reactions to windows in general, most pilots rated helicopter windows somewhere between "adequate" and "satisfactory." The most common complaint concerned restrictions on windshield wiper use. Pilots wanted some better method of rain removal, or glass windshields so that wipers could be used as needed.

## BALLISTIC DAMAGE TOLERANCE TESTS

The purpose of this series of tests was to evaluate ballistic damage criteria for helicopter transparent enclosures, establishing limits on

The amount of spall consistent with aircrew safety.  
Visibility after ballistic impact.

Spall consists of many small fragments that are produced and ejected when a material is impacted by a high-speed projectile or shock wave. Transparencies that necessarily enclose large portions of the crew-occupied helicopter areas are particularly susceptible to spallation.

Data<sup>9,10</sup> compiled during the hostilities in the Republic of Vietnam indicated that spall from the transparencies of U. S. Army helicopters posed a significant hazard to the aircrews and passengers. This spall was generated primarily by small arms fire impacting on the aircraft cast acrylic transparencies. Although spall rarely caused permanent injury, it nonetheless hindered aircraft operations. Aircrew wounding was the primary cause cited for aborted missions.

Several transparency materials were ballistically tested to quantify spallation characteristics, residual visibility, and the ability of the panel to support aerodynamic pressure loads after impact. In addition, the following conditions were varied, in turn, during the test to evaluate their effects.

- a. Edge attachment (bolted vs clamped edges)
- b. Pressure vs zero pressure during impact
- c. Impact velocity
- d. Ammunition (ball vs armor piercing)

### Test Specimens

The test specimens consisted of approximately two-foot-square panels of various transparency materials. Table 33 is a list and description of specimen types. The abbreviations listed will be used to represent these materials in all subsequent tables of this report.

- 
9. Bernier, P. G., Smith, H. C., "U. S. Army Casualties Aboard Aircraft in the Republic of Vietnam (1962 through 1967)," BRL MR 2030, Ballistic Research Laboratories, Aberdeen Proving Ground, Md, March 1970.
  10. Malick, D., et al, Falcon R&D Corp, "U. S. Army Casualties Aboard Aircraft in the Republic of Vietnam (1968 through 1970)", BRL CR-257, Confidential, Ballistic Research Laboratories, Aberdeen Proving Ground, Md, August 1975.

TABLE 33. MATERIAL DESCRIPTIONS FOR BALLISTIC TESTS

Source	Type	Thickness (in.)	Material	Abbreviation
PPG Industries	laminate	.095	Semitempered soda lime glass	GG
		.075	Polyvinyl butyral	
		.095	Semitempered soda lime glass	
Sierracin	laminate	.085	Chemcor 0401 glass	GA
		.075	Polyvinyl butyral	
		.080	Stretched acrylic	
MIL-P-8184	monolithic	.080	Cast acrylic	CA
MIL-P-8184	monolithic	.187	Cast acrylic	CA
MIL-P-25690	monolithic	.080	Stretched acrylic	SA
MIL-P-83310	monolithic	.080	Polycarbonate	PC

#### Test Equipment

All specimens were mounted to a pressure box as shown in Figure 136. The test specimen could be attached to the pressure box in two ways. By one method, the specimen was drilled and bolted to a support frame which was bolted in turn to the pressure box as shown in Figure 137. By the alternate method, the specimen was placed over the support frame gasket. Then a gasketed aluminum retainer was placed over the specimen periphery and bolted to the support frame to clamp the specimen in place. A vacuum pump was also connected to the pressure box. This enabled a differential pressure to be applied to the specimen, simulating aerodynamic loading.

The ballistic rounds were fired from the mount and barrel shown in Figure 138. The round velocity was determined by the device shown in Figure 139, which measured the time of flight over a three-foot distance. Each round was either 7.62mm ball or 7.62mm armor-piercing ammunition.

7.62mm weapons are standard issue for hostile ground forces, and constitute the most prevalent threat faced by helicopters operating in combat zones. The criteria and test methodologies described herein are nevertheless suitable for evaluating spall generated by larger caliber threats even though ballistic damage would be considerably greater.



Figure 136. Pressure Box and Pump.

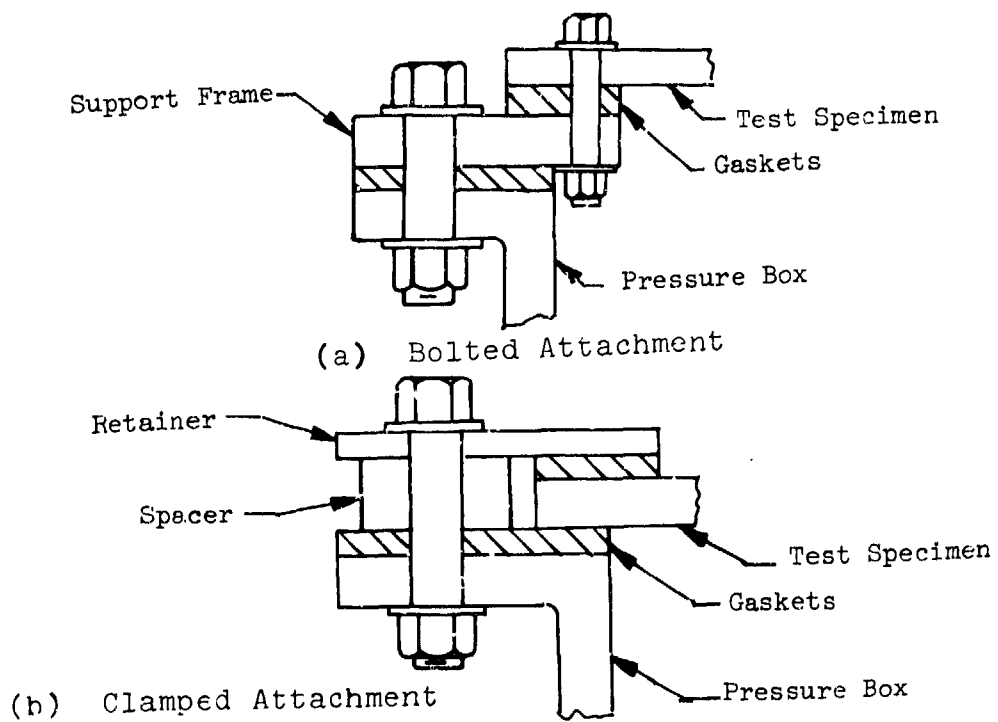


Figure 137. Methods of Attaching Test Specimens.

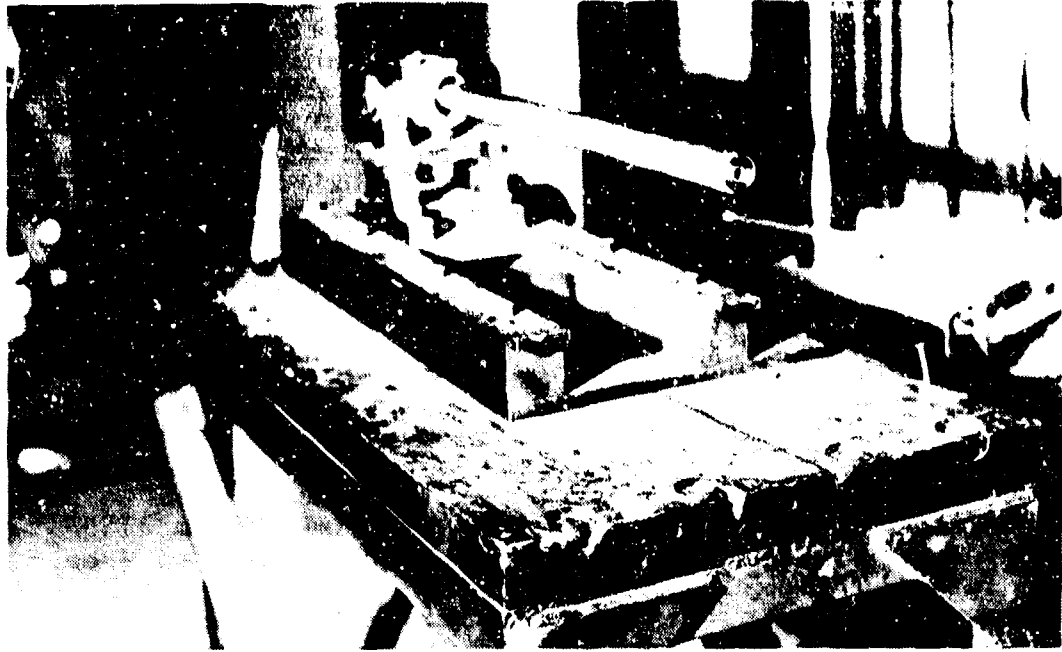


Figure 138. Mann Barrell and Mount.



Figure 139. Velocity Measuring Equipment.

The pressure box was designed to aid in determining the energy of any spall fragments ejected from the specimen at impact. Six inches behind the specimen was a 0.002-inch-thick aluminum foil witness sheet for recording spall dispersion patterns. A wooden frame maintained a 1-inch space behind the witness sheet. The presence of this void aided in differentiating between those fragments which merely punctured the foil and fell back and those which fully penetrated the foil. Behind the spacer were five layers of one-half-inch-thick expanded polystyrene foam (1 lb/cu ft density). This foam was also used to characterize the energy of spall fragments.

SCREENING TEST

Before conducting the primary tests, it was necessary to determine the most damaging angle and velocity of ballistic impact for the various specimen types. Consequently, two specimens, each of the all-glass laminate, glass-acrylic laminate and monolithic cast acrylic (0.080 inch), were subjected to multiple ballistic impacts at velocities ranging from 800 to 2750 ft/sec and angles of obliquity ranging from 0 to 60 degrees (see Figure 140). The bullet exit hole from the pressure box is also shown in Figure 140. These holes were subsequently plugged with modeling clay and tape during the pressure tests.

Some of the screening tests were performed with a wooden test box shown in Figure 141. An aluminum foil witness sheet and layers of wall board were placed in the box to evaluate spall damage. The criteria for ballistic damage included size, amount and density of spall as well as reduction in visibility.

The results of these screening tests are given in Table 34.

TABLE 34. RESULTS OF PRELIMINARY SCREENING TEST

Material	Most Damaging Condition	
	Velocity (fps)	Angle of Obliquity (deg)
All-Glass laminate	1000	60
Glass-Acrylic laminate	1200	60
Cast Acrylic	1200	0

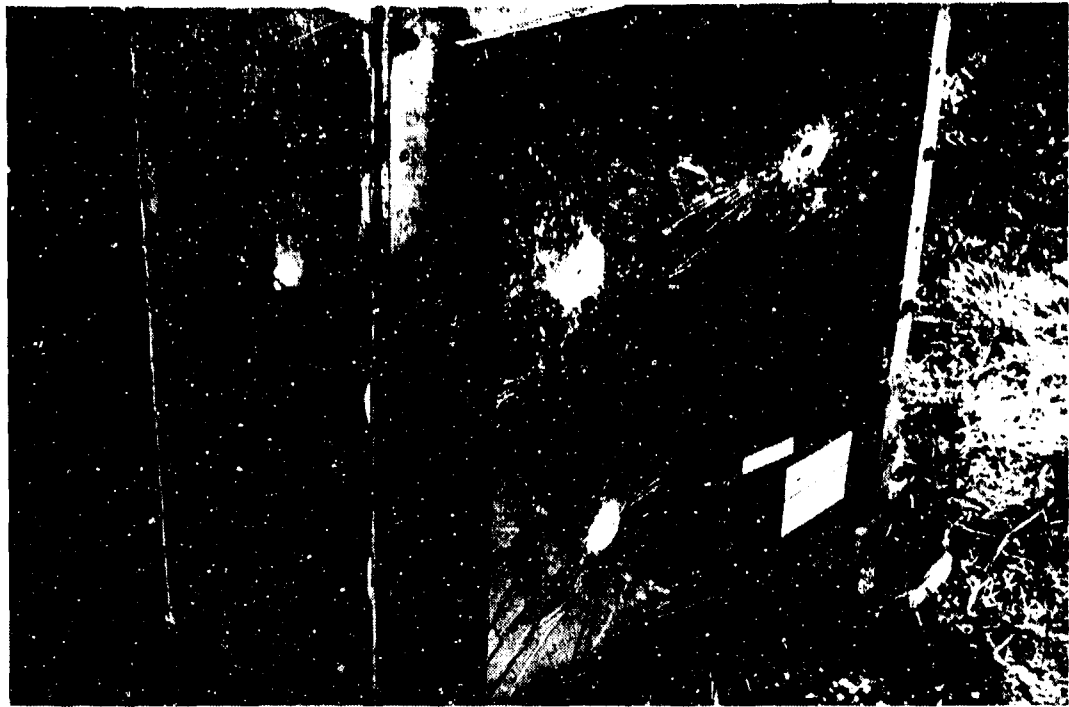


Figure 140. Multiple Ballistic Impacts.

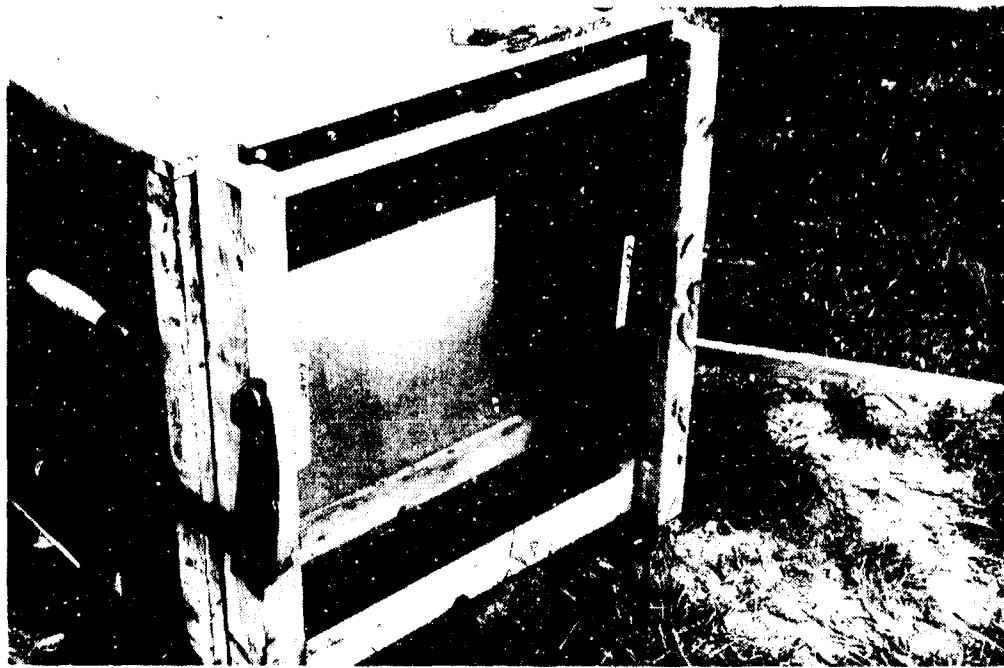


Figure 141. Screening Test Fixture.

## BALLISTIC IMPACT TEST PROCEDURE

Each specimen was attached to the support frame, set at a specified angle of obliquity, and pressurized as recorded in Table 35. An attempt was made to impact specimens at incremental velocities around those found most damaging during the screening tests. However, since the ammunition used was hand loaded, a large variance in velocity was observed. The types of ammunition and measured velocities are also recorded in Table 35. The final three rounds for each material were intended to be fired at a velocity close to that which caused the most damage.

After a round was fired, the specimen was photographed and a fail-safe test was performed. The specimen was first examined for residual visibility, noting severity of crack patterns and dicing. Then the witness sheet was studied to determine the amount and density of spall penetration. Finally, the foam backup sheets were examined for spall fragments. The spall fragments found in various portions of the pressure box were weighed and qualitatively studied.

Two glass/acrylic panels were cracked before testing during installation. The damage occurred because the flexibility of the edge reinforcement was sufficiently low to permit excessive bending to occur between fasteners when they were torqued. This created undue stresses which cracked the glass. However, the resultant cracks in the glass were widely spaced and did not interfere with the target area, which enabled the damaged panels to be successfully tested (Figures 142 and 143).

### FAIL-SAFE TEST

After ballistic penetration, each specimen was subjected to a fail-safe test to determine whether or not the damaged specimen was capable of supporting the required aerodynamic loads. The entry hole created by the test round was sealed by a soft rubber gasket, as shown in Figure 144, and the original pressure was reinstated. In most cases where the specimen supported this load, pressure was maintained for one minute to test for any time-dependent effects.



Figure 142. Damaged Ballistic Specimen.



Figure 143. Ballistic Impact on Damaged Specimen.

TABLE 35. TEST CONDITIONS FOR BALLISTIC TESTS

Specimen	7.62mm Ammunition	Velocity (ft/sec)	Attachment	Obliquity (deg)	Pressure (psi)
GG1	Ball	1254	bolted	60	1
GG2	Ball	1048	bolted	60	1
GG3	Ball	1284	bolted	60	1
GG3A*	Ball	705	bolted	60	1
GG4	AP	1278	bolted	60	1
GG5	Ball	1064	clamped	60	1
GG6	Ball	1207	bolted	60	0
GA1	Ball	1505	bolted	60	1
GA2	Ball	1254	bolted	60	1
GA3	Ball	1124	bolted	60	1
GA4	AP	904	bolted	60	1
GA5**	Ball	1090	clamped	60	1
GA6**	Ball	1138	bolted	60	0
SA1	Ball	1485	bolted	0	.25
SA2	Ball	1262	bolted	0	.25
SA3	Ball	1104	bolted	0	.25
SA4	AP	1467	bolted	0	.25
SA5	Ball	1077	clamped	0	.25
SA6	Ball	1138	bolted	0	0
CA1	Ball	1497	clamped	0	.25
CA2	Ball	1289	clamped	0	.25
CA3	Ball	1075	clamped	0	.25
CA4	AP	1432	clamped	0	.25
CA5***	Ball	1155	clamped	0	.50
CA6	Ball	1066	clamped	0	0
PC1	Ball	1501	bolted	0	.25
PC2	Ball	1299	bolted	0	.25
PC3	Ball	1098	bolted	0	.25
PC4	AP	1479	bolted	0	.25
PC5	Ball	1080	clamped	0	.25
PC6	Ball	1254	bolted	0	0

\*No penetration, bullet ricocheted  
 \*\*Damaged on installation  
 \*\*\*Used 0.187-inch-thick sheet

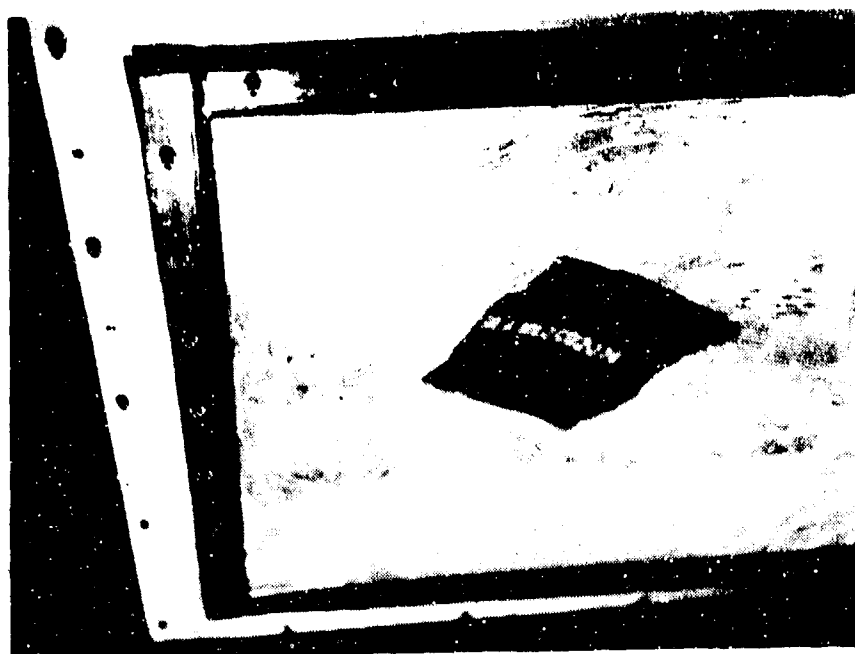


Figure 144. Soft Rubber Patch Maintains Vacuum for Fail Safe Test.

## RESULTS

### Visibility Results

The extent to which visibility through the test specimens was reduced is presented in Table 36. Three types of data are summarized: bullet hole diameter, maximum dimension across the pulverized opaque area adjacent to the bullet hole, and the maximum dimension circumscribing areas of poor visibility. Areas of poor visibility are defined as regions where the dicing density is greater than 1000 particles per square foot.

The polycarbonate showed excellent residual visibility. No surface cracks occurred and the entry hole closed up to become smaller than the round itself, as shown in Figure 145.

The stretched acrylic also behaved well. The penetration hole was equal to the round diameter. In several cases two fine radial cracks less than one-half inch long developed, as shown in Figure 146.

TABLE 36. VISIBILITY DATA FROM BALLISTIC TESTS

Specimen	Bullet Hole Size (in.)	Maximum Dimension Across Pulverized Area (in.)	Maximum Dimension Circumscribing Region of Poor Visibility (in.)
GG1	1	3	3
GG2	2-1/2	3-1/2	7-1/2
GG3	2	2-3/4	4-1/2
GG4	2	4	4
GG5	1-1/2	3-1/2	3-1/2
GG6	1	2-1/2	3
GA1	smaller than round	2	2
GA2	smaller than round	2	2
GA3	smaller than round	2-1/2	2-1/2
GA4	smaller than round	3	3
GA5	smaller than round	2	2
GA6	smaller than round	2-1/2	2-1/2
SA1	round diameter	0	0
SA2	round diameter	0	0
SA3	round diameter	0	0
SA4	round diameter	0	0
SA5	round diameter	0	0
SA6	round diameter	0	0
CA1	1	0	0
CA2	1-1/2	0	0
CA3	1-1/2	0	0
CA4	1	0	0
CA5*	round diameter	0	0
CA6	1	0	0
PC1	smaller than round	0	0
PC2	smaller than round	0	0
PC3	smaller than round	0	0
PC4	smaller than round	0	0
PC5	smaller than round	0	0
PC6	smaller than round	0	0

\*Used 0.187-in.-thick sheet.

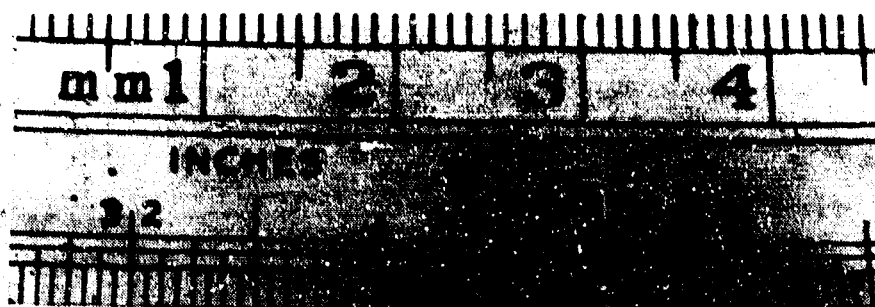


Figure 145. Ballistic Penetration of Polycarbonate.

The cast acrylic specimens suffered primarily localized damage. The entry holes were typically about one-inch across with some material being torn out by the round. Little damage was sustained beyond a 3-inch diameter for the 0.080-inch sheets (Figure 147). Cracking was somewhat more extensive for the 0.187-inch sheets, as shown in Figure 148.

The glass/glass laminates sustained considerably more surface damage than any of the monolithic specimens. The entry holes were from 1 to 2 inches across (Figure 149). Since the specimens were shot at a 60-degree angle of obliquity, the pulverized areas were oblong, ranging up to 4 inches across.

In some of the glass/glass specimens, areas of poor visibility appeared. The largest such area, as noted in Table 36, was 7 1/2 inches across, as shown in Figure 150.

The glass/acrylic laminates sustained considerable surface damage from ballistic impact, as shown in Figure 151. Entry holes were very small with the soft interlayer tending to close the hole, as shown in Figure 152. The pulverized area of each specimen was from 2 to 3 inches across. The crack patterns outside the neighborhood of impact did not exceed the poor visibility level, although in many areas they did reach about 800 particles per square foot.

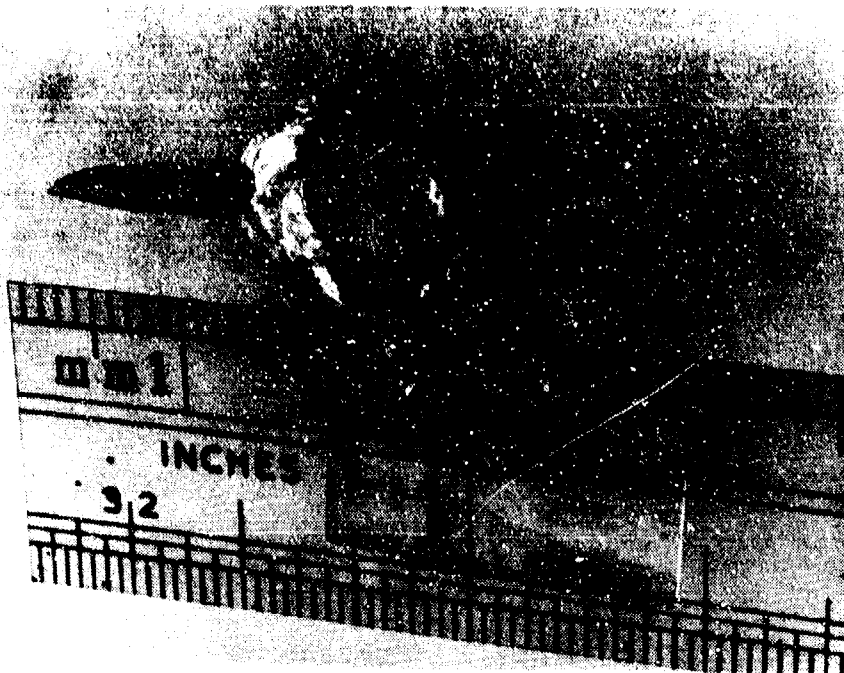


Figure 146. Ballistic Penetration of Stretched Acrylic.

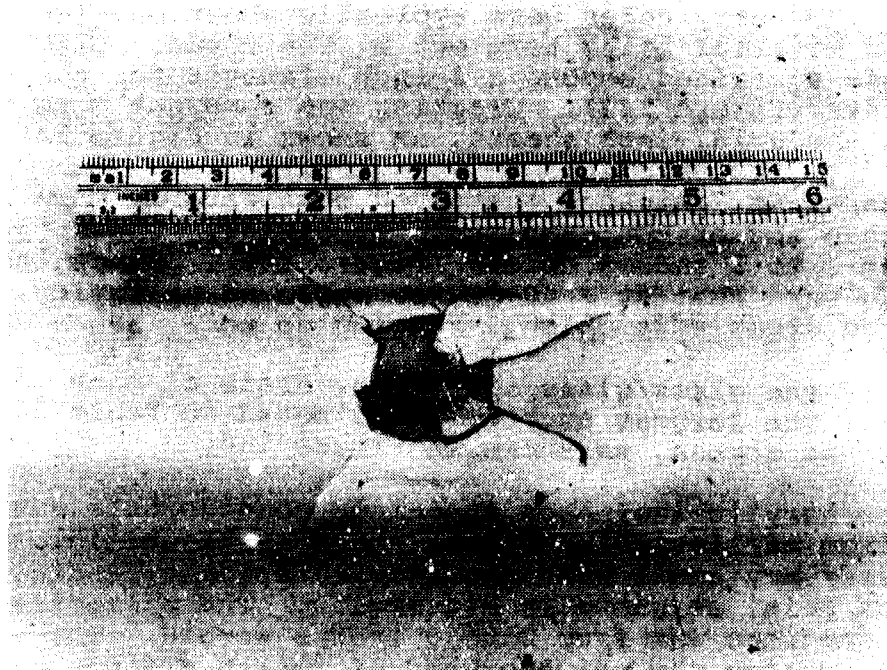


Figure 147. Ballistic Penetration of 0.080 Inch Cast Acrylic.



Figure 148. Ballistic Penetration of 0.187  
Inch Cast Acrylic.

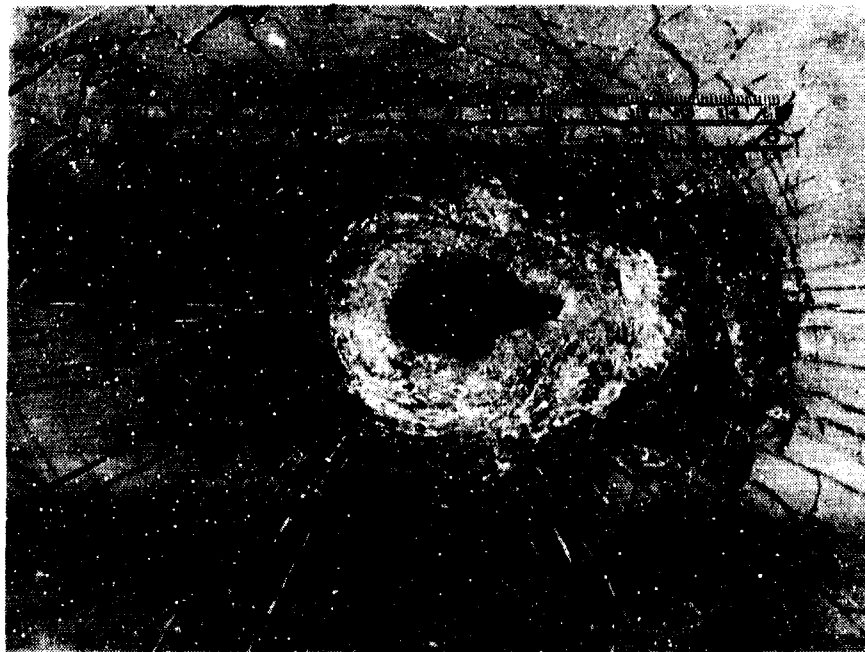


Figure 149. Ballistic Penetration of  
All-Glass Laminate.



Figure 150. All-Glass Laminate After Ballistic Impact.

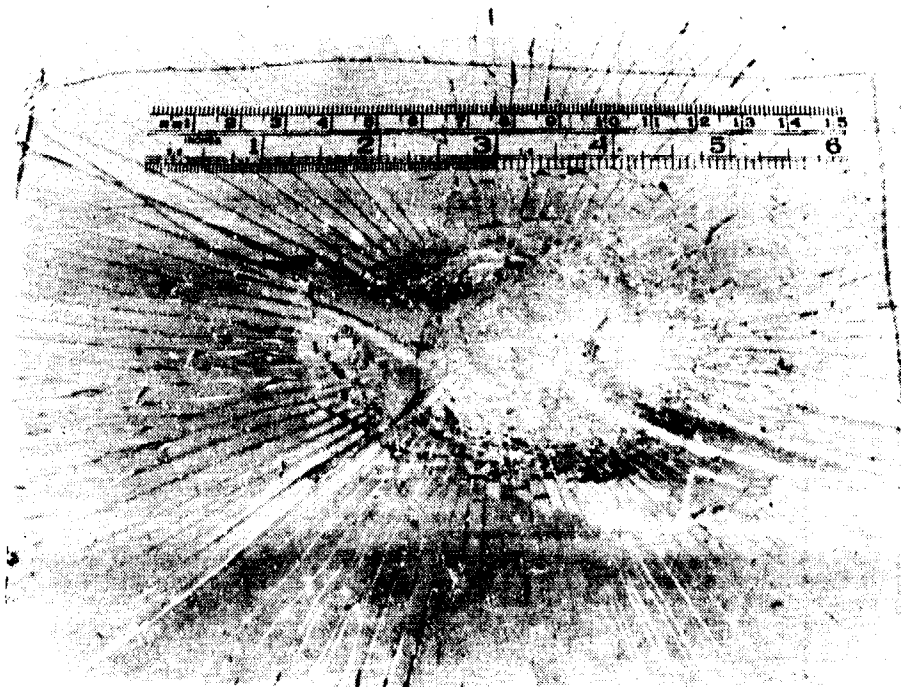


Figure 151. Ballistic Penetration of Glass/Acrylic Laminate.

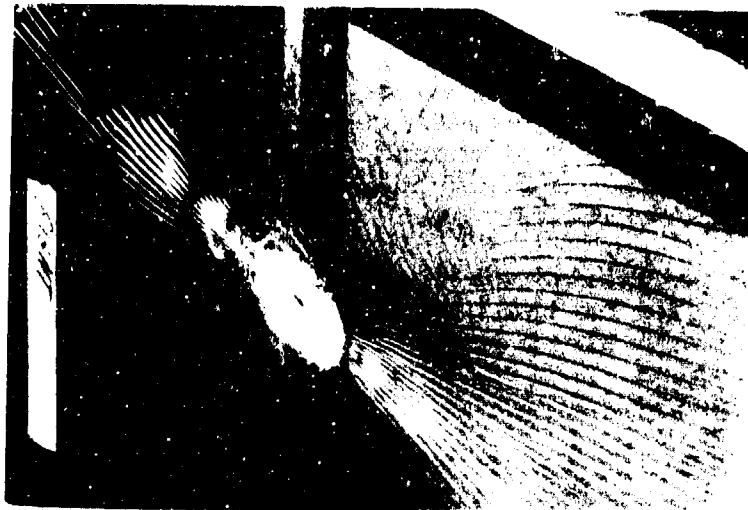


Figure 152. Glass/Acrylic Laminate After Ballistic Impact.

#### Fail-Safe Test Results

In all cases, the impacted specimens were able to support the pressure load applied to them originally. Most tests were held for 1 minute to check for creep. It should be noted that the glass/acrylic laminate, although holding the load, deflected severely under pressure. Deflections went up to 6 inches, and caused tearing in the acrylic layer, as well as considerable secondary cracking in the glass layer. The magnitude of the deflections are evident in Figure 153 by the rubber patch being partially obscured from view due to the sunken shape of the panel.

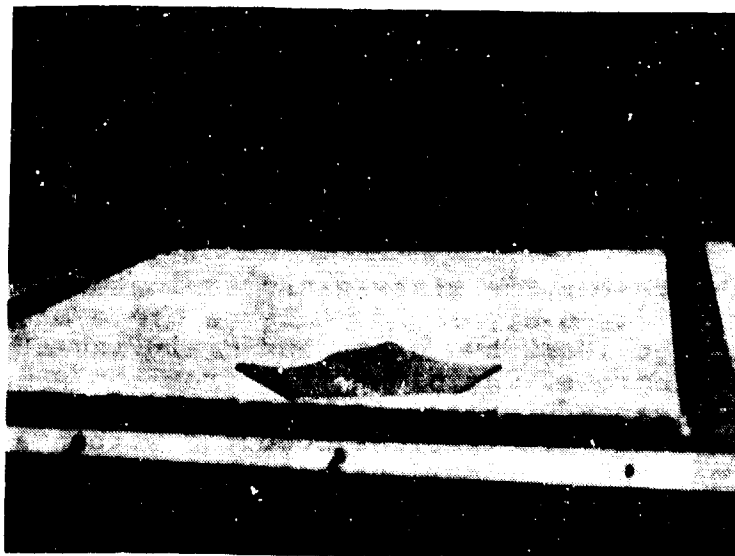


Figure 153. Fail-Safe Test of Glass/Acrylic Laminate at 1 psi.

### Witness Sheet Damage

A measure of witness sheet damage for each specimen is reflected in Table 37. Two dimensions are listed. The first represents the maximum distance measured across the penetrated area of the witness plate. The second dimension represents the diameter of a circle which could be circumscribed around 80 percent of the penetrations.

The monolithic polycarbonate showed little spall damage to the witness sheet. One or two particles generally made minute penetrations of the sheet within 2 inches from the impact position. A typical polycarbonate witness sheet pattern is shown in Figure 154.

The stretched acrylic sheets also exhibited minor witness sheet damage. Generally, about six small penetrations were made within 5 inches of the impact center. In this same region, a large number of particles dented the sheet but were unable to penetrate. A typical penetration pattern for stretched acrylic is shown in Figure 155.

The cast acrylic specimens caused several penetrations in a compact area. In general, ten or more particles penetrated the aluminum foil within 4 inches of the impact center. Also within that area was a number of dents roughly equal to the number of penetrations. The 0.187-inch specimen exhibited the same pattern but appeared to cause slightly larger penetrations. A typical witness sheet for the cast acrylic is shown in Figure 156.

A typical witness sheet for the glass/acrylic laminate is shown in Figure 157. Since the specimens were impacted at a 60-degree angle of obliquity, the damage is located in an oblong area of the foil. Typically, this area was thickly covered with a mixture of dents and various sized penetrations, most being less than a quarter inch across. Most damage occurred within a 10- by 6-inch rectangle, the more serious being done closer to the impact point. The zero pressure round seemed to cause less scatter than the others. The AP round caused fewer penetrations.

The witness sheets for the glass/glass laminates sustained serious damage. For every round, a large piece of the interlayer, weighing at least two grams and measuring at least an inch and a half across, was blown free from the specimen. This projectile caused severe rips in the foil. A large number of additional penetrations occurred within a 14-inch by 10-inch area, the most serious being in the neighborhood of ballistic impact. A typical witness sheet is shown in Figure 158. The penetration pattern for this sheet is shown in Figure 159. It should be noted that the amount and scatter of damage were much less for the clamped specimen, as reflected in Figure 160.

TABLE 37. DISPERSION OF PENETRATIONS IN WITNESS SHEET

Specimen	Maximum Dispersion Across Penetrations (in.)	Maximum Dispersion Across Area Containing 80% of Penetrations (in.)
GG1	28.5	23.0
GG2	28.0	22.0
GG3	38.0	30.0
GG4	28.0	20.0
GG5	9.0	7.0
GG6	24.0	13.0
GA1	24.0	18.0
GA2	9.0	13.0
GA3	22.5	15.0
GA4	16.5	14.0
GA5	16.0	13.0
GA6	19.0	12.0
SA1	(11.0)	7.7 (8.0)
SA2	(11.0)	5.0 (8.0)
SA3	(11.0)	8.2 (8.0)
SA4	(12.0)	7.5 (8.0)
SA5	(13.0)	8.0
SA6	(14.0)	(10.0)
CA1	8.2	5.5
CA2	8.5	5.8
CA3	8.5	4.5
CA4	8.2	5.5
CA5	6.5	5.0
CA6	7.8	4.5
PC1	4.8	4.6
PC2	3.2	3.2
PC3	1.5	1.5
PC4	0	0
PC5	2.5	2.5
PC6	0	0

NOTE: Numbers in parentheses include dents.



Figure 154. Typical Witness Sheet Penetration Pattern for Polycarbonate.

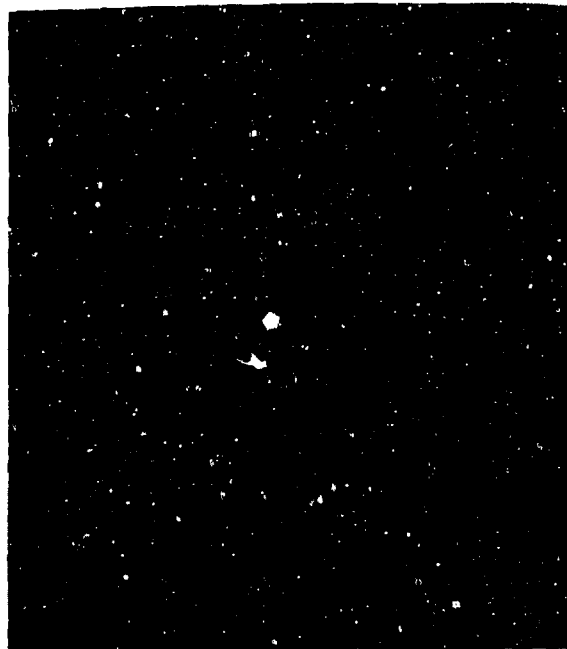


Figure 155. Typical Witness Sheet Penetration Pattern for Stretched Acrylic.



Figure 156. Typical Witness Sheet Penetration Pattern for Cast Acrylic.

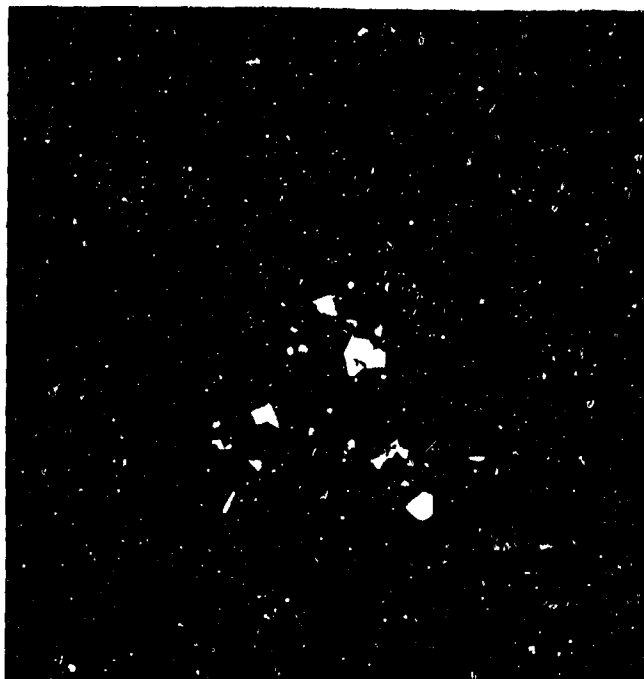


Figure 157. Typical Witness Sheet Penetration Pattern for Glass/Acrylic Laminate.

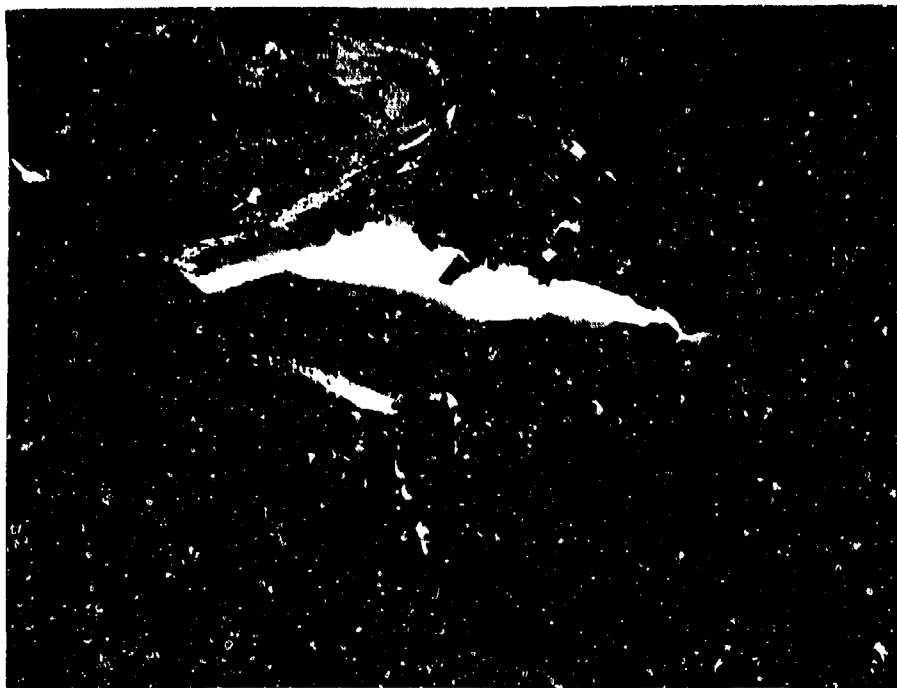


Figure 158. Typical Witness Sheet for All-Glass Laminate.

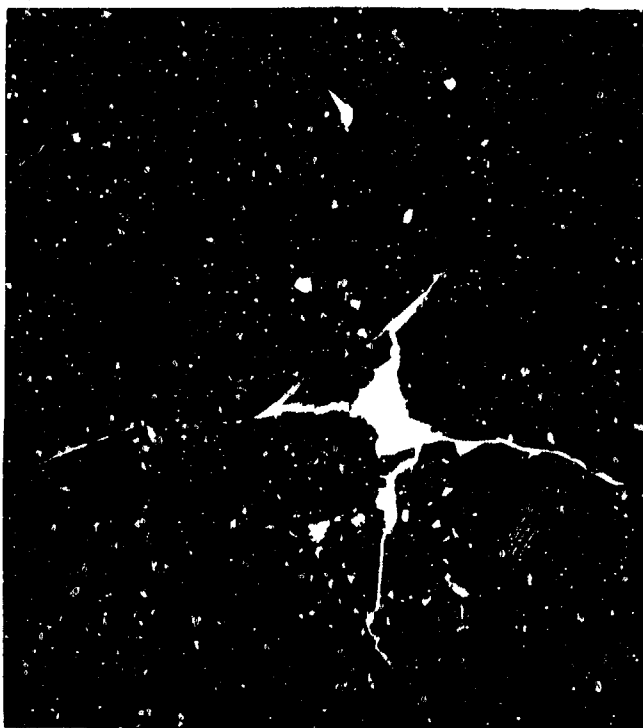


Figure 159. Typical Witness Sheet Penetration Pattern for All-Glass Laminate.

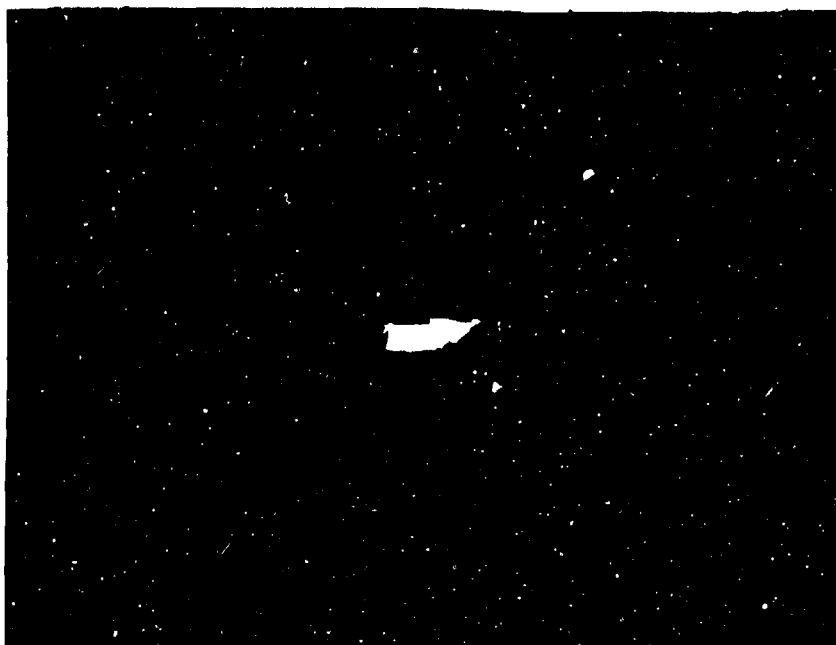


Figure 160. Witness Sheet Spall Penetration  
Pattern for Clamped All-Glass Laminate.

#### Foam Penetration

No penetration of foam sheets occurred for either the polycarbonate or the stretched acrylic specimens.

In tests conducted on the cast acrylic, from two to six fragments penetrated the foam, some going into the second sheet. For the 0.187-inch specimen, one fragment reached the third sheet. All fragments were found within 4 inches of the impact center.

For the glass/glass laminates, from one to five fragments penetrated as far as the fourth sheet. All fragments were in relatively close proximity to each other. For the glass/acrylic laminates, from one to nine fragments penetrated as far as the fourth sheet, the fragments occasionally being dispersed over the oblong damage area.

The number of fragment penetrations for each foam sheet and general dispersion information are presented in Table 38. These numbers do not include very tiny fragments which could only be partially collected. Their presence is noted by ">".

TABLE 38. FOAM PENETRATION DATA

Specimen	No. of Fragments in Foam Sheets* (#1, #2, #3, #4)	Scatter in Foam (in.)
GG1	3, 0, 0, 0	Close
GG2	4, 0, 0, 0	Close
GG3	>0, 3, 1, 1	Close
GG4	>0, 2, 0, 0	Close
GG5	>1, 0, 0, 0	Close
GG6	>1, 3, 1, 0	Close
GA1	2, 1, 1, 0	Dispersed
GA2	4, 1, 0, 0	Dispersed
GA3	4, 2, 0, 0	Close
GA4	1, 0, 0, 0	----
GA5	8, 0, 0, 1	Close
GA6	1, 1, 1, 0	Close
SA1	----	----
SA2	----	----
SA3	----	----
SA4	----	----
SA5	----	----
SA6	----	----
CA1	4, 0, 0, 0	4
CA2	3, 0, 0, 0	3-1/4
CA3	4, 2, 0, 0	2
CA4	2, 0, 0, 0	2-1/2
CA5	2, 4, 1, 0	3-1/4
CA6	2, 3, 0, 0	2-1/2
PC1	----	----
PC2	----	----
PC3	----	----
PC4	----	----
PC5	----	----
PC6	----	----

\*> indicates presence of very small fragments.

### Spall Weight and Description

For each test, spall was collected from the area in front of the aluminum witness sheet (pre-witness sheet area), behind the aluminum witness sheet (post-witness sheet area), and imbedded in the foam sheets. The weights of these fragments are listed in Table 39. During the glass/glass laminate tests, the large pieces of soft interlayer previously mentioned tore large holes in the witness sheets. Consequently, the spall weights in the post-witness sheet area may include some spall that passed through these holes rather than actually penetrating the foil.

Table 40 contains a general description of the spall fragments collected for each type of material. These fragments can be seen in Figures 161, 162 and 163.

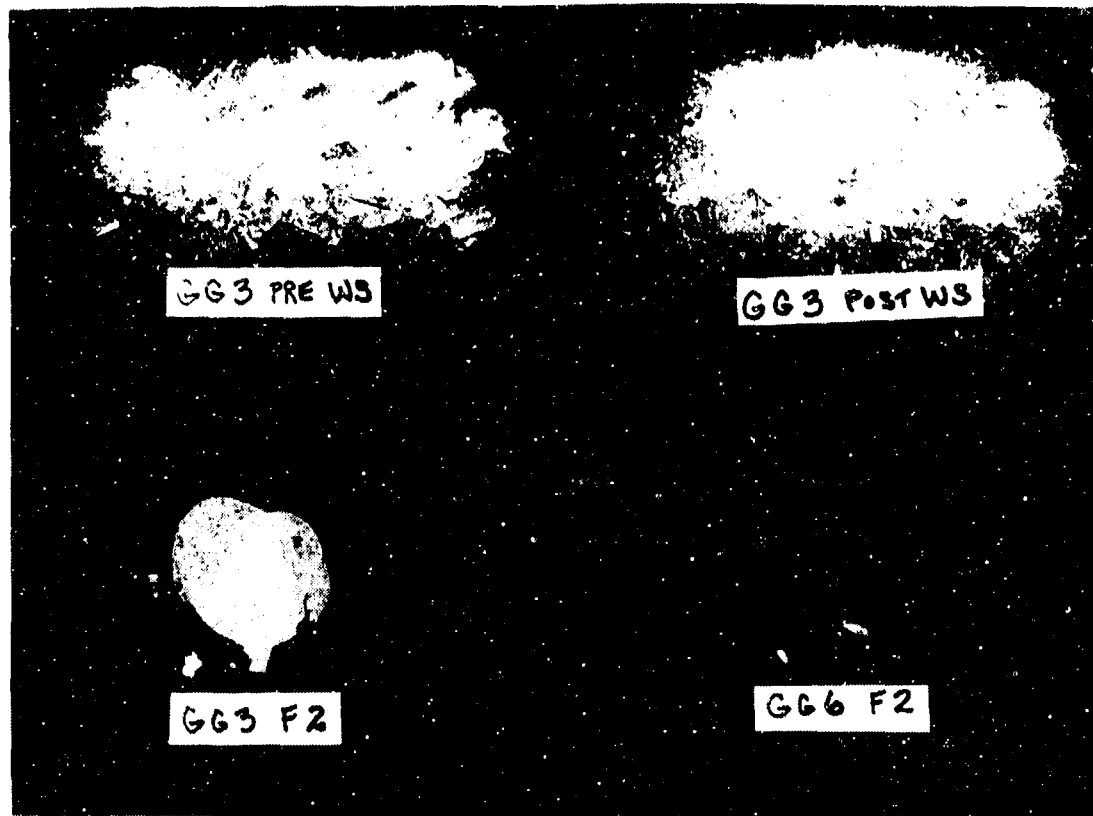


Figure 161. Typical Spall Fragments From All-Glass Laminates.

TABLE 39. TOTAL WEIGHT OF SPALL FRAGMENTS

Specimen	Pre-witness Sheet	Post-witness Sheet	Foam 1	Foam 2	Foam 3	Foam 4
GG1	4.363	9.748 (1.730)	.060	--	--	--
GG2	16.931	4.243	2.998 (.712, 2.033)	--	---	---
GG3	5.619	10.645	.061	2.951 (2.882)	---	.189
GG4	12.363	4.452	.045	2.827 (2.801)	---	---
GG5	14.173	2.052	10.975 (10.388)	---	---	---
GG6	8.908	2.322	1.853 (1.852)	.007	.015	---
GA1	1.165	.233	.018	.013	.007	---
GA2	1.483	.398	.138	.023	---	---
GA3	1.184	.678	.094	.038	---	---
GA4	1.250	.476	.010	---	---	---
GA5	.788	.306	.342	---	---	.076
GA6	1.920	.610	.005	.051	.109	---
SA1	.089	.012	---	---	---	---
SA2	.109	---	---	---	---	---
SA3	.117	---	---	---	---	---
SA4	.113	.017	---	---	---	---
SA5	.114	---	---	---	---	---
SA6	.010	---	---	---	---	---
CA1	.265	.075	.039	---	---	---
CA2	.590	.129	.269	---	---	---
CA3	.519	.071	.150	.052	---	---
CA4	.397	.007	.052	---	---	---
CA5	.176	.071	.359	.065	.024	---
CA6	.252	.096	.065	.088	---	---
PC1	---	---	---	---	---	---
PC2	.001	---	---	---	---	---
PC3	---	---	---	---	---	---
PC4	.013	---	---	---	---	---
PC5	.008	---	---	---	---	---
PC6	---	---	---	---	---	---

NOTE: Numbers in parentheses indicate portion of spall weight contained in large chunks of PVB interlayer.

TABLE 40. GENERAL DESCRIPTION OF SPALL FRAGMENTS

Specimen	Prewitness Sheet	Postwitness Sheets	Foam Sheets
Glass/Glass Laminate (See Figure 161.)	Powdered glass with a large proportion of small jagged fragments up to 1/8 inch across and a few larger jagged fragments up to 3/4 inch across.	Powdered glass with small jagged fragments up to 1/8 inch across and a few larger jagged fragments up to 1/2 inch across.	Large flat plug of soft inter-layer, primarily circular but with frequent jagged protrusions of up to 1-1/2 inches across. Also, a small number of fragments up to 1/4 inch across in the shape of a sliver or wedge.
Glass/Acrylic Laminate (See Figure 162.)	Some powdered acrylic with several thin jagged acrylic fragments up to 3/4 inch across.	Several small, thin, jagged, acrylic fragments less than 1/4 inch across and a small number of larger wedge-shaped fragments up to 1/2 inch across.	A few thin jagged wedge-like pieces up to 3/4 inch across.
Cast Acrylic (See Figure 163.)	A few very small fragments and about a half dozen jagged, wedge-like fragments up to 3/8 inch across.	A few small fragments about 1/16 inch across and several jagged wedge-like fragments up to 1/4 inch across.	A small number of jagged, wedge-like fragments up to 1/4 inch across.

TABLE 40. (Continued)

Specimen	Prewitness Sheet	Postwitness Sheets	Foam Sheets
Stretched Acrylic (See Figure 163.)	Several small shavings of pulverized acrylic up to 1/8 inch across.	A very small number of similar fragments.	None observed.
Polycarbonate	A couple of very small fragments less than 1/16 inch across.	None observed.	None observed.

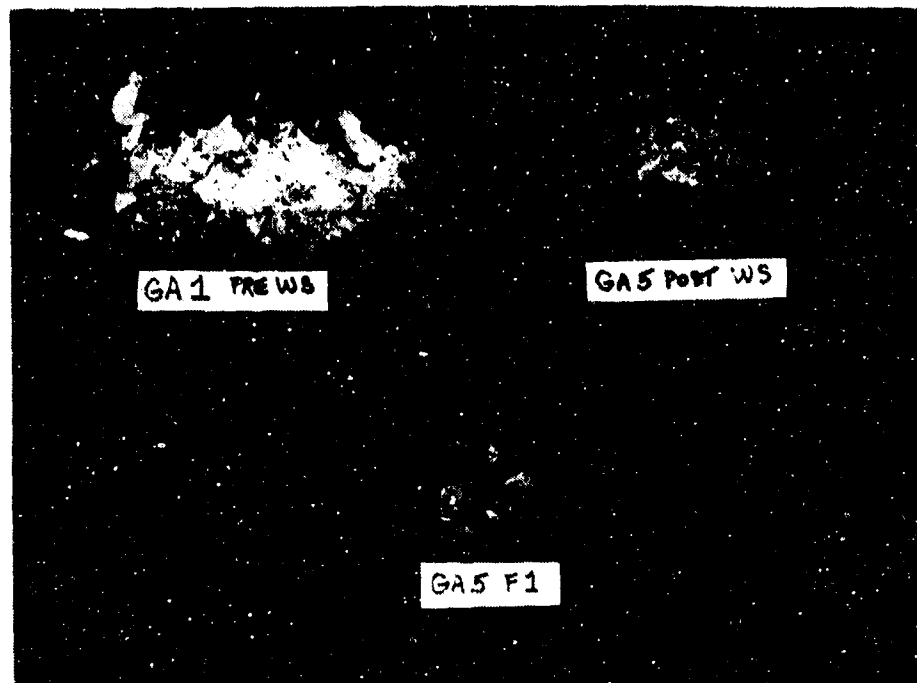


Figure 162. Typical Spall Fragments From Glass/Acrylic Laminate.

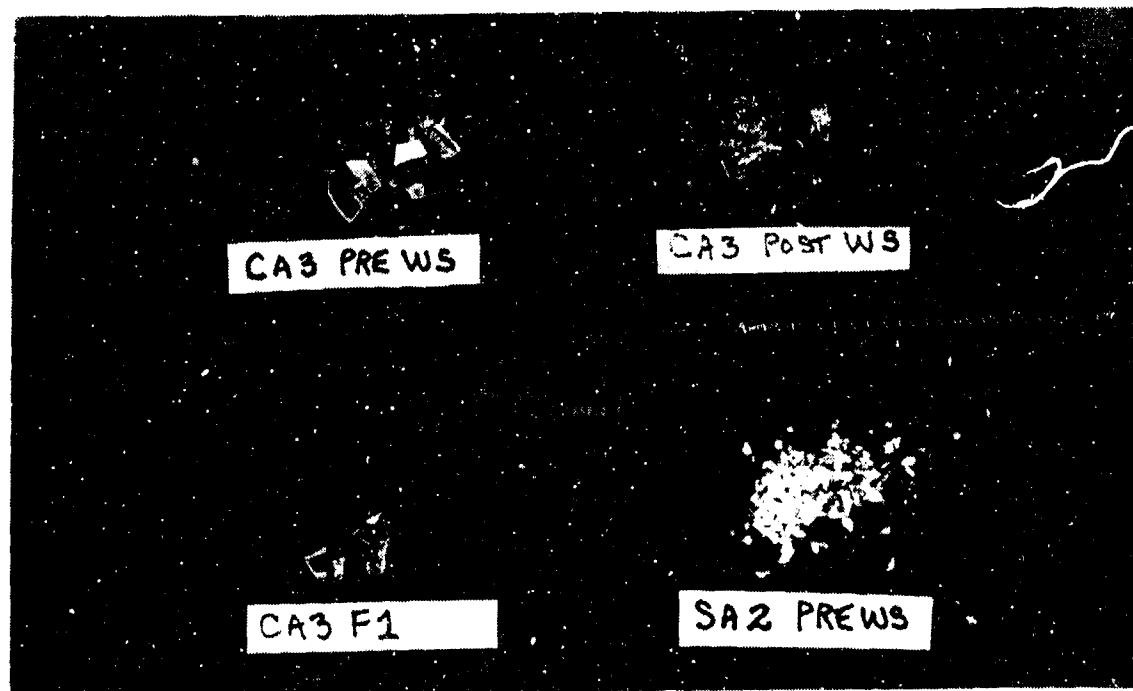


Figure 163. Typical Spall Fragments From Acrylic Specimen.

### SPALL CRITERIA

The areas of the body most vulnerable to spall wounding are those which are not protected by clothing: the head, neck, hands and arms. In particular, the eyes must be protected by visors or goggles. Even the smallest of spall fragments hitting the eye can temporarily incapacitate a pilot and have serious consequences.

Figure 164 shows combinations of fragment mass and velocity that represent a threshold for lacerating or penetrating the skin. The model was derived from several wounding models and empirical data.<sup>11,12</sup> Fragments whose mass and velocity describe a point below the threshold line have less than a 5-percent chance of effecting a wound. The model may, therefore, be considered as a conservative criterion for evaluating the spall resistance of candidate transparent materials.

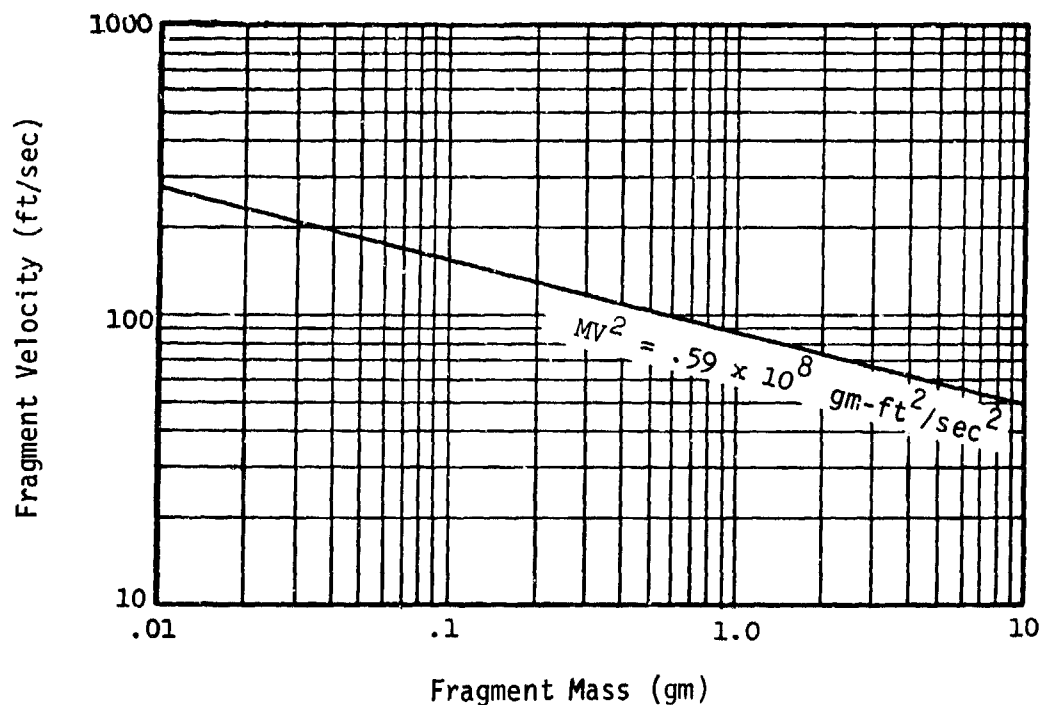


Figure 164. Wounding Model, Skin Laceration by Glass Fragments.

- 11 Feinstein, D. I., "Personnel Casualty Study," IITRI Report J6067, IIT Research Institute, Chicago, Ill., July 1968.
- 12 White, C. S., et al, Lovelace Foundation for Medical Education and Research, "The Environmental Medical Aspects of Nuclear Blast," DASA 1341, November 1962.

Incapacitation caused by spall hitting the eyes must be considered a special case, because temporary blindness can result from extremely minute particles normally categorized as dust. Thus, to be completely effective, the criteria should specify that no measurable spall be generated from ballistic impact. However, this requirement is considered too stringent for currently available transparent materials other than thin polycarbonate, and since the eyes represent a very small percentage of the total vulnerable area, alternate methods of protection in the form of fragment resistant visors or goggles can be used effectively.

#### Foil and Foam Calibration

After the spall data had been collected, it was important to correlate this data with the potential for causing wounds or injuries. Thus, it became necessary to associate a velocity with the spall fragments. A precise calibration of the foil and foam witness plates was considered to be impractical because of the number of impact variables (size, shape, weight, velocity and orientation). Therefore, the following procedure was used to obtain rough estimates of the energies necessary to penetrate various combinations of witness materials.

To obtain a fragment penetration velocity range for a given foil-foam configuration, four different projectile geometries were used. Their characteristic shapes were:

1. A blunt end as found on a retracted ball point pen. This shape was representative of the largest fragments.
2. A sharp wedge as found in a typical fragment. An actual spall fragment was attached to a thin metal wire to simulate this shape.
3. A conical shape, as found on a sharpened pencil.
4. A sliver-like shape. This configuration, which exhibited the greatest ease of penetration, was represented by a long, hard, sharpened drawing lead.

Each projectile was weighed and then dropped onto the foil and varying numbers of foam sheets. The height at which a dropped projectile just penetrated the foil-foam configuration was measured. In most cases, weights were added to the projectiles to decrease the necessary height. Once the height and mass were known for each situation, the potential energy was computed. This was then equated with the kinetic energy of an average spall fragment to determine its impact velocity.

The average spall fragment was found to weigh about 0.05 gram. The velocities required to give an 0.05-gram mass sufficient kinetic energy to penetrate the various foil-foam combinations were calculated and are presented in Table 41.

TABLE 41. VELOCITY NECESSARY TO PENETRATE VARIOUS COMBINATIONS OF WITNESS MATERIAL, FRAGMENT MASS = 0.05 GRAM

Witness Combination	Fragment Shape		Velocity (ft/sec)	
	Blunt	Wedge	Cone	Sliver
Foil	150	120	120	60
Foil + 1 foam	450	290	240	150
Foil + 2 foam	-	410	420	250
Foil + 3 foam	-	-	-	370

Using this data and the test results contained in Table 38, the spall characteristics for the five materials tested are compared to the wound model in Figure 165.

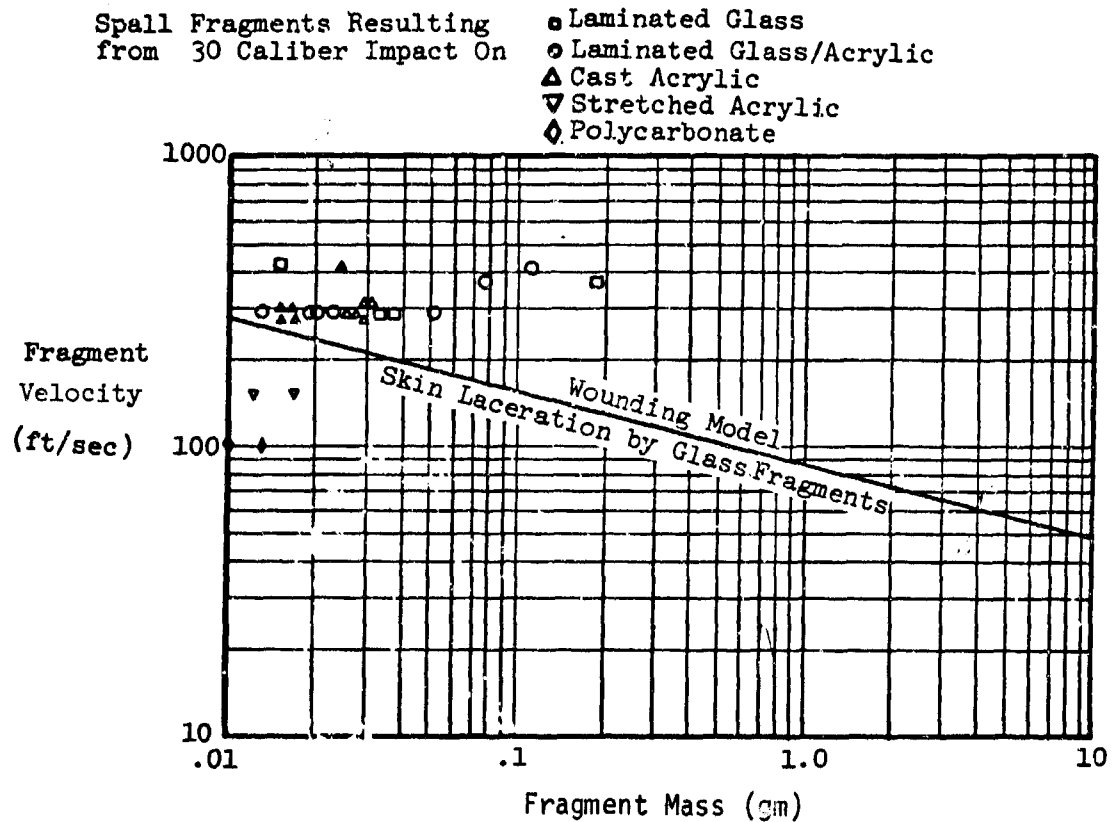


Figure 165. Spall Data Compared to Wounding Model.

## BALLISTIC TEST CONCLUSIONS

1. All materials tested exhibited satisfactory residual visibility after ballistic impact. However, the laminated specimens contained small regions adjacent to the point of impact that were difficult to see through.
2. All specimens tested showed acceptable fail-safe behavior.
3. The monolithic polycarbonate and monolithic stretched acrylic produced negligible spall.
4. The monolithic cast acrylic, the glass/acrylic laminate and the glass/glass laminate each produced spall of sufficient energy to be a potential source of injury to personnel.
5. The two types of ammunition used produced generally negligible differences in test results.
6. The greatest amount of spall was produced at relatively low impact velocities (approximately 1000 ft/sec). However, differences in spallation were not apparent for small (< 500 ft/sec) incremental velocity changes.
7. Only slight differences could be observed between the pressurized and the nonpressurized test results.
8. Except for a reduced dispersion of spall during one glass/glass laminate test, the method of attachment showed no significant differences in test results.
9. The test criteria and test methods provided realistic correlation to service experience.

## LOW-ENERGY IMPACT TESTS

Impact characteristics of transparent materials are of interest for the following reasons:

- a. Foreign Object Damage (FOD) resulting from low impact strength adversely affects aircraft operational readiness and reliability.
- b. Gross postcrash deformations that cause breakage of transparencies could produce sharp edges which would hinder rescue or emergency egress operations.
- c. Secondary fragments ejected from a transparency as a result of impact by stones, tools, and other low-energy projectiles can be hazardous to personnel.

A series of low-energy impact tests were performed to study the impact strength and fracture mechanisms of several common transparent materials in an effort to establish design and test criteria. The tests were conducted at room temperature, as well as high and low temperatures, to evaluate any temperature-dependent effects.

### Test Equipment

The basic test setup for the impact tests is shown in Figure 166. The test specimens were secured to an aluminum box designed for ballistic and impact tests. The specimen was held rigidly in place by two different methods. In both cases, the specimen rested on a support frame rimmed by a rubber gasket. A metal retainer fit over the periphery of the specimen, leaving most of it exposed. In one configuration, this frame was secured to the test box by twelve spring clamps (Figure 167). In an alternative configuration, the metal retainer was bolted to the box by capscrews placed in drilled, tapped holes along the frame rim (Figure 168).

A 0.002-inch aluminum foil witness plate and five layers of 1/2-inch-thick expanded polystyrene foam (1 lb/cu ft density), respectively, were placed 6 inches below the specimen to characterize the energy of any ejected fragments.

The impact projectile was a 2-pound cylindrical steel dart as shown in Figure 169. This dart was dropped from a height of 10 feet above the specimen through the pipe shown in Figure 166. The impact energy of the dart was therefore 20 ft-lb, which was arbitrarily chosen as being representative of FOD hazards and also sufficient to enable characterization of material shattering effects.



Figure 166. Dart Impact Test Setup.

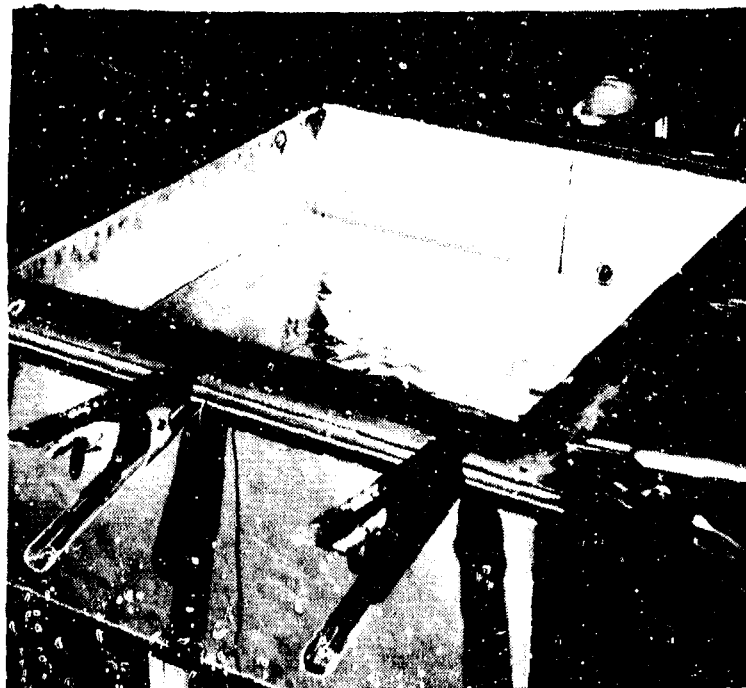


Figure 167. Clamped Attaching Arrangement.

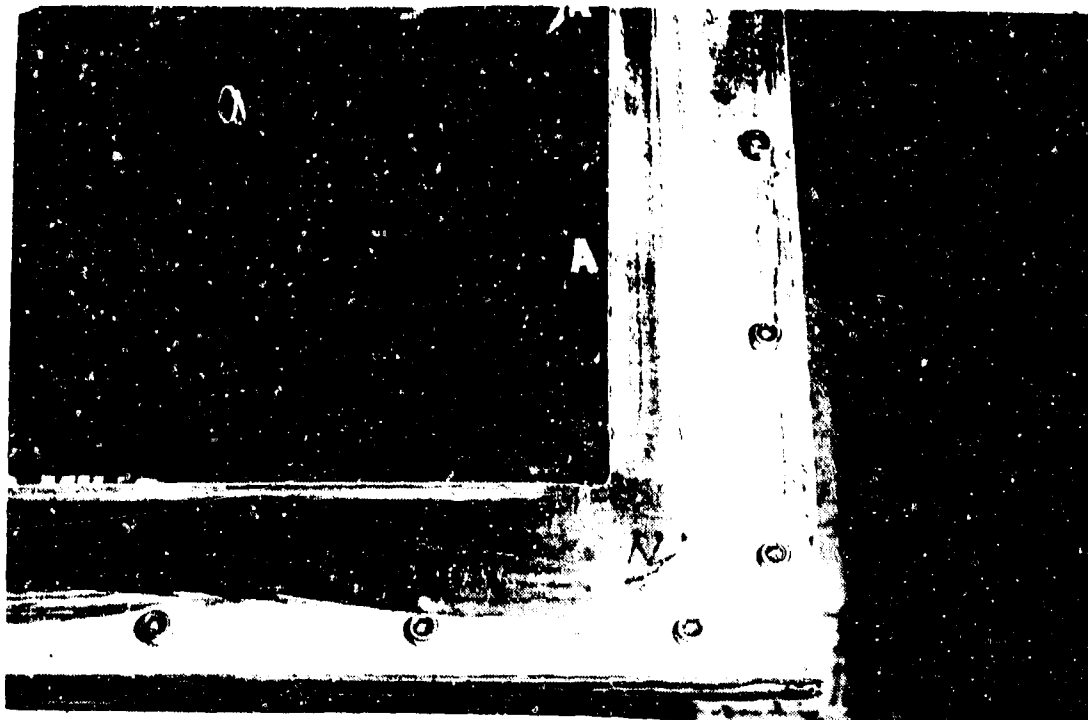


Figure 168. Bolted Attaching Arrangement.

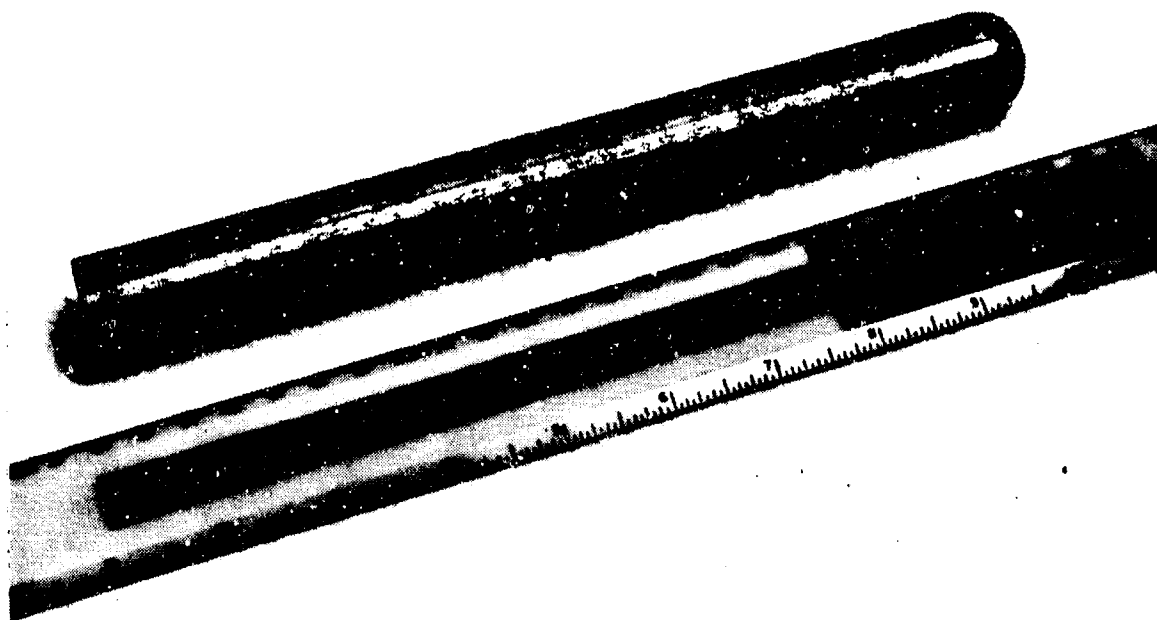


Figure 169. Impact Dart.

### Test Specimens

The test specimens were 2-foot-square panels of various laminated and monolithic transparent materials. Their descriptions are contained in Table 42. The abbreviations listed will be used to represent these materials in all subsequent tables of this report.

TABLE 42. MATERIAL DESCRIPTION FOR LOW-ENERGY IMPACT TESTS

Source	Type	Thickness (in.)	Material	Abbreviation
PPG Industries	laminate	.095	Semitempered soda lime glass	GG
		.075	Polyvinyl butyral	
		.095	Semitempered soda lime glass	
Sierracin	laminate	.085	Chemcor 0401 glass	GA
		.075	Polyvinyl butyral	
		.080	Stretched acrylic	
MIL-P-8184	monolithic	.080	Cast acrylic	CA (.080)
MIL-P-8184	monolithic	.125	Cast acrylic	CA (.125)
MIL-P-8184	monolithic	.250	Cast acrylic	CA (.250)
MIL-P-25690	monolithic	.080	Stretched acrylic	SA
MIL-P-83310	monolithic	.080	Polycarbonate	PC

### TEST PROCEDURE

The test specimen was either clamped or bolted onto the test box. Then, the 2-pound dart was dropped onto the specimen from a height of 10 feet, creating an impact energy of 20 ft-lb. The specimen was subsequently examined for crack patterns, dart penetration, and visibility characteristics. Appropriate photographs were taken.

Any spall was collected, weighed, and qualitatively examined. The witness sheet was checked for spall penetration or other damage. Finally, where necessary, the foam sheets were studied to detect any imbedded fragments.

High-temperature tests were performed using an identical procedure except as modified herein. Prior to testing, the specimens were placed in an environmental chamber at 150°F and allowed to soak overnight. This temperature was maintained during installation by a heat lamp. Temperature just prior to impact was recorded by means of a thermocouple bonded to the specimen surface.

Low-temperature tests were also performed using the same basic procedure except the specimens were placed in an environmental chamber at -65°F and allowed to soak overnight. Temperature just prior to impact was recorded by means of a thermocouple bonded to the specimen surface.

A complete list of test conditions is found in Table 43. Forty-nine specimens were tested.

TABLE 43. TEST CONDITIONS FOR IMPACT TESTS

Specimen	Temperature (°F)/Configuration		
	Ambient	High Temperature	Low Temperature
GG1	Bolted	136/clamped	-52/clamped
GG2	Clamped	141/clamped	-42/clamped
GG3	Bolted	134/bolted	-50/clamped
GA1	Bolted	140/clamped	-52 clamped
GA2	Clamped	126/bolted	*
GA3	Clamped	140/clamped	-52/clamped
SA1	Bolted	137/clamped	-25/clamped
SA2	Bolted	142/clamped	-50/clamped
SA3	Clamped	139/clamped	-46/clamped
CA1 (.080)	Bolted	140/clamped	-44/clamped
CA2 (.080)	Clamped	134/clamped	-49/clamped
CA3 (.080)	Clamped	139/clamped	-48/clamped
CA1 (.125)	Bolted	-----	-----
CA2 (.125)	Clamped	-----	-----
CA3 (.125)	Clamped	-----	-----
CA1 (.250)	Bolted	140/clamped	-44/clamped
CA2 (.250)	Clamped	-----	-----
CA3 (.250)	Clamped	-----	-----
PC1	Bolted	140/clamped	-46/clamped
PC2	Bolted	-----	-----
PC3	Clamped	-----	-----

\*Specimen damaged during low-temperature soak in environmental chamber.

## RESULTS

Visibility and fragment data for the 49 test specimens are presented in Tables 44 through 49. Whenever a specimen was damaged by impact, a photograph was taken for subsequent analysis. A discussion of each parameter follows.

TABLE 44. SPECIMEN APPEARANCE AFTER AMBIENT TEMPERATURE TESTS

Specimen	Surface Cracks	Pulverized Diameter (in.)	Poor Visibility Diameter (in.)	Dart Penetration
GG1	Yes	1/2	1/2	No
GG2	Yes	3/4	1-1/2	No
GG3	Yes	1/2	1/2	No
GA1	Yes	3	3	No
GA2	Yes	1-1/4	1-1/4	No
GA3	Yes	1-3/4	1-3/4	No
SA1	No	0	0	No
SA2	No	0	0	No
SA3	No	0	0	No
CA1 (.080)	Yes	0	0	Yes
CA2 (.080)	Yes	0	0	Yes
CA3 (.080)	Yes	0	0	Yes
CA1 (.125)	Yes	0	0	Yes
CA2 (.125)	Yes	0	0	Yes
CA3 (.125)	Yes	0	0	Yes
CA1 (.250)	No	0	0	No
CA2 (.250)	No	0	0	No
CA3 (.250)	No	0	0	No
PC1	No	0	0	No
PC2	No	0	0	No
PC3	No	0	0	No

TABLE 45. SPECIMEN APPEARANCE AFTER HIGH-TEMPERATURE TESTS

Specimen	Surface Cracks	Pulverized Diameter (in.)	Poor Visibility Diameter (in.)	Dart Penetration
GG1	Yes	3	7	No**
GG2	Yes	1-1/2	5-1/2 *	No
GG3	Yes	1	4	No
GA1	Yes	1	Most Areas	No
GA2	Yes	1-1/2	13-1/2	No
GA3	Yes	1	Most Areas	No
SA1	No	0	0	No
SA2	No	0	0	No
SA3	No	0	0	No
CA1 (.080)	Yes	0	0	Yes
CA2 (.080)	Yes	0	0	Yes
CA3 (.080)	Yes	0	0	Yes
CA1 (.250)	No	0	0	No
PC1	No	0	0	No

\*Scattered areas of poor visibility exist.

\*\*Dart made 1/2 inch indentation.

**TABLE 46. SPECIMEN APPEARANCE AFTER LOW-TEMPERATURE TESTS**

Specimen	Surface Cracks	Pulverized Diameter (in.)	Poor Visibility Diameter (in.)	Dart Penetration
GG1	No	0	0	No
GG2	Yes	1-3/4	7-3/4	No
GG3	Yes	1-3/4	7-3/4	No
GA1	Yes	1/2	4-1/2+corners	No
GA2	Specimen broken in environmental chamber			No
GA3	Yes	1-1/2	corners	No
SA1	Yes	0	1/2	No
SA2	Yes	0	0	No
SA3	Yes	0	0	No
CA1 (.080)	Yes	0	0	Yes
CA2 (.080)	Yes	0	0	Yes
CA3 (.080)	Yes	0	0	Yes
CA1 (.250)	No	0	0	No
PC1	No	0	0	No

TABLE 47. SPALL DATA - AMBIENT TEMPERATURE TESTS

Specimen	Spall Weight (grams)	Witness Sheet Damage	Spall Description
GG1	0	None	---
GG2	.067	None	small slivers most < 1/16 inch
GG3	.021	None	small slivers most < 1/16 inch
GA1	0	None	---
GA2	0	None	---
GA3	0	None	---
SA1	0	None	---
SA2	0	None	---
SA3	0	None	---
CA1 (.080)	0*	Dart Tear	---
CA2 (.080)	0*	Dart Tear	---
CA3 (.080)	0*	Dart Tear	---
CA1 (.125)	0*	Dart Tear Large Frag- ment Tears	---
CA2 (.125)	.008*	Dart Tear Large Frag- ment Tears	3 small flat chips < 1/8 inch diameter
CA3 (.125)	0	Dart Tear	---
CA1 (.250)	0	None	---
CA2 (.250)	0	None	---
CA3 (.250)	0	None	---
PC1	0	None	---
PC2	0	None	---
PC3	0	None	---

\*Does not include large pie-shaped fragments.

TABLE 48. SPALL DATA - HIGH-TEMPERATURE TESTS

Specimen	Spall Weight (grams)	Witness Sheet Damage	Spall Description
GG1	1.085	None	Jagged fragments up to 3/8 inch
GG2	.742	None	Jagged fragments and slivers up to 3/8 inch
GG3	.006	None	Small jagged fragments less than 1/16 inch
GA1	0	None	---
GA2	0	None	---
GA3	0	None	---
SA1	0	None	---
SA2	0	None	---
SA3	0	None	---
CA1 (.080)	0	Dart Tear	---
CA2 (.080)	0	Dart Tear	---
CA3 (.080)	0	Dart Tear	---
CA1 (.250)	0	None	---
PC1	0	None	---

TABLE 49. SPALL DATA - LOW-TEMPERATURE TESTS

Specimen	Spall Weight (grams)	Witness Sheet Damage	Spall Description
GG1	0	None	---
GG2	.011	None	3 small jagged frag- ments less than 1/4 inch
GG3	.078	None	Small jagged fragments less than 1/4 inch
GA1	0	None	---
GA2	Specimen broken in environmental chamber		
GA3	0	None	---
SA1	.154	None	Thin, jagged fragments up to 1/2 inch
SA2	.014	None	Small jagged fragments up to 1/8 inch
SA3	0	None	---
CA1 (.080)	.148*	Dart Tear Large Frag- ment Tear	1 clean fragment 1/2 inch long, .080 inch thick
CA2 (.080)	0*	Dart Tear Large Frag- ment Tear	---
CA3 (.080)	0*	Dart Tear	---
CA1 (.250)	0	None	---
PC1	0	None	---

\*Does not include large pie-shaped fragments.

### Surface Cracks

The polycarbonate and 0.250-inch cast acrylic sheets were the only materials sustaining no damage throughout the test. The stretched acrylic was undamaged at high temperatures and ambient conditions. However, at low temperatures, this material did crack. The typical cracks were long, jagged and sheared in a layer-like fashion similar to mica, as shown in Figure 170.

The 0.125-inch and 0.080-inch cast acrylic cracked at all temperatures tested. The cracks were long and clean, usually four or five, radially emanating from the impact point, as shown in Figure 171.

The glass/glass laminate exhibited surface cracks at all conditions. In most cases, large numbers of fine, long, radial cracks were present in both glass layers, as shown in Figure 172. The resistance to cracking was somewhat temperature dependent as evidenced by one specimen sustaining no impact damage when tested at  $-52^{\circ}\text{F}$ .

The glass/acrylic laminate exhibited varying crack patterns. The ambient and high-temperature tests exhibited radial patterns as shown in Figure 173. However, the low-temperature tests, due to high thermal stresses, produced concentric patterns (Figure 174). One specimen was actually broken in the environmental chamber by these high thermal stresses (Figure 175).

### Surface Pulverization

Only the laminates sustained such damage, their glass layers being pulverized locally by the dart. Close-up shots of this damage are shown in Figures 176 and 177.

In the all-glass laminates, the diameter of pulverization was least at ambient conditions, being about three or four times greater for both hot and cold conditions. The glass/acrylic laminate showed more pulverization at ambient conditions.



Figure 170. 0.080-Inch Stretched Acrylic Specimen, Low-Temperature Impact Test.



Figure 171. 0.080-Inch Stretched Acrylic Specimen, High-Temperature Impact Test.

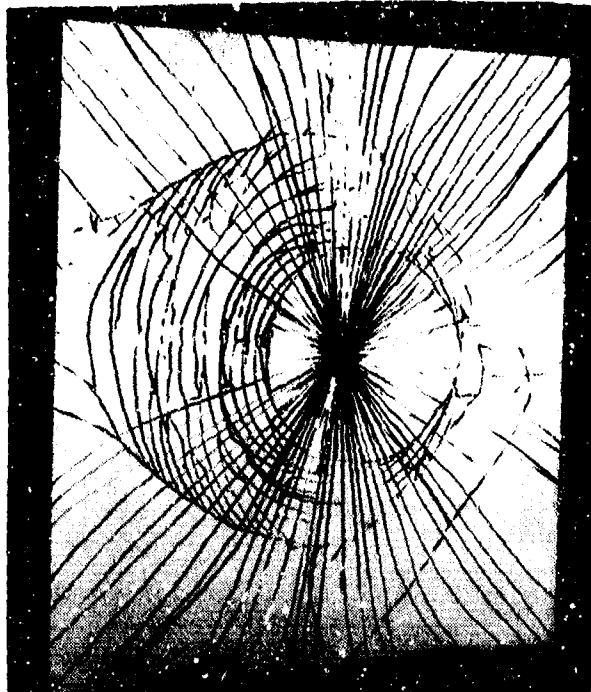


Figure 172. Glass/Glass Laminate, Ambient-Temperature Impact Test.

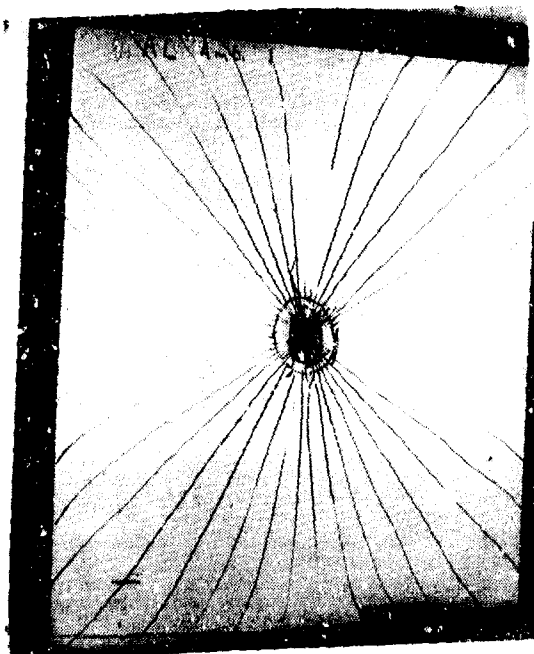


Figure 173. Glass/Acrylic Laminate, Ambient-Temperature Impact Test.



Figure 174. Glass/Acrylic Laminate, Low-Temperature Impact Test.



Figure 175. Glass/Acrylic Laminate Broken in Environmental Chamber at Low Temperature.

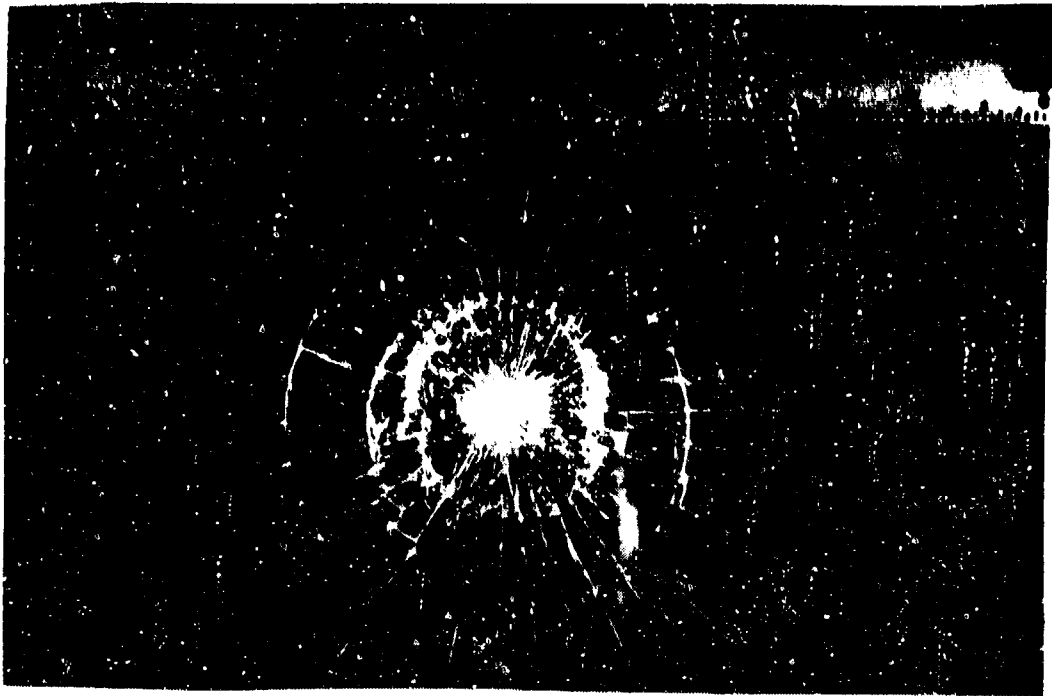


Figure 176. Close-up of Glass/Acrylic Laminate Impact Area.



Figure 177. Close-up of Glass/Glass Laminate Impact Area.

### Impaired Visibility

Impaired visibility was a result of any combination of surface cracks and pulverization which yielded a severely distorted or obscured view. In previous tests, described earlier in this report, a study was made of the residual visibility through cracked and shattered transparency materials. It was determined that a particle density of 1000 per square foot was the threshold for impaired visibility. In the impact tests, this critical level was reached only by the laminated specimens. In most cases, this damage occurred only in the immediate vicinity of impact or other isolated areas.

Severe cracking occurred in the all-glass laminate at both temperature extremes. It extended typically two to three inches beyond the diced area as shown in Figure 178. Such damage was generally limited to the impact center and specimen edges in the glass/acrylic laminate at cold and ambient conditions. However, at high temperatures, the glass layer was severely shattered, badly impairing visibility as shown in Figure 179.

### Dart Penetration

Dart penetration occurred only for the 0.080-inch and 0.125-inch cast acrylic sheets. Particularly at low temperatures, the 0.080-inch specimens showed little resistance to penetration. The dart generally made a clean entry, leaving radial cracks that closed on themselves, except for occasional large pie-shaped fragments which were broken off.

The all-glass laminate was almost penetrated at high temperatures, and the dart made a 1/2-inch indentation in one case.

### Spall Weight and Description

Very little spall occurred during the impact tests. Except for isolated instances as noted in the tables, only two materials exhibited spall. The stretched acrylic at low temperatures gave off a small number of thin jagged chips less than 1/8 inch across.

The glass/glass laminate spalled at all temperature conditions. Most fragments were small and jagged, some in the form of slivers. All were less than 3/8 inch across. The most spall occurred at high temperature (almost a gram) and at low temperature (almost a third of a gram). Ambient temperature spall was typically less than .05 gram.



Figure 178. Glass/Glass Laminate, High-Temperature Impact Test.



Figure 179. Glass/Acrylic Laminate, High-Temperature Impact Test.

### Spall Energy

Spall fragments had low energy and did not penetrate or significantly damage the witness sheet during any test.

Witness sheet damage occurred only in the tests of the 0.080-inch and .125-inch cast acrylics. This was primarily due to dart penetration. However, for certain specimens, primarily of the .125-inch thickness, the witness sheet was occasionally punctured or torn by large pie-shaped fragments broken off by the dart. The clean sharp points of these acrylic chunks could possibly cause tissue injuries to aircraft personnel. The area vacated by such fragments can be seen in Figure 180.

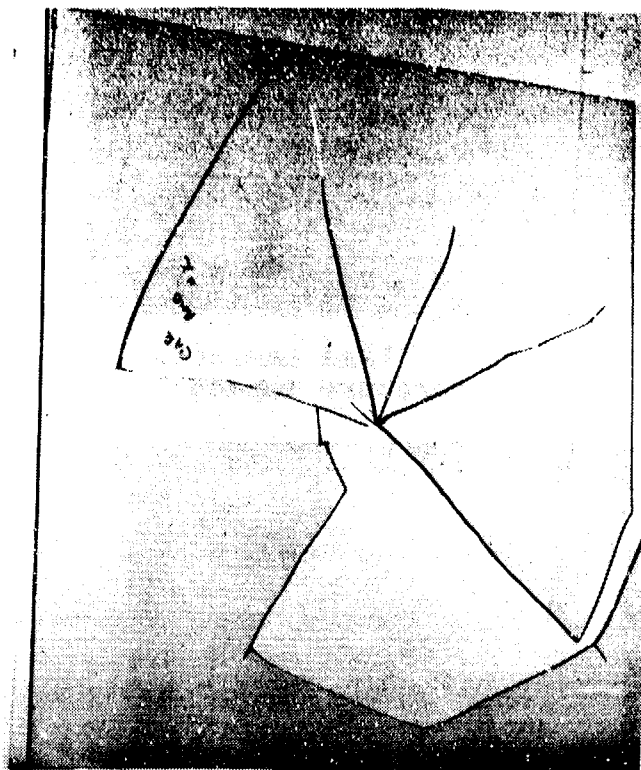


Figure 180. 0.125-Inch Cast Acrylic Specimen,  
Ambient Temperature Impact.

### Attachment Method

Based on the ambient temperature tests conducted on the laminated specimens, the bolted specimens generally appeared to sustain less damage than the clamped specimens.

### IMPACT TEST CONCLUSIONS

1. The 0.080-inch cast acrylic material was very susceptible to impact damage, as evidenced by extensive cracking and ejection of large pie-shaped fragments. Impact strength improved drastically as the thickness was increased.
2. Polycarbonate material was unbreakable for the conditions tested.
3. Stretched acrylic material showed good impact strength and cracked only at low temperatures; even then, the dart did not penetrate the sheet. However, cracks tended to be jagged and sharp.
4. The all-glass and glass/acrylic laminates exhibited good impact strength. Spall ejection was insignificant.
5. Large areas of closely spaced cracks that restricted visibility were noted only on the glass/acrylic laminates during high temperature impact tests.
6. With the exception of polycarbonate, all materials exhibited temperature dependent effects.
7. Based on the performance of the materials tested, a 20-ft/lb dart impact appears to be a reasonable standard for evaluating impact characteristics of helicopter transparencies.

## USAGE SPECTRUM

The purpose of this task was to prepare a typical helicopter windshield usage spectrum as a basis in formulating endurance tests.

In order to formulate meaningful endurance tests for transparencies, the magnitude as well as frequency of occurrence for all loading conditions must be known. This total loading environment for helicopters includes the effects of aerodynamic pressure, maneuvers and gust loads, temperature, humidity and vibration, all of which may be coupled to various degrees.

For test purposes, environmental conditions were generalized. However, a structural environment cannot be generalized and it was, therefore, based on a specific aircraft's characteristics and mission profile.

### TEMPERATURE ENVIRONMENT FROM NATURAL CLIMATIC CONDITIONS

The effects of temperature environment on structural integrity for helicopter windshields can be considered as short term and simulated in real time during endurance tests. Critical temperature conditions result from exposure to natural weather, and operation of windshield heating systems.

A single usage spectrum of temperature and humidity could not be developed due to the wide variations in world weather conditions and lack of criteria to place the aircraft in any one environment for a given period of time. Undue conservatism would result if extreme MIL-SPEC<sup>13</sup> environments shown in Table 50 were assumed to occur continuously and simultaneously with all structural loading conditions.

Helicopter operations are essentially conducted at low altitude where local geographic weather conditions prevail. Therefore, to establish a realistic temperature spectrum, actual worldwide climatic variations were reviewed and typical climates were analyzed. Figures 181 through 184 show a sampling of representative annual temperature distributions for the different climates<sup>14</sup> that were analyzed during this study.

13 "Research, Development, Test and Evaluation of Material for Extreme Climatic Conditions," AR-70-38, July 1969.

14 Anon, "U. S. Naval Weather Service Worldwide Airfield Summaries," Vol. I, VII, IX.

TABLE 50. SUMMARY OF TEMPERATURE AND RELATIVE HUMIDITY  
DIURNAL EXTREMES

CLIMATIC CATEGORY	OPERATIONAL CONDITIONS		STORAGE AND TRANSIT CONDITIONS	
	AMBIENT AIR TEMPERATURE °F	AMBIENT RELATIVE HUMIDITY %	INDUCED AIR TEMPERATURE °F	INDUCED RELATIVE HUMIDITY %
Wet-Warm	Nearly constant 75	95 to 100	Nearly constant 80	95 to 100
Wet-Hot	78 to 95	74 to 100	90 to 160	10 to 85
Humid-Hot Coastal Desert	85 to 100	63 to 90	90 to 160	10 to 85
Hot-Dry	90 to 125	5 to 20	90 to 160	2 to 50
Inter- mediate Hot-Dry	70 to 110	20 to 85	70 to 145	5 to 50
Inter- mediate Cold	-5 to -25	Tending toward saturation	-10 to -30	Tending toward saturation
Cold	-35 to -50	Tending toward saturation	-35 to -50	Tending toward saturation
Extreme Cold	-60 to -70	Tending toward saturation	-60 to -70	Tending toward saturation

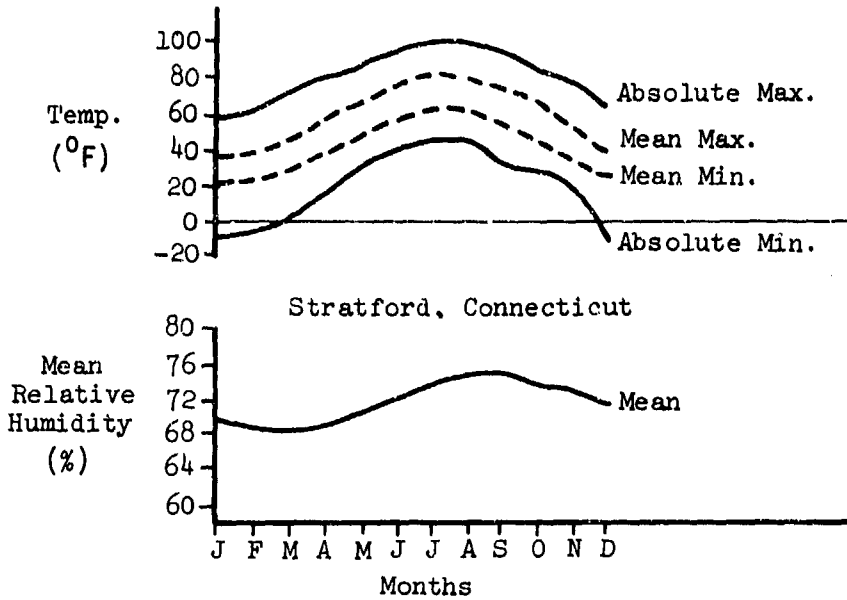


Figure 181. Typical Moderate Climate, Annual Diurnal Temperature/Humidity Variation.

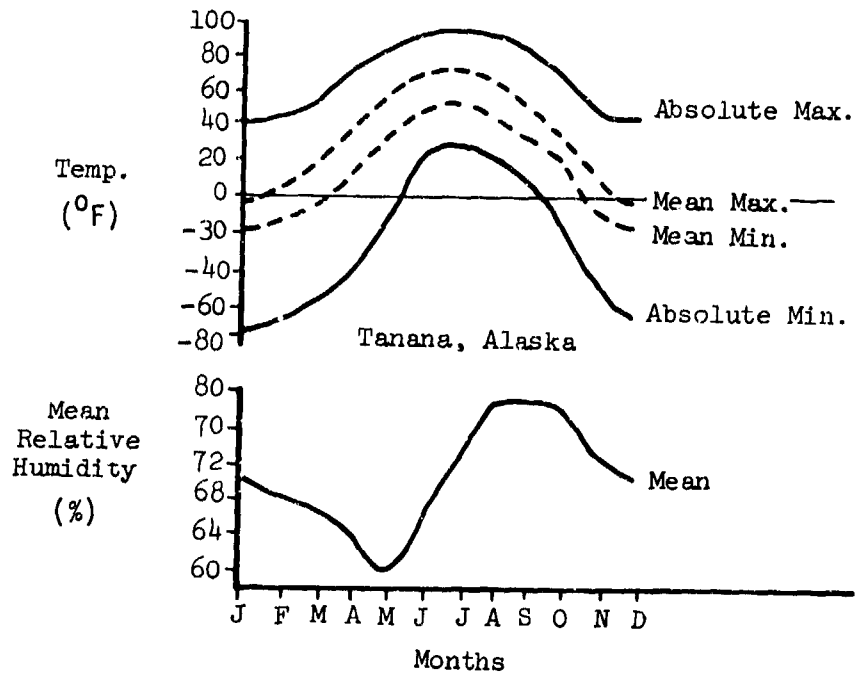


Figure 182. Typical Extreme Cold Climate, Annual Diurnal Temperature/Humidity Variation.

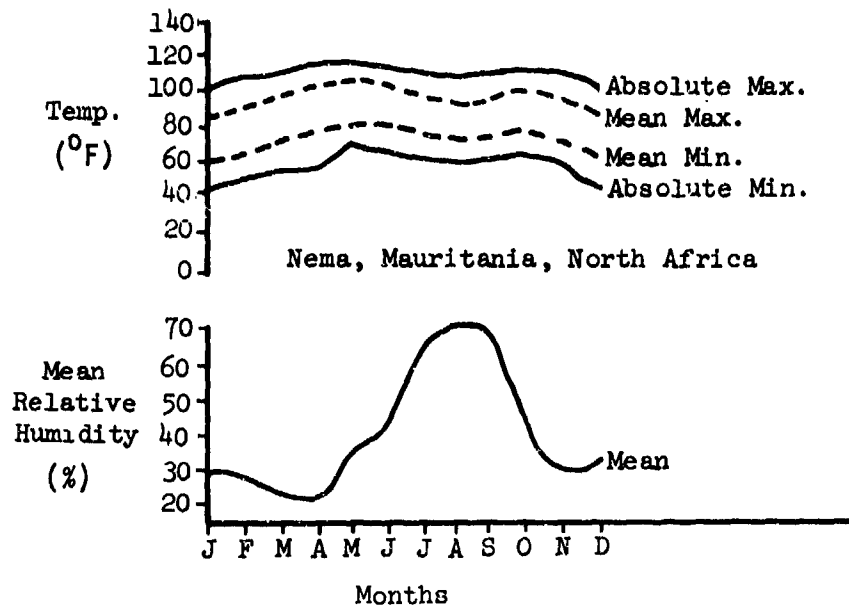


Figure 183. Typical Hot/Dry Climate, Annual Diurnal Temperature/Humidity Variations.

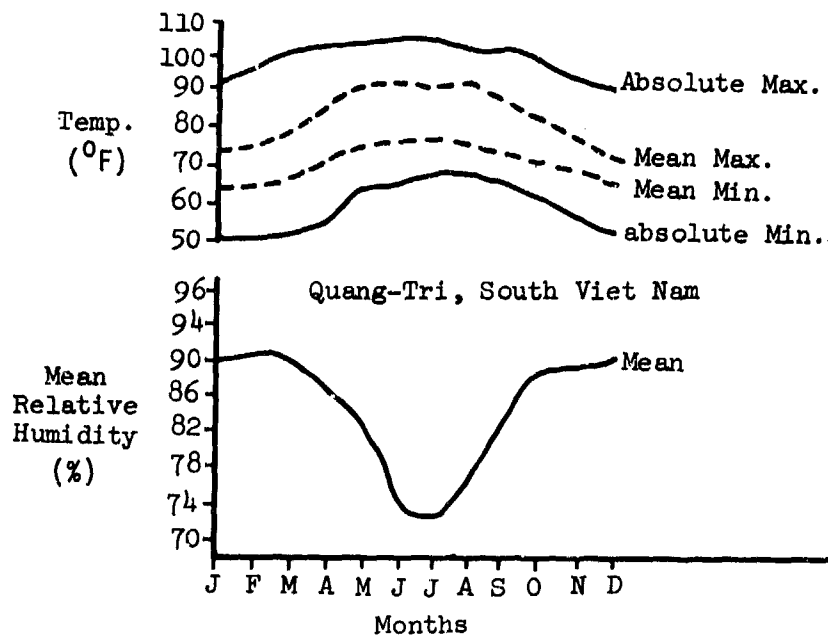


Figure 184. Typical Hot/Wet Climate, Annual Diurnal Temperature/Humidity Variations.

From this analysis, two idealized climates were conservatively created to represent a hot climate and a cold climate for structural endurance testing. Tables 51 and 52 summarize this effort. High temperature (160°F) exposure is omitted from the hot-climate tabulation because it is not representative of flight conditions, but only ground or storage conditions.

TABLE 51. COLD CLIMATE TEMPERATURE DISTRIBUTION

<u>Temperature</u>	<u>Percent of Time</u>
+40°F	45
+25°F	25
-25°F	25
-65°F	5

TABLE 52. HOT CLIMATE TEMPERATURE DISTRIBUTION

<u>Temperature</u>	<u>Percent of Time</u>
100°F	95
125°F	5

STRUCTURAL LOADING CONDITIONS

The structural loading conditions for the usage spectrum were based on an analysis of ground-air-ground (GAG) cycles. By definition, a GAG cycle contains the maximum loads that are encountered in a single flight. Since absolute maximum load conditions do not occur every flight, a load spectrum was also generated to show frequency of occurrence for critical conditions.

### Aerodynamic Pressure

Aerodynamic pressure loads are predominantly a function of airspeed and aircraft attitude (pitch and yaw), and are calculated by the following equation:

$$p = \frac{(C_p) \rho V^2}{288}$$

where

- p = pressure, psi
- C<sub>p</sub> = coefficient of pressure
- ρ = density of air (.00238 slug/ft<sup>3</sup>)
- V = velocity, ft/sec

For cargo or utility helicopters, the basic mission calls for level flight at cruise speed between origin and destination, and the aerodynamic pressure GAG cycle for this condition would simply appear as shown in Figure 185. The average pressure coefficient was assumed to be 1.0 for this case. Similar GAG cycles for other airspeeds were constructed in a like manner.

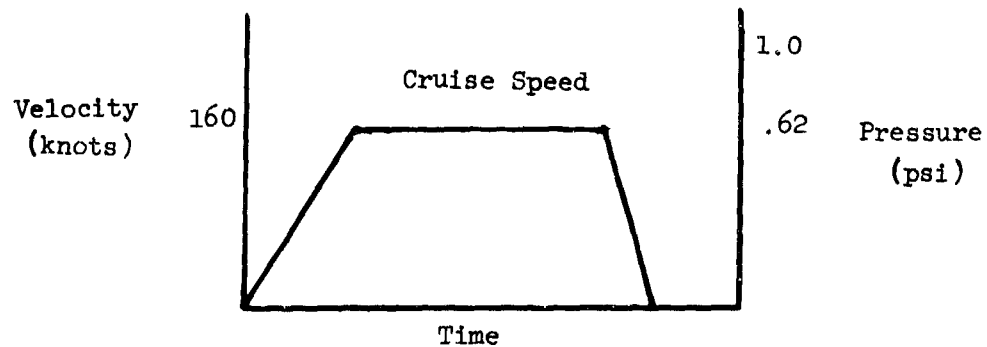


Figure 185. Aerodynamic Pressure Ground-Air-Ground Cycle, UTTAS Helicopter.

## Aircraft Velocity and Load Factor

Data on aircraft velocity and load factors were obtained for an Army Utility Tactical Transport Aircraft System (UTTAS) mission profile.<sup>15,16</sup> A load spectrum was then derived using the UTTAS criterion of four landings per flight hour, coupled conservatively with the 20,000 peak flight load occurrences per 5000 flight hours. The load spectrum is shown in Table 53.

TABLE 53. FLIGHT LOAD SPECTRUM FOR A UTTAS HELICOPTER

Velocity Range (kts)	Corresponding Maximum Vertical Load Factor (Nz)	Number of Exceedances per 5000 Flight Hours
176-217	1.0	1000
151-175	2.25	1000
0-150	3.0	1000
0-150	2.25	7000
0-150	1.5	10000

## VIBRATION

Flight test data from the NH-3A<sup>17</sup> (high speeds) and the CH-53A<sup>18</sup> (low speeds) were used to generate a curve of windshield vibration level versus velocity as shown in Figure 186. The increment in vibration above the 1-g level as a function of load factor was also estimated from flight test data and is presented in Table 54. The dashed lines in the figure indicate the range of data for the condition. This increment was assumed to be zero for load factors equal to or less than 1.0 g.

For the 1.0-g baseline curve, vertical vibrations were assumed to be equal to those of lateral and twice those of longitudinal.

- 15 "Structural Design Criteria Report, YUH-60A," SER-70534, Sikorsky Aircraft Div, Stratford, Conn, January 1973.
- 16 Anon, Prime Item Development Specification for UTTAS, DAAJ01-73-C-0006 (P40), Attachment 2, Army Aviation Systems Command, St. Louis, Mo, July 1972.
- 17 Anon, "NH-3A Vibratory Airloads and Vibratory Rotor Loads," SER-611493, Sikorsky Aircraft Div, Stratford, Conn, January 1970.
- 18 Anon, "CH53A Main Rotor and Stabilizer Vibratory Airloads and Forces," SER-65593, Sikorsky Aircraft Div, Stratford, Conn, June 1970.

TABLE 54. WINDSHIELD VIBRATION SENSITIVITY TO AIRCRAFT LOAD FACTOR

Velocity Range (kts)	Vibration Increment $\Delta g_{vib}/(N_z-1)$		
	Vertical Component	Lateral Component	Longitudinal Component
0 to 88	.15	.15	.10
89 - 150	.20	.20	.15
151 - 210	.25	.25	.20

Note:  $N_z$  = vertical load factor.

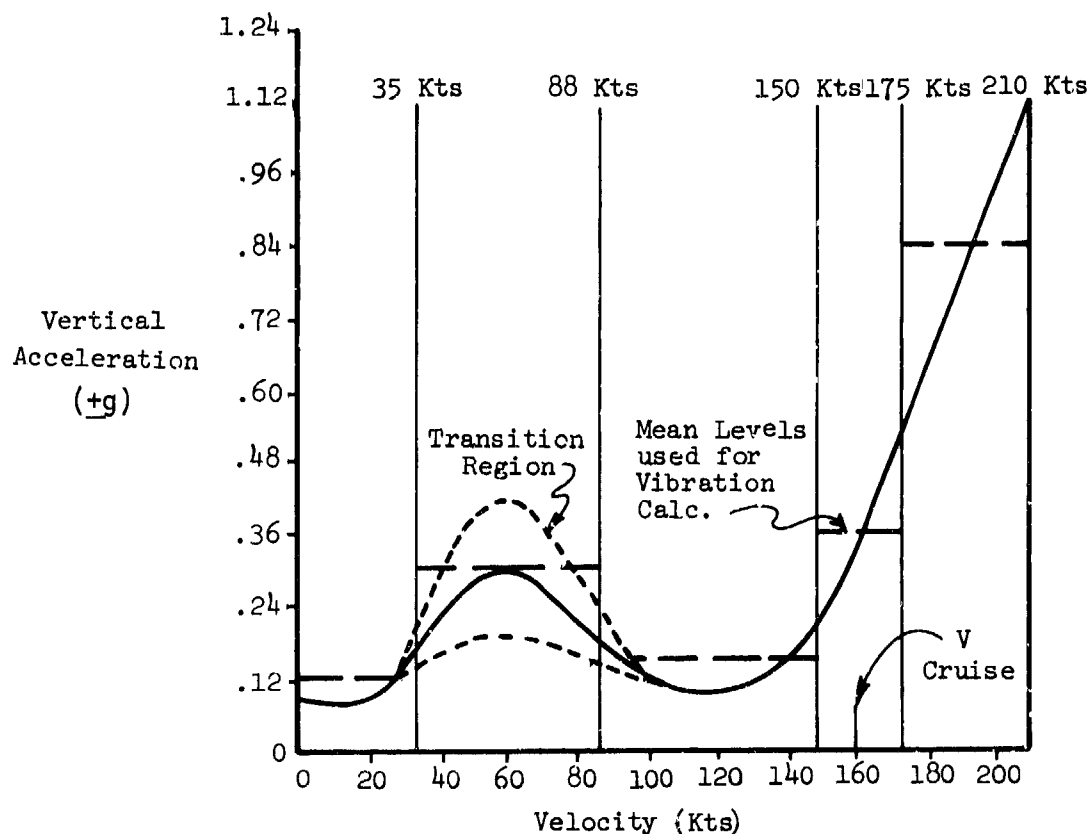


Figure 186. Windshield Vibration vs Aircraft Velocity, 1.0 g Level Flight.

## STRUCTURAL LOADING SPECTRUM

The complete structural loading spectrum for the windshield is presented in Table 55. The effects of load factor are shown as in-plane running loads applied to the edges of the windshield. Typical edge loads were obtained from a NASTRAN analysis of a Sikorsky UTTAS airframe under similar loading conditions.

The vibration was assumed to be orthogonal to the windshield, with a magnitude equivalent to the vertical component previously derived. Frequency of vibration was considered to fall in a range between 9 and 30 hertz, being a function of main rotor blade speed.

TABLE 55. TYPICAL UTILITY HELICOPTER LOADING SPECTRUM

Velocity Range (kts)	Vertical Load Factor (Nz)	Aerodynamic Pressure (psi)	In-Plane Edge Load (lb/in.)	Vibration (g)	Percent Time
176-210	1.0	1.0	70	0.84	5
151-175	2.25	0.75	50	0.61	5
0-150	3.0	0.60	40	0.80	5
0-150	2.25	0.60	40	0.61	35
0-150	1.5	0.60	40	0.42	50

## INSTRUMENTED WINDSHIELD TESTS

This series of tests was formulated to establish the effects of combined structural and environmental loadings on a selection of windshield configurations.

Various parameters were simulated, both singly and in combination, on each of three types of windshield construction, all of which were fully instrumented.

The first part of the program was to establish which parameters were significant, and to determine which of these would be most useful for future qualification testing. The second part of the program was to subject a selected windshield to repeated applications of a complex loading combination, considered to most accurately represent helicopter service conditions.

The tests were performed by the Triplex Safety Glass Co, Ltd, Birmingham, England. Windshield specimens were supplied by PPG Industries, Huntsville, Ala, and Sierracin/Sylmar, Sylmar, Calif.

### TEST SPECIMENS

Three different types of flat, heated, anti-ice windshield designs were tested:

- 101, Two-Ply Glass Construction.
- 102, Glass Faced Stretched Acrylic.
- 103, Polyester Faced Stretched Acrylic.

The anti-ice integral heating film of each windshield type operated from a 195-volt, A.C. supply and gave a nominal power density of 366 watts/sq in. Each windshield incorporated one 300-ohm temperature-sensing element.

Detail design was based on the requirements of the Sikorsky YUH60A Utility Tactical Transport Aircraft System (UTTAS).

Four windshields of each of the three types were provided; Table 56 lists the serial numbers and relevant manufacturers; Figure 187 illustrates the configuration details of all three types. Temperature uniformity checks had been conducted prior to testing, either by the manufacturer or by Triplex, and the results are given in Table 57. The locations of the hot spots correspond to the dimensions shown in Figure 188.

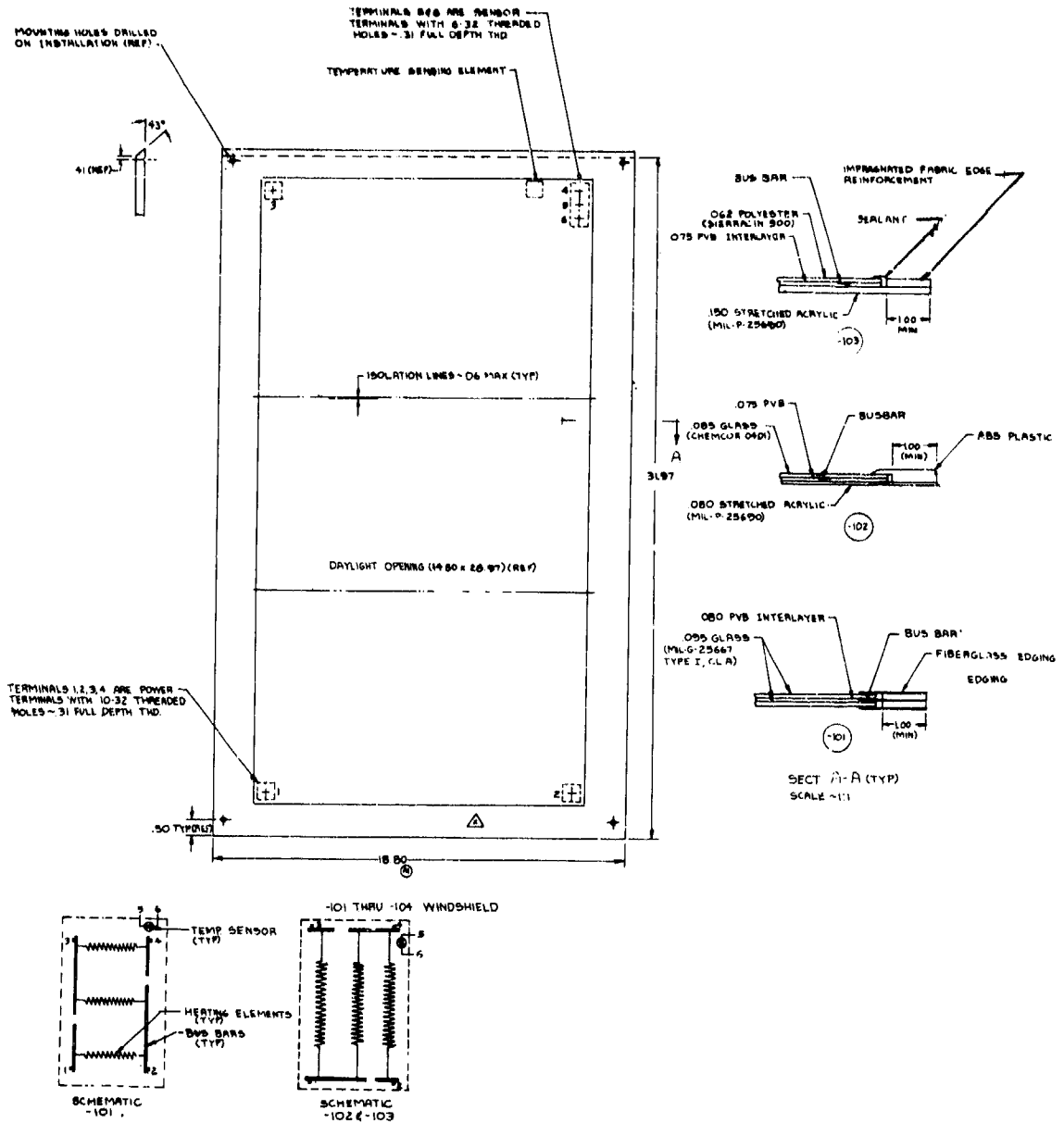


Figure 187. Windshield Test Specimens.

TABLE 56. PART AND SERIAL NUMBERS OF TEST SPECIMENS

Drawing Suffix	Configuration (Outside/Inside)	Manufacturer	Serial Numbers
-101	Glass/Glass	PPG	6-24-75-9 7-1-75-5 7-7-75-1 7-10-75-4
-102	Glass/Acrylic	Sierracin	001 002 003 009
-103	Polyester/Acrylic	Sierracin	005 006 007 008

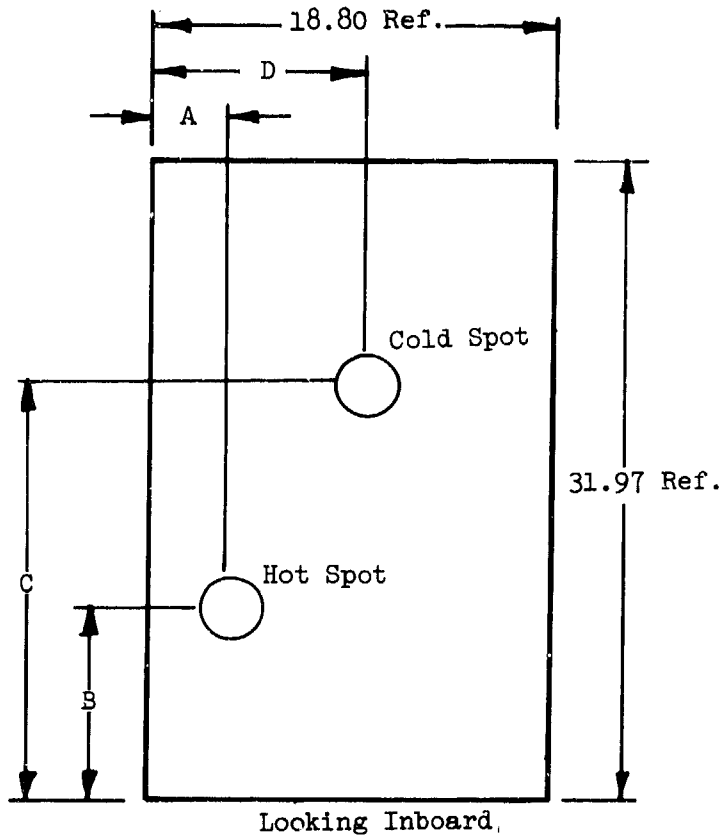


Figure 188. Hot and Cold Spot Locations.

TABLE 57. WINDSHIELD TEMPERATURE UNIFORMITY MEASUREMENTS

Drawing Suffix	Serial No.	Hot Spot Power Const K <sub>H</sub>	Cold Spot Power Const K <sub>L</sub>	Hot Spot		Location		Cold Spot		Location		Phase Resistance (Ohms)			
				Dim A (in.)	Dim B (in.)	Dim A (in.)	Dim B (in.)	Dim C (in.)	Dim D (in.)	1-2	1-3	1-4	2-4	3-4	
-101	6-24-75-9	1.28	0.90	16.3	23.0	8.5	2.7	74.3	-	73.9	-	76.1	-	-	
-101	7-1-75-5	1.00	0.76	14.8	4.5	16.5	6.0	72.3	-	75.4	-	73.6	-	-	
-101	7-7-75-1	1.07	0.88	16.3	6.5	29.0	5.2	68.8	-	66.9	-	70.1	-	-	
-101	7-10-75-6	1.11	0.74	16.3	12.0	21.5	10.5	64.2	-	64.6	-	66.7	-	-	
-102	001	-	-	Outer Glass Cracked on Receipt				-	-	-	-	-	-	-	-
-102	002	1.21	0.89	11.3	8.0	28.0	12.8	-	-	69.0	64.3	66.9	-	-	
-102	003	-	-	Outer Glass Cracked on Receipt				-	-	-	-	-	-	-	-
-102	009	1.30	0.93	5.0	5.0	12.0	2.5	-	-	74.5	76.0	73.1	-	-	
-103	005	1.16	0.88	10.5	24.0	15.0	16.8	-	-	69.6	64.6	66.7	-	-	
-103	026	1.22	1.00	13.0	3.2	Sensor	-	-	-	72.1	70.3	68.3	-	-	
-103	007	1.30	0.96	9.0	4.0	18.0	15.8	-	-	71.0	72.2	80.2	-	-	
-103	008	1.30	0.93	12.8	5.0	28.0	3.0	-	-	78.6	68.2	72.0	-	-	

## SPECIMEN INSTALLATION

All specimen windshields were required to be installed in a fully representative portion of canopy structure. An actual section of the YUH60A cockpit structure was used for this purpose. A cross-sectional view showing a typical part of this structure with a windshield installed is shown in Figure 189.

On windshields of glass/acrylic (-102) and polyester/acrylic construction (-103), a steel reinforcing ring was required to be fitted around the windshield aperture to represent the stiffness of the adjacent structures. This was necessary since these windshields had relatively low transverse stiffness and behaved more as a membrane than a plate. The resulting in-plane membrane loads would thus be reacted by the reinforcing ring.

Windshields of glass/glass configuration, being far stiffer, and thus likely to behave as a plate, did not require any such edge reinforcing.

## TEST PARAMETERS

The following requirements for environmental and loading parameters were used:

### Parameter 1. Low Temperature

Reduce airstream temperature to provide an external air temperature of  $-65^{\circ}\text{F}$  ( $-54^{\circ}\text{C}$ ) while maintaining an internal air temperature of  $+40^{\circ}\text{F}$  ( $+4^{\circ}\text{C}$ ).

### Parameter 2. High Temperature

Raise airstream temperature to provide an external air temperature of  $+125^{\circ}\text{F}$  ( $+52^{\circ}\text{C}$ ) while allowing the windshield inner and outer surfaces to achieve a stabilized condition approximating this level.

### Parameter 3. Thermal Shock

With an outside air temperature of  $-65^{\circ}\text{F}$  ( $-54^{\circ}\text{C}$ ) and an internal air temperature of  $+40^{\circ}\text{F}$  ( $+4^{\circ}\text{C}$ ), apply full electrical power to the windshield until operational temperature, as indicated by the temperature sensing element, is reached. The thermal shock is applied in quiescent air conditions.

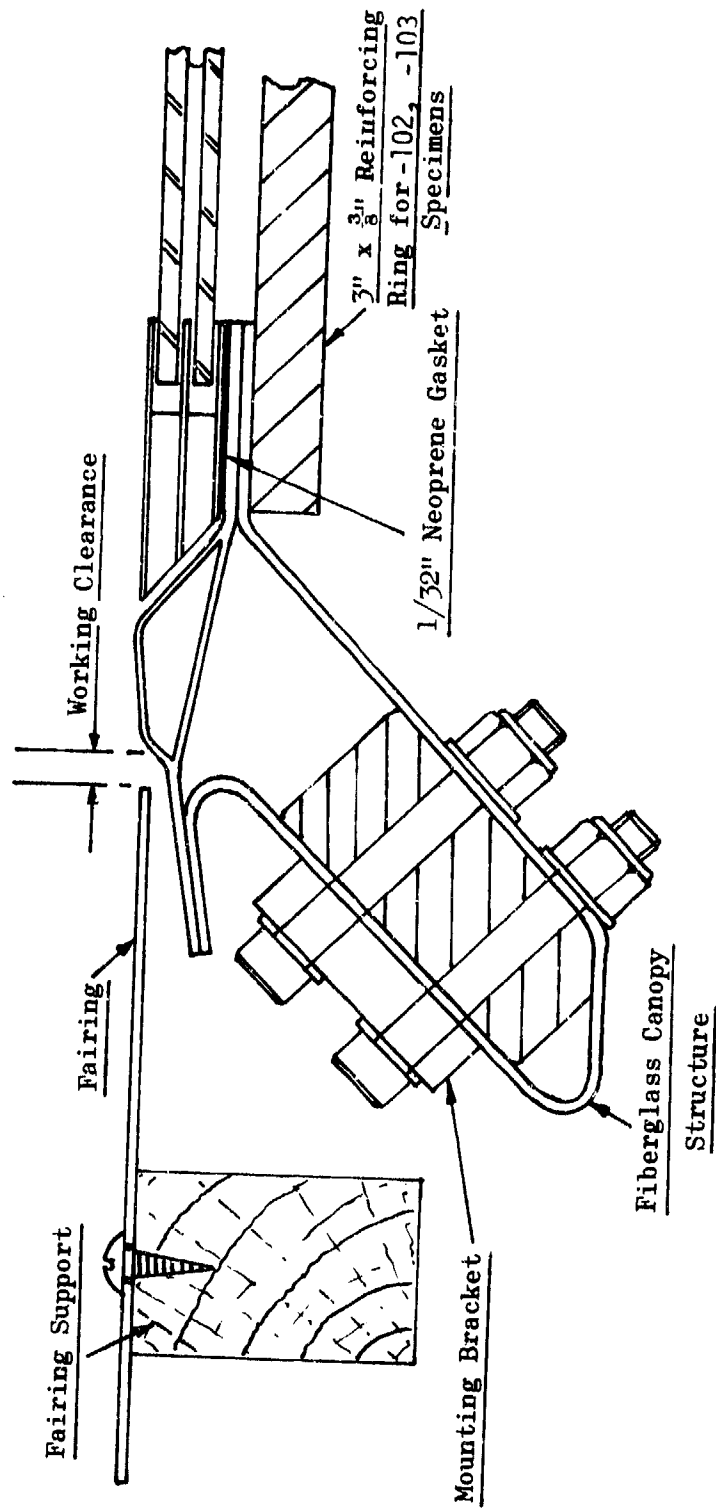


Figure 189. Assembly of Windshield Canopy Structure and Reinforcing Ring.

#### Parameter 4. Cold Shock

This parameter requires the simulation of a rapid down shock, as would be experienced when flying from dry cold air into cloud formation containing supercooled moisture. Conditions are initially stabilized at +25°F (-4°C). Full electrical power is then applied and the temperature is allowed to stabilize at operational temperature. The airflow temperature is reduced at a minimum rate of 2°F/second (approximately 1°C/second) until the outer glass surface is lowered to 32°F (0°C).

#### Parameter 5. Aerodynamic Pressure

Subject the windshield to an outward acting pressure differential of 1 psi.

#### Parameter 6. Edge Loading

On the glass/glass (-101) windshield only, apply an inplane load of 2000 lb uniformly distributed along the windshield's longer edge.

#### Parameter 7. Vibration

Excite the windshield and its supporting canopy structure at a +1g vibratory amplitude. Conduct a frequency sweep over the range of 9 to 30 Hertz to determine whether a resonant frequency is present in this range.

#### Parameter 8. Installation Preload

Simulate a contour mismatch by installing a tapered shim, designed to introduce a bow of 0.10 in. between one long edge of the windshield and the supporting canopy structure.

#### PROCEDURE

The preceding schedule of parameters was applied as relevant to each of the three windshield configurations. Then, various combinations of parameters were applied to establish their interaction. As testing proceeded, some loading conditions were seen to create only negligible effects and in such cases, they were subsequently omitted from the program. Tables 58, 59 and 60 show the loading matrix finally evolved for each of the three configurations and include both single and combination tests. For simplicity, each parameter is identified by the preceding parameter numbers, and each test, whether involving single or multiple application of parameters, has been allocated a 'Case Number.'

TABLE 58. LOADING PARAMETER MATRIX FOR THE GLASS/GLASS  
(-101) WINDSHIELD

Case No.	Parameters Included
1	1 (Low Temperature)
2	2 (High Temperature)
3	3 (Thermal Shock)
4	4 (Cold Shock)
5	5 (Aerodynamic Pressure)
6	6 (Edge Loading)
7	7 (Vibration)
8	8 (Installation Preload)
9	1, 5
10	1, 6
11	1, 7
12	1, 8
13	2, 5
14	2, 6
15	2, 7
16	2, 8
17	3, 5
18	3, 6
19	3, 8
20	4, 5
21	4, 5
22	4, 6
24	4, 8
25	5, 6
27	5, 8
29	6, 8
32	5, 6, 8
34	5, 6, 1
35	5, 6, 2
36	5, 6, 3
37	5, 6, 4
38	5, 6, 8, 1
39	5, 6, 8, 2
40	5, 6, 8, 3
41	5, 6, 8, 4

TABLE 59. LOADING PARAMETER MATRIX FOR THE GLASS/  
ACRYLIC (-102) WINDSHIELD

Case No.	Parameters Included
1	1 (Low Temperature)
2	2 (High Temperature)
3	3 (Thermal Shock)
4	4 (Cold Shock)
5	5 (Aerodynamic Pressure)
7	7 (Vibration)
9	1,5
11	1,7
13	2,5
15	2,7
17	3,5
21	4,5

TABLE 60. LOADING PARAMETER MATRIX FOR THE  
POLYESTER/ACRYLIC (-103) WINDSHIELD

Case No.	Parameters Included
1	1 (Low Temperature)
2	2 (High Temperature)
3	3 (Thermal Shock)
4	4 (Cold Shock)
5	5 (Aerodynamic Pressure)
7	7 (Vibration)
9	1,5
11	1,7
13	2,5
15	2,7
17	3,5
21	4,5

### Inspection Requirements

During and after each loading cycle, the windshields were visually inspected for any sign of degradation. Particular attention was made to observe delamination, cracking, bubbling, and seal or edging separation.

### Calibration Requirements

Calibration of all test equipment was required to be in accordance with MIL-C-45662A. This specification, in turn, permits other countries' National Standards, provided they align with International or U. S. National Standards.

The U. K. Ministry of Defense (Procurement Executive) Specification DEF. STAN. 05-26, under which Triplex is qualified, provides for calibration traceability to U. K. National Standards and thus falls into this category.

### TEST FACILITY

The test rig was essentially a continuous loop of ducting with a working section to accept a test specimen mounted parallel to the airflow. Each specimen was mounted in an individual pressure box that was inserted into this working section and surrounded by suitable fairings to maintain a flush surface around the specimen.

The basic circuit of the loop was a rectangular cross section with radiused bends. The loop was efficiently lagged to minimize thermal losses within the rig itself. Careful attention was given to the transition zones between the rectangular and the working sections of the system so as to provide a constant velocity profile in the working section. The circulating air was driven around the endless loop by a centrifugal fan, and the air was heated or cooled as required. Velocity was constant at approximately 70 knots (120 ft/sec) with a corresponding heat transfer coefficient (h) of 28 Btu/hr-ft<sup>2</sup>-°F.

For heating, a bank of electrical resistance elements were mounted in the duct. Cooling was achieved by the controlled injection of gaseous nitrogen, fed from a liquid nitrogen bulk storage tank. A general schematic of the facility is shown in Figure 190. All of the required parameters could be controlled manually if necessary with a master programmer defining the sequence and control of the various operations for cyclic testing.

Details of special features incorporated in the rig for this program are discussed in the following paragraphs.

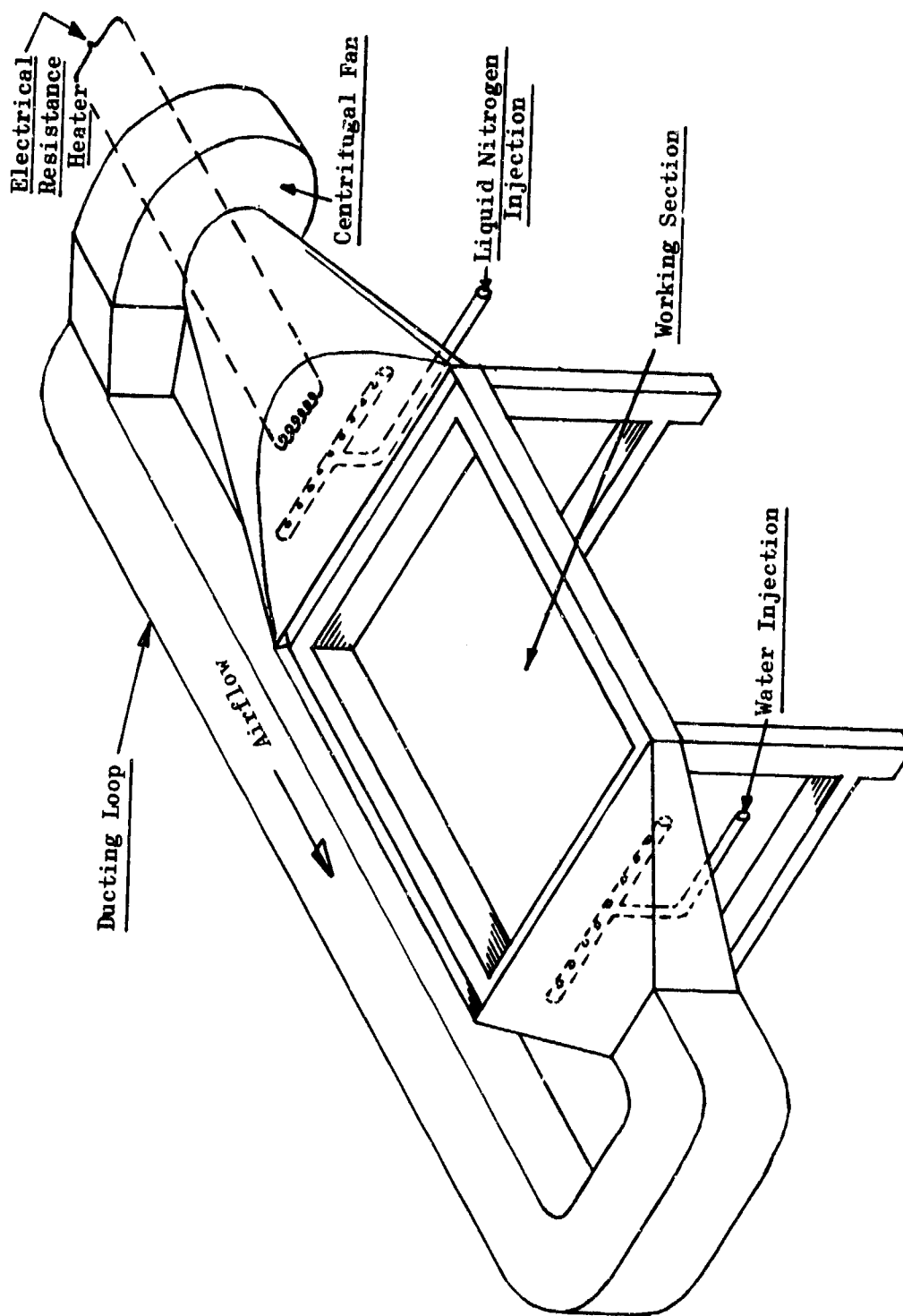


Figure 190. Schematic View of Basic Testing Facilities.

### Edge Loading

The in-plane edge loading was applied to an outside flange of one of the canopy posts, which because of its relatively low stiffness, transmitted a significant proportion of the load to the windshield. Load was applied, nominally distributed evenly along the post, via eight bolted attachments, locally reinforced to further distribute the point load concentration.

The total load was applied by a pneumatically actuated dead load system, acting through a suitable lever mechanism and incorporating a load cell in the circuit. General views of this system are shown in Figures 191 and 192. The three pneumatic actuators shown in Figure 192 allow automatic selection of three differing load levels, if required.

### Mounting of Canopy Structure

Basically, the structure was supported at its four corners, i.e., at the ends of the windshield's horizontal upper and lower sills. On the side remote from the applied in-plane load, the supports were pin-jointed, and the end attachment plates incorporated universal ball joints on these pins to give full rotational freedom. The ball joints themselves could slide on the pins to remove the risk of any degree of binding.

The other two corners were fully floating, although a spreader beam was attached between them. This also incorporated full freedom of movement and provided (at its center point) a means of attaching:

- a) the vibratory input
- b) a balance system to react the applied aerodynamic pressure load
- c) a mass balance system to react the weight of the windshield and its adjacent structure.

This is shown schematically in Figure 193.

### Windshield Installation and Pressure Box

The windshield was attached to the canopy structure using 0.187-inch-diameter screws at approximately three-inch-spacings. Hole diameter was 0.312 inch for the glass/glass (-101) windshields, and 0.201 inch for the polyester/acrylic and glass/acrylic windshields. In the case of the glass/glass windshields, anchor nuts were provided, prefixed to thin aluminum strips. In all other cases, the fasteners attached directly into threaded holes in the steel reinforcing plate.

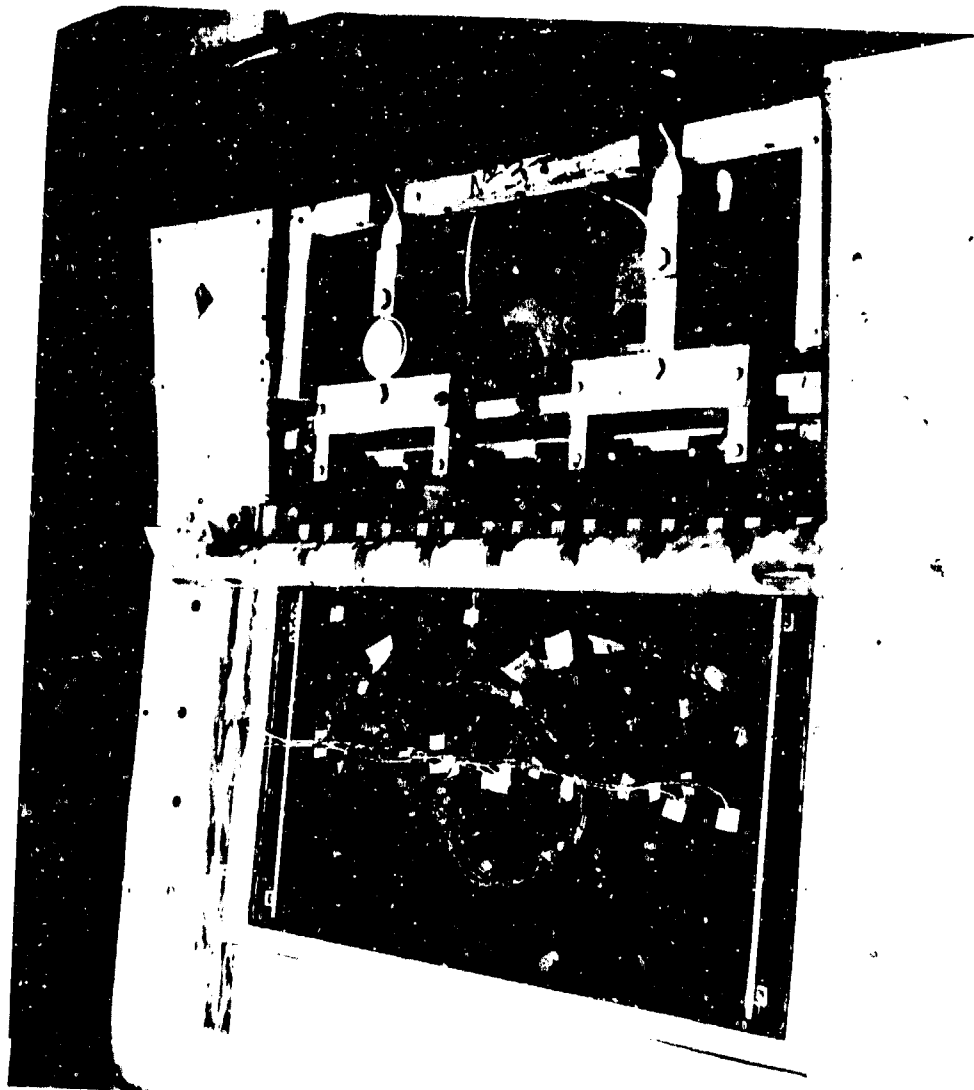


Figure 191. View of Edge Loading Attachment Showing  
8-Point Load Input and Load Cell.

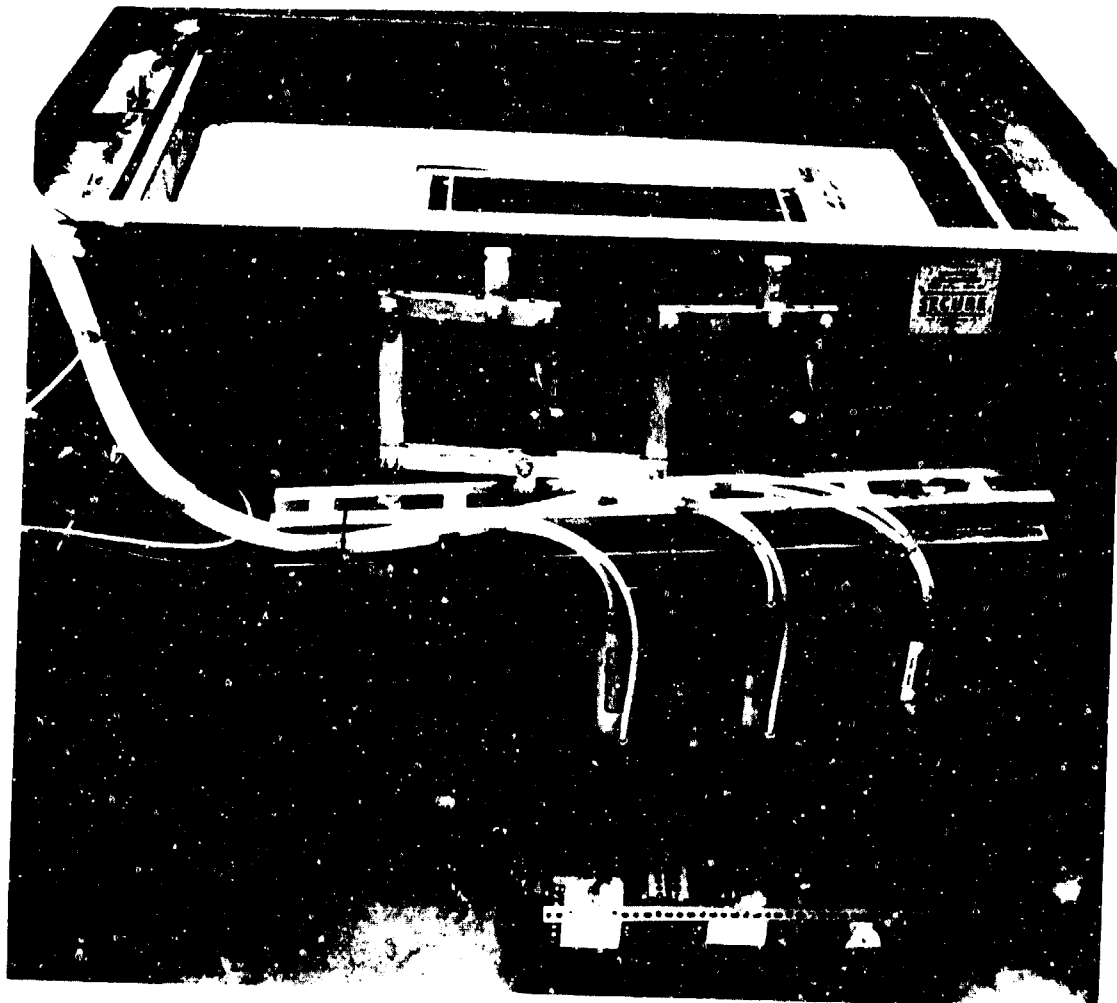


Figure 192. View of Mechanism for Applying Load to Edge Load System.

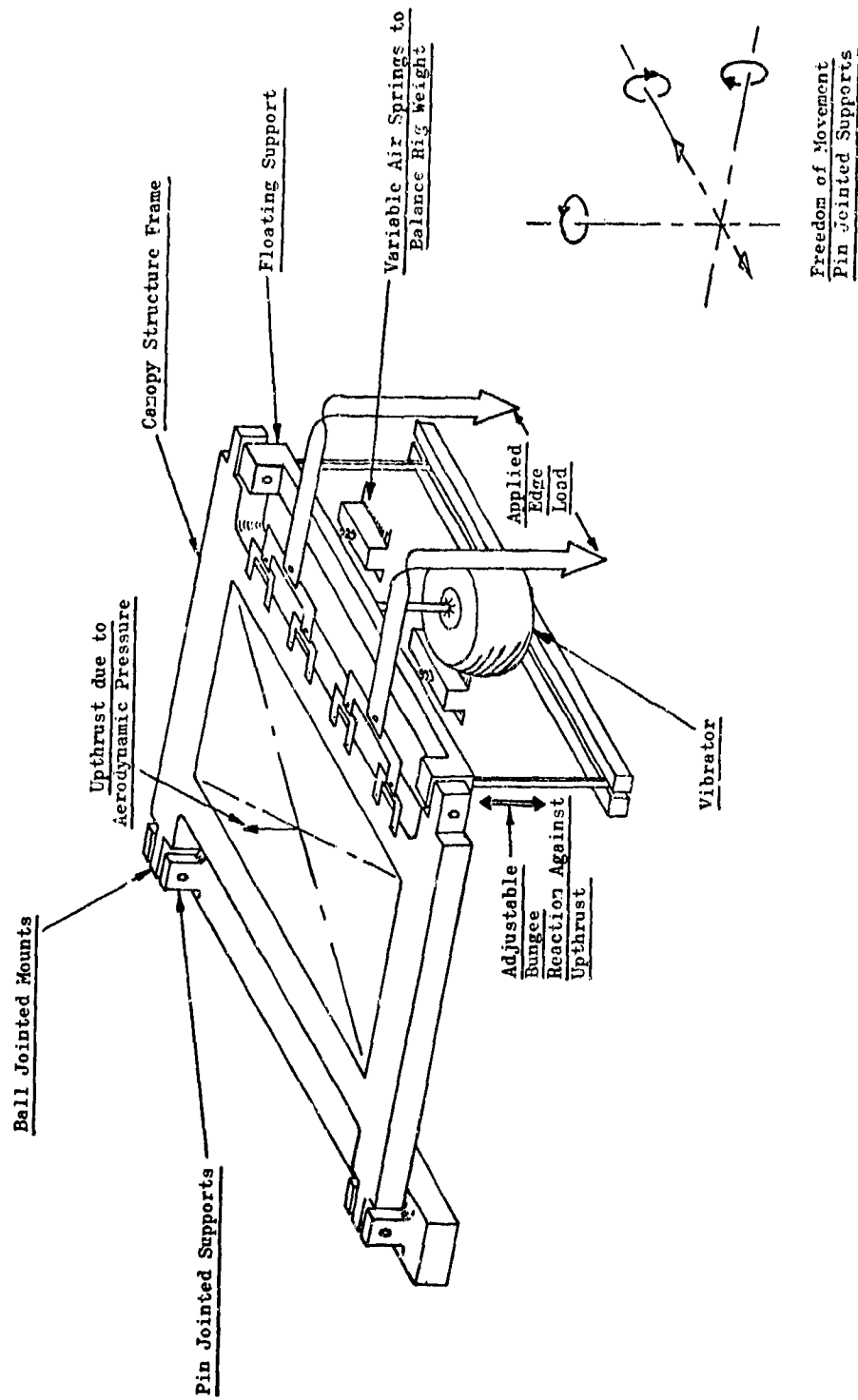


Figure 193. Schematic View of the Frame Support and Mass Balance System.

Because it was important to maintain the correct edge stiffness and because the entire windshield structure had to float under vibratory excitation, the pressure box had to be structurally independent. This was achieved by attaching the posts and sills of the structure to the steel pressure box with a reinforced neoprene "skirt," as illustrated in the typical edge shown in Figure 194.

#### Vibration System

The vibratory input was on the free edge of the pin-joint mounted canopy structure. The vibrator itself was firmly anchored on a subframe off the main rig framework.

It was necessary to carefully mass balance the loads applied to the windshields either because of the aerodynamic pressure or the specimen and structural dead weight. This was to ensure that the exciter commenced its action from a neutral unloaded condition. Bungee loops and inflated air bags provided a good means of achieving this condition. These are shown schematically in Figure 193 and photographically in Figure 195.

#### INSTRUMENTATION

Instrumentation as described herein was provided to monitor and record the following test parameters:

##### Strain

Three-arm rosette strain gauges were selected, manufactured by Micro-Measurements Inc., Romulus, Michigan. They were of the temperature-compensating type since the "dummy bridge" principle was not practical due to the presence of severe temperature gradients, both in-plane and normal to the windshield surface.

The following Inc. part numbers were used:

For glass, WK-05-250RA-350W  
For acrylic, WK-15-250RA-350W  
For polyester, EA-50-250RD-350W

Gauges were bonded to the surface using 'M' Bond AE10/15 adhesive (manufactured by Micro-Measurements Inc.) and the gauges were held in contact during adhesive curing by the use of a vacuum bag. A thin protective coating of silicone rubber was applied over the gauges. Gauges were positioned and orientated as shown in Figure 196.

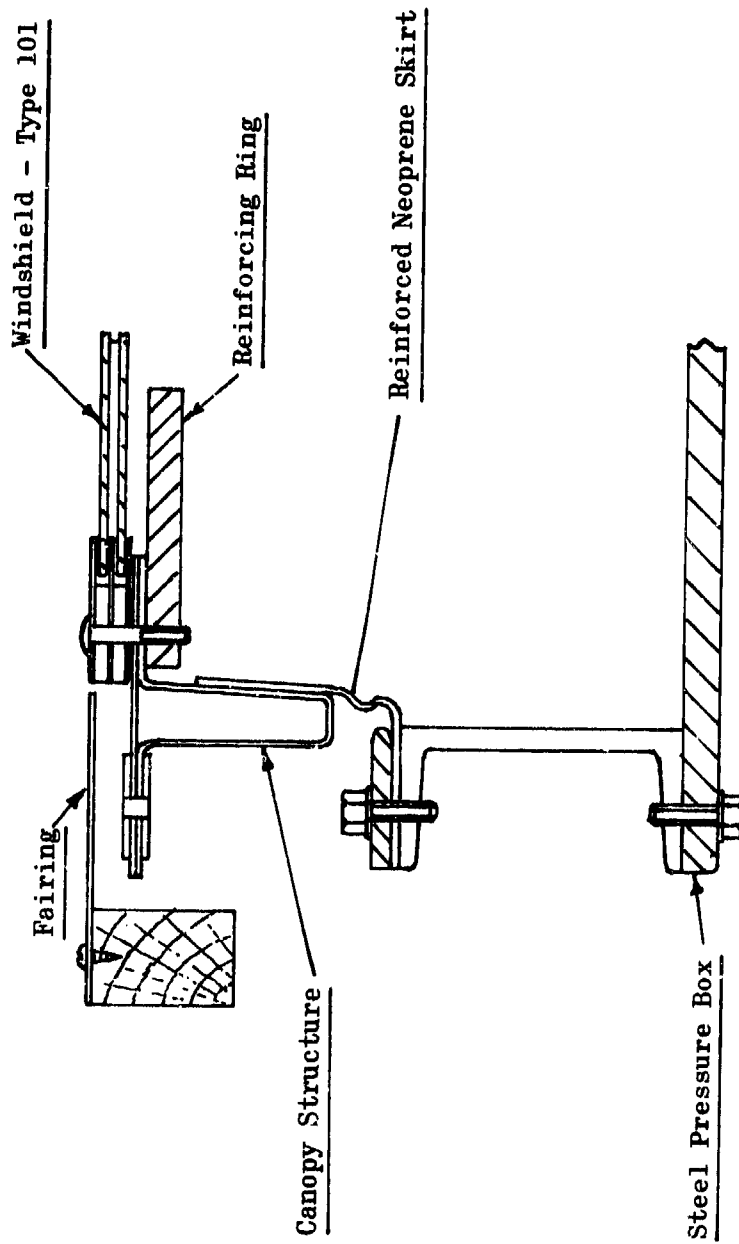


Figure 194. Windshield Installation and Pressure Box.

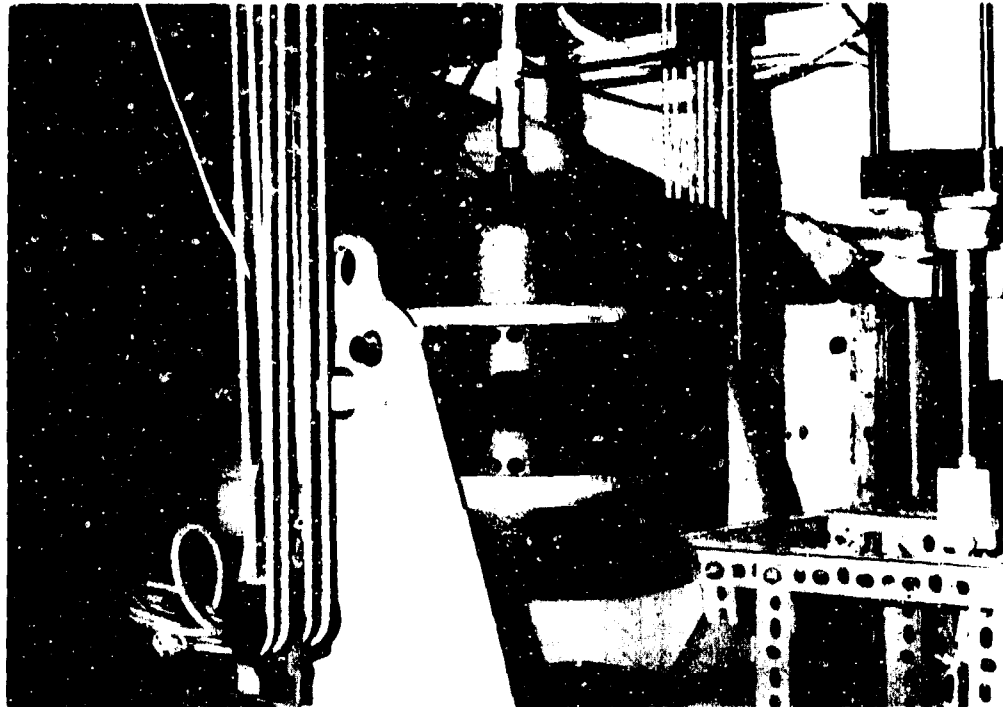


Figure 195. View of "Bungee" Loops to Restrain Floating Canopy Structure in Neutral Attitude When Pressurized.

Strain gauge signals were fed through a carrier amplifier system to U. V. Chart Recorders that ran continuously through a given test.

As far as possible, the temperature-compensating factors of these gauges had been selected to suit the materials used. However, this was only achieved accurately in the case of glass. It was considered that any error in gauge/coefficient matching could be allowed for by establishing an apparent strain curve for each material type and applying this as a correction to the results. This would assume that the precise temperature of the gauge at any moment was known.

As testing proceeded, it rapidly became apparent that the presence of the instrumentation itself could cause errors, and accurate temperature compensation proved to be virtually impossible at temperatures other than ambient, particularly in the case of transient conditions.

These problems are discussed in greater detail in Appendix B of this report.

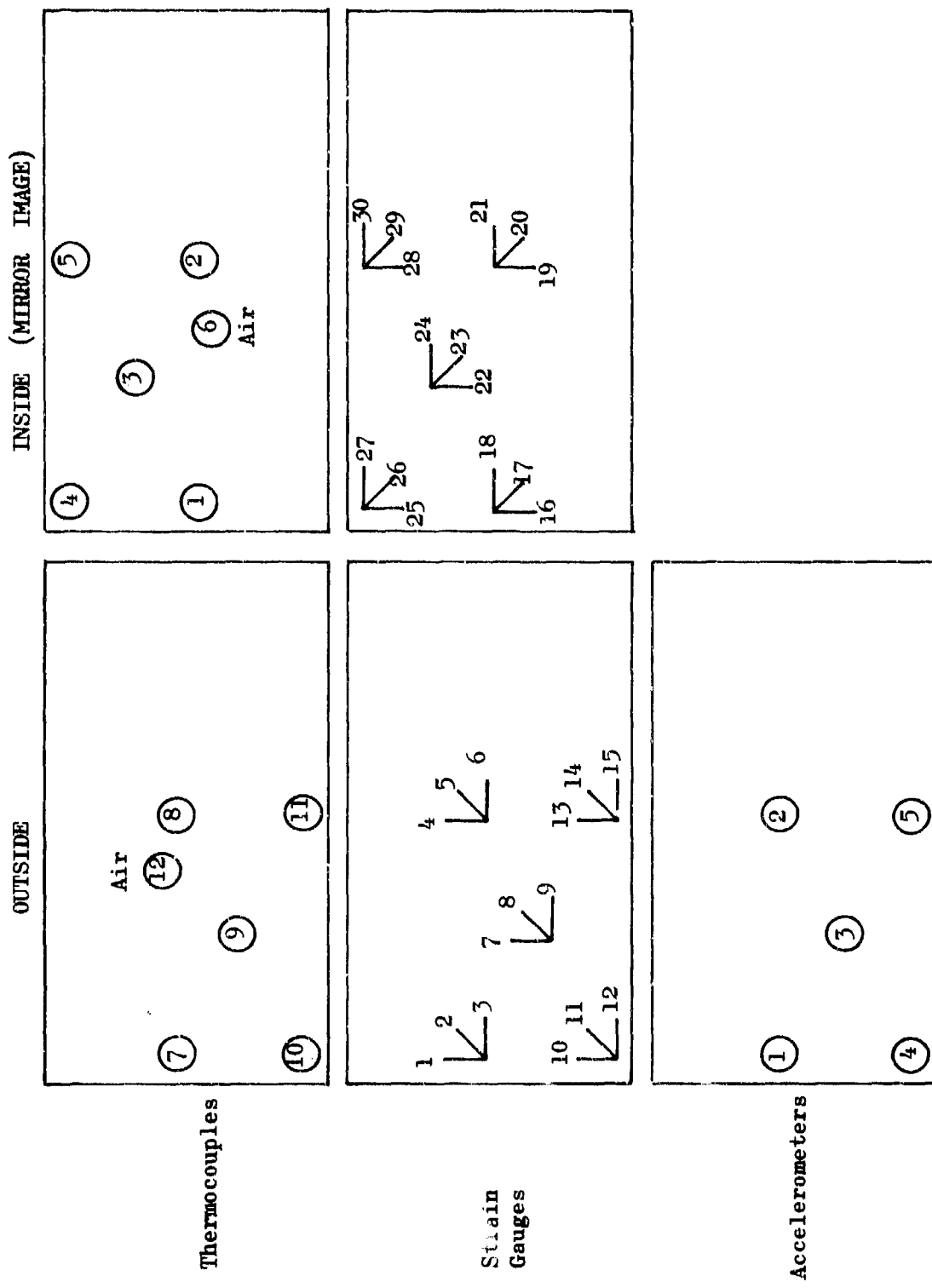


Figure 196. Location of Instrumentation.

### Strain Gauge Limitations

All tests conducted at or near ambient conditions were capable of being instrumented with acceptable accuracy. Tests which applied a certain parameter at stable elevated or depressed temperatures could only be reliably instrumented for strain in part. That is, the strain induced by temperature alone could not be proven, but, providing a zero setting was obtained once the test temperature stabilized, the strain caused by the application of other parameters at that temperature could be determined.

Any test cases involving transient effects, such as thermal shock or cold shock, could not be instrumented for strain within the present limitations of equipment and strain gauge availability. Test cases where results were thought to be suspect were treated as proof loads, with instrumentation employed for such aspects as deflection, acceleration and temperature.

### Temperature

Copper-Constantan thermocouples were used at positions as near as possible to the strain gauge locations shown in Figure 197. Thermocouples were also used to determine inside and outside air temperatures, and, in some cases, hot and cold spots on the windshield were monitored. Temperatures were recorded on continuously running chart recorders.

### Edge Load

The in-plane edge load was measured by a calibrated load cell, installed in the loading linkage. The cell generated a signal that was continuously displayed on a digital voltmeter scale.

### Aerodynamic Pressure

This was similarly measured by a calibrated pressure transducer in conjunction with a digital voltmeter display.

### Deflection

The central deflection of a windshield was monitored using dial indicators. Three instruments were used, one at the panel center and one each at the top and bottom windshield edges on the longitudinal center-line. Since the entire windshield structure was floating about its pin-jointed mounting, it was necessary to install the indicators in a line parallel to the hinge line. The latter two gauges were therefore necessary to provide a datum plane.

Linear transducers had initially been employed, but these were discarded after considerable problems were experienced over the temperature range required.

### Vibration

Five accelerometers were bonded to the outside surface of the specimen in use at positions as close as possible to the strain gauge locations shown in Figure 196. As a control, a sixth accelerometer was installed on the floating support described in Figure 193, exactly in line with the vibratory input.

The accelerometers provided a signal that was fed through normalizing amplifiers and 'g' meters and presented a continuous trace on U. V. chart recorders.

### Windshield Controller

The test facility incorporated an electronic Fielden controller to maintain the windshield operating temperature at its correct level. The controller was modified to be compatible with the Westinghouse (300 ohm) AVK 1160 sensing element within each windshield. Control temperature was maintained at  $118 \pm 1^{\circ}\text{F}$  ( $47.5 \pm 0.5^{\circ}\text{C}$ ).

## RESULTS

### Glass/Glass (-101) Windshields

As this was the first windshield to be tested, many test runs were found to be necessary in order to set up procedures and to remove minor problems. Only the definitive test runs were reported, however.

During application of Case 21 (cold shock and aerodynamic pressure), a failure of the facing ply occurred on windshield serial number 7-10-75-4. As shown by the overall view from outside in Figure 197, only the outboard glass ply was broken. Fracture started in the vision area 6-1/2 inches from the right edge and 8-1/2 inches from the top edge. Subsequent analysis revealed that the fracture origin was located on the outboard surface at a severe scratch 0.40 inch long. Fissures from this damage were about 0.017 inch deep, which almost completely penetrated the 0.020-inch compression layer. Because of this severe surface damage, very little mechanical or thermal load was required to cause fracture. This is supported by the fact that the origin fracture face revealed that the tension stress at failure was less than 1500 psi.

The sequence of testing was slightly altered at this stage, and other types of windshield were tested prior to installing the second glass/glass (-101) item, Serial No. 6-24-75-9.

Regular inspections of the specimen during subsequent testing revealed no signs of degradation.

#### Glass/Acrylic (-102) Windshields

When these windshields arrived at Triplex, it was discovered during unpacking that specimens 001 and 003 had broken facing plies, probably due to inadequate packaging material. The remaining specimens were permanently bowed in both directions. When placed on a flat surface with the windshields' outer face down, the gap from the surface of the table was in the order of 0.5 inch on the long edges and 0.25 inch on the short edges.

During installation, the facing ply of specimen serial number 002 cracked, despite meticulous efforts to remove the bow uniformly during bolting in. This windshield is shown in Figure 198.

Prior to installing the next glass/acrylic windshield, serial number 009, its strain gauges were adjusted to zero with the windshield in an unrestrained state. This procedure enabled strains to be monitored as the windshield was installed. Using extra care, the windshield was successfully installed, and measured strain levels equivalent to approximately 3000 psi were recorded in the glass. Thus, all subsequent tests for this specimen were conducted with a built-in preload stress that could not be removed.

Testing was conducted in accordance with the matrix previously presented in Table 59. This matrix of tests was substantially abbreviated as compared to the matrix of tests for the glass/glass windshields, as shown previously in Table 58. This was due to the recording of very small strains during the single parameter tests, which allowed the number of multiple parameter tests to be reduced. Only the definitive test runs are reported, and the most cost-effective sequence of testing was used.

For the reasons previously mentioned, strain measurements on this windshield (and subsequently also on the Polyester/Acrylic, -103, windshield) proved to be suspect at nonambient conditions. In such cases the test run was treated as a proof load, and instrumentation did not include strain measurement. In certain cases, where instrumentation difficulties at non-ambient temperatures were encountered, the strain recording equipment was zeroed once the high or low temperature had been stabilized, and strain was then recorded to indicate the increment due to the application of a second parameter only.



Figure 197. Failure of Glass/Glass (-101) Windshield,  
Serial No. 7-10-75-4, During Run 61, Case 21.

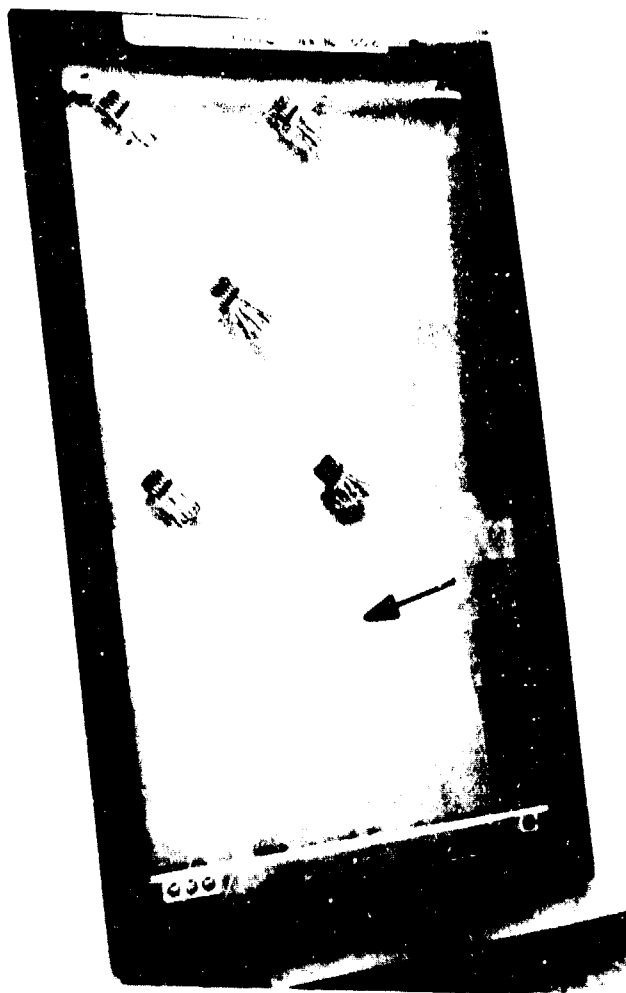


Figure 198. Failure of Glass/Acrylic (-102) Windshield, Serial No. 002, During Installation.

Inspection of the specimen windshield during testing did not show degradation of any kind.

After testing was completed, this specimen suffered a broken facing ply during removal despite extremely careful precautions being taken to allow it to return to its natural state uniformly.

#### Polyester/Acrylic (-103) Windshields

Specimen serial number 006 was tested in accordance with the matrix shown previously in Table 60 which shows only the definitive test runs. This matrix was also condensed for the same reasons given for the glass/acrylic windshields.

The inspections, conducted during testing, did not reveal any defects or degradation.

#### ANALYSIS OF RESULTS

For comparative purposes, a summary of the maximum stresses obtained for each condition is presented in Table 61. The highest individual strain measurement for each case was converted to stress by multiplication with an appropriate modulus of elasticity as listed in Table 62.

TABLE 61. SUMMARY OF MAXIMUM RECORDED STRESSES

Case	Condition	Stress (psi)				
		-101	-102	-102	-103	-103
		Glass Ply	Stretched Acrylic Ply	Polyester Ply	Stretched Acrylic Ply	
	Initial Installation	1133	-3210	276	-157	301
1	Low Temperature	-4223	-5885	-1067	1093	-1336
2	High Temperature	607	1498	293	468	814
5	Aerodynamic Pressure	2317	3049	-289	663	-514
6	Edge Load	-721	--	--	--	--
7	Vibration	+ 83	+481	+ 63	+17	+ 70
8	Installation Preload	-1010	--	--	--	--
9	Low Temp, Pressure	-4583	2083*	-442*	145*	-242*
10	Low Temp, Edge Load	-3347	--	--	--	--
11	Low Temp, Vibration	+257	+374	+33	+32	+80
12	Low Temp, Installation Preload	480	--	--	--	--
13	High Temp, Pressure	3193	3424*	226*	352	579*
14	High Temp, Edge Load	2729	--	--	--	--
15	High Temp, Vibration	+257	+642	+39	+75	+90
16	High Temp, Installation Preload	721	--	--	--	--
25	Pressure, Edge Load	-1545	--	--	--	--
27	Pressure, Installation Preload	2781	--	--	--	--
29	Edge Load, Preload	927	--	--	--	--
32	Pressure, Edge Load, Installation Preload	597	--	--	--	--
34	Low Temp, Pressure, Edge Load	-4120	--	--	--	--
35	High Temp, Pressure, Installation Preload	2935	--	--	--	--
38	Low Temp, Pressure, Edge Load, Installation Preload	-4429	--	--	--	--
39	High Temp, Pressure, Edge Load, Installation Preload	3193	--	--	--	--

\*Value does not include stress increment due to differential thermal expansion/contraction.

TABLE 62. MODULUS OF ELASTICITY OF FACING MATERIALS

Material	Temperature (°F)	Modulus of Elasticity (psi)
Glass (Thermally Tempered)	All	$10.3 \times 10^6$
Glass (Chemically Tempered)	All	$10.7 \times 10^6$
Stretched Acrylic	70	$.5 \times 10^6$
Stretched Acrylic	-65	$.8 \times 10^6$
Stretched Acrylic	125	$.45 \times 10^6$
Polyester	70	$.45 \times 10^6$
Polyester	-65	$.75 \times 10^6$
Polyester	125	$.3 \times 10^6$

Deflections for the glass/glass windshield ranged from 0.0795 inch to 0.301 inch for the pressure load conditions. Temperature was the most important variable, with deflections increasing in proportion to temperature.

Deflections for the glass/acrylic windshield ranged from 0.1125 inch to 0.3425 inch under pressure load conditions.

Deflections for the polyester windshield ranged from 0.177 inch to 0.772 inch under pressure load conditions.

Individual parameters are discussed below for each windshield configuration.

#### Glass/Glass (-101) Windshields

Low Temperature - Of all the parameters examined, low temperature effects, creating substantial temperature gradients, induced the most significant strains. The compressive stresses shown on both inside and outside windshield surfaces reached a maximum level of approximately 4200 psi compression.

High Temperature - With only slight temperature gradients through the windshield, strain levels were very low. The maximum (tensile) stresses noted were in the order of 600 psi.

Thermal Shock - This parameter indicated the highest relative change in strain levels. Changes in surface strain measurements occurring during windshield warmup reached a maximum of 600 microinches per inch as shown in Figure 199.

Cold Shock - Owing to the very short time scale during which the cold shock occurs, highly significant hysteresis effects were considered to be present in the strain gauge circuits. The analysis of strain gauge signals naturally depends upon the gauge itself being at the temperature of the glass surface. Because of rapidly changing temperature gradients this was not so; thus, large errors could be present. Surface temperatures during cool-down are shown in Figure 200.

Aerodynamic Pressure - The maximum principal stress seen on the outside glass surface for this condition was about 2300 psi. Generally, predominantly bending strains were seen, but some additive diaphragm effects were present. These diaphragm stresses, which were in the order of only 180 psi, significantly reduce the stresses that would occur due to pure bending. Strain gauge data is shown in Table 63.

Edge Loading - Edge loading effects were low. Strains were generally tensile in the direction of the applied load, although at the loaded edge, some local bending was indicated. This was probably attributable to the slight offset of the applied load relative to the windshield's neutral plane. The maximum stress level observed was 721 psi.

Vibration - During vibration sweeps (9 Hz to 30 Hz) strain levels were exceedingly low. They approximately varied proportionally to the applied 'g' load, and also varied inversely as the frequency. No resonance was seen, although some 'g' magnification, relative to the input level, was seen. It was apparent from viewing the vibration tests that transparency dither would become visually disturbing to flight crews prior to posing any structural problems.

Installation Preload - The specimens, although substantially flat, showed slightly more strain induced on their original installation than they did due to the intentionally installed contour mismatch. Generally, however, the strain level was low and very local bending effects were evident. The maximum stress seen was approximately 1000 psi.

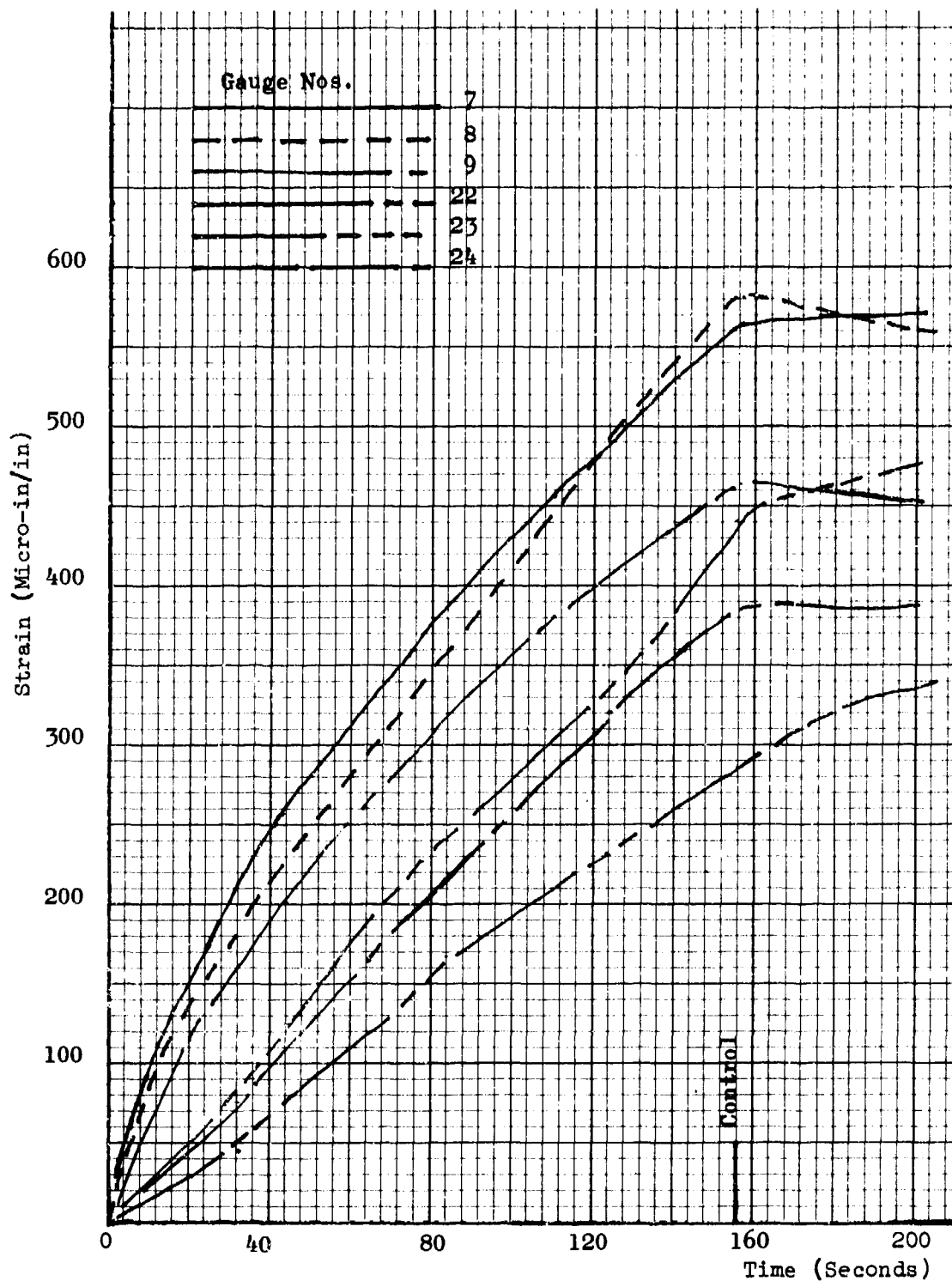


Figure 199. Strain Gauge Data  
 Glass/Glass Windshield (-101)  
 Thermal Shock, Case No. 3.

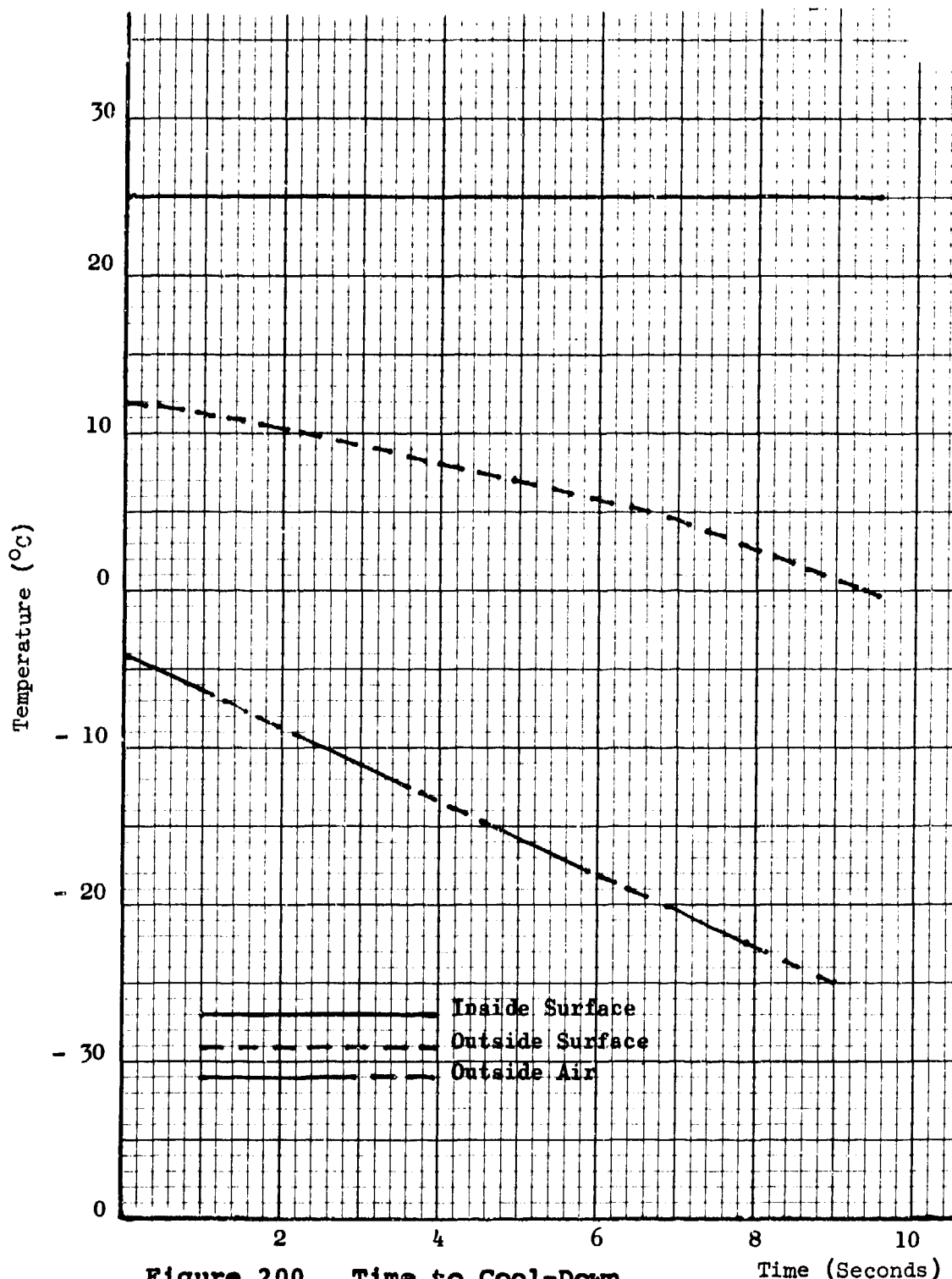


Figure 200. Time to Cool-Down  
 Glass/Glass Windshield (-101)  
 Cold Shock, Case No. 4.

TABLE 63. STRAIN GAUGE DATA  
 GLASS/GLASS WINDSHIELD (-101)  
 AERODYNAMIC PRESSURE, CASE NO. 5

Outside Face		Inside Face	
Gauge No.	Microstrain $\frac{M-in.}{in.}$	Gauge No.	Microstrain $\frac{M-in.}{in.}$
1	+ 215	16	- 170
2	+ 165	17	- 25
3	+ 30	18	- 90
4	+ 195	19	- 215
5	+ 225	20	- 205
6	+ 205	21	- 185
7	+ 180	22	- 165
8	+ 170	23	- 145
9	+ 150	24	- 130
10	+ 95	25	- 80
11	+ 75	26	- 45
12	+ 50	27	- 35
13	+ 110	28	- 85
14	+ 150	29	- 140
15	+ 85	30	- 175

Deflection at Center = 0.098 in.

Combined Effects - Basically, combined parameters behaved such that the mathematical addition of strains appeared logical. No magnification effects were evident, indicating strain levels no greater than the sum of the constituent parameters. The most severe conditions were those combinations which occurred at low temperature.

#### Glass/Acrylic (-102) Windshields

Low Temperature - Inside surface strains on the acrylic material were not reliably recorded. Outside surface strains in the glass were noted at a maximum level of 550 microstrain (compressive), which was significantly higher than those recorded on glass/glass (-101) windshields.

High Temperature - As with the glass/glass (-101) windshields, strains in the outer glass surface were fairly low, reaching a maximum value of 140 microstrain (compressive). Inner surface strains were not reliably recorded.

Thermal Shock - The highest changes in outer surface strains were noted for this panel, and these were very similar to the glass/glass (-101) item; a transient tensile strain of 640 microstrain was the maximum noted. Inner surface values were not considered reliable.

Cold Shock - For the reasons stated previously, instrumented values for this parameter were not meaningful, although it would be expected that transient strains would be high. No specimen damage was noted.

Aerodynamic Pressure - Compared with the glass/glass (-101) configuration, the strains indicated more diaphragm effect. The maximum tensile stress seen on the outer (glass) surface was 2935 psi microstrain, whereas the peak stress on the inner (acrylic) surface was compressive, being 290 psi. This indicated that most of the load was supported by the glass ply.

Vibration - In common with the glass/glass (-101) windshield, the level of strain was very small, being at a maximum level of only +45 microstrain on the outer glass surface and +125 microstrain on the inner acrylic surface.

Installation Preload - Although no tests were conducted with the 0.10-inch shim installed, owing to exceedingly low predictions for the strain likely to result, measurements made before and after installation indicated substantial bending strains. Tensile strains of up to 550 microstrain were seen on the inner (acrylic) surface, with up to 300 compressive microstrain noted on the outer glass.

Combined Effects - Addition of the strain levels recorded for the various parameters did not produce any magnification effect exceeding the values obtained by straightforward mathematical addition. However, this can only be said for the outer surface strains as no reliance could be put on strains recorded for the acrylic inner surface.

#### Polyester/Acrylic (-103) Windshields

Thermal Tests - No reliable strains were recorded during these tests, although the panel was satisfactory after the tests.

Aerodynamic Pressure - Owing to the basic flexibility of the specimen, strains were not very significant, although a central deflection of 0.375 inch was noted. Stresses were predominantly diaphragm, although bending stresses were also present. Stresses of 664 psi (tensile) were noted on the outer polyester surface, with 514 psi (compressive) noted on the inner acrylic surface.

Vibration - As with the other types of specimens, strains were relatively low at a maximum level of +260 microstrain on the outer polyester surface and +140 microstrain on the inner acrylic member.

Combined Effects - No strains greater than those obtained by straightforward mathematical addition of the component parameters were observed. However, in general the correlation in this manner was not as good as that for the glass/glass (-101) specimens. This was attributed to the basic difficulties encountered in the strain measurement techniques.

#### INSTRUMENTED TEST CONCLUSIONS

1. It was generally noted that the strains recorded for all three types of construction were relatively low. In no case did any particular loading parameter indicate a strain level which by itself could be considered as likely to promote a failure. No combination of loading parameters induced any significant multiplying effects on the three variants tested.
2. The strain levels induced by vibratory inputs were exceedingly low, and no resonances were noted for any of the windshields tested.

3. The effect of curvature mismatch was very significant, particularly on the glass-faced plastic windshields. Strain values could be obtained while bolting in badly matched contours that were of a magnitude equivalent to that induced by any of the loading parameters.
4. Temperature was shown to have a major effect on the strain levels induced in the windshields when applied separately and in combination with other loading conditions. Maximum strain levels were obtained at elevated and reduced temperatures.
5. Accurate strain measurement of stretched acrylic and polyester materials could not be obtained in dynamic thermal environments.

## WINDSHIELD ENDURANCE TESTS

A series of endurance tests was performed on -103 polyester/acrylic windshields to demonstrate how cyclically applied combinations of structural loads and aggressive environments can be used to simulate the useful design life of a component in the laboratory. By condensing the time between applications of loads, service time is greatly accelerated to enable the early detection of potential design/process flaws, thereby permitting corrective actions to be implemented and verified in an expeditious, cost-effective manner.

### TEST DESCRIPTION

Two endurance tests were performed: a cold weather test and a hot weather test. The loading schedules for these tests are presented in Tables 64 and 65, which were derived from the loading spectrum and climates previously presented in the section on Usage Spectrums. Each load application represented one ground-air-ground cycle. Some modifications were made to the original loading spectrum based on the following considerations.

In-plane edge loads from fuselage wracking (inertia, maneuvers) were assumed to be nonapplicable due to the polyester/acrylic windshield's compliant flexibility.

Vibration and aerodynamic pressure were conservatively applied at maximum levels throughout the test since their worse effects were found to be only minimal during the instrumented tests.

#### High-Temperature Endurance Test

During the high-temperature endurance test, the airspeed was held constant at 70 knots, with the vibration held constant at a frequency producing the worst effect.

Aerodynamic pressure was then applied for a duration long enough to reach the required level, and then reduced to zero between cycles.

TABLE 64. HIGH-TEMPERATURE ENDURANCE TEST SPECTRUM

Number of Cycles	Aerodynamic Pressure (psi)	Vibration (+g)	Temperature (°F)	Relative Humidity (%)
380	1.0	0.9	+ 100	95
20	1.0	0.9	+ 125	95

### Low-Temperature Endurance Test

Table 65 describes the required test spectrum, representing 100 hours of flight (or 400 flight cycles) in arctic conditions.

During this spectrum, the airspeed was held constant at 70 knots, together with a constant frequency vibration similar to that in the high-temperature endurance test. The loading sequence was as follows:

- a) With the air temperatures stabilized, the windshield temperature, as indicated by the temperature sensing element, was allowed to stabilize.
- b) Aerodynamic pressure was applied.
- c) When required, full anti-ice power was applied until operational temperature was achieved, allowing the power to cycle off and on once.
- d) When specified in Table 65, a cold shock (as described in the section on Windshield Instrumented Tests) was applied.
- e) Aerodynamic pressure was removed.

TABLE 65. LOW-TEMPERATURE ENDURANCE TEST SPECTRUM

Number of Cycles	Aerodynamic Pressure (psi)	Vibration (+g)	Outside Temp (°F)	Inside Temp (°F)	Cold Shock	Power
180	1.0	0.9	+ 40	+ 70	No	No
100	1.0	0.9	+ 25	+ 70	Yes	Yes
100	1.0	0.9	- 25	+ 50	No	Yes
20	1.0	0.9	- 65	+ 40	No	Yes

### Inspection

The windshields were visually examined after the end of the first load application and then after each 50 cycles or on completion of each loading condition. The inspection criterion was the same as that described in the section on Instrumented Tests.

### RESULTS

The final test schedule comprised three high-temperature test spectra and one low-temperature test spectrum.

Minor modifications were made to the test procedures as testing progressed due to unforeseen complications in the loading sequences.

### First High-Temperature Test Spectrum

Specimen serial number 008 was used for this spectrum and the procedure was as described previously with vibration held constant at 9 Hz  $\pm$  0.9 g.

No damage was observed other than some apparent partial breakdown of the bond between the terminal blocks and the acrylic face.

### Low-Temperature Test Spectrum

Specimen serial number 007 was used for this spectrum, and for the first 280 cycles, the procedure was as specified in Table 65.

The remaining cycles at lower OAT's were carried out to the following procedure after difficulties were encountered involving failure of the windshield to attain control temperature due to the high heat transfer coefficient of the test facility.

- a) Windshield temperatures stabilized with  $-25^{\circ}\text{F}$  ( $-32^{\circ}\text{C}$ ) OAT and  $+40^{\circ}\text{F}$  ( $+10^{\circ}\text{C}$ ) IAT.
- b) Aerodynamic pressure and vibration applied at 9 Hz  $\pm$  0.9 g.
- c) Duct air circulation stopped.
- d) Windshield power on and controller allowed to cycle off and on twice.
- e) Windshield power off.
- f) Air circulation restarted.
- g) Aerodynamic pressure removed.
- h) Windshield temperatures stabilized.

Inspection of the windshield after 230 cycles showed, on the long sides, a gap between the rubber edge seal and the edge reinforcement of 0.010 inch at ambient temperature and 0.050 inch at  $+25^{\circ}\text{F}$  ( $-4^{\circ}\text{C}$ ). After 280 cycles the windshield had developed a permanent outward bow of 0.080 inch measured at the center of the windshield. After 330 cycles the bow had increased to 0.32 inch.

Deflection measurements taken under various conditions after 345 cycles are shown in Table 66.

During cycle 355 an apparent heating film failure occurred. Inspection revealed a failure of the polyester component caused by a film fuse, which in turn led to massive delamination due to local overheating.

Damage to the windshield is recorded in Figures 201 and 202.

TABLE 66. DEFLECTION MEASUREMENTS (CENTER RELATIVE TO EDGE) TAKEN DURING LOW-TEMPERATURE TEST

Condition	Deflection (Inches)
Ambient Pressure, Ambient Temperature, Heat Off	0.32
Ambient Pressure, -25°F OAT, 40°F IAT, Heat Off	0.13
One psi Pressure, -25°F OAT, 40°F IAT, Heat Off	0.35
Ambient Pressure, -25°F OAT, 40°F IAT, Heat On	0.45
One psi Pressure, -25°F OAT, 40°F IAT, Heat On	0.74

#### Second High-Temperature Test Spectrum

Specimen serial number 008 was subjected to a second high-temperature climate test spectrum as defined previously with the addition of a ten-minute "power on" period at the end of each batch of 50 cycles. The "power on" period simulated defog conditions.

No further damage was observed upon completion of the test.

#### Third Tropical Climate Test Spectrum

In an attempt to accelerate a failure under tropical conditions, a further modified test spectrum was implemented.

The modification was a prolonged exposure to high relative humidity at elevated temperature and was conducted on two specimens simultaneously. The specimens were serial number 008, previously subjected to two test spectra, and serial number 005, which was "as new" and included for control purposes.

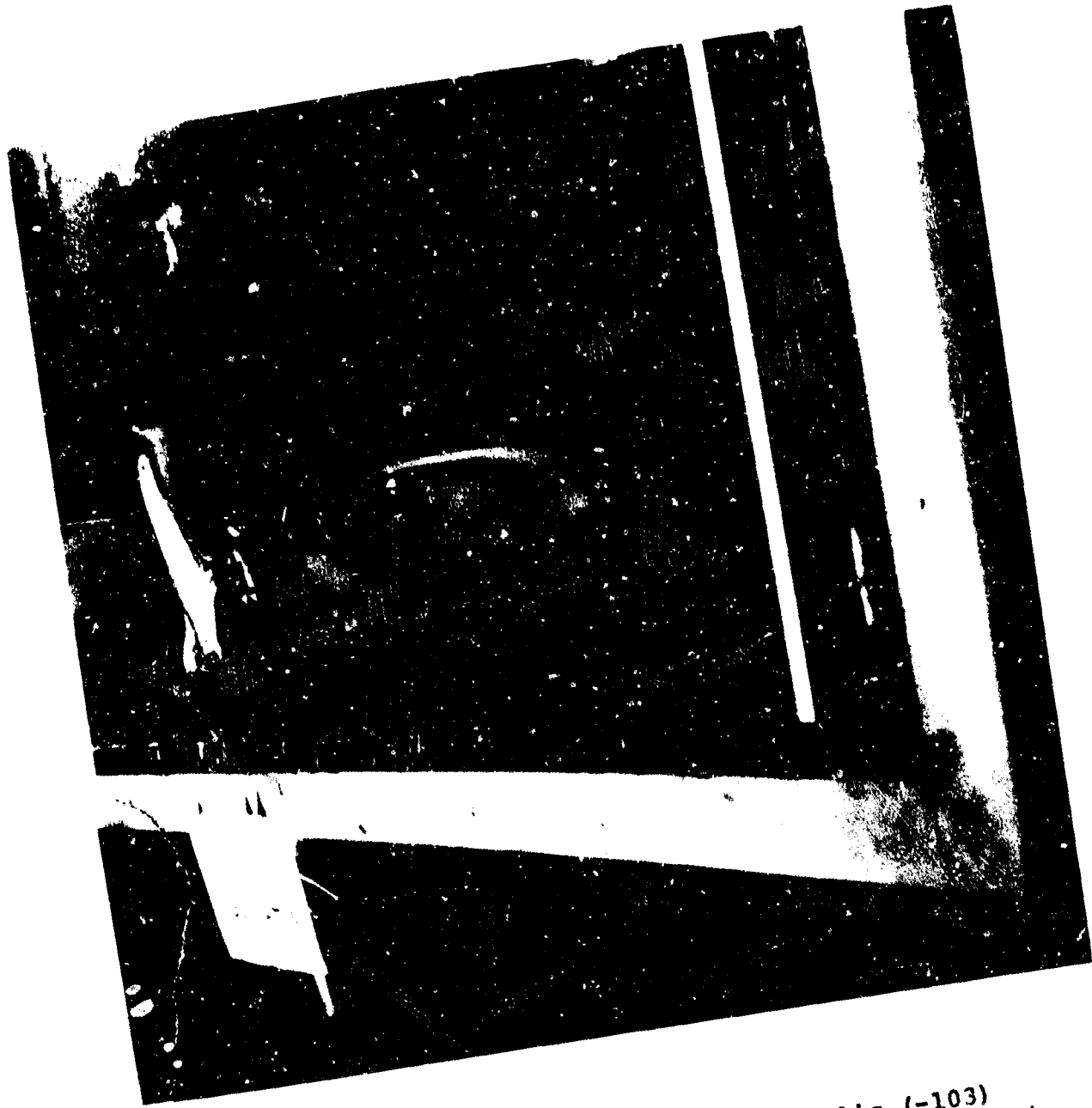


Figure 201. Failure of Polyester/Acrylic (-103)  
Windshield During Low-Temperature Test  
Spectrum.

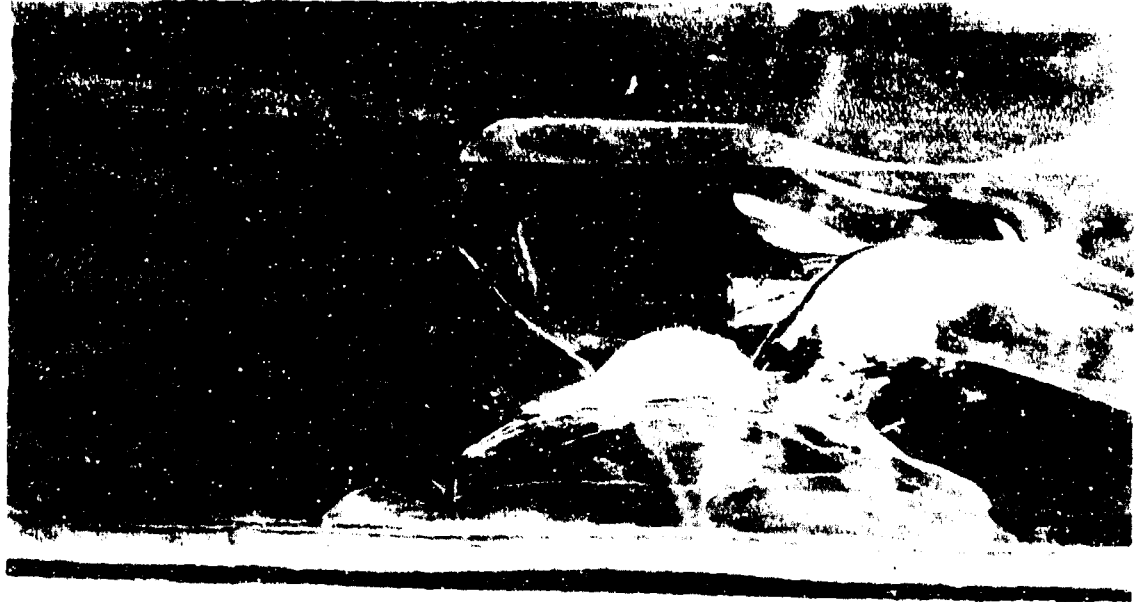


Figure 202. Failure of Polyester/Acrylic (-103) Windshield During Low-Temperature Test Spectrum, Also Showing Nib Seal Separation.

The test conditions were 90% relative humidity and 158°F (70°C), maintained for seven days, after which the specimens were inspected and one was selected for testing. On both specimens, excessive bubbling of the interlayer had occurred. This was apparently caused by moisture absorption via the acrylic component, thereby increasing the moisture content of the interlayer which subsequently gassed off at the elevated temperature.

Also, both specimens had developed a considerable "dished" shape approximately 2 inches and 1/2 inch measured on the long and short sides, respectively. The damage to both specimens is illustrated in Figures 203 through 206.

The degree of damage being apparently equal on both specimens, serial number 008 was selected for the additional spectrum as being the most likely to produce a classic failure.

However, no further damage occurred during the test spectrum.

When the specimen was removed from the test frame, the distortion was considerably less but returned to the pre-test extent within 48 hours.

Approximately one week after completion of the spectrum, it was noticed that delamination of the acrylic material had occurred around the perimeter of the windshield. Inspection of the other windshield exposed to high humidity also showed damage of a similar nature and extent. Figure 206 illustrates the degree to which the specimens were affected.

#### ENDURANCE TEST CONCLUSIONS

1. The low-temperature endurance test produced a massive delamination failure at 355 cycles, which corresponds to about 355 hours flight time for a cargo helicopter. The failure mode and time to failure were considered to be realistic for polyester/acrylic windshields.
2. The delamination failures during the low-temperature tests, taken in consonance with the instrumented test findings, show that the most severe windshield loadings occur at low temperature.
3. Accelerated humidity testing of polyester/acrylic windshields produced interlayer bubbling which was similar to service failures experienced in tropical climates. However, the test conditions (158°F, 90% relative humidity) were severe compared to even extreme hot-wet conditions found in the tropics (100°F, 100% relative humidity), and the rate of acceleration for moisture permeation was therefore unknown.

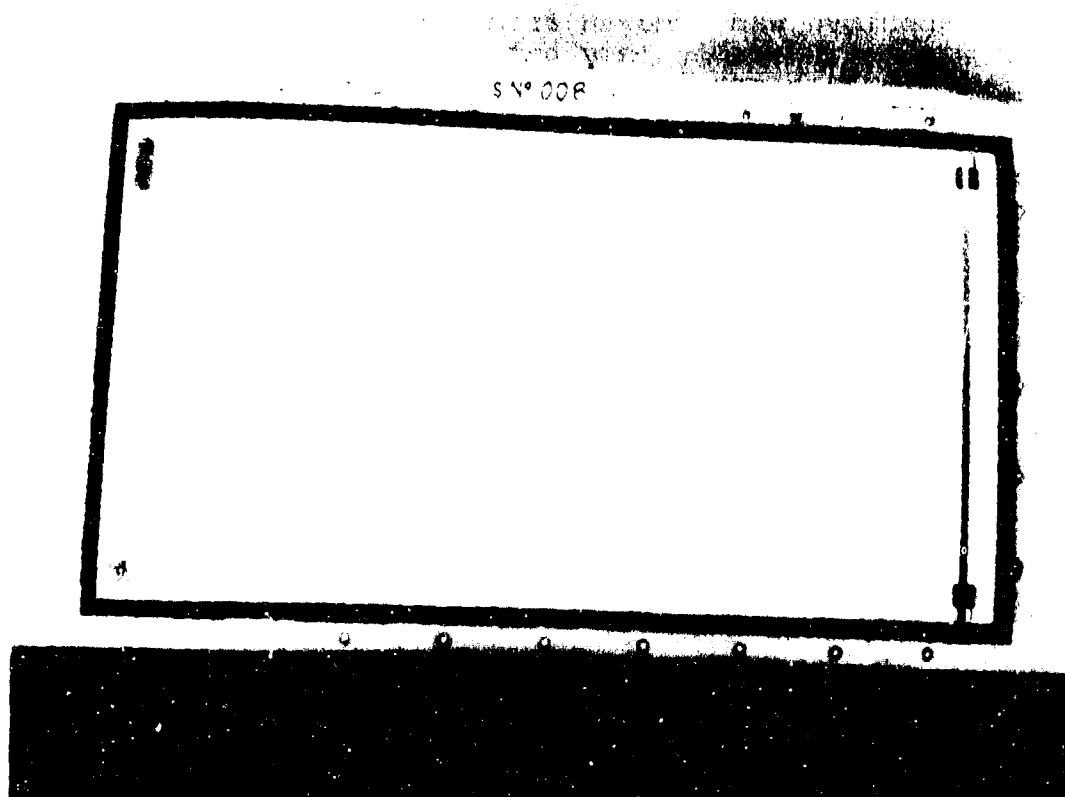


Figure 203. Overall View of Interlayer Bubbling on Polyester/Acrylic (-103) Windshield After Prolonged Humidity Exposure.

S. N° 008

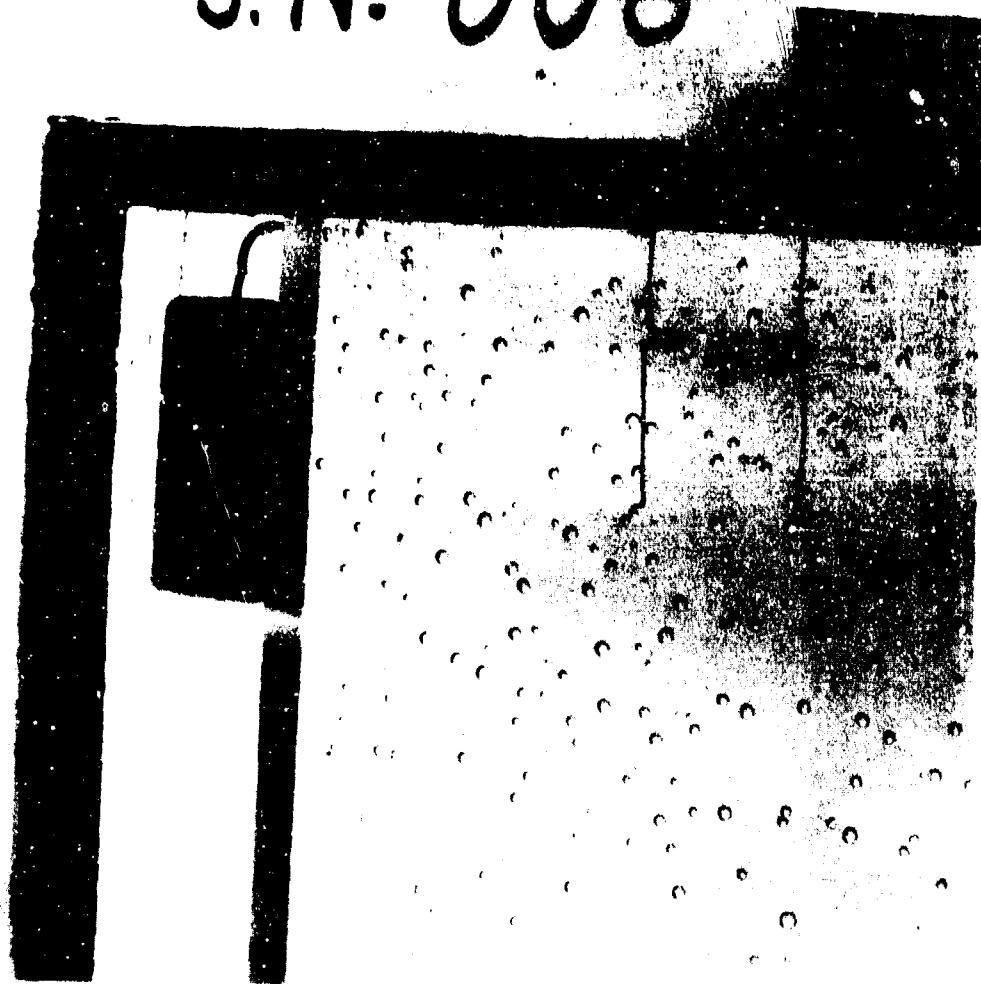


Figure 204. Close Range View of Interlayer Bubbling on Polyester/Acrylic (-103) Windshield After Prolonged Humidity Exposure.



Figure 205. "Dished" Shape of Polyester/Acrylic (-103) Windshield After Prolonged Humidity Exposure.

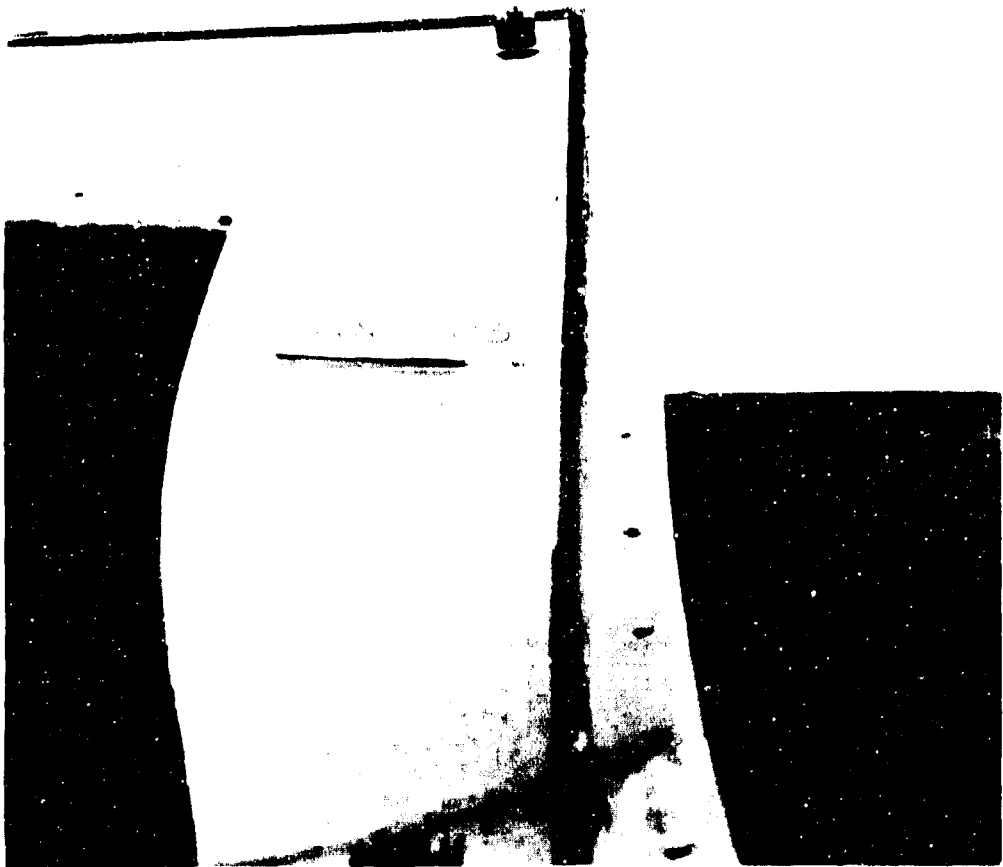


Figure 206. Delamination of Acrylic Edge Material on Polyester/Acrylic Windshield (-103).

4. During the high temperature endurance test, an equivalent of 1200 hours of cargo helicopter flight time was simulated on the acrylic/polyester windshield with no failures. This was approximately three times greater than the historical MTBF for this type of windshield in effect when this program was initiated in 1974. However, since that time, the windshield manufacturers have incorporated changes in the laminating process used to fabricate their plastic windshields, and recent reliability data indicates that windshield MTBF's have been substantially improved as a result. It is now felt that the tendency for acrylic/polyester windshields to delaminate under moderate to hot environmental conditions has largely been overcome.
5. Endurance testing of windshields prior to making production commitments is an extremely cost-effective method for substantiating component reliability.

## MAJOR CONCLUSIONS

Major conclusions reached in each program task are summarized here:

### Abrasion Tests

1. The rubbing abrasion, windshield wiper and falling sand tests realistically simulate aggressive mechanism of abrasion, yield failure modes experienced in service, and are viable tests for assessing or comparing the abrasion resistance of candidate materials.
2. Due to the random nature of abrading phenomenon, it is not possible to correlate test results with service life.

### NASTRAN Analysis

1. The NASTRAN finite element analysis was found to be suitable for analyzing homogeneous transparencies of the following types:
  - a. Flat plates and curved shells where the transverse deflections are small in comparison to the thickness of the part.
  - b. Curved shells where the pressure loads are resisted by in-plane forces (similar to hoop tension or compressive arch).
2. The NASTRAN analysis was not suitable for analyzing transversely loaded flat plates where the load is carried partially or entirely by membrane effects. Flat helicopter transparencies generally fall into this category.
3. The NASTRAN analyses conclusively showed how fuselage racking can and does induce loads into transparencies. For the specific loading and airframe stiffnesses analyzed, these loads were found to be approximately the same magnitude as the primary pressure loads.

### Thermal Expansion, Installation Preload and Assembly Tests

Installation preload forces can create critical loading conditions for certain types of laminated transparencies, particularly those containing glass plies. The stresses can be induced from mismatch of contours between the panel and the airframe, or from uneven torquing of fasteners. These conditions are highly sensitive to edge attachment design.

### Field Survey of Army Helicopter Transparencies

The most common Army helicopter pilot complaint concerned restrictions on windshield wiper use. They want a better method of rain removal, or glass windshields so that wipers could be used as needed. Wipers and poor cleaning practices abrade transparencies, yielding excessive haze. The threshold of haze acceptability, the point at which most flight crews will demand replacement, was found to be 30%.

### Ballistic Damage Tolerance Tests

The criteria (spall mass-velocity relationships) and test methods developed for evaluating spall provided realistic correlation with actual service experience.

### Low-Energy Impact Tests

Based on the performance of the materials tested, a 20 ft-lb dart impact appears to be a reasonable standard for use in evaluating impact characteristics of helicopter transparencies.

### Instrumented Windshield Tests

1. Temperature was shown to have a major effect on the strain levels induced in the windshields when applied separately and in combination with other loading conditions. Maximum strain levels were obtained at elevated and reduced temperatures.
2. The strain levels induced by vibratory inputs were exceedingly low, and no resonances were noted for any of the windshields tested.
3. The effect of curvature mismatch was very significant, particularly on the glass-faced plastic windshields. It was seen that strain values could be obtained while bolting in badly matched contours that were of a magnitude equivalent to that induced by any of the loading parameters.

### Windshield Endurance Tests

1. Low temperature endurance testing was shown to be the most severe test condition.
2. Endurance testing of windshields prior to making production commitments is an extremely cost-effective method for substantiating component reliability.

## RECOMMENDATIONS

The findings derived from this program have been incorporated in a general specification<sup>17</sup> and a design handbook<sup>18</sup> for helicopter transparent enclosures. It is recommended that the criteria and design information contained in these documents be adopted for use on future helicopter development programs.

In addition, during the course of this program, several areas needing further research were discerned. They are summarized below along with some of the major recommendations that were incorporated in the general specification and design handbook.

### 1. Abrasion Tests

The rubbing abrasion, windshield wiper, and falling sand tests that were evaluated should be adopted as a means for ranking abrasion resistance of candidate transparent materials.

### 2. Effect of Impingement on Structural Integrity of Glass

Thin chemically tempered glass is susceptible to pitting from impingement by blowing sand or foreign objects which can cause severe loss of strength and/or cracking. Tests should be developed to quantify the relationship between particle size, energy, and losses in glass strength.

### 3. Hard Coats

Hard coats provide significant improvements in abrasion resistance. However, they are subject to environmental deterioration. Development of more durable hard coats are required, or alternatively, nonscratching rain removal systems.

### 4. Chemical Attack on Transparent Materials

Certain chemicals commonly used in aircraft environments can attack transparent materials. A comprehensive documentation of the effects of chemical contact with such materials would help to avoid such chemicals and subsequent damage to transparencies.

---

17 Kay, B. F., Sikorsky Aircraft Division, "Helicopter Transparent Enclosures, Volume II, General Specification," USARTL-TR-78-25B, Applied Technology Laboratory, U. S. Army Research and Technology Laboratories (AVRADCOM), Ft. Eustis, Virginia, November 1978.

18 Kay, B. F., Sikorsky Aircraft Division, "Helicopter Transparent Enclosures, Volume I, Design Handbook," USARTL-TR-78-25A, Applied Technology Laboratory, U. S. Army Research and Technology Laboratories (AVRADCOM), Ft. Eustis, Virginia, November 1978.

5. Finite Element Analysis of Fuselage Deformations

Finite element analyses should be adopted as a means to determine the structural effects of fuselage wracking on transparencies.

6. Finite Element Analysis of Curved Transparencies

Finite element analyses should be used to analyze curved transparencies where pressure loads are resisted by in-plane forces.

7. Finite Element Analysis of Thin Windshields

Current state-of-the-art finite element analysis cannot analyze flat membrane-like structures subject to pressure loads. A nonlinear finite element analysis should be developed to handle this deficiency.

8. Installation Preload and Thermal Stresses

The effects of installation preload and thermal stresses should be considered during structural design, and appropriate manufacturing tolerances, stress allowances, or design features should be adopted to prevent service difficulties.

9. Ballistic Spall Criteria

The test methods and criteria developed in this program for evaluating ballistic spall should be applied to combat helicopter transparencies.

10. Spall Resistant Windshields

Ballistic tests conducted on current generation laminated windshield configurations indicate none to be spall resistant. Development is required for advanced composite heated panels that will meet this requirement.

11. Low-Energy Impact Tests

The 20 ft-lb dart impact should be adopted as a standard for evaluating impact characteristics of helicopter transparencies.

## 12. Effect of Temperature on Fail-Safety

Fail-safe tests conducted on ballistically damaged transparencies at room temperature showed current generation transparencies to be inherently fail safe. Since transparency material properties change with temperature, fail-safe tests should also be performed at low temperatures and high temperatures to evaluate any temperature-dependent effects.

## 13. Vibration Testing

Structural vibration testing is not recommended for helicopter transparencies because it was apparent from instrumented vibration tests that transparency dither would become visually disturbing to flight crews prior to posing any structural problems.

## 14. Windshield Endurance Tests

Heated windshields should undergo endurance testing prior to making production commitments. These tests should include simultaneous cycling of anti-ice heating systems, application of pressure loads, and exposure to temperature extremes.

## 15. Humidity Testing

Certain transparency materials are susceptible to damage from prolonged exposure to moisture. During qualification testing the effects of moisture can be accelerated by increasing the temperature; however, the rate of acceleration is unknown. Accelerated humidity tests should be correlated with actual service environments.

## 16. Birdproofing

As helicopter speeds are increased, the hazards from potential bird strikes also increase. A study should be undertaken to correlate the probability of helicopter/bird strikes against airspeed.

## 17. Glint Intensity

Current techniques for evaluating glint signatures utilize maps of sun reflection contours relative to the helicopter. Procedures do not adequately consider relative size, intensity and background illuminance, which are necessary to determine whether or not the object can be detected. Additional analytical/experimental work should be aimed at including the latter parameters.

## APPENDIX A

### ABRASION TEST METHODS

Abrasion test methods and procedures are described in this Appendix.

#### DRY RUBBING ABRASION TEST (TEST 1)

This type of abrasion test method was performed to evaluate the rubbing abrasion properties of the different materials from simulated dry wiping of dirty transparencies.

#### Apparatus

The apparatus consisted of a reciprocating motion abrader designed to provide a wiping action that simulates conditions encountered during field cleaning of transparencies by aircraft personnel. Abrading head pressure was adjustable up to 1 psi (see Figure A-1). The abrasive was 400 grit boron carbide impregnated in a dry felt pad with 500 grams of load. The Gardner Hazemeter, shown in Figure A-2, was used in Tests 1, 2, and 3 to measure haze.

#### Procedure

Prior to testing, haze measurements were obtained for all samples.

A 1-inch-diameter disc of 100% wool felt, 1/8 inch thick, cemented to the abrading head was impregnated with dry 400 grit boron carbide. The head was weighted with 500 grams of load.

The test was run at a speed of approximately 50 cycles per minute. The abrading head was reimpregnated after each 25-cycle period.

Periodic haze measurements were taken at intervals corresponding approximately to each 5% increase in haze.

Testing continued until a haze level of approximately 30% was measured. Testing hard-coated materials was terminated in some cases prior to reaching 30% haze because further testing served only to polish the specimens and did not produce a measurable increase in haze.

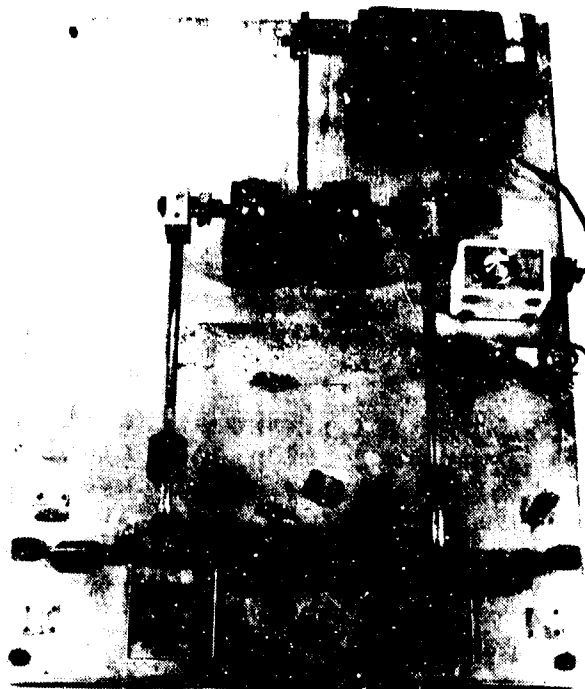


Figure A-1. Apparatus for Dry Rubbing Abrasion Test.

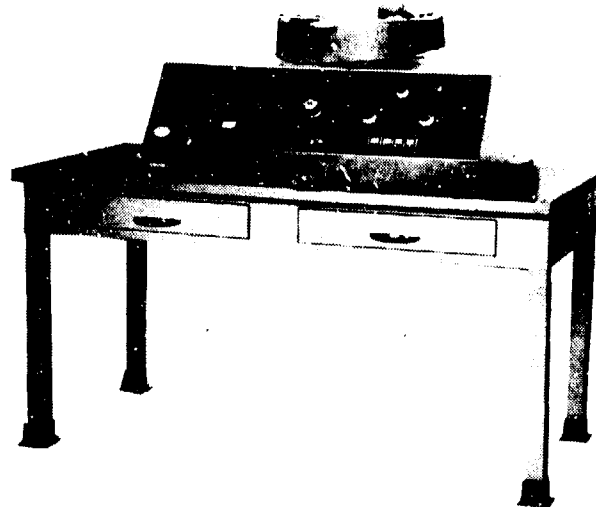


Figure A-2. Gardner Hazemeter.

## FALLING SAND TEST (TEST 2)

This type of abrasion test method was performed in compliance with ASTM D673-70 (except that the measurement of gloss was not required) to evaluate the effect of impingement by falling abrasive particles.

### Apparatus

The apparatus consisted of a hopper and glass tube rotating about 7 rpm, which allowed abrasive to free fall at 200 to 250 grams/minute from the fixed height of 25 inches. The test specimen was 3 x 6 inches and was held at a 45° position to the falling abrasive particles (see Figure A-3).

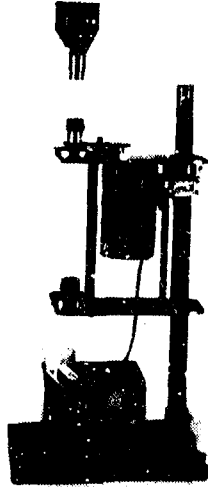


Figure A-3. Apparatus for Falling Sand Test.

### Materials

The abrasive was Silicon Carbide, No. 80 Mesh, Type GG. It was selected for its "blockiness", which assures a more even flow in the tester. The "blockier" silicon carbide particle was found to be less apt to spall and otherwise break than would be expected were silicon carbide dendrites used.

### Procedure

The ASTM test method procedure required that particles adhering to the surface or imbedded in it be removed before making any measurements; it suggests that a mild air blast may be effective. This procedure removed all silicon carbide particles used in the falling sand test, and the values reported reflect this procedure. The samples tested had a fine dusting of material spalled from the samples themselves, which required solvent washing for removal. They appeared to be held on by a static charge. Their removal would have yielded a lower effective

haze value for each material. This was not done, as the procedure appeared at variance with the aim of the ASTM standard test procedure. Published literature appears to give this value for many materials, but it is believed that the test data as reported is more representative of the haze which would be present on a part.

#### WINDSHIELD WIPER TEST (TEST 3)

This test method was performed to simulate the effect of windshield wiper operation on dirty windshields. The presence of an abrasive medium was used in this test because soft rubber wiper blades would otherwise be incapable of abrading most windshield materials.

#### Apparatus

The apparatus consisted of a specimen holding fixture mounted at approximately 45° with provisions to mount material specimens. A 12-inch Hycar rubber wiper blade (30 to 40 shore hardness) and a windshield wiper driver arm were attached to an aircraft type motor which was mounted to the test fixture. A system for regulating and discharging the abrasive slurry onto the 16-x-21-inch test specimen at 300 ML/minute rate was attached to the test fixture (see Figure A-4). A peristaltic pump was used to recirculate and apply the slurry. The haze measurements were confined to specific locations by the use of a marking mask. Eight holes were located on the mask periphery, Figure A-5, as well as in the middle of the mask.

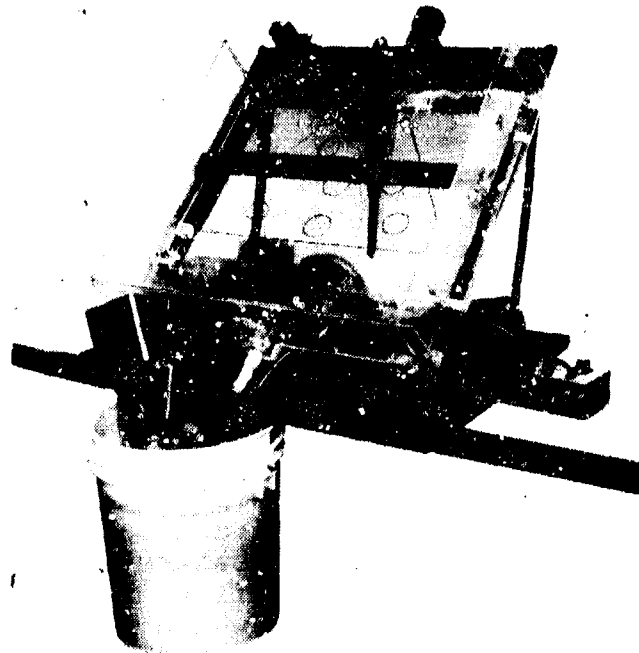


Figure A-4. Windshield Wiper Test Apparatus.

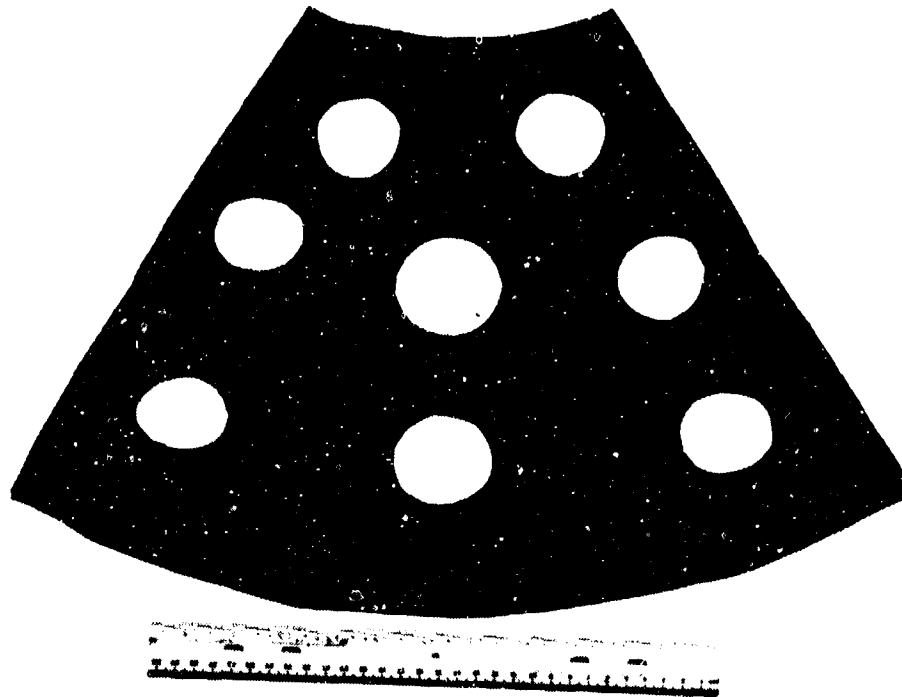


Figure A-5. Windshield Wiper Locating Mask.

Materials

The specimen size was 16 inch x 21 inch. The abrasive slurry mixture was 100 grams of AC air cleaner test dust, coarse (50% 30 to 80 micron) size, mixed with 1 liter of water.

Procedure

The windshield wiper blade pressure was adjusted to 0.5 lb per linear inch of blade length, and the operating speed was 100 cycles per minute. Every 12,000 cycles, the windshield wiper blades were changed and additional slurry was added as required. During the operation of the test, vigorous stirring of the reservoir was required to prevent settling of the abrasive.

#### WET RUBBING ABRASION TEST (TEST 4)

This test was performed to simulate the effects of wiping dirty, wet windshields, wherein the dirt contains abrasive particles. The specimens were mounted on a turntable and rotated at 10 rpm, while continually applying a slurry of water and fine sand through a 3-inch tube placed vertically over the specimen.

#### Apparatus

The apparatus consisted of a 3.0-inch-diameter slurry tube, 17 inches long, positioned with its centerline vertical and located 1-1/2 inches out from the center of a circular rotating platform as shown in Figure A-6. A piece of foam rubber was wrapped around and fastened to the bottom of the tube which rested on the specimen during the test. Pressure was maintained at 1 pound per square inch by keeping the slurry level at 15 inches.

This simulated a wiping effect which reasonably duplicated field service conditions.

A Hazemeter as specified in ASTM, Method D-1003; was used to obtain all haze measurements as shown in Figure A-7.

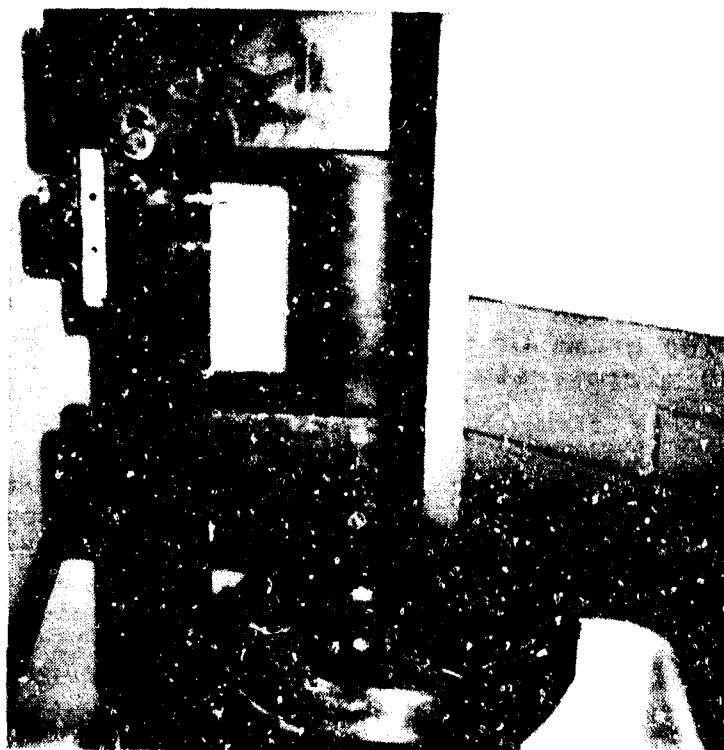


Figure A-6. Wet Rubbing Abrasion Test Setup.

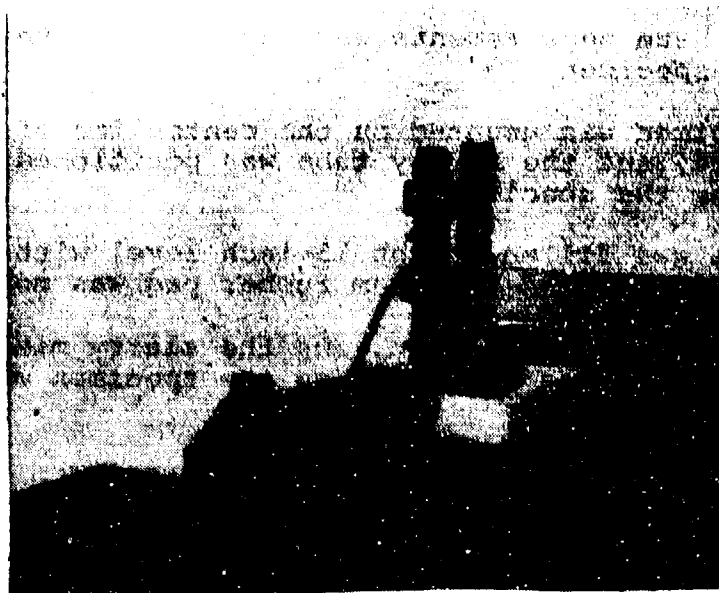


Figure A-7. Digital Readout Hazemeter and Wet Rubbing Abrader.

### Materials

Specimen size was 6 in. x 6 in. The abrasive and slurry mixture consisted of white sand and three other ingredients to keep the sand in suspension. The mixture and the mixing procedure were as follows:

Water	3 liters
Milk of Magnesia	125 grams
Bentonite U.S.P.	300 grams
White Sand	2.5 liters

The combination was mixed with a ball mill for 3 hours, then left standing in a closed container for 24 hours prior to use. Water was added as required during testing. Size characteristics of the white sand were as follows:

2.0% greater than U.S. Std.	30 mesh sieve (0.0232 in.)
15.0% greater than U.S. Std.	40 mesh sieve (0.0164 in.)
64.0% greater than U.S. Std.	60 mesh sieve (0.0098 in.)
15.0% greater than U.S. Std.	100 mesh sieve (0.0059 in.)
4.0% less than U.S. Std.	100 mesh sieve (0.0059 in.)

### Procedure

1. Initial haze measurements were taken prior to abrading a clean specimen.
2. One specimen was mounted on the centerline of the turntable, and the slurry tube was positioned to seat firmly on the specimen.
3. The tube was filled to the 15-inch level with the slurry mixture and the foam rubber pad was moistened.
4. The abrader was turned on, and the slurry mixture was kept at 15 inches in height as the specimen was abraded.
5. The abrader was turned off, and the specimen was removed to record the haze measurements.
6. The specimen was washed and dried thoroughly.
7. Haze measurements were taken and recorded.
8. The specimen was replaced on the turntable.
9. Steps 2 through 7 were repeated until a 30% haze was recorded.

### BLOWING SAND AND DUST TEST (TEST 5)

This test was conducted to simulate sand and dust blowing at 40 mph against a transparency.

### Apparatus

The test facility was a chamber with accessories to control dust concentration, velocity, temperature and humidity of dust-laden air in accordance with MIL-STD-810B, Method 510.

### Materials

The abrasive used was "140 Mesh Silica Flour", as listed in MIL-STD-810B, Method 510.

### Procedure

The test was conducted in accordance with the MIL-STD-810 procedure, except that the chamber was operated at an airflow setting of 3500 fpm. Haze measurements were taken initially for all specimens and periodically during the test.

## APPENDIX B

### ANALYSIS OF INSTRUMENTATION DIFFICULTIES WITH STRAIN MEASUREMENT AT NONAMBIENT TEMPERATURES

During the windshield instrumented tests, strains were measured under a wide range of loading and temperature conditions. Three types of windshield material were used; namely, glass, stretched acrylic, and polyester. On completion of a series of tests on glass windshields, the first tests on plastic materials at nonambient temperatures showed such divergent results that their validity was questioned. In the following analysis, it was found that the instrumentation requirements to accurately measure strains in polyester and stretched acrylic material in a dynamic thermal environment have exceeded the state of the art.

#### Background to Choice of Strain Gauge Method

During the preparation of the test plan for this project, the test subcontractor, Triplex Safety Glass Co, Ltd, considered the use of:

- a) Strain gauges plus "dummy" temperature compensating gauges.
- b) Temperature compensating strain gauges with matching expansion coefficients.

Alternative a) was quickly discarded since it was incorrect to assume that the dummy gauge would be at the temperature of the active gauge. This was not only due to the temperature gradients both through the windshield thickness and in the windshield plane, but due to the fact that the dummy was more likely to be at air temperature than windshield temperature. Therefore, the decision was made to use temperature compensating gauges, and numerous discussions were held with strain measurement suppliers regarding the best gauges to use. Although no gauges were traceable, worldwide, with exactly matching coefficients, three types of biaxial gauges with properties most suitable for use with glass, polyester and acrylic were eventually selected. For glass only, the match was good. For the other materials, differences were apparent.

At that time, it was considered that any error in gauge/coefficient matching could be allowed for by establishing an apparent strain curve for each material type and applying this as a correction to the results. This would assume that the precise temperature of the gauge at any moment was known. Correction curves were established and these are shown in Figures B-1 and B-2.

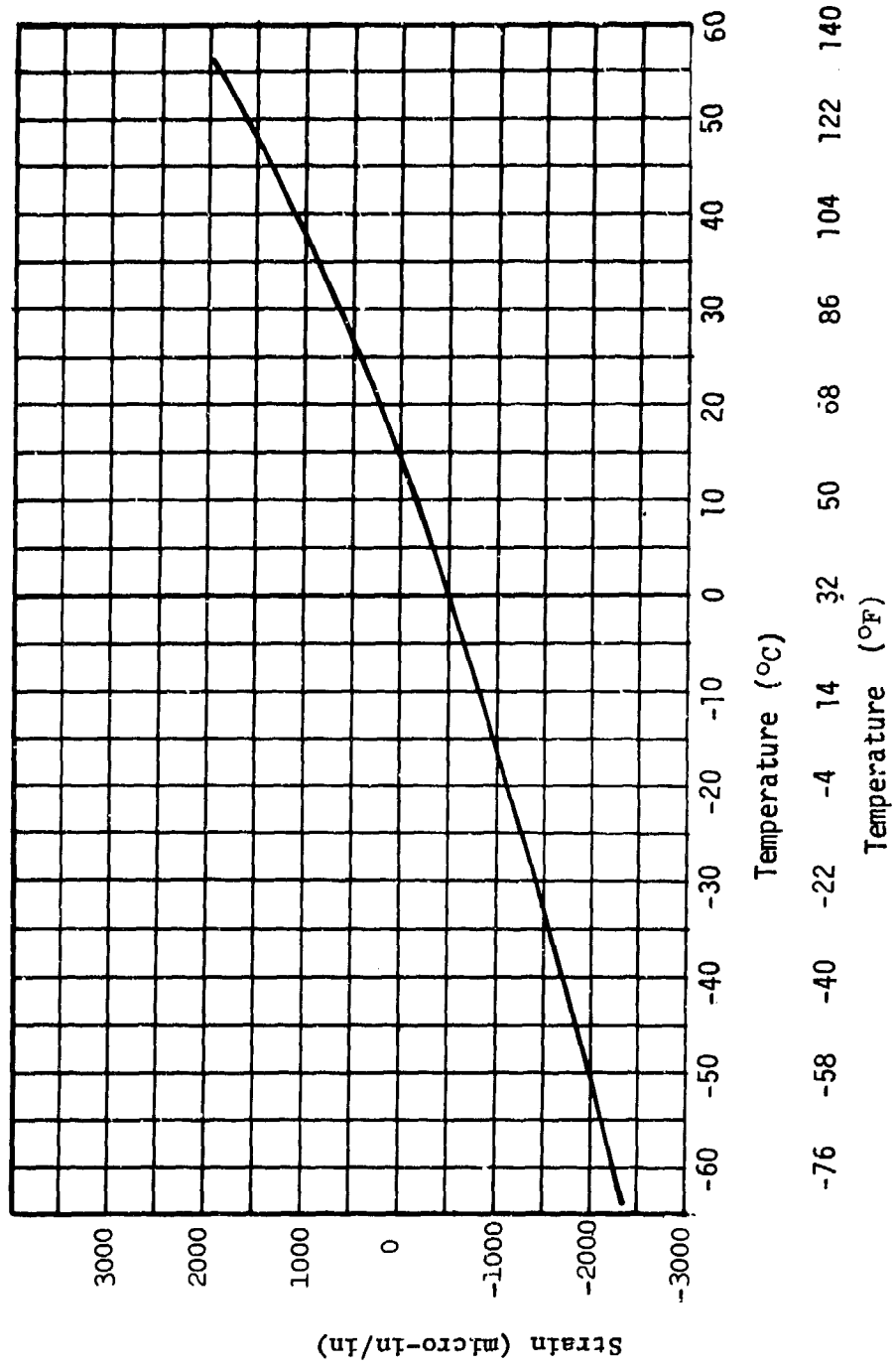


**Figure B-1. Temperature Induced Apparent Strain on Stretched Acrylic.**

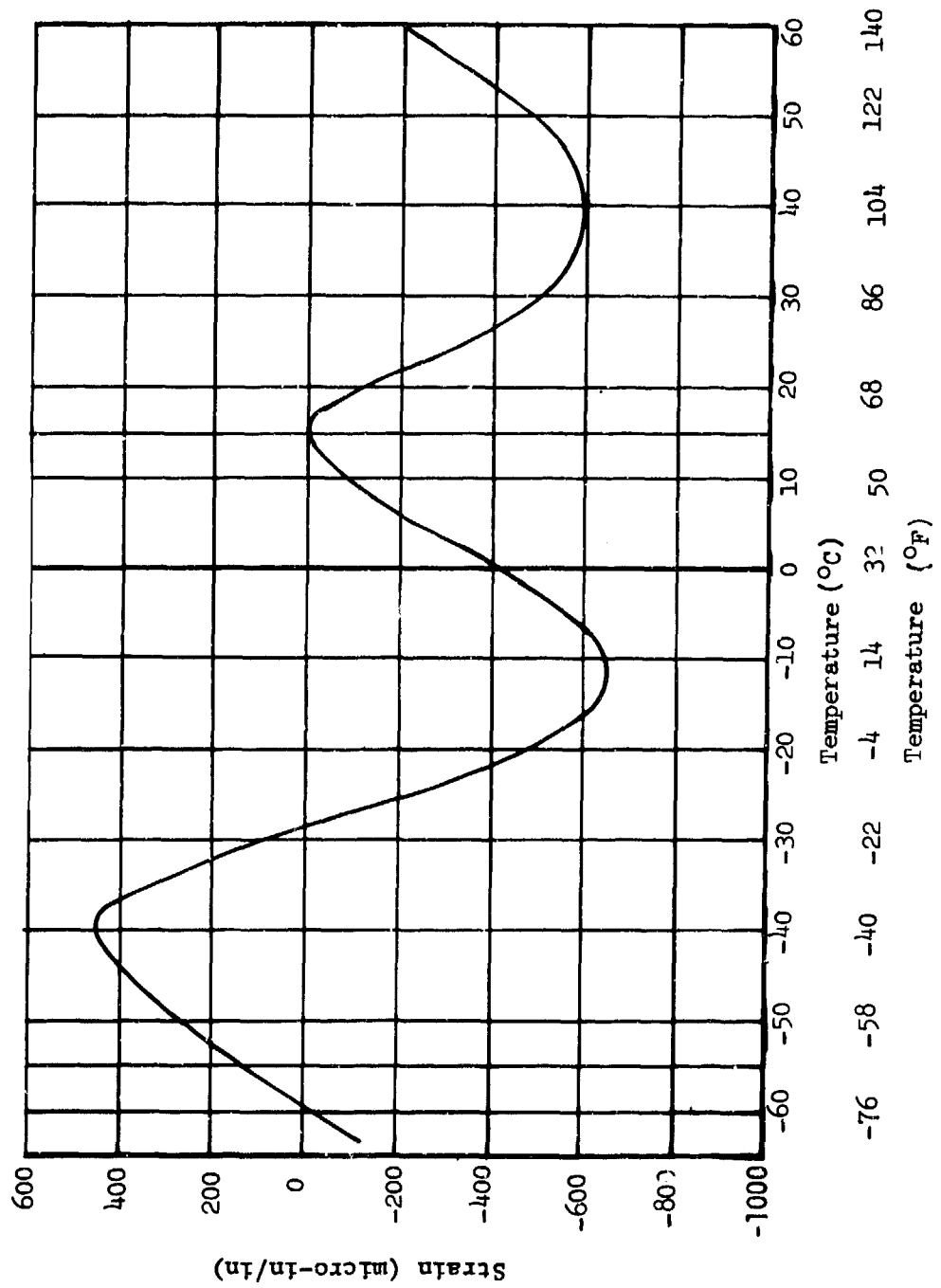


**Figure B-2. Temperature Induced Apparent Strain on Polyester.**

### Problems Experienced

Corrections required to temperature compensate the strain gauges were found to exceed the value of the strains actually being measured. For example, as shown in Figure B-1, at 125°F the strain gauge correction factor for stretched acrylic is approximately 30  $\mu$ -in./°F. Measured strains were on the order of 150  $\mu$ -in. This meant that a temperature variation between thermocouple and strain gauge as small as 5°F could create an error of 100%. Even more of a problem was the non-regular correction curve for polyester. Because of the apparent illogical wave-form seen, the calibration plot was repeated numerous times using three different gauge arms and completely separate instrumentation methods. All of these repeatedly indicated the same trend.

Compounding this problem was the basic difficulty of determining the actual gauge temperature. Laterally, there was some nonuniformity of panel temperature, and in the worst case there was a KH factor at the 1.30 limit level. As the thermocouples were at the side of the rosette, there were also temperature gradients which could be slightly different from that at the thermocouple itself. In addition, it was considered that the combined bulk of an accelerometer, a thermocouple, and a strain gauge rosette, together with their leads, locally affected the temperature gradients both laterally and through the thickness of the specimen by unrepresentatively disturbing the boundary layer of the airflow around a given instrumentation point. This altered the local heat transfer coefficient, giving rise to further nonrepresentative effects. The net result was that the strain gauge and its adjacent thermocouple experienced different temperatures which, linked with their differing hysteresis rates, made any temperature correction near meaningless.

This phenomenon was most significant during transient temperatures, but even at stable elevated or depressed temperatures, the evidence indicates that little reliance could be put on the results.

### Implications on Existing Results

Since the difficulties discussed thus far highlight the significance of temperature gradient effects and hysteresis delays, the failure of the Type -101, glass windshield (Serial No. 7-10-75-4) was further considered. It was thought that, at the moment of failure, the strain gauges on the surface may have been acting at temperatures nearer those of the air stream than those of the glass surface and thus indicate lower than actual strain levels. This was particularly likely under the very high rate of temperature drop of 2°F/sec (minimum).

Recorded strains at the time of failure were very low and were nowhere near the level expected at rupture, although some glass bending would have occurred under this temperature gradient; and in the absence of strain (or temperature) gauges within the laminate, this was impossible to extrapolate.

#### Alternatives Evaluated

The following possible alternatives for strain measurements were evaluated.

Alternative Gauge Type - Special universally temperature compensating gauges capable of working in conjunction with any material, over a wide temperature range, were considered. However, these gauges required an input signal based on temperature and therefore did not offer any significant advantages.

Brittle Lacquer Techniques - More commonly, these techniques are difficult to accurately quantify and the lacquers usually need fairly sophisticated temperature maintenance. The nature of Triplex's facility was also very restrictive for such an application, since the test windshield is enclosed out of sight during running. Apart from removing the specimen from the test rig after each parameter application, it would be impossible to assess inside surfaces for lacquer cracking. The concept would be further invalidated by any setting up run or stabilizing period.

Photo-Elasticity - Similar comments apply as in the brittle lacquer technique. Although photoelastic methods are used within Triplex's parent group, readily adaptable equipment was not available for this type of facility. In addition, stress profiles, through an assembly embodying three types of material, would be exceedingly difficult to determine.

Imbedded Temperature Sensors - For any new test specimens to be procured in the future, it is suggested that these might include further instrumentation within the interlayer of the laminate. This has been found in the past to provide valuable data on such parameters as internal temperature, which permit a more accurate assessment of internal interlayer forces.

Strain Measurement Conclusions

It is considered that the requirements for achieving the level of instrumentation intended stretched available technology beyond the limits imposed by budgetary considerations.

The inability to provide matching strain gauges for the materials concerned has been the prime cause of this. Temperature gradient effects, both laterally and through the laminate, have further compounded the difficulties.

This Document Contains Pages  
Reproduced From  
Best Available Copy